Atypical ways of signaling:

The adhesion GPCR Latrophilin as a regulator of reproduction

Inaugural thesis

presented to the Faculty of Mathematics and Natural Sciences

of Heinrich Heine University Düsseldorf

for the degree of

Doctor of Philosophy in Natural Sciences

by

Willem Berend Post

from Veenendaal, the Netherlands

Düsseldorf, May 2026

From the Institute of Cell Biology

of Heinrich Heine University Düsseldorf

Printed with permission of the Faculty of Mathematics and Natural Sciences of

Heinrich Heine University Düsseldorf

Examiners:

1. Prof. Dr. Simone Prömel
2. Prof. Dr. Sebastian Fraune

Day of Oral Defence: 27th October 2026

Table of Contents

Table of Figures **4**
Abbreviations **5**
Summary **6**
1 Introduction **8**

1.1 Adhesion G Protein-Coupled Receptors 8
1.1.1 G Protein-Coupled Receptors (GPCR) 8
1.1.2 Adhesion G Protein-Coupled Receptors and their physiological relevance 9
1.1.3 Structure of Adhesion GPCRs 10
1.1.4 Molecular functions of Adhesion GPCRs 11
1.1.5 Latrophilins 15

1.2 *C. elegans* 15
1.2.1 *C. elegans* as model organism to study adhesion GPCRs *in vivo* 15
1.2.2 The *C. elegans* gonad as a test tube for probing cellular division and development 16
1.2.3 The Notch pathway is essential for metazoan functioning 18
1.2.4 The *C. elegans* ADGRL homolog LAT-1 is essential for several physiological functions 21
1.2.5 LAT-2 remains poorly characterized 23

2 Aims of this thesis **24**
3 The N terminus-only (*trans*) function of the Adhesion GPCR Latrophilin-1 controls multiple processes in reproduction of *C. elegans* **26**
4 Notch activity is modulated by the aGPCR Latrophilin binding the DSL ligand in *C. elegans* **43**
5 The Adhesion GPCR ADGRL2/LPHN2 Can Protect Against Cellular and Organismal Dysfunction **61**
6 Discussion **79**

6.1 Notch and aGPCRs: a conserved mechanism uncovered? 80
6.2 The role of alternative splicing to establish N terminus-only functions 81

7 References **84**
8 Supplementary material **92**

8.1 Supplementary material for 'The N terminus-only (*trans*) function of the Adhesion GPCR Latrophilin-1 controls multiple processes in reproduction of *C. elegans*' 92
8.2 Supplementary material for 'Notch activity is modulated by the aGPCR Latrophilin binding the DSL ligand in *C. elegans*' 97
8.3 Supplementary material for 'The Adhesion GPCR ADGRL2/LPHN2 Can Protect Against Cellular and Organismal Dysfunction' 128
8.4 Curriculum Vitae 133
8.5 List of publications 137

9 Statement of Authorship **138**
10 Acknowledgments **139**

Table of Figures

Figure 1: GPCR structure, activation and downstream signaling

Figure 2: Typical structure of Adhesion GPCRs

Figure 3: Signaling and functions of aGPCRs

Figure 4: Anatomy of an adult *C. elegans* hermaphrodite and its gonad

Figure 5: Core Notch signaling pathway

Figure 6: aGPCR homologs in *C. elegans*

Abbreviations

7TM	Seven transmembrane
AC	Anchor cell
ADAM	A Disintegrin And Metalloprotease domain
aGPCR, Adhesion GPCR	Adhesion G Protein-Coupled Receptor
AID	Auxin inducible degradation
BBB	Blood-brain barrier
BFPP	Bilateral frontoparietal polymicrogyria
C. elegans	*Caenorhabditis elegans*
Cirl	Calcium independent receptor for Latrotoxin
cAMP	Cyclic adenosine monophosphate
CSL	CBF-1/Suppressor of hairless/LAG-1
CTF	C terminal fragment
D. melanogaster	*Drosophila melanogaster*
DSL	Delta, Serrate, LAG-2
DTC	Distal Tip Cell
Dvl	Disheveled
ECM	Extracellular matrix
ECR	Extracellular region
EGF	Epidermal growth factor-like
ER	Endoplasmic Reticulum
Fz	Frizzled
GAIN domain	GPCR Autoproteolysis Inducing Domain
GPCR	G Protein-Coupled Receptor
GPS	GPCR Proteolysis Site
HRM, HBD, HormR	Hormone Binding Domain
LRR	Leucine rich repeats
MAML	Mastermind-like protein
MMP-14	Metalloproteinase 14
NICD	Notch intracellular domain
NTF	N terminal fragment
NRR	Negative regulatory region
RBL	Rhamnose Binding Lectin
Reck	Reversion-inducing cysteine-rich protein with kazal motifs
RNAi	RNA interference
TA	Tethered Agonist
TIA	Tethered Internal Agonist
VPCs	Vulval precursor cells
Vstat-40	Vasculostatin-40
Vstat-120	Vasculostatin-120

Summary

Proper cell-cell communication is key for all multicellular organisms, with severe cellular and organismal consequences upon disruption. Among the molecules most essential to realize this communication are G protein-coupled receptors, of which adhesion GPCRs (aGPCRs) are one class. They possess unusually long N-terminal regions that enable the receptors to mediate cell-cell and cell-matrix adhesion as well as classical G protein-mediated signals. Additionally, and maybe most intriguingly, the N termini can act as “signal/information giver” for pathways on opposing cells, a function that is called *trans*/N terminus-only/7TM-independent. Due to this complexity, aGPCRs remain highly enigmatic, in particular regarding the ways they mediate their molecular mechanisms. Delineating these requires informative analyses *in vivo*, which is often complicated and costly, in particular in higher animals. Therefore, in this thesis, the adhesive and signaling functions of aGPCRs are explored using the simple model organism *Caenorhabditis elegans*, focusing on the conserved aGPCR group Latrophilins. Two homologs, *lat-1* and *lat-2*, exist in the nematode. While for LAT-2 not much is known yet, LAT-1 mediates G protein signals to orient cell division plane orientations in the early embryos. Additionally, it mediates N terminus-only functions in several, not well-defined contexts.

This thesis first clarified the contexts in which the LAT-1 N terminus-only function is required. Broad expression of *lat-1* was found in several gonadal tissues of *C. elegans*. *lat-1* null mutants displayed reduced sperm guidance, slower ovulation rates, and poorer oocyte quality as well as increase in germ cell apoptosis. These defects could largely be rescued by the sole receptor N terminus, highlighting that the N-terminus-only function of LAT-1 is crucial for the regulation of nematode fertility and reproduction. Transcriptome analyses revealed numerous *lat-1* variants with some only containing the N terminus giving rise to the hypothesis that N terminus-only functions might be modulated by alternatively spliced *lat-1* transcripts.

To understand the molecular mechanisms underlying the N terminus-only LAT-1 function, the progenitor zone of the *C. elegans* gonad was further investigated. This region is key for

germ cell self-renewal and differentiation and is under tight control by the Notch pathway. *lat-1* mutant nematodes display a reduced progenitor zone, which could also lead to a reduced brood size. A potential interplay between LAT-1 and the Notch pathway was observed as in *lat-1* mutants, a reduction of Notch activity was observed. Using a variety of methods, it was shown that the LAT-1 N terminus can interact with the Notch ligand LAG-2 on the distal tip cell of the gonad and thus, modulate Notch activity, affecting germ cell maintenance in this manner. Key residues in the N terminus of LAT-1 responsible for this interaction were identified and confirmed. Given the strong conservation of Notch and Latrophilins, these findings raise the question of whether aGPCRs may modulate Notch signaling across cellular contexts.

To broaden the study, the Latrophilin homolog LAT-2 was characterized. Similar to LAT-1, a prerequisite for investigating molecular functions of LAT-2 is a thorough understanding of its biological impact. Thus, in this thesis, *lat-2* null mutant nematodes were phenotypically analyzed. It was found that LAT-2 affects oxidative stress resistance in *C. elegans*. *lat-2* null mutants were shown to have increased levels of reactive oxygen species, a reduced lifespan and an upregulation of stress-related genes. These results form a basis for further analyses addressing the question of whether an N terminus-only mechanism is underlying this LAT-2 function.

Taken together, the findings presented in this thesis indicate that aGPCRs can modulate Notch activity via their N terminus-only function, thereby underlining the importance and diversity of ways that aGPCRs can integrate and transduce signals beyond canonical G protein signaling. They open up valuable avenues for additional research to grasp a more comprehensive picture how these receptors can fulfill such a large variety of roles.

1 Introduction

1.1 Adhesion G Protein-Coupled Receptors

1.1.1 G Protein-Coupled Receptors (GPCR)

Eukaryotic organisms require intricate mechanisms to receive and respond to extracellular stimuli, elicited either via other cells, or by their larger environment. Sensing and transmitting these signals is essential for proper functioning of organisms. One of the largest groups of molecules responsible for this signal transduction are G Protein-Coupled Receptors (GPCR, 7TM receptors, serpentine receptors), with over 800 GPCRs encoded by the human genome. These receptors are located on the cell surface and have some key characteristics. All GPCRs consist of seven transmembrane helices spanning the cell membrane, interconnected through extracellular and intracellular loops, with an extracellular N terminus and an intracellular C terminus (**Figure 1**). Their name stems from their capacity to signal via heterotrimeric G proteins. These G proteins allow a GPCR to transduce extracellular stimuli into cells, ultimately resulting in a cellular response.

The extracellular ligands that are able to interact with GPCRs are diverse, and contain compounds such as neurotransmitters, peptides, lipids, olfactory molecules, and light. Binding of these compounds to the GPCR leads to conformational changes, causing a shift from inactive to active state. The heterotrimeric G protein complex consists of a Gα, Gβ and Gγ subunit. Receptor activation results in the dissociation of the G protein from the receptor, affecting four main signaling pathways, mediated by distinct subclasses of G proteins, which are defined according to the Gα subunit (summarized in **Figure 1**). All lead to distinct cellular responses, highlighting how GPCRs can affect cellular functioning on many different levels. This variety in responses also explains why GPCRs are seen as promising drug targets. This is underlined by two additional reasons. The first one being that GPCR mutations can cause diseases, for example retinitis pigmentosa [1–3] and Usher Syndrome type IIC [4,5]. More prominent, however, is the fact that GPCRs are easily druggable, due to their accessibility on

the cell surface, affecting their downstream pathways in this manner. Additionally, their wide involvement in virtually all physiological processes makes them highly relevant as drug target.

Within the superfamily of GPCRs, several classes can be identified. GPCRs are commonly classified using the GRAFS system, grouping GPCRs based on their sequence homology to either Glutamate, Rhodopsin, Adhesion, Frizzled/Taste2 or Secretin [6]. This thesis focuses specifically on the class of adhesion GPCRs.

1.1.2 Adhesion G Protein-Coupled Receptors and their physiological relevance

The second largest class of GPCRs according to the GRAFS system are the Adhesion G Protein-Coupled Receptors (Adhesion GPCRs, aGPCRs), containing 33 genes in humans [7]. Although the adhesion class is not as large as the Rhodopsin class, which contains over 700 GPCRs, Adhesion GPCRs are very enigmatic, with many members still considered as orphan receptors and sparse knowledge on their signaling mechanisms and functions. Within the class of aGPCRs, nine subfamilies can be distinguished, based on their conserved seven transmembrane (7TM) region [8].

Adhesion GPCRs are broadly expressed in virtually all organs, fulfilling numerous functions (reviewed by [9,10]). For example, GPR126/ADGRG6 is involved in brain

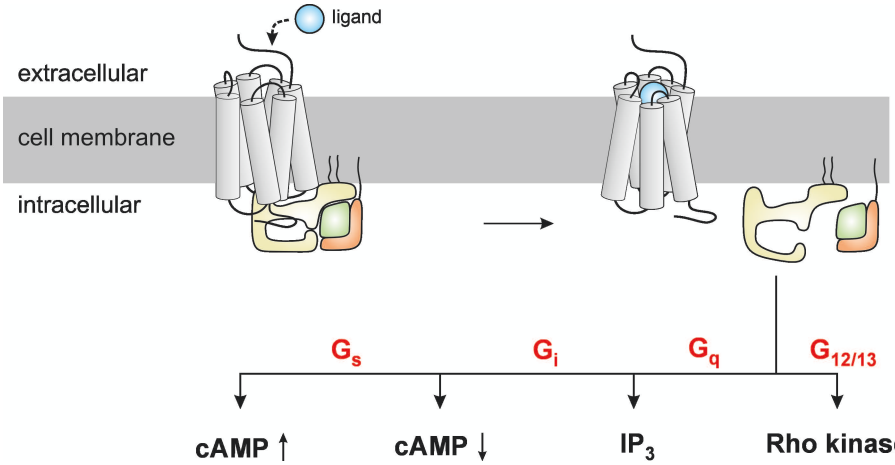


Figure 1: GPCR structure, activation and downstream signaling. Upon binding of a ligand to the GPCR, a conformational change takes place, leading to the recruitment of GTP by the Gα subunit, as well as dissociation of the bound GDP. This exchange triggers dissociation of the G protein complex from the GPCR, as well as dissociation of the Gα and Gβγ subunits. Eventually, this results in, cAMP levels raised or lowered via Gs and Gi, respectively, or IP_3 production (Gq), leading to an increase of cytosolic Ca^{2+}, or cytoskeletal remodeling takes place via Rho kinase ($G_{12/13}$).

vascularization, angiogenesis as well as cardiac development, and is additionally key for myelination of glial cells, impacting signal propagation in the nervous system.

Involvement of aGPCRs in the nervous system has long been established, for example for CELSRs/ADGRC, which affect axon guidance and synaptogenesis (reviewed by [9,10]). Additionally, Latrophilins/ADGRL are essential for synapse formation. Many more functions exist for aGPCRs, but these examples underline the functional diversity of them in a variety of contexts.

A strong link between aGPCRs and diseases exist, with three receptors showing monogenic pathologies (reviewed by [10]). VLGR1/ADGRV1 mutations have been shown to cause Usher syndrome type II, GPR56/ADGRG1 mutants can cause bilateral frontoparietal polymicrogyria (BFPP) [11] and EMR2/ADGRE2 mutants can give rise to vibratory urticaria [12]. Additionally, many other aGPCRs have been implicated in other pathologies, such as severe neurodevelopmental defects (for example neural tube defects and spina bifida) that are often embryonically lethal (reviewed by [9]). Lastly, members of all aGPCR subfamilies are associated with cancer, making them potential future therapeutic targets.

1.1.3 Structure of Adhesion GPCRs

As the name suggests, aGPCRs are known for their role in cell-cell and cell-matrix adhesion. To achieve this, aGPCRs have an extensive extracellular region (ECR), which is considered their key characteristic (**Figure 2**). The ECR can contain a plethora of domains that aid in fulfilling their roles as receptors as well as adhesion-mediating modules. Examples of these domains are diverse types of lectin domains, leucine rich repeats (LRRs), diverse types of laminin domains, etc. A key domain present in all aGPCRs except ADGRA1 is the GPCR-Autoproteolysis Inducing Domain (GAIN), located immediately upstream the 7TM [13]. The GAIN domain of most but not all aGPCRs has the intrinsic capability to autoproteolytically cleave the receptor into an N terminal and a C terminal fragment (coined NTF and CTF, respectively), which occurs at a conserved site of ~50 residues within the GAIN domain named GPCR Proteolytic Site (GPS). This cleavage occurs immediately after receptor biosynthesis in the

endoplasmic reticulum (ER) [14]. Upon cleavage, NTF and CTF remain non-covalently attached, consisting as one entity. Although highly conserved, the function of receptor autoproteolysis remains enigmatic, with contrasting evidence. Some studies indicate that it is important for receptor trafficking and folding [15] while other studies suggest that the presence of the GPS motif and not the proteolysis is the key importance for receptor functionality [16,17]. There is also a line of evidence that suggests NTF / CTF dissociation is a necessary step in activation for

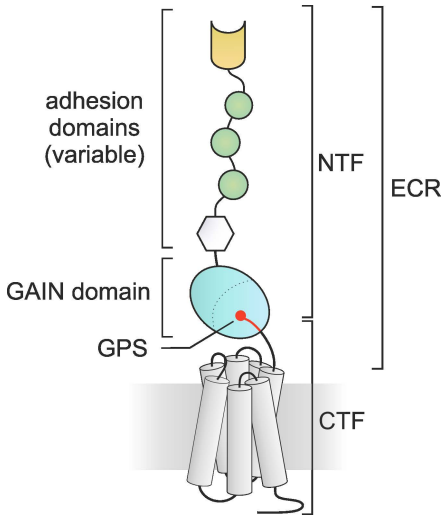


Figure 2: Typical structure of Adhesion GPCRs. aGPCRs consist of an ECR that contains a number of adhesion-related domains in variable composition. Just upstream the 7TM domain, the receptor contains the GAIN domain, which induces autoproteolytic cleavage at the GPS. All domains upstream of the GPS are referred to as NTF whereas the remaining GAIN domain fragment (Stachel/tethered agonist/tethered internal agonist), 7TM and C terminus are referred to as CTF.

some of the receptors, which will be further outlined below (**chapter 1.1.4**). Importantly, for some aGPCRs, GPS cleavage does not occur, or abolishing cleavage does not affect receptor functionality, highlighting a varied mechanism that to date is not fully understood.

1.1.4 Molecular functions of Adhesion GPCRs

Adhesion GPCRs can mediate functions through multiple mechanisms. In addition to canonical G protein–dependent/*cis* signaling, a largely uncharacterized yet intriguing mode of functioning, referred to as *trans*/N terminus-only/7TM-independent signaling, has been described for aGPCRs. Furthermore, cell-cell and cell-matrix adhesion play key roles in shaping aGPCR function.

Cis signaling

As described, canonical (*cis*) signaling of GPCRs uses G proteins to mediate receptor activation and thus induce downstream signaling cascades. aGPCRs can couple G proteins, generally having a preference for $G_{12/13}$ [18] (**Figure 3**). Fascinatingly, aGPCRs contain an embedded agonistic sequence embedded in the GAIN domain, immediately upstream the 7TM. This highly hydrophobic ß-sheet, referred to as *Stachel*, tethered agonist (TA) or, as recently suggested, tethered internal agonist (TIA) can activate the receptor [19,20], leading to canonical G protein dependent downstream signaling. This was initially shown for GPR126/ADGRG6, GPR133/ADGRD1, GPR56/ADGRG1 and GPR110/ADGRF1, but has been shown for other aGPCRs as well, and is currently considered the key activation mechanism of aGPCRs [18,21–24]. This *in vitro* discovery has been supported by a number of *in vivo* evidences, such as from the Latrophilin/ADGRL homolog Cirl (Calcium independent receptor for Latrotoxin/ADGRL) in *Drosophila melanogaster* (*D. melanogaster*) [25] and LAT-1 in *Caenorhabditis elegans* (*C. elegans*) [26].

Initially, it was hypothesized that ligand binding could cause NTF-CTF dissociation, leading to exposure of the tethered agonist (referred to as the *dissociation* or *one-and-done* [20] *model*), leading to receptor activation, however, uncleavable receptor variants are often still functional, indicating N-C dissociation is not a strict requirement (reviewed by [27,28]). Recent research has shown that for some aGPCRs, there is potential for tethered agonist exposure in an NTF-CTF heterodimer, suggesting a mode of aGPCR activation that does not require dissociation (referred to as *non-dissociation*, *displacement* or *tunable model* [20]) [29]. Structural elucidations of ADGRL3 have shown that small movements of the ECR are also able to activate the receptor [30]. Since not all aGPCRs are autoproteolytically cleaved, this method would allow also those receptors to be activated by the TA. Separation or movement of the NTF can be elicited through binding of the NTF with other cell surface proteins, or extracellular matrix (ECM) components. The multiplicity of receptor activation mechanisms highlights the diversity and complexity of aGPCR signaling and likely do not yet fully cover modes of *cis* signaling.

Trans function

To date, it has been shown for seven of the 33 aGPCRs that they are able to engage in G protein-independent / N terminus-only / 7TM independent / *trans* functions (reviewed by [31]). This is a highly intriguing mode distinctive from *cis* signaling due to its independence from 7TM, C terminus as well as G protein coupling, therefore differing distinctly (**Figure 3**). Due to the lack of a comprehensive set of second messengers such as for *cis*, it is a much more enigmatic mode, often requiring researchers to step away from *in vitro* methodologies. Importantly, N terminus-only functions are distinct from cell-cell or cell-matrix adhesion, which can also be elicited by aGPCRs. N terminus-only functions result in an effect on opposing cells, for example by acting as a ligand. This is in contrast to adhesion, which is considered as structural, not eliciting a molecular signal. Below, several examples will be elaborated, showcasing the large variety of cellular processes that can be affected by N terminus-only functions.

A key example of a N terminus-only function is ADGRA2/GPR124. Although G protein coupling has not been shown for ADGRA2, it has been shown that it interacts with the Wnt pathway in the blood-brain barrier (BBB) [32–35]. Canonically, the extracellular molecule

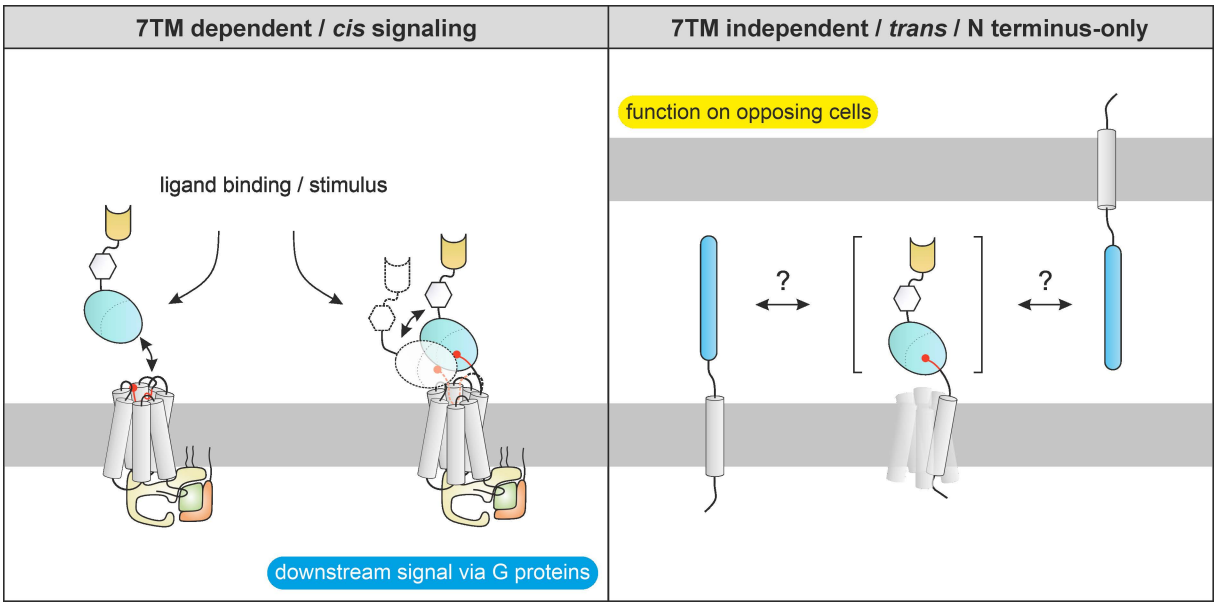


Figure 3: Signaling and functions of aGPCRs. Canonical (*cis*) activation of aGPCRs involves G protein and classical second messengers, and can occur by movement or dissociation of the NTF, exposing the TIA. This movement or dissociation can occur due to ligand binding or mechanical stimuli. Additionally, many aGPCRs display N terminus-only functions which are solely mediated by the NTF, eliciting a response on opposite cells.

Wnt7 binds to Frizzled (Fz) and Lrp5/6, in turn leading to ß-catenin signaling via disheveled (Dvl) . Alternatively, Wnt7 can be bound by R membrane-bound Reck (reversion-inducing cysteine-rich protein with kazal motifs), therefore making Wnt7 unavailable for Fz and Lrp5/6. However, when ADGRA2 interacts with the Reck/Wnt7 complex, it facilitates the assembly of a larger complex of ADGRA2, Reck, Fz and Lrp5/6. This in turn enhances ß-catenin signaling, controlling angiogenesis. This highlights how aGPCRs can be deeply integrated into signaling networks that do not rely on G protein signaling.

Another prominent aGPCR, ADGRG6/GPR126 has shown both *cis* and N terminus-only functionality. Primarily, ADGRG6 NTF secretion by endocardial cell has been shown, as well as binding of the NTF to cardiomyocytes and pericardial cells [36]. More details remain enigmatic, but it is hypothesized that the NTF acts as ligand or coreceptor, triggering an unknown signaling pathway in cardiomyocytes. Additionally, ADGRG6 is involved in radial axon sorting by Schwann cells [37]. The current hypothesis is that the N terminus-only function is mediated by laminin-211 and ß1-integrin, eventually affecting radial sorting [38]. Simultaneously, the CTF is activated by NTF dissociation, triggering Schwann cell differentiation, thus coupling both N terminus-only function and G protein-coupling together into a single biological process.

Lastly, ADGRB1/BAI1 has been quite extensively characterized for its N terminus-only function as part of its antiangiogenic function in the brain (reviewed by [31]). Fascinatingly, ADGRB1 can produce two NTF's, one via GPS cleavage, called vasculostatin-120 (Vstat-120) [39,40] as well as a smaller N terminus, Vstat-40, which is produced via cleavage by matrix metalloproteinase 14 (MMP-14) [41]. Both these soluble proteins can interact with CD36 on endothelial cells, affecting angiogenesis [39,41]. The exact reason why both fragments are produced, remains unclear, however, it has been suggested that the ratio between Vstat-40 and Vstat-120 may be of importance [41].

These examples show the conservation as well as diversity of N terminus-only functions across aGPCRs, playing roles in various cellular roles. However, this diversity makes N terminus-only functions complicated to study. Without confined cellular outcomes such as cyclic adenosine monophosphate (cAMP), it is essential to study these functions in their native

contexts as much as possible, requiring model organisms. Some of the pressing open questions regarding N terminus-only functioning are: do receptors fulfil both *cis* and *trans* function simultaneously, as well as: how is *trans* function realized *in vivo*? Many of these questions are as of yet unanswered in the current body of research, and the N terminus-only function will be a key concept under investigation in this thesis.

1.1.5 Latrophilins

A highly conserved subfamily within aGPCRs are the Latrophilins/ADGRLs which, in humans, consist of four members (LPHN1-3 and ELTD1, ADGRL1-4). This subfamily is among the oldest and most conserved, encompassing all the typical features of aGPCRs, such as the long N terminus, containing the GAIN domain as well as G protein signaling capability (reviewed by [10]). Latrophilins are conserved in a plethora of organisms, ranging from humans and mice to the zebrafish *Danio rerio* and invertebrate models such as *Drosophila melanogaster* and, as mentioned *C. elegans*, making it a key subfamily of aGPCRs for fundamental and structural research, allowing researchers to leverage advantages from these model organisms. The name Latrophilin is derived from its original identification as a receptor for α-Latrotoxin, a potent neurotoxin which is a key component in the black widow spider venom [42–45]. Latrophilins are most well-known for their key role in neurogenesis (reviewed by [46]), yet have functions in other organs as well, such as for example the pancreas [47]. Furthermore, expression of ADGRLs in several other tissues hypothesizes further, undiscovered functions (reviewed by [10]).

1.2 *C. elegans*

1.2.1 *C. elegans* as model organism to study adhesion GPCRs *in vivo*

Adhesion GPCR signaling is extremely varied and diverse, making it essential to study them in their native context as much as possible. However, classical murine animal models are often too complex to efficiently delineate signaling mechanisms from. Conversely, *in vitro* systems are often based on overexpression and heterologous expression, thereby introducing

a certain level of artificiality. Optimally, a simple model organism that endogenously expresses conserved aGPCR homologs can be utilized.

In the last century, the soil-dwelling roundworm *Caenorhabditis elegans* has been gradually established as a well-known model organism for a wide variety of topics, varying from epigenetics to ecology. In the late 20th century, technological advancements allowed for mapping the nematode's genome [48] as well as defining its invariant post-embryonic cell lineage [49]. Strikingly, it was the first multicellular organism to have its whole genome sequenced [50]. *C. elegans* is seen as a particularly useful model organism due to its small size (~1 mm), limited, defined cell number and lineage (~1000 somatic cells in adult nematodes), short life span as well as transparency and genetic amenability, making it a key model organism for fundamental biological questions. Despite its small size and cell number, the nematode contains a diversity of cell types and organs such as a pharynx, gonad, gut as well as an elaborate nervous system (**Figure 4a**).

The nematode commonly exists as hermaphrodite, which is a benefit for laboratory maintenance. Additionally, males do exist, albeit at low frequencies (approximately 0.1%), allowing for genetic variability. Additionally, the high number of offspring (200-300 eggs per hermaphrodite) is seen as a key advantage, allowing researchers to cultivate large amounts of worms in a short period of time. This can be further manipulated using temperature, which is commonly kept between 15 °C – 25 °C. Wild-type nematodes can grow from egg to self-fertilizing adult in approximately 3 days at 20 °C. All these features make *C. elegans* a very powerful model organism.

Additionally, *C. elegans* expresses three conserved homologs to aGPCRs named *lat-1*, *lat-2*, and *fmi-1. lat-1* and *lat-2* will be addressed in more detail in **chapter 1.2.4**.

1.2.2 The *C. elegans* gonad as a test tube for probing cellular division and development

In this thesis, the major focus will be on the *C. elegans* gonad. These large, tubular structures exist in duplicate and are responsible for production of oocytes, which is a tightly

regulated process (**Figure 4b**). The gonad can be divided into a somatic part and the germline. At the distal end of the gonad, a capping cell named Distal Tip Cell (DTC) is present, which is a key somatic cell playing a major role in promoting the proliferative germ cell fate [51]. This cell is highly elaborated, containing very thin processes extending into the germ cell pool, creating a microenvironment in which germ cells undergo a stem-cell like mitotic renewal process [52]. The microenvironment is often referred to as the proliferative zone or progenitor zone and is mainly controlled via the highly conserved Notch pathway [53–55], which will be described in more detail in **chapter 1.2.3**.

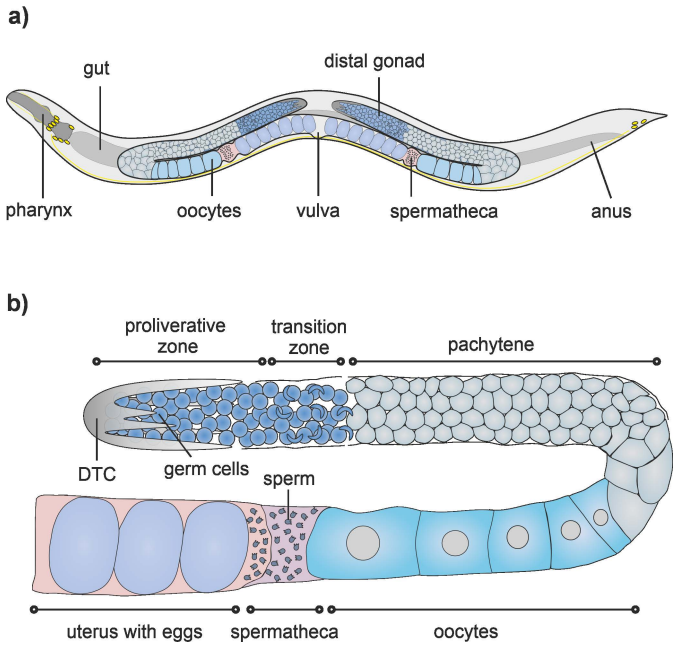


Figure 4: Anatomy of an adult *C. elegans* hermaphrodite and its gonad. a) General anatomy of *C. elegans*. Despite its small size, the nematode features several distinct organs such as a pharynx, gut and anus as well as an elaborate hermaphroditic gonad. b) The gonad can be divided into several zones, in which germ cells divide, grow and eventually get fertilized by sperm produced in earlier stages.

Proximal to the DTC, the germ cells are covered by pairs of gonadal sheath cells, which promote several factors in germ line development, as well as germ cell engulfment following apoptosis. The proximal sheath cells are also responsible for oocyte maturation, ovulation and pass on yolk protein to the developing oocytes (reviewed by [56]). Additionally, they are responsible for contraction, which pulls the spermatheca over the most proximal oocyte for fertilization.

In the germline, sperm is produced during the L4 stage, in which each gonad arm commits approximately 37 diploid germ cells to sperm production (reviewed by [57]). They form primary

spermatocytes, attached to the central canal connecting the gonad, called rachis. Following migration of the primary spermatocytes past the pachytene, they detach from the rachis and complete meiosis, generating a total of approximately 250 haploid spermatids per nematode. These spermatids are then pushed into the spermatheca for storage. Upon sperm activation, the spermatids develop a pseudopod which provides motility, and they can subsequently locate and fertilize oocytes pushed through the spermatheca.

Contrary to the sperm, the number of oocytes produced outnumbers the set amount of sperm, making the sperm the limiting factor for the number of offspring generated. Oocyte production is a continuous process starting at adulthood. At the distal end, germ cells undergo a mitotic self-renewal process under control of the DTC. Upon mitotic division, bulk flow makes germ cells migrate out of the DTC influence into the pachytene region of the gonad, transitioning from a mitotic to a meiotic fate. At this stage, crossover recombination takes place. In the late pachytene, it is estimated that about half of the germ cells undergo apoptosis as part of a natural process [58], leading to corpse engulfment by the gonadal sheath cells. The leading theory for this major germ cell apoptosis is that the apoptotic germ cells provide a nutrient source for the developing oocytes. This maintains a high quality of the oocytes and regulates their number. As germ cells migrate further, they grow in size, taking up additional nutrients, and finally form into fully cellularized oocytes. These then get fertilized by sperm stored in the spermatheca and get excreted by the nematode, for further *ex utero* development and eventual hatching.

1.2.3 The Notch pathway is essential for metazoan functioning

One key pathway responsible for proper germ cell division and differentiation in the *C. elegans* germline is the Notch pathway. This pathway is highly conserved among metazoa and malfunctioning of key Notch components can have severe consequences. Notch is involved in a large variety of processes, often being responsible for self-renewal of stem cells, cell fate determination and tissue homeostasis (reviewed by [59]). Examples of physiological processes that involve Notch are for example the regulation of osteoblasts, chondrocytes and osteoclasts

in bone tissue. In heart tissue, Notch regulates the ratio of cardiomyocytes to non-cardiomyocytes.

The typical highly conserved Notch pathway consists of the Notch receptor in conjunction with a Notch ligand (**Figure 5**). During production, the Notch receptor undergoes cleavage in the Golgi (S1 cleavage) and exists as a heterodimer on the cell surface. It can bind to DSL (Delta, Serrate, LAG-2) ligands, which are located on opposite cells. Upon interaction the ligand undergoes endocytosis, taking with it the extracellular part of the Notch receptor. This opens the negative regulatory region (NRR), exposing a cleavage site located within Notch, making it accessible for A Disintegrin And Metalloprotease domain (ADAM) proteases, which cleaves the receptor, releasing the Notch extracellular domain (S2 cleavage). Following S2 cleavage, the receptor undergoes S3 cleavage by γ-secretase, in turn liberating the Notch intracellular domain (NICD). The NICD translocates to the nucleus of the receiver cell and initiates target gene transcription with the transcription factor CBF-1/Suppressor of hairless/LAG-1 (CSL) and the coactivator Mastermind-like protein (MAML). All key Notch components are well conserved within mammalians as well as invertebrate models such as *Drosophila* and *C. elegans*, making them valuable model organisms to study Notch signaling *in vivo*.

In *C. elegans*, there are two Notch ligands (LAG-2 and APX-1) as well as two Notch receptors (GLP-1 and LIN-12), playing diverse roles in a number of tissues. In the germline, Notch is initiated by LAG-2, which is expressed on the DTC, interacting with GLP-1 which is expressed in the germline (reviewed by [60]). Activation of GLP-1 promotes meiotic entry while simultaneously blocking mitotic self-renewal. Failure to activate GLP-1 results in smaller germlines with few to no offspring, making it an essential process for nematode reproduction.

Other cells in the nematode where Notch plays highly conserved roles are the vulval precursor cells (VPCs) (reviewed by [61]). In the early nematode, VPC specification is essential for proper vulval development, with three different fates (1° - 3°) possible. These fates follow a set pattern, controlled by Ras-mediated inductive signaling mediated from the anchor cell (AC) and Notch-mediated lateral signaling. In this scenario, LIN-12 acts as the Notch ligand,

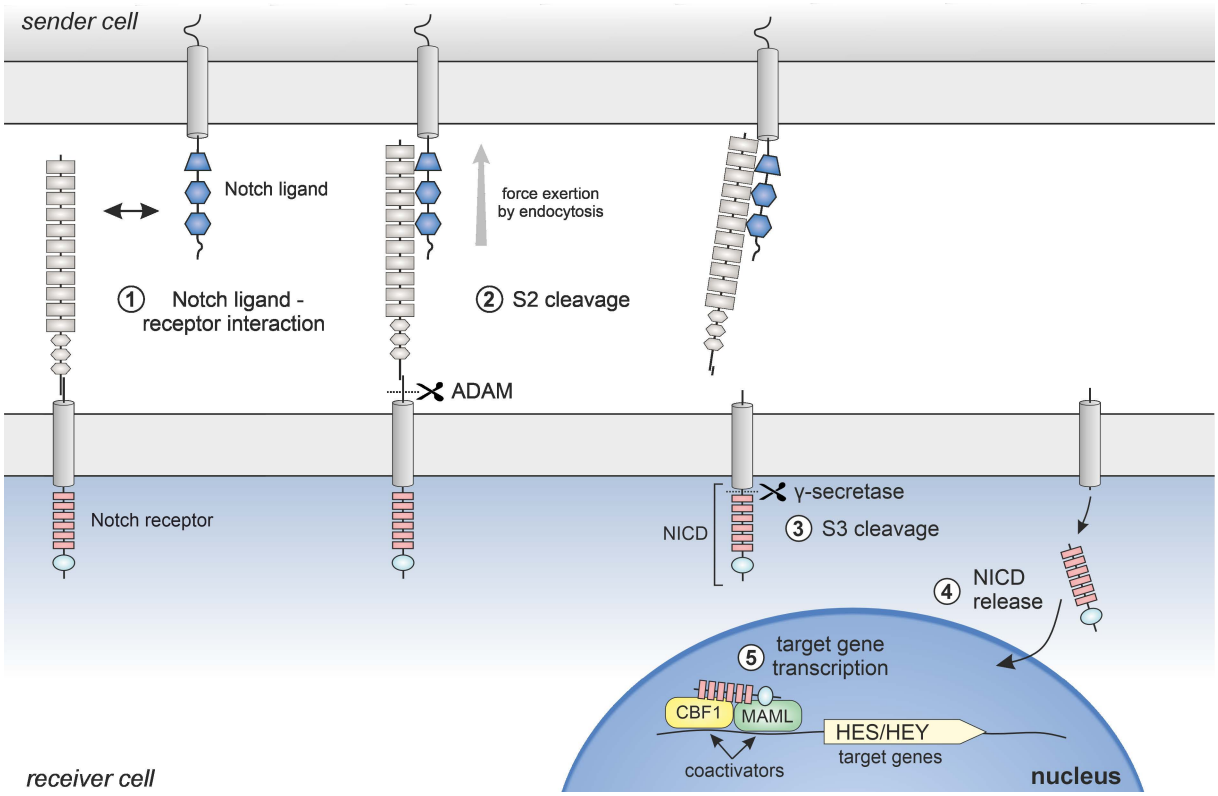


Figure 5: Core Notch signaling pathway. Notch ligand and receptor interact (1), exposing a cleavage site allowing for cleavage by ADAM (2). This in turn allows for intracellular cleavage by γ-secretase (3), releasing the NICD as a soluble fraction (4). The NICD locates to the nucleus and, together with coactivators, induces target gene transcription (5).

expressed on cells that eventually specify the 2° fate. Nematodes that fail proper VPC specification can be vulvaless or display multiple vulvas.

Additionally, Notch plays various roles throughout *C. elegans* embryogenesis (reviewed by [62]). One example is pharyngeal development, which depends on two separate occasions where Notch is induced, once in the four-cell stage embryo and later in 12-cell stage. Contrary to the gonad, APX-1 is considered the dominant ligand in this tissue. The two interactions are critical to define which AB descendants will become pharyngeal cells. Following these two interactions, a third interaction is necessary to form the symmetrical nematode head. Failure to induce this interaction is causative for a so-called twisted nose phenotype. Interestingly, this interaction is again dependent on LAG-2 as ligand. Lastly, a fourth interaction specifies the development of the excretory cell.

These various examples highlight both the conservation and the widespread involvement of Notch signaling within *C. elegans* development.

1.2.4 The *C. elegans* ADGRL homolog LAT-1 is essential for several physiological functions

All three adhesion GPCRs in *C. elegans* contain the canonical 7TM and GAIN domain as well as Hormone Binding Domain (HormR, HBD, HRM) (**Figure 6a**). Upstream of these domains, the composition varies, with the latrophilin homologs containing the Rhamnose Binding Lectin (RBL) domain, and LAT-2 additionally containing a C-type Lectin. FMI-1 has a large NTF consisting of multiple cadherin, laminin type G and epidermal growth factor-like (EGF) domain.

LAT-1 has been studied thoroughly in the past and has been implicated in a myriad of nematode functions, which revolve around two major phenotypes in null-mutants, requiring different kinds of receptor architecture to be ameliorated.

Cis-dependent receptor functionality

Previous research showed that the null mutant *lat-1(ok1465)* (hereafter referred to as *lat-1* mutant) shows severe embryonic and larval arrest, due to disturbed cell division planes in the early embryo [16]. From this global phenotype, it was delineated that LAT-1 is responsible for alignment of division axes in the early embryo. Later research showed that these defects are dependent of cAMP increase, hence, signals via G_s which was shown using Forskolin stimulation as well as by activating the receptor using peptides encoding the TA [26].

N terminus-only functions

A second observed phenotype is a reduction in the amount of produced embryos, reducing from ~228 eggs in wild-type nematodes to ~117 in *lat-1* mutants [17] (**Figure 6b**). Strikingly, this phenotype can be ameliorated back to wild-type levels by solely expressing a membrane-tethered NTF, indicating that, contrary to the polarity defect described above, this loss of fertility is due to distinctly different receptor functions, where G protein signaling is irrelevant, yet the receptor needs to be membrane tethered. Additionally, GAIN and RBL domain are deemed essential. These findings indicate an N terminus-only function of LAT-1, establishing brood size in *C. elegans*. Fascinatingly, enforcing N terminus-only functions by

truncating the receptor, effectively removing six of seven TM's, still retains significant receptor functionality, ameliorating observed fertility defects. However, the exact way in which fertility is affected by N terminus-only functions is still unknown. Resolving these molecular details would greatly advance our knowledge of the diversity of endogenous aGPCR functionality.

Additionally, several minor functions have been identified. The involvement of LAT-1 in the copulation machinery of the male nematode has been shown [63]. In *lat-1* mutants, several morphological changes in neurons have been observed, and copulation efficiency is severely reduced. This furthermore emphasizes the diversity of biological processes that involve LAT-1, as well as the wider involvement of N terminus-only functions in receptor activity.

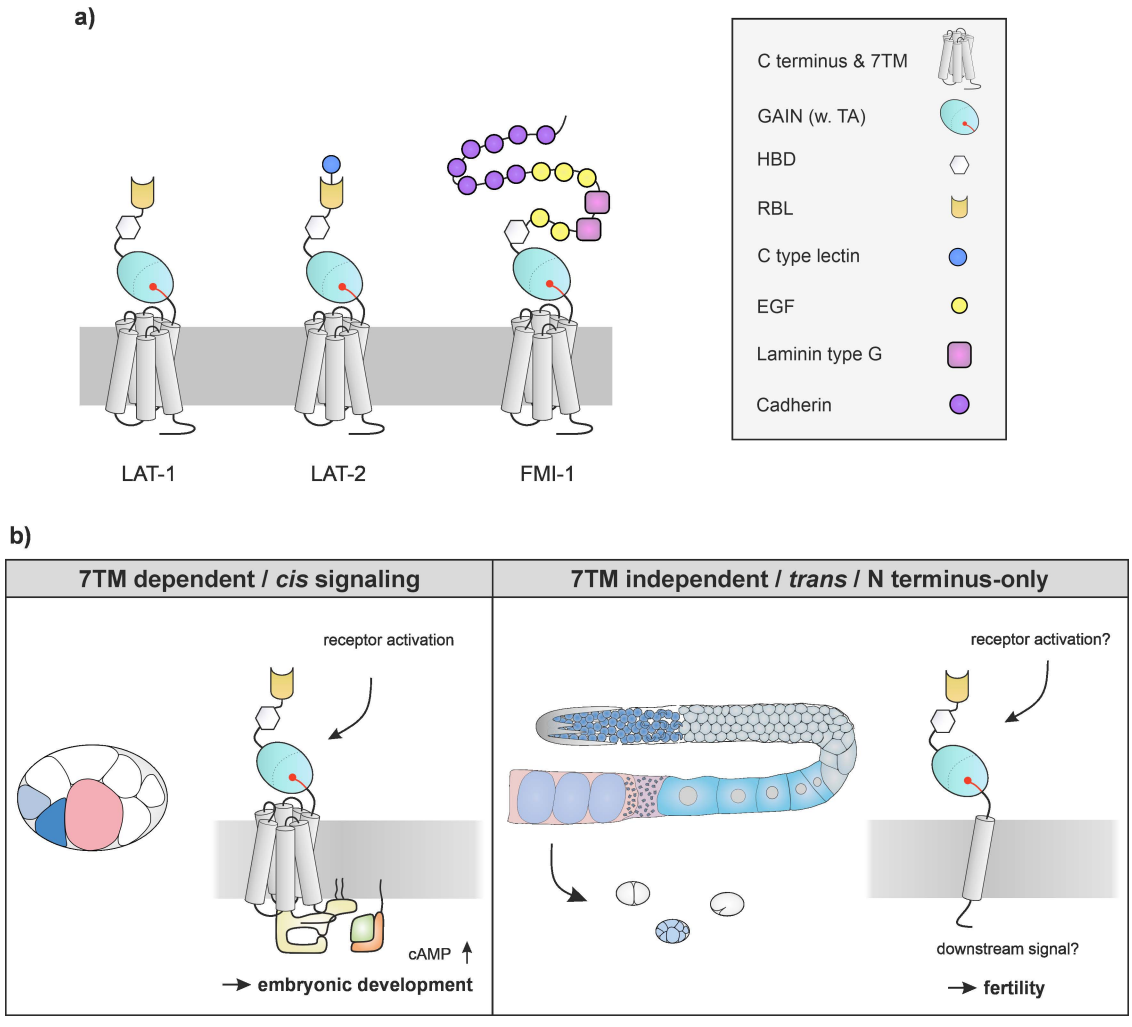


Figure 6: aGPCR homologs in *C. elegans*. a) *C. elegans* has three conserved aGPCR homologs, LAT-1, LAT-2 (ADGRL/LPHNs) and FMI-1 (ADGRC/CELSR). b) LAT-1 has two distinct functions, defined as 7TM / *cis* signaling and 7TM independent / *trans* / N terminus-only function. *Cis* signaling plays a dominant role in cell polarity in the developing embryo whereas N terminus-only functions have a major effect on the establishment of brood size. However, it's exact mode of action is unknown

1.2.5 LAT-2 remains poorly characterized

Contrary to LAT-1, *lat-2* loss-of-function mutants are superficially phenotypically wild-typical and therefore its functions remain largely unknown [16,64,65]. Expression analyses showed that *lat-2* expression is mostly confined to the pharynx as well as the excretory cell [16]. A partial overlap in functionality with LAT-1 has however, been shown, with double *lat-1, lat-2* mutants displaying increased lethality [16]. Additionally, the GPS of LAT-2 is able to restore fertility defects of LAT-1, however, not the tissue polarity defect in embryonic development [17]. To date, distinct phenotypes are still lacking. By finding LAT-2 specific phenotypes, a valuable contribution could be provided in providing a broader understanding of the diversity of aGPCR signaling.

In summary, previous research on LAT-1 has shown that the receptor is able to perform a variety of functions, either in *cis*, or as N terminus-only function. The latter is poorly understood, but due to distinct phenotypes, *C. elegans* allows us to study N terminus-only function in great detail. Additionally, due to its conservation, LAT-1 acts as a prototypical receptor for studying N terminus-only functions in aGPCRs. Therefore, delineating how LAT-1 can integrate this large variety of signaling capacities would give valuable insights in aGPCR functioning. Additionally, LAT-2 has been shown as enigmatic receptor, with no clearly defined function. Pinpointing processes in which LAT-2 can play a role would aid in generating a clearer understanding of the broad functionality that aGPCRs can exhibit.

2 Aims of this thesis

Adhesion GPCRs are essential molecules in cellular contexts with highly varied functions in physiology, being able to mediate a plethora of signals in a variety of environments. This wide involvement makes them promising drug targets. Both 7TM-dependent and -independent functions show the complexity at which these receptors function, yet particularly the *trans*/7TM-independent/N terminus-only function remains poorly understood, with limited knowledge on mechanistics, interaction partners and affected pathways. These limitations preclude utilizing aGPCRs as drug targets.

As mentioned, N terminus-only functions substantially broaden the functional repertoire of aGPCRs, potentially involving interactions on opposing cells or the extracellular matrix that necessitate the use of an *in vivo* model for accurate characterization. Additionally, in order to understand the signaling behind N terminus-only functions, a detailed knowledge in the processes in which these functions are involved is crucial. Therefore, in this thesis, *C. elegans* is utilized as a model organism. Previously, the N terminus-only function of LAT-1 has been characterized as an essential modulator of brood size, therefore providing an ideal starting point for further characterization of this highly unusual and enigmatic mode of aGPCR functioning.

In **chapter 3**, the N terminus-only function will be dissected in detail, providing high resolution insight in expression pattern and functional diversity of the receptor throughout the *C. elegans* gonad. This will provide valuable entry points and cellular context on which follow-up research can be conducted on signaling and mechanistics.

The knowledge acquired in **chapter 3** will be utilized as a starting point for **chapter 4**. To come to a more complete understanding of aGPCR function, specifically their N terminus-only function, it is essential to understand how they can be integrated into various pathways and molecular networks. In this subsequent chapter, the mechanistic basis of N terminus-only functions will be examined, with a focus on identifying the molecular interactions and clarifying how aGPCRs are integrated in signaling cascades.

For comprehensive understanding of aGPCR signaling, it is essential to understand the functional diversity of this receptor family. In this context, the limited knowledge on signaling, and physiological roles of LAT-2 presents a large research gap. In **chapter 5**, functions of LAT-2 in *C. elegans* will be investigated, expanding our knowledge of ADGRL functioning in various contexts, thereby providing a foundation to understand signaling of LAT-2 in more detail.

Summarized, the various chapters presented in this thesis will aid significantly in our understanding of the functional diversity of aGPCRs and their integration in various cellular processes. Additionally, the signaling cascades that are affected by N terminus-only functions will be addressed, providing a deeper understanding in how aGPCR can affect a plethora of cellular functions and probing into their potential as pharmaceutical targets.

3 The N terminus-only (*trans*) function of the Adhesion GPCR Latrophilin-1 controls multiple processes in reproduction of *C. elegans*

Authors: Daniel Matúš[#], Willem Berend Post[#], Victoria Elisabeth Groß, Alexander Bernd Knierim, Christina Katharina Kuhn, Franziska Fiedler, Darian Benno Tietgen, Johanna Lena Schön, Torsten Schöneberg and Simone Prömel

[#]These authors contributed equally to this work

Journal: G3 Genes | Genomes | Genetics

Publisher: Oxford Academic

Impact Factor: 2.2

Submitted: 24 July 2024

Accepted: 16 August 2024

Published: 07 September 2024

Keywords: Adhesion GPCR, Latrophilin, *trans* function, germ cells, sperm guidance, ovulation, apoptosis

DOI: 10.1093/g3journal/jkae206, previously online as pre-print on BioRxiv (DOI: 10.1101/2023.02.18.529090)

PubMed ID: 39243387

G3, 2024, **14(11)**, jkae206
https://doi.org/10.1093/g3journal/jkae206
Advance Access Publication Date: 7 September 2024
Investigation

The N terminus-only (*trans*) function of the adhesion G protein-coupled receptor latrophilin-1 controls multiple processes in reproduction of *Caenorhabditis elegans*

Daniel Matúš,[1,2,†] Willem Berend Post,[3,†] Victoria Elisabeth Groß ,[3] Alexander Bernd Knierim,[1,4] Christina Katharina Kuhn,[1,5] Franziska Fiedler,[1] Darian Benno Tietgen,[3] Johanna Lena Schön,[1,6] Torsten Schöneberg,[1,7] Simone Prömel [3,*]

[1]Medical Faculty, Rudolf Schönheimer Institute of Biochemistry, Leipzig University, 04103 Leipzig, Germany
[2]Department of Molecular and Cellular Physiology, Stanford University, Stanford, CA 94305, USA
[3]Department of Biology, Institute of Cell Biology, Heinrich Heine University Düsseldorf, 40225 Düsseldorf, Germany
[4]IFB Adiposity Diseases, Leipzig University Medical Center, 04103 Leipzig, Germany
[5]Department of Diagnostics, Fraunhofer Institute for Cell Therapy and Immunology (IZI), 04103 Leipzig, Germany
[6]Department of Dermatology, Venereology and Allergology, Leipzig University Medical Center, Leipzig University, 04103 Leipzig, Germany
[7]School of Medicine, University of Global Health Equity, Kigali 6955, Rwanda

*Corresponding author: Department of Biology, Institute of Cell Biology, Heinrich Heine University Düsseldorf, Universitätsstr. 1, 40225 Düsseldorf, Germany.
Email: proemel@uni-duesseldorf.de
[†]These authors contributed equally to this work.

Adhesion G protein-coupled receptors are unique molecules. They are able to transmit classical signals via G protein activation as well as mediate functions solely through their extracellular N termini, completely independently of the seven transmembrane helices domain and the C terminus. This dual mode of action is highly unusual for G protein-coupled receptors and allows for a plethora of possible cellular consequences. However, the physiological implications and molecular details of this N terminus-mediated signaling are poorly understood. Here, we show that several distinct seven transmembrane helices domain-independent/*trans* functions of the adhesion G protein-coupled receptor latrophilin homolog latrophilin-1 in the nematode *Caenorhabditis elegans* together regulate reproduction: sperm guidance, ovulation, and germ cell apoptosis. In these contexts, the receptor elicits its functions in a noncell autonomous manner. The functions might be realized through alternative splicing of the receptor specifically generating N terminus-only variants. Thus, our findings shed light on the versatility of seven transmembrane helices domain-independent/N terminus-only/*trans* functions of adhesion G protein-coupled receptor and discuss possible molecular details.

Keywords: adhesion GPCR; latrophilin; *trans* function; germ cells; sperm guidance; ovulation; apoptosis

Introduction

Cellular communication mediated by G protein-coupled receptors (GPCR) typically involves the transduction of extracellular signals into a cell, primarily realized through intracellular activation of G proteins via the receptor's seven transmembrane helices domain (7TM). This concept has also been confirmed for most members of the class of adhesion GPCR (aGPCR) (Bohnekamp and Schöneberg 2011; Gupte *et al.* 2012). Like other GPCR, these receptors play essential roles in various physiological and pathophysiological processes (summarized in Hamann *et al.* 2015; Rosa *et al.* 2021; Einspahr and Tilley 2022). However, they harbor structural features that distinguish them as a separate class within the GPCR superfamily (summarized in Hamann *et al.* 2015; Liebscher *et al.* 2022; Seufert *et al.* 2023). One of these features is their extraordinarily long extracellular N terminus comprising various domains. This structure enables the receptors to mediate signals and participate in cell–cell or cell–matrix adhesion (summarized in Hamann *et al.* 2015).

Remarkably and in contrast to other GPCR, members of the class of aGPCR are capable of transmitting functions solely via these complex N termini, indicating noncanonical signaling mechanisms completely independent of their 7TM and C terminus (N terminus-only/7TM-independent/*trans* function). This intriguing mode of function is in stark contrast to the canonical 7TM-dependent/*cis* signaling employed by all GPCR, which requires the entire receptor molecule and is limited to transmitting signals into the cell the receptor is expressed on. Conversely, 7TM-independent/*trans* functions have the potential to affect adjacent cells (potentially noncell autonomously) by mediating adhesion or even activation of other surface receptors. This dual mode of action is highly uncommon for GPCR. Our work and that of others suggest that several aGPCR, such as latrophilins/LPHN/ADGRL (Prömel *et al.* 2012; Matus *et al.* 2022), BAI1/ADGRB1 (Tu *et al.* 2018), GPR126/ADGRG6 (Patra *et al.* 2013), and CD97/ADGRE5 (Ward *et al.* 2018), harbor the ability to act in such bidirectional manner, with evidence for more (Okajima *et al.* 2010; Steimel *et al.* 2010; Patat *et al.* 2016). These cases imply

Received on 24 July 2024; accepted on 16 August 2024
© The Author(s) 2024. Published by Oxford University Press on behalf of The Genetics Society of America.
This is an Open Access article distributed under the terms of the Creative Commons Attribution License (https://creativecommons.org/licenses/by/4.0/), which permits unrestricted reuse, distribution, and reproduction in any medium, provided the original work is properly cited.

Downloaded from https://academic.oup.com/g3journal/article/14/11/jkae206/7750701 by Universitaets- und Landesbibliothek Duesseldorf user on 04 May 2026

that the unique dual mode of function is a common feature of this receptor class, and data from several studies indicate that the sole N terminus independent of the 7TM and C terminus is always sufficient to mediate effects (Prömel et al. 2012; Patra et al. 2013; Tu et al. 2018; Ward et al. 2018; Matus et al. 2022). However, while evidence for the existence of N terminus-only/7TM-independent/*trans* functions is growing and models of their possible cellular consequences are beginning to take shape, essential questions regarding the molecular framework of this concept remain unanswered. For instance, while it was observed that this mode of function affects cells surrounding the aGPCR-expressing cells, it is not shown whether the receptor is activating signaling cascades in these cells or whether its noncell autonomous effect is mediated, for example, via adhesion. Furthermore, it is unclear whether the whole receptor molecule is intact at all times or whether the N terminus could be released or produced independently of the C-terminal parts to mediate its function. Autocatalytic cleavage at the G protein-coupled receptor proteolysis site (GPS) (Lin et al. 2004) yielding an N-terminal fragment and a C-terminal fragment occurs in many aGPCR and might offer a possible mechanism for realizing the N terminus-only/7TM-independent/*trans* function. However, our previous work showed that this cleavage is not absolutely vital for the 7TM-independent receptor mode of latrophilin-1 (LAT-1), a latrophilin homolog in the nematode *Caenorhabditis elegans* (Prömel et al. 2012), thus indicating that other mechanisms exist. More attempts to understand the mechanistic details of the N terminus-only/7TM-independent/*trans* aGPCR functions have been made in vitro and ex vivo (Okajima et al. 2010; Tu et al. 2018; Ward et al. 2018). However, these systems are not too well equipped to address the noncell autonomous roles of aGPCR, how they act in diverse multicellular settings, and how they are connected to and integrated with the classical G protein-mediated receptor functions. In vivo studies are more suitable to grasp the integration of the classical G protein-mediated and the 7TM-independent function and their physiological consequences.

Here, we provide evidence that the N terminus-only/7TM-independent/*trans* function of the aGPCR LAT-1 in *C. elegans* is vitally involved in a wide spectrum of physiological processes within the nematode. Previous studies have shown that the receptor controls anterior–posterior cell division plane orientation in the early *C. elegans* embryo (Langenhan et al. 2009) via *cis* signaling (Prömel et al. 2012) through a Gs protein cascade (Müller et al. 2015). Furthermore, an N terminus-only/7TM-independent/*trans* function has been described in neuron morphogenesis (Matus et al. 2022) and in reproduction (Prömel et al. 2012). In the current study, we show that LAT-1 regulates sperm guidance, ovulation, germline apoptosis, and potentially the quality of germ cells. All these functions together cumulate in contributing to reproduction and brood size control. At first glance, *lat-1* expression in both the affected germ cells and the surrounding somatic cells of the gonad does not necessarily imply a noncell autonomous mechanism. However, we show that sole *lat-1* expression in the cells of the somatic gonad is sufficient for many of its functions in the reproductive system. Additionally, we discuss the possibility of realizing isolated *trans* functions through alternative splicing of the receptor specifically generating N terminus-only variants.

Materials and methods

Materials and reagents

All standard chemicals were from Sigma-Aldrich, Thermo Fisher Scientific, or Carl Roth unless stated otherwise. All enzymes were obtained from New England Biolabs.

Caenorhabditis elegans maintenance and strains

C. elegans strains were maintained according to standard protocols (Brenner 1974) on *Escherichia coli* OP50 at 22°C unless stated otherwise. Strains carrying *nIs13 [pie-1p::vab-1::GFP + unc-119(+)]; ltIs44 [pie-1p::mCherry::PH(PLC1delta1) + unc-119(+)]* were kept at 25°C.

Wild-type worms were *C. elegans* var. Bristol strain N2 (Brenner 1974). The following alleles were obtained from the *Caenorhabditis* Genetics Center (CGC), which is funded by the NIH Office of Research Infrastructure Programs (P40 OD010440): *lat-1(ok1465)* (generated by the *C. elegans* gene knockout consortium), *qIs153[lag-2p::MYR::GFP; ttx-3p::DsRed]* (Byrd et al. 2014), *nIs13[pie-1p::vab-1::GFP; unc-119(+)]*; *ltIs44[pie-1p::mCherry::PH(PLC1delta1); unc-119(+)]* (Cheng et al. 2008), *tnIs6[lim-7p::GFP; rol-6(su1006)]* (Hall et al. 1999), and *bcIs39[lim-7p::ced-1::GFP; lin-15(+)]* (Zhou et al. 2001). The following strains containing extrachromosomal or integrated arrays were generated in this study: *lat-1(ok1465) aprEx192[pTL20; myo-2::mCherry; pBSK]*, *lat-1(ok1465) aprEx193[pJL13; myo-2p::mCherry; pBSK]*, *lat-1(ok1465) aprEx194[pJL14; myo-2::mCherry; pBSK]*, *lat-1(ok1465) aprEx216[pDM3; myo-2::mCherry; pBSK]*. Strains *lat-1(knu846[lat-1 KO/KI mCherry intronic loxP::hygR::loxP])* [NemaMetrix Inc. (Eugene, OR, USA)] and *lat-1(apr1[lat-1(1-581)::GFP^{hygR}])* were generated using CRISPR/Cas9 genome editing. The following combinations of transgenes/alleles were obtained using standard genetic techniques (Brenner 1974): *lat-1(knu846 [lat-1 KO/KI mCherry intronic loxP::hygR::loxP])*; *tnIs6[lim-7p::GFP; rol-6(su1006)]*, *lat-1(knu846[lat-1 KO/KI mCherry intronic loxP::hygR::loxP])*; *qIs153[lag-2p::myr::GFP; ttx-3p::DsRed]*, *lat-1(ok1465)*; *nIs13[pie-1p::vab-1::GFP; unc-119(+)]*; *ltIs44[pie-1p::mCherry::PH(PLC1delta1)*; *unc-119(+)]*, *lat-1(ok1465)*; *nIs13[pie-1p::vab-1::GFP; unc-119(+)]*; *ltIs44[pie-1p::mCherry::PH(PLC1delta1)*; *unc-119(+)]; aprEx192[pTL20 myo-2::mCherry pBSK]*, and *bcIs39[lim-7p::ced-1::GFP; lin-15(+)]; lat-1(ok1465)*.

Generation of transgenic *C. elegans* lines

All transgenic strains with stably transmitting extrachromosomal arrays were generated using DNA microinjection. Plasmids were injected at a concentration of 1 ng/µl together with the coinjection marker, a modified pPD118.33 containing *myo-2p::mCherry* (kind gift of Ralf Schnabel (Technical University Braunschweig, Germany) (30 ng/µl), and pBluescript II SK + vector DNA (Stratagene) as stuffer DNA to achieve a final concentration of 120 ng/µl. DNA was injected into the syncytial gonad of hermaphrodites. Transgenic progeny were isolated, and stable lines were selected. Multiple independent transgenic lines were established for each transgene tested.

For the CRISPR/Cas9-mediated genetic modifications, the injection cocktail consisted of *Peft-3::cas9-SV40_NLS::tbb-2 3′UTR*, respective sgRNA plasmids, a respective repair template plasmid (injected at 50 ng/µl each), pCFJ104 (5 ng/µl), pCFJ90 (2.5 ng/µl), and pMA122 (10 ng/µl). pCFJ104, pCFJ90, and pMA122 were kind gifts from Erik Jorgensen (Addgene plasmids #19328, #19327, and #34873, respectively. The Cas9 expression plasmid was a kind gift from John Calarco (Addgene plasmid #46168). Correctly modified worms were selected based on hygromycin resistance after heat shock.

Brood size and lethality assay

Hermaphrodite L4 larvae were individually placed on NGM plates containing *E. coli* OP50 to lay eggs at 22°C and transferred onto a fresh plate every 24 h. Each day, progeny was counted until egg laying ceased. For the lethality assay, offspring were incubated at 22°C and the number of adult/L4 animals was scored 48 h after the mother was removed. Sterile and semi-sterile (< 25 eggs) mothers were excluded from the assay.

Downloaded from https://academic.oup.com/g3journal/article/14/11/jkae206/7750701 by Universitaets- und Landesbibliothek Duesseldorf user on 04 May 2026

Larval development assay

To assess the time of development, ~800 synchronized wild-type and *lat-1* L1 larvae were placed on *E. coli* OP50-seeded NGM plates and incubated at 22°C. After 8, 16, 24, 36, and 48 h, the number of larvae in different developmental stages (L1, L2, L3, L4, and adult) was scored.

Ovulation rate assay

Ovulation rates were determined in hermaphrodites 24 and 96 h post-L4, respectively. Hermaphrodites were placed separately on *E. coli* OP50-seeded NGM plates, and eggs and oocytes inside the uterus were counted. After 4 h at 22°C, eggs/oocytes on the plate and inside the uterus of the mother were counted. The ovulation rate per gonad was calculated as ([eggs + oocytes in and out of uterus after 4 h] – [initial eggs + oocytes inside uterus])/(2 × 4 h).

MitoTracker Red staining

To assess sperm movement in vivo, sperm was labeled using MitoTracker Red (Kubagawa *et al.* 2006). L4 males were kept isolated overnight to ensure sperm accumulation. The following day, young adult males were stained with 10 µM MitoTracker Red CM-H2XRos (Thermo Fisher) in M9 for 2 h in the dark at room temperature and then left overnight to recover on plates seeded with *E. coli* OP50. The next day, 25 stained males and 25 young adult hermaphrodites, which were first anesthetized using 300 µM levamisole (AppliChem), were mated on a 5-µl spot of overnight grown *E. coli* OP50. Copulation was monitored. Successfully inseminated hermaphrodites (indicated by transfer of fluorescent sperm into the uterus) were transferred separately into the wells of a 72-well plate containing 1.5 mM levamisole. Thereafter, hermaphrodites were mounted on 2% agarose pads and microscopy was conducted 1 h postinsemination. The resulting stack images of MitoTracker Red-stained sperm in the hermaphrodite uterus were evaluated as average intensity Z-projections. Correct localization of sperm was defined as proximal of the first egg next to the spermatheca, including all sperm around this egg. The percentage of correctly localized sperm was calculated as (mean fluorescence intensity of correctly localized sperm/mean fluorescence intensity of all sperm inside uterus).

Sperm activation assay

Sperm activation was studied as previously described (Hammerquist *et al.* 2021) with minor modifications. L4 male nematodes were placed on separate NGM plates with *E. coli* OP50 and kept isolated to avoid premature sperm activation. The following day, nematodes were dissected in Sperm Medium buffer containing BSA and treated with 200 ng/µL pronase (Sigma) for 15 min. Following stimulation, differential interference contrast (DIC) microscopy was conducted within 5 min and sperm was scored as activated (with full pseudopod) or not activated (spherical, lobed, and spiked). At least 100 spermatids were scored per replicate.

SYTO staining

Adult hermaphrodites (24 h post-L4) were washed off NGM plates with NGM lacking phosphate buffer and incubated overnight in the dark at room temperature with 33 µM SYTO 12 green fluorescent nucleic acid stain (Thermo Fisher) in NGM and a small amount of *E. coli* OP50. To remove the stained bacteria, worms were washed 3 times with NGM and transferred to NGM plates with fresh *E. coli* OP50 for 1 h. Subsequently, stained worms were anesthetized with 300 µM levamisole (AppliChem) in M9 and mounted on 2% agarose pads for microscopy.

CED-1::GFP imaging

Adult *bcIs39[lim-7p::ced-1::GFP; lin-15(+)]* and *bcIs39[lim-7p::ced-1::GFP; lin-15(+)]; lat-1(ok1465)* hermaphrodites were anesthetized with 300 µM levamisole (AppliChem) in M9 and mounted on 2% agarose pads for microscopy. CED-1::GFP was scored per gonad.

Antibody and DAPI staining

Antibody and DAPI stainings were performed on extruded germlines. For this purpose, germlines of precisely synchronized hermaphrodites were dissected, fixed, and stained as previously described (Francis *et al.* 1995; Jones *et al.* 1996). Adult hermaphrodites (24 h post-L4) were transferred into 300 µM levamisole (AppliChem) in 0.1% Tween in PBS (PBST) for immobilization, and gonad arms were exposed by cutting off the heads/tails with a scalpel blade. Gonads were either fixed in 4% formaldehyde/PBST solution for 15 min (DAPI only) or 10 min (antibody staining). After washing with PBST, the specimens were postfixed in 100% ice-cold methanol at -20°C for 5 min (DAPI only).

To boost the expression signals of genome-edited *LNT::GFP* (strain *lat-1(apr1[lat-1(1-581)::GFP^{hygR}])*), antibody staining was performed following permeabilization in PBST + 0.1% Triton X-100 for 30 min and blocking with PBST + 1% BSA for 1 h at room temperature. Samples were subsequently incubated in rabbit anti-GFP antibody (Invitrogen, G10362) (1:100 in PBST + 1% BSA) overnight at 4°C. Goat anti-rabbit StarRED (Aberrior, 1:500 in PBST + 1% BSA with 1 ng/µl DAPI) (for overview gonad and spermatheca stainings) or goat anti-rabbit Alexa 568 (Invitrogen, 1:1,000 in PBST + 1% BSA with 1 ng/µl DAPI) [for distal tip cell (DTC) and gonadal sheath cell stainings] were used as secondary antibodies for 1 h at room temperature. After three brief wash steps in PBST, the gonads were mounted on 2% agarose pads in Fluoromount-G (Thermo Fisher) for microscopy. To stain gonads exclusively with DAPI, formaldehyde/methanol-fixed gonads were incubated for 2 h at 4°C in the dark with 1 ng/µl DAPI. Gonads were washed 3 times with M9 and mounted as described above. Because of the faint mCherry expression of *lat-1(knu846 [lat-1 KO/KI mCherry intronic loxP::hygR::loxP])*, strains carrying this marker were not fixed and gonads were mounted in their native form for microscopy.

Microscopy

All specimens were imaged using confocal imaging techniques. DIC and fluorescence imaging were performed using a Leica SP8 microscope and an Olympus FluoView FV1000 microscope. Z-stacks were taken with a spacing of 0.5–2 µm, depending on the specimen (2 µm for whole worms, 0.5–1 µm for germlines, and 0.5 µm for sperm). Microscopic images were evaluated using Fiji (Schindelin *et al.* 2012) and ImageJ (Schneider *et al.* 2012).

Oocyte size and area measurements

To asses oocyte size, strains of different genotypes expressing *tnIs13[pie-1p::vab-1::GFP; unc-119(+)], ltIs44[pie-1p::mCherry::PH(PLC1delta1); unc-119(+)]* containing a cell membrane as well as a cytoplasmic marker were utilized. Worms were grown at 25°C to induce marker expression, anesthetized at young adult stage with 300 µM levamisole (AppliChem) in M9, and mounted on 2% agarose pads for microscopy. Stack images of oocytes were acquired with stack borders set on the last visible part of oocyte membrane, visualized by mCherry fluorescence. Every 2 adjacent images were used to reconstruct part of the oocyte modeled as a truncated pyramid with the volume $V = 1/3 \times$ (slice spacing) $\times [A1 + A2 + \mathrm{sqrt}(A1 \times A2)]$, with $A1$ and $A2$ being the

Downloaded from https://academic.oup.com/g3journal/article/14/11/jkae206/7750701 by Universitaets- und Landesbibliothek Duesseldorf user on 04 May 2026

area enclosed by the oocyte membrane in both respective images. The full oocyte volume was determined by summing the volumes of all truncated pyramids.

For determining oocyte area, oocytes of L4 + 1-day-old hermaphrodites were anesthetized using 300 µM levamisole (AppliChem) in M9 and mounted on 2% agarose pads. Images of the middle section of an oocyte were taken using a microscope with DIC, and the area was measured using Fiji (Schindelin *et al.* 2012).

Generation of transgenes

To obtain the constructs used in this study, recombineering was conducted. Existing protocols (Dolphin and Hope 2006; Tursun *et al.* 2009) were modified as previously described (Langenhan *et al.* 2009; Prömel *et al.* 2012) to generate LAT-1 transgenes using cosmids, PCR-amplified targeting cassettes, and positive antibiotic selection. All transgenes are based on a construct comprising the genomic locus of *lat-1* containing *lat-1p::lat-1(1-581)::GFP* (pTL20) (Prömel *et al.* 2012). To replace the promoter with tissue-specific promoters, a recombineering targeting cassette consisting of two parts, a spectinomycin selection cassette and the promoter sequence, was generated. For generating CRISPR/Cas9-based integrations, a plasmid-based approach was used as described previously (Chen *et al.* 2013; Dickinson *et al.* 2013; Friedland *et al.* 2013). For primer sequences, see Supplementary Table 1 in Supplementary File 1.

lag-2p::lat-1(1-581)::GFP (lag-2p::LNT::GFP, pJL13)

A 2-kb promoter region of *lag-2* was amplified with primers lat1_1088F/lat1_1089R from genomic DNA of a mixed population of N2 and ligated into vector pCR2.1 using the TOPO TA Cloning Kit (Thermo Fisher). From this vector, the promoter was again amplified with primers lat1_1090F/lat1_1091R with the forward primer introducing a *PstI* site and the reverse primer containing an overhang with a homology to the vector pTL20. In parallel, the spectinomycin resistance gene was amplified from the Gateway cloning vector backbone pDON223 (Invitrogen) with primers lat1_1080F (introducing an overhang with a homology to pTL20) and lat1_1081R (containing a *PstI* site). Both fragments were digested by *PstI* and ligated together using a T4 DNA ligase. The ligated cassette was subsequently recombineered into pTL20 (*lat-1p::lat-1(1-581)::GFP*) replacing the *lat-1* promoter using electrocompetent *E. coli* SW105 cells with a heat-induced recombinase of the λ-Red recombinase system (Warming *et al.* 2005).

plc-1p::lat-1(1-581)::GFP (plc-1p::LNT::GFP, pJL14)

The promoter region of *plc-1* (2 kb) was obtained by amplification from genomic DNA of a mixed N2 population using primers lat1_1084F/lat1_1085R. Following ligation into vector pCR2.1 using the TOPO TA Cloning Kit (Thermo Fisher), the promoter was amplified with primers lat1_1086F/lat1_1087R. While the forward primer introduced a *PstI* site, the reverse primer contained an overhang with a homology to the vector pTL20. In parallel, the sequence of the spectinomycin resistance gene was amplified from the Gateway cloning vector backbone pDON223 (Invitrogen) with primers lat1_1080F (containing an overhang with a homology to pTL20) and lat1_1081R (introducing a *PstI* site). Both fragments were digested by *PstI* and ligated with a T4 DNA ligase, and the resulting fragment was recombineered into pTL20 (*lat-1p::lat-1(1-581)::GFP*) replacing the *lat-1* promoter using electrocompetent *E. coli* SW105 cells with heat-induced recombinase of the λ-Red recombinase system (Warming *et al.* 2005).

lim-7p::lat-1(1-581)::GFP (lim-7p::LNT::GFP, pDM3)

The promoter region of *lim-7* (2 kb) was retrieved by PCR with primers lat1_1082F (containing a *PstI* site) and lat1_1083R (harboring a homology sequence to pTL20) from vector pOH323, which was a kind gift from Oliver Hobert (Columbia University, New York, NY, USA) (Hall *et al.* 1999). In parallel, primers lat1_1080F (containing an overhang with homologies to pTL20) and lat1_1081R (introducing a *PstI* site) were used to amplify the spectinomycin resistance gene from the Gateway cloning vector pDON223 (Invitrogen). Both PCR products were digested with *PstI* (NEB) and ligated using a T4 DNA ligase. The resulting fragment was recombineered into pTL20 (*lat-1p::lat-1(1-581)::GFP*) replacing the *lat-1* promoter using electrocompetent *E. coli* SW105 cells with heat-induced recombinase of the λ-Red recombinase system (Warming *et al.* 2005).

Repair template for *lat-1(1-581)::GFP*^{HygR} *(LNT::GFP*, pSP231)

A 1.5-kb fragment of *lat-1(1-581)* fused to GFP was amplified from pTL20 (*lat-1p::lat-1(1-581)::GFP*) (Langenhan *et al.* 2009) as 5′ flanking site using primers lat1_1896F/lat1_1897R. A fragment encoding the hygromycin resistance gene was amplified from plasmid IR98 (Radman *et al.* 2013) using primers lat1_1898F/lat1_1921R. 1.5 kb of the 3′ UTR and downstream sequence of *lat-1* was amplified from plasmid pTL2 (Langenhan *et al.* 2009) (encoding the *lat-1* genomic locus) using primers lat1_1900F/lat1_1901R. The fragments were inserted into IR98 by Gibson assembly (Gibson *et al.* 2009) using primers lat1_1902F/lat1_1903R. This was performed using NEBuilder HiFi assembly (New England Biolabs) according to manufacturer's instructions, followed by transformation into chemically competent *E. coli* DH5α.

sgRNA plasmids

For CRISPR–Cas9 engineering of endogenous loci, sgRNA was cloned into vector pJJR50 as described by Waaijers *et al.* (2016). pJJR50 was a kind gift from Mike Boxem (Addgene plasmid #75026). gRNA was cloned into *Bbs*I-digested pJJR50 using annealed oligonucleotides 5′-ggactggctccagtggacga-3′/5′-tcactcatctttgagctcgg-3′ with primer pairs lat1_1904F/lat1_1905R and lat1_1906F, lat1_1907R, respectively. Ligation was performed using a T4 ligase (Thermo Fisher) according to the manufacturer's instruction, followed by transformation into chemically competent *E. coli* DH5α cells.

RNA extraction and rapid amplification of 5′ cDNA-ends with PCR

Total RNA was extracted from a mixed population of wild-type hermaphrodites using TRI Reagent (Sigma) according to the manufacturer's protocol and transcribed into cDNA with the second-generation 5′/3′ RACE Kit (Roche) in combination with the Expand High Fidelity PCR System (Roche) as described in the supplier's instructions using 2 different gene-specific primers (lat-1_1772R and lat-1_1772R). Before the PCR, the 3′ end of the cDNA was tailed with dATP and TdT. The cDNA mix was directly utilized as a template for the 5′ rapid amplification of cDNA-ends with PCR (RACE-PCR). Amplification was run with an Oligo-d(T) anchor primer and the gene-specific primers above, respectively. PCR products were separated via gel electrophoresis, cut out, purified with the Wizard SV Gel and PCR Clean-Up System (Promega), and cloned into the vector pCR2.1 using the TOPO TA Cloning Kit (Thermo Fisher) for further analysis. For primer sequences, see Supplementary Table 1 in Supplementary File 1.

Downloaded from https://academic.oup.com/g3journal/article/14/11/jkae206/7750701 by Universitaets- und Landesbibliothek Duesseldorf user on 04 May 2026

Transcript variant analyses

Publicly available RNA-seq datasets from adult wild-type hermaphrodite *C. elegans* var. Bristol N2 were downloaded via the Sequence Read Archive (Leinonen *et al.* 2011; Kodama *et al.* 2012), and paired-end reads with an average length of 101 bases were aligned to the WBcel235 genome (Howe *et al.* 2017) using STAR (Dobin and Gingeras 2015) The mapped reads were assembled into transcripts and quantified by StringTie (version v2.1.3b) (Pertea *et al.* 2015) using the genome annotation as initial set of transcript variants. Full-length transcripts and newly identified transcripts were inspected (Supplementary Table 2 in Supplementary File 1), and further analyses including visualization were conducted with the Integrated Genomics Viewer (Robinson *et al.* 2011). Accession numbers and mapping statistics are given in Supplementary Table 3 in Supplementary File 1.

Statistical analysis

Numerical assay data were analyzed with GraphPad Prism version 9.2.0 (GraphPad Software). If not stated otherwise, the data are presented in box plots with 90% confidence interval. Statistical analyses were performed using a two-tailed Student's *t*-test for comparing two groups and a one-way ANOVA in combination with a Bonferroni post hoc test for comparing multiple groups, respectively. *P* values of $P \leq 0.05$ were considered statistically significant. All details are given in the respective figure legends.

Results

LAT-1 controls sperm guidance in hermaphrodites

Previously, we showed that the LAT-1 N terminus (LNT) tethered to the membrane by its first transmembrane helix (aa 1-581, termed LNT) is sufficient to ameliorate the fertility defects in *C. elegans* homozygous for the null allele *lat-1(ok1465)* (hereafter referred to as *lat-1*), which are overall characterized by a reduced brood size (wild type: 228.2 ± 3.6; *lat-1*: 117.4 ± 4.0) (Langenhan *et al.* 2009; Prömel *et al.* 2012). These findings indicate that the unusual 7TM-independent/*trans* function of the receptor is involved in controlling aspects of reproduction of the self-fertilizing *C. elegans* hermaphrodite. The hermaphrodite gonad produces a fixed number of sperm during larval development, which are subsequently stored in the spermatheca, and variable amounts of oocytes are generated during adulthood (Fig. 1). We therefore asked whether the LAT-1 function affects only one or possibly several cellular processes or cell types culminating in the regulation of reproduction. To address this question, we dissected the defects of the *lat-1* mutants in greater detail.

We first analyzed *lat-1* mutant sperm as previously obtained data led to the hypothesis that LAT-1 plays some role in sperm function (Prömel *et al.* 2012). Mutant hermaphrodites produced approximately the same amount of sperm as wild-type individuals (Fig. 2a and b), and the number of anucleate residual bodies generated during sperm production appeared to be constant (Fig. 2c and d). During larval stages, the germ cells that enter meiosis I proximally of the transition zone are called primary spermatocytes. Cytokinesis of meiosis I can be incomplete, i.e. the cytoplasm of the resulting secondary spermatocytes is still connected. During meiosis II, the secondary spermatocytes divide into spermatids and bud off the common cytoplasm to form individual haploid cells. The remaining anucleate cytoplasm is called a residual body and is eventually resorbed. Spermatids are activated to functional spermatozoa just before fertilization in the spermatheca (summarized in L'Hernault 2006). Our data indicate largely intact sperm development and the correct timing of the sperm–oocyte switch during the transition of the last larval stage into adulthood.

When crossing *lat-1* males with wild-type feminized hermaphrodites, we previously observed a reduced number of progeny compared to wild-type males (Prömel *et al.* 2012), suggesting either a reduced sperm function or decreased sperm transfer. As *lat-1* males also display a defective mating behavior (Matus *et al.* 2022), the observed reduced progeny of *lat-1* males could be attributed to sperm transfer during mating rather than sperm function. To exclude a defect in functionality of *lat-1* sperm, we treated spermatids from unmated males with pronase, which should activate them. As no difference was observed between wild-type and *lat-1* spermatid activation (Fig. 2e), we hypothesized that *lat-1* sperm was grossly functional.

As *lat-1* nematodes lay overall fewer fertilized eggs (Prömel *et al.* 2012) and thus use less sperm than wild-type worms in a given time period, this should result in an accumulation of residual sperm over time. To assess a possible change in the amount of sperm during the fertilization period, we examined sperm in the spermatheca 48 h after the first ovulation (Fig. 2f) together with the course of egg laying (Fig. 2g). Sperm amounts in the spermatheca 48 h after the first ovulation were not elevated, but slightly, albeit not significantly reduced compared to the amount in wild types. At the same time, significantly less sperm was used for fertilization indicating a loss of sperm during adulthood. This sperm loss was evaluated by subtracting the number of laid eggs and residual sperm within the spermatheca from the initial sperm count (Fig. 2f). As sperm loss can be caused by impaired motility or defective directed locomotion of sperm, which leads to them being flushed out during egg laying (summarized in Han *et al.* 2010), our data suggest that LAT-1 could play a role in sperm movement. Consistent with this hypothesis, the ovulation rate in *lat-1* mutants, which was initially similar to the one of wild-type worms, declined more rapidly over time (Fig. 2h). This is plausible as in *C. elegans*, ovulation is stimulated by signals produced in spermatozoa (reviewed in Han *et al.* 2010). Both phenotypes were rescued by the transgenic LNT (Fig. 2f and h), showing that the role in sperm movement is mediated by the 7TM-independent function of LAT-1. It should be noted that worms were precisely staged in all experiments, also to account for the fact that some *lat-1* mutants are developmentally slower than wild-type controls (Langenhan *et al.* 2009) (Supplementary Fig. 1 in Supplementary File 1).

To further assess the hypothesis that LAT-1 is essential for sperm movement, we monitored MitoTracker Red-labelled sperm after mating of males and hermaphrodites of different genotypes. Sperm of *lat-1* mutant males did not show impaired movement toward the spermatheca of wild-type hermaphrodites, indicating largely intact sperm motility (Fig. 2i and j). In contrast, wild-type sperm inside *lat-1* hermaphrodites did not localize near the spermatheca to the same extent as in the respective wild-type control. This defect was ameliorated by transgenic expression of the *LNT* in the hermaphrodite. Thus, our data indicate a defect in sperm guidance originating from *lat-1* hermaphrodites rather than impaired sperm function.

LAT-1 modulates germ cell apoptosis and affects oocyte quality

Besides the effect on sperm movement, we found that the 7TM-independent mode of LAT-1 also affects oocytes. We observed an increase of germ cell apoptosis by SYTO 12-staining of *lat-1* mutant hermaphrodites, which was rescued by transgenic expression of the *LNT* (Fig. 3a and b). We also confirmed the

Downloaded from https://academic.oup.com/g3journal/article/14/11/jkae206/7750701 by Universitaets- und Landesbibliothek Duesseldorf user on 04 May 2026

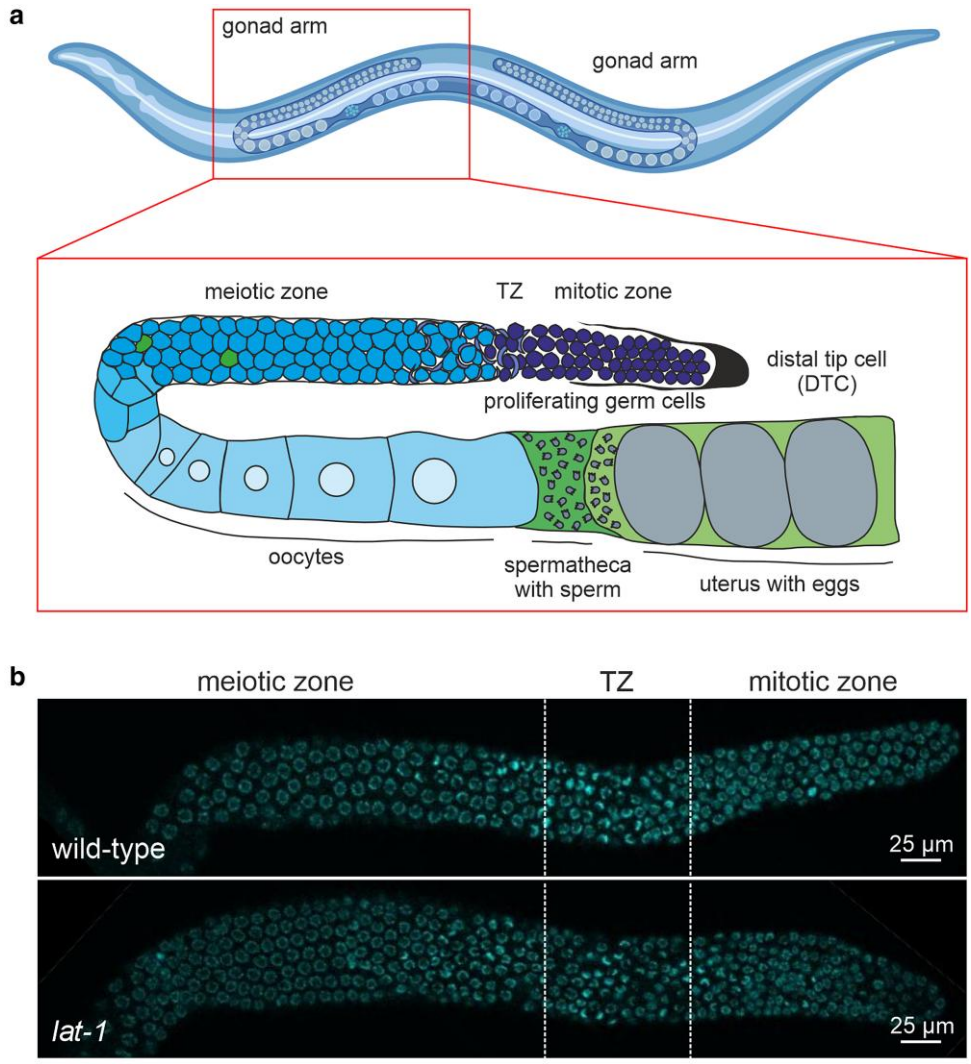


Fig. 1. The *C. elegans* gonad. a) Shown is one of the two symmetrical U-shaped gonad arms of a *C. elegans* adult hermaphrodite. In the fourth larval stage (L4), a fixed number of sperm (~150 per gonad) are produced and stored inside the spermatheca. Subsequently, the gonad switches to continuous oocyte production only. In the distal gonad, germ cell nuclei are not surrounded by a complete membrane but reside in a common cytoplasm. They continually self-renew by mitotic division in the proliferative (mitotic) zone, which is distally enclosed by the DTC. Subsequently, germ cells enter meiotic divisions (crescent-shaped nuclei) and progress further through meiosis, where some germ cells undergo apoptosis. Here, the cells are surrounded by the gonadal sheath cells (not shown). Near the loop, nuclei start to cellularize and to obtain individual plasma membranes. Due to coordinated contraction of the gonadal sheath cells, oocytes are pushed into the spermatheca, fertilized, and eggs are flushed into the uterus. After completing the first set of embryonic divisions, they are laid through the vulva (not shown). Parts of the figure were created in Biorender. Prömel, S. (2024) BioRender.com/u05l303. b) Dissected and DAPI-stained distal gonads of L4 + 1-day-old wild-type and *lat-1* hermaphrodites.

increase in apoptotic bodies independently using a CED-1::GFP reporter (Zhou *et al.* 2001), which labels germ cells that are being engulfed by the somatic gonadal sheath cells (Supplementary Fig. 2 in Supplementary File 1). During adult stages, germ cells normally form oocytes, and it is a physiological process during *C. elegans* oogenesis that some of them undergo apoptosis (Fig. 1) (summarized in Gartner *et al.* 2008). While its role is debated, one possible function is to provide nutrients for other developing oocytes (Gumienny *et al.* 1999; Andux and Ellis 2008). Mutants of the apoptosis pathway (*ced-3* and *ced-4*) showed a reduced oocyte size (Andux and Ellis 2008). Thus, oocytes gaining too little nutrients are of inferior quality, reflected by reduced oocyte size (Andux and Ellis 2008) and increased embryonic lethality (Carranza-Garcia and Navarro 2019). Surprisingly, *lat-1* oocytes displayed both characteristics: smaller oocytes which can be ameliorated by the presence of the LNT (Fig. 3c–e), and increased lethality (Fig. 3f). As nematodes null for *lat-1* generally show embryonic lethality due to the receptor's function in early development (Langenhan *et al.* 2009; Müller *et al.* 2015), it is impossible to assess oocyte quality by directly quantifying embryonic lethality. Thus, we investigated *lat-1* worms expressing the *LNT*. As this construct has been observed to rescue fertility defects, but not embryonic defects (Prömel *et al.* 2012), any amelioration of embryonic death detected in the corresponding strain is more likely to stem from maternal, postembryonic LAT-1 function. Comparison with *lat-1* mutants revealed that embryonic lethality is less pronounced in the presence of the LNT (Fig. 3f), indicating a cause other than developmental defects such as inferior oocyte quality. It must be noted that rescue by the LNT occurs to a much lesser extent than rescue by the full-length receptor, which is due to the fact that the latter one is essential for embryonic development (Langenhan *et al.* 2009; Müller *et al.* 2015).

Downloaded from https://academic.oup.com/g3journal/article/14/11/jkae206/7750701 by Universitaets- und Landesbibliothek Duesseldorf user on 04 May 2026

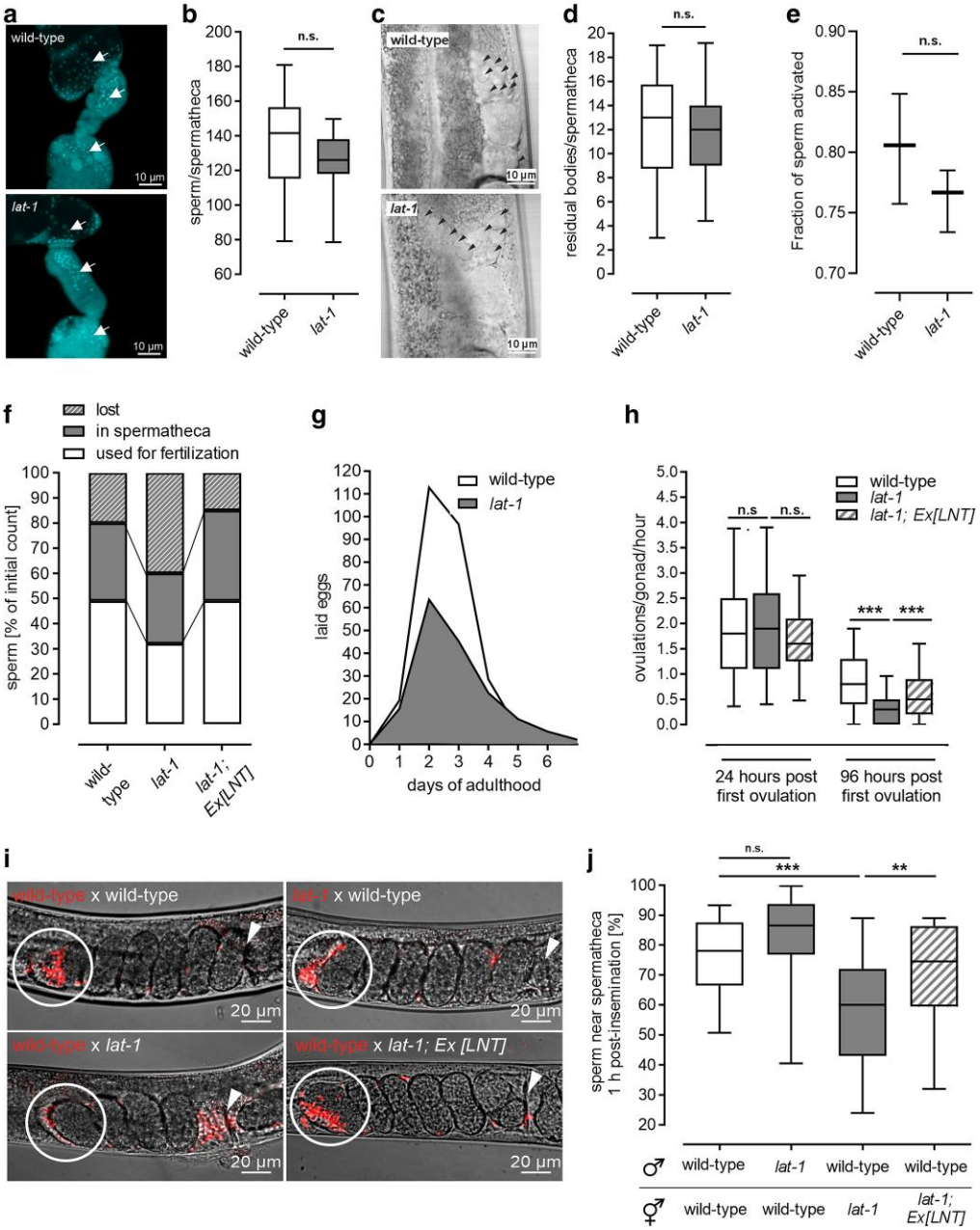


Fig. 2. Nematodes lacking *lat-1* display impaired sperm movement. a) Spermathecae of L4 + 1-day-old *lat-1* mutant hermaphrodites contain the same amount of sperm (white arrows) as wild-type specimen. Gonads of adult hermaphrodites were dissected and subsequently stained with DAPI. b) Quantification of DAPI stainings as shown in (a) reveals that the number of sperm inside the spermatheca is indifferent from the one in wild-type nematodes. $n \geq 20$ in 4 independent experiments. n.s., not significant. c) Residual bodies (black arrowheads) located close to the spermatheca in *lat-1* mutant and wild-type gonads. Shown are DIC images of unstained living L4 + 1-day-old hermaphrodites. d) Quantification of anucleate residual bodies based on DIC images as displayed in (c) revealed no significant difference in number between wild-type nematodes and *lat-1* mutants. Data from 4 independent experiments, $n \geq 24$. n.s., not significant. e) Activation of spermatids by pronase treatment. Dissected spermatids from L4 + 1-day-old *lat-1* males showed a similar level of activation as wild-type controls. Data from 3 independent experiments, $n \geq 100$. n.s., not significant. f) Sperm amount 48 h after the first ovulation. Sperm was DAPI-stained and sperm loss was calculated (for details, see '*Materials and methods*'). This loss is ameliorated in transgenic lines expressing LNT. It should be noted that due to experimental limitations, the initial sperm count in the spermatheca had to be taken from different animals than the count after 48 h. $n \geq 15$. g) Hermaphrodites lacking *lat-1* exhibit a continuously smaller brood size over their entire reproductive period with the maximal reduction being visible on the second and third day of egg laying. $n \geq 75$ in nine independent replicates. h) The ovulation rate in *lat-1* mutants is similar to the one in wild types 24 h after the first ovulation but decreases faster than in wild-type individuals or in *lat-1* mutants expressing the LNT. At 96 h after the first ovulation, it is significantly lower. Data of 4 independent experiments, $n \geq 51$. n.s., not significant; $^{***}P < 0.001$. i) Representative images showing the distribution of male *lat-1* and wild-type sperm, respectively, after mating to hermaphrodites of different genotypes. The motility of *lat-1* sperm after mating with wild-type hermaphrodites appears to be intact, as indicated by correct localization near the spermatheca (white circle) 1 h postinsemination. Conversely, wild-type sperm inside *lat-1* hermaphrodites do not reliably localize next to the spermatheca and remain close to the vulva (white arrowhead). Mating assays were performed with wild-type and *lat-1* mutant nematodes in different constellations. Sperm was stained with MitoTracker Red by incubation of living young adult males prior to the mating, and sperm location was monitored 1 h after mating occurred. j) Sperm of wild-type males do not properly migrate to the spermatheca in *lat-1* mutant hermaphrodites after mating, while sperm of *lat-1* mutant males show no impaired movement toward the spermatheca of wild-type hermaphrodites. The former effect can be rescued by transgenic complementation of the LNT. Quantification was performed from images as shown in (h). Data were acquired in at least three independent experiments with $n > 20$ biological replicates. n.s., not significant; $^{**}P < 0.01$; $^{***}P < 0.001$.

Downloaded from https://academic.oup.com/g3journal/article/14/11/jkae206/7750701 by Universitaets- und Landesbibliothek Duesseldorf user on 04 May 2026

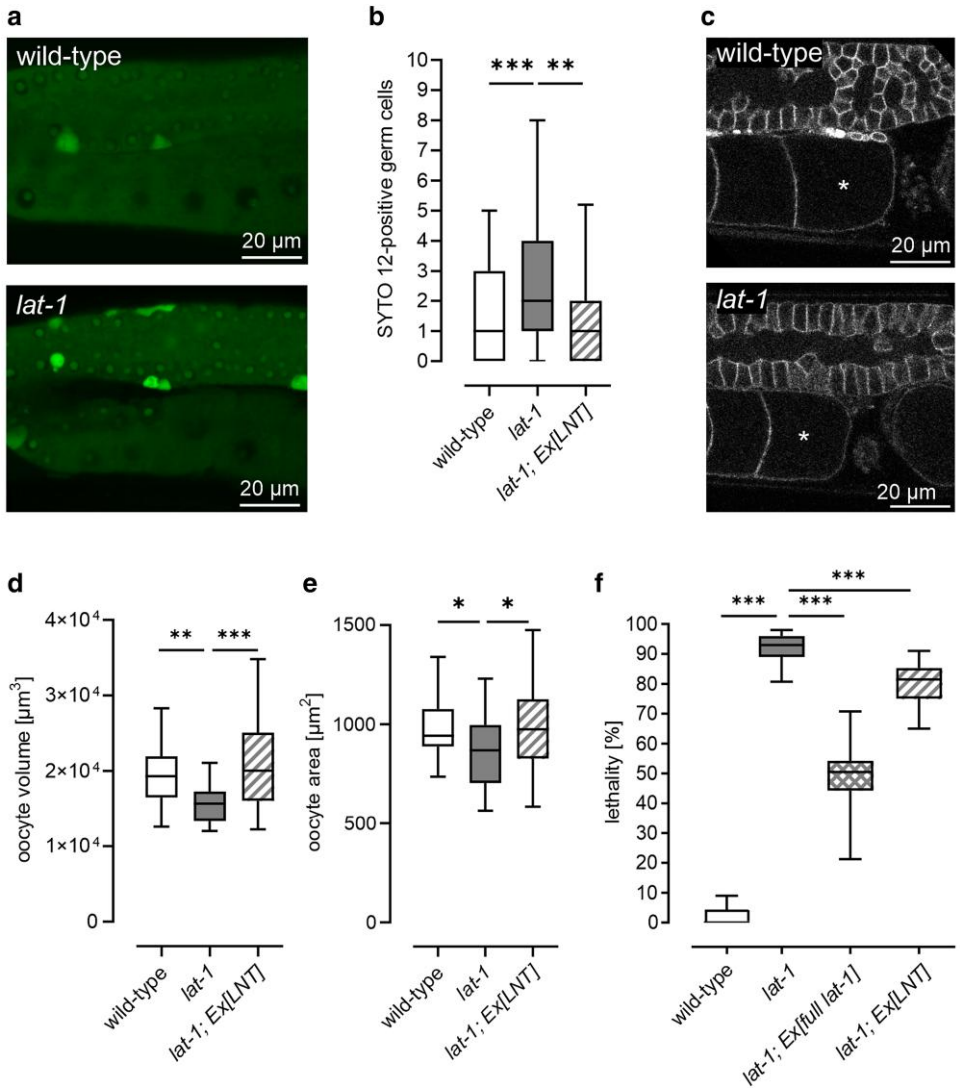


Fig. 3. In the absence of LAT-1 function, germ cell apoptosis is increased. a) Germlines of *lat-1* mutants exhibit more SYTO 12-stained germ cells compared with wild-type controls. Living adult nematodes 24 h post-L4 were stained with SYTO 12 as a marker for apoptotic cells. Shown are representative images. b) Quantification of SYTO 12 stainings from (a). Reintroduction of the LNT rescues the increased number of apoptotic cells. Given are numbers per gonad. $n \geq 33$. $^{**}P < 0.01$; $^{***}P < 0.001$. c) Oocytes (marked with an asterisk) are significantly smaller in *lat-1* mutants than in wild-type individuals. Oocyte membranes were visualized in living young adult hermaphrodites by expression of the construct *pie-1p::mCherry::PH(PLC1delta1)*. Shown are representative images. d) Quantification of (c) reveals that oocyte size is decreased in *lat-1* mutants. This defect can be ameliorated by expression of the *LNT*. $n \geq 18$. $^{**}P < 0.01$; $^{***}P < 0.001$. e) Oocyte size determination by area measurements confirms data from (d). This way of measuring oocyte dimension was employed to supplement the volume measurements. Data from at least 5 independent experiments of area measurements, $n \geq 39$, $^{*}P < 0.05$. f) The LNT rescues embryonic lethality of *lat-1* mutants to a small but significant extent, while amelioration by the full-length *lat-1* construct is much stronger and is considered the maximum rescue that can be reached. Assays were performed in 4 independent experiments, $n \geq 30$, $^{***}P < 0.001$.

These data point toward *lat-1* oocytes gaining too few nutrients, which can imply insufficient apoptotic events/clearance of apoptotic cells rather than too many. Therefore, *lat-1* worms may not display a genuine increase in apoptosis but have other defects resulting in apoptotic cell accumulation.

LAT-1 elicits its functions from the somatic gonad in *trans*

All functions of LAT-1 identified in this study, in sperm guidance, ovulation, and germ cell apoptosis/oocyte quality, have been shown to be 7TM-independent functions of the aGPCR. To gain insights into the mechanisms underlying these functions, we addressed the question, from which cells the LAT-1 function originates. Thus, we first generated a detailed expression profile of the receptor in the hermaphrodite gonad. Utilizing a CRISPR/Cas9 genome-edited *LNT::GFP (lat-1(1-581)::GFP)*, we observed *lat-1* expression in the entire somatic gonad of adult hermaphrodites, including the DTC, the gonadal sheath cells, and the spermatheca (Fig. 4a–c). Furthermore, LAT-1 seemed to be present in germ cells and developing oocytes. To verify expression in DTC and gonadal sheath cells, a CRISPR/Cas genome-edited transcriptional *lat-1p::mCherry* was combined with a marker for the DTC (*lag-2::myr::GFP*) (Fig. 4d) or the gonadal sheath cells (*lim-7p::GFP*) (Fig. 4e), respectively.

To test whether the somatic gonad is the origin of the LAT-1 7TM-independent function, we specifically expressed the *LNT* in the DTC (*lag-2p::LNT*), the gonadal sheath cells (*lim-7p::LNT*), and the spermatheca (*plc-1p::LNT*) of *lat-1* mutants, respectively. First, brood size was quantified to assess whether the LNT in distinct cells has the capability to ameliorate the fertility defects in

Downloaded from https://academic.oup.com/g3journal/article/14/11/jkae206/7750701 by Universitaets- und Landesbibliothek Duesseldorf user on 04 May 2026

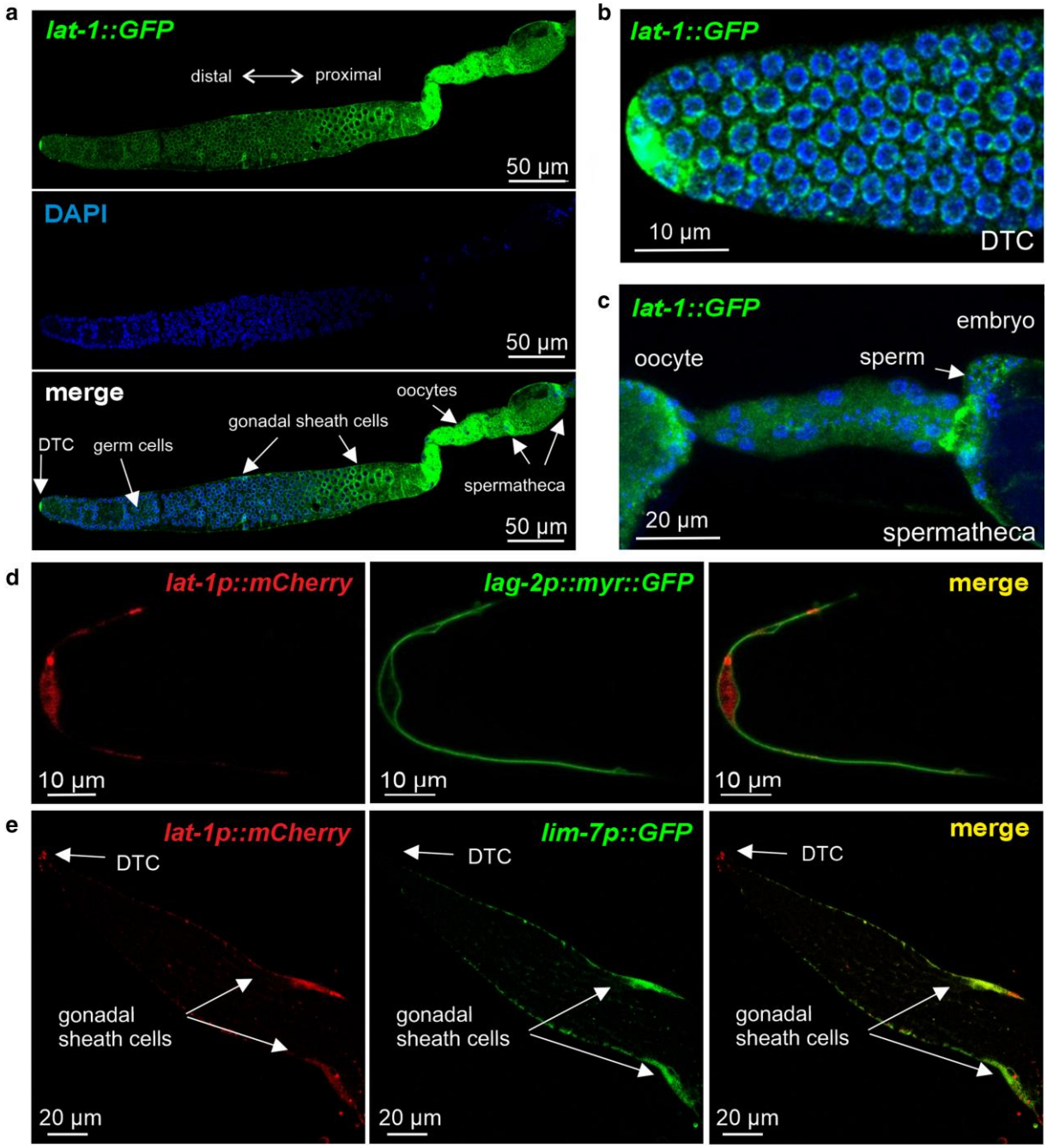


Fig. 4. Expression of *lat-1* in the hermaphrodite gonad. a) The receptor is present in all somatic cells of the gonad as well as germ cells. b), d) *lat-1* is expressed in the DTC. It is further localized c) in the spermatheca and e) in gonadal sheath cells. For visualizing *lat-1* expression, either a CRISPR/Cas9 genome-edited single-copy integrated *LNT::GFP* (*lat-1(1-581)::GFP*) was used with signal amplification by an anti-GFP antibody (a–c) (for details, see '*Materials and methods*') or a CRISPR/Cas9 genome-edited single-copy integrated *lat-1p::mCherry* (d, e) was employed. The DTC was visualized (d) by expressing *lag-2p::myr::GFP* and the gonadal sheath cells by using *lim-7p::GFP* (e). It should be noted that LAT-1 is not visible in germ cells in (d and e) likely due to the weak expression and the fact that no signal amplification by antibodies was employed here.

general (Fig. 5a). While expression in the DTC and gonadal sheath cells rescued at least partially (to a lesser extent than the LNT driven by its endogenous promoter), expression in the spermatheca did not. Focusing on the two tissues, in which *LNT* expression had an effect, we next elucidated whether it exerts a function from the DTC and/or the gonadal sheath cells specifically in the observed phenotypes: ovulation rate at 96 h after the first ovulation, sperm guidance, apoptosis, and oocyte size. While its presence in either the DTC or the gonadal sheath cells led to a partial amelioration of the ovulation rate (Fig. 5b), no significant rescue was achieved for sperm guidance (Fig. 5c). Receptor expression on the gonadal sheath cells had a rescuing effect on the increased apoptosis rate of germ cells in *lat-1* mutant hermaphrodites (Fig. 5d). The same rescuing effect was observed with regards to oocyte size (Fig. 5e).

These data highlight the fact that the LAT-1 7TM-independent/*trans* function is sufficient to control aspects of reproduction at least partially in a noncell autonomous manner.

Downloaded from https://academic.oup.com/g3journal/article/14/11/jkae206/7750701 by Universitaets- und Landesbibliothek Duesseldorf user on 04 May 2026

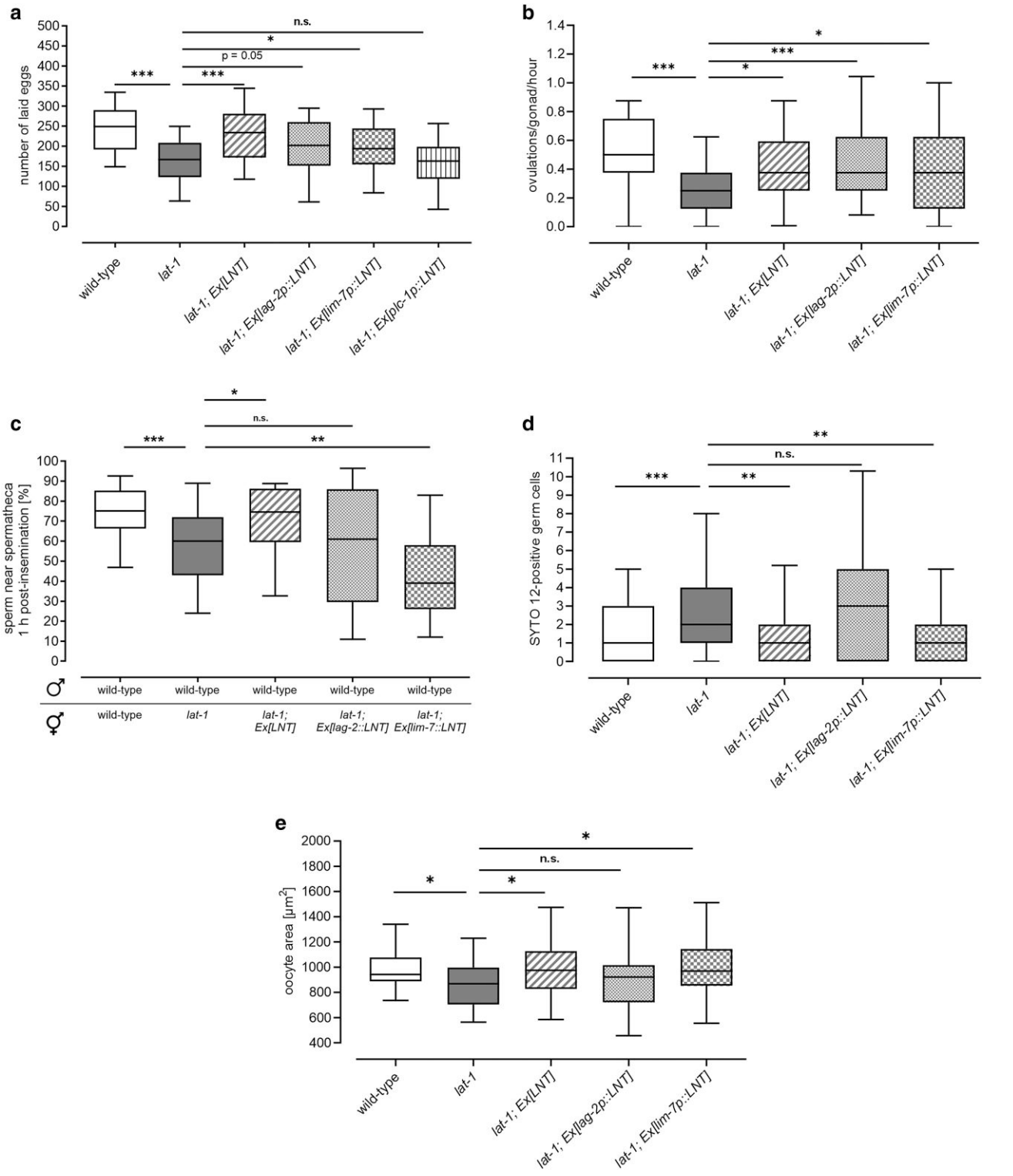


Fig. 5. The LNT acts from somatic cells of the *C. elegans* gonad in a noncell autonomous manner. Tissue-specific expression of the LNT tethered to the membrane (LNT) using promoters with activity restricted to the DTC (*lag-2p::LNT*), the gonadal sheath cells (*lim-7p::LNT*), or the spermatheca (*plc-1p::LNT*) reveals whether a *trans* mode of the receptor fulfills its functions in different contexts on germ cells and in which location it is required. a) While expression of LNT in the DTC and the gonadal sheath cells generally results in a partial amelioration of the overall brood size defect of *lat-1* mutants, sole expression in the spermatheca (*plc-1p::LNT*) does not. b) The ovulation defect 96 h after the first ovulation of worms lacking *lat-1* is rescued by the LNT in both, the DTC and the gonadal sheath cells. c) Sperm migration to the spermatheca is rescued by the sole presence of LAT-1 neither in the DTC nor in the gonadal sheath cells. Data were acquired in at least three independent experiments with $n > 20$ biological replicates. n.s., not significant; $^{*}P < 0.05$; $^{**}P < 0.01$; $^{***}P < 0.001$. Note that some controls in this dataset (wild type, *lat-1*, *lat-1*; *Ex[LNT]*) are the same as in Fig. 2j. d) The increased apoptosis rate in *lat-1* mutants is ameliorated by the presence of the receptor in the gonadal sheath cells, but not in the DTC. Numbers are given per gonad. Data from at least 3 independent experiments, $n \geq 28$. n.s., not significant; $^{*}P < 0.05$; $^{**}P < 0.01$; $^{***}P < 0.001$. Note that the controls in these data (wild type, *lat-1*, *lat-1*; *Ex[LNT]*) are the same as in Fig. 3b. e) The decreased oocyte size observed in *lat-1* mutant nematodes can be ameliorated by expressing the LNT in the gonadal sheath cells, but not in the DTC. Data from at least 5 independent experiments of area measurements, $n \geq 39$. n.s., not significant; $^{*}P < 0.05$. Note that the controls in these data (wild type, *lat-1*, *lat-1*; *Ex[LNT]*) are the same as in Fig. 3e.

Downloaded from https://academic.oup.com/g3journal/article/14/11/jkae206/7750701 by Universitaets- und Landesbibliothek Duesseldorf user on 04 May 2026

The LAT-1 transcript variant repertoire contains N terminus-only receptor versions

As the LAT-1 7TM-independent functions act in a completely different biological context than that of its 7TM-dependent signal in embryogenesis (Langenhan *et al.* 2009; Prömel *et al.* 2012), the question arose as to why such a large receptor molecule is produced, when only the extracellular entity is mediating a function in distinct contexts. The release of the N terminus by cleavage of the aGPCR at the GPS, the motif in the GAIN domain capable of autoproteolysis, could be one mechanism. However, our previous findings indicate that cleavage is not essential for overall LAT-1 function (Prömel *et al.* 2012). Interestingly, a recent study suggests the presence of several premature poly-A sites within *lat-1* transcripts that, among others, render LAT-1 molecules consisting only of the N terminus (Tourasse *et al.* 2017). To gain insights into the prevalence of such variants, we analyzed existing transcriptome data generated by RNA-Seq from day 1 adult wild-type hermaphrodites (Chen *et al.* 2015), in which the coverage was sufficient for splice variant analyses (Fig. 6a). Generally, with more than 20 transcript forms, the repertoire of *lat-1* variants can be considered extensive. Although the largest fraction consisted of the entire receptor molecule, ~1.5% of the variants comprised only the N-terminal exons in different combinations and versions, which are potentially able to transmit the 7TM-independent/*trans* function (Fig. 6b). A RACE-PCR from the mRNA of wild-type hermaphrodites confirmed the general presence of N terminus-only variants (Fig. 6c, Supplementary Fig. 3 in Supplementary File 1), suggesting that these variants of *lat-1* exist in vivo. It has to be noted that, to ensure correct transcript composition, rescue analyses were always performed with constructs containing the genomic locus of *lat-1* or modifications of it.

Discussion

It is becoming increasingly clear that the highly unusual dual mode of classical *cis* signaling via G proteins and *trans* functions mediated solely through the N terminus (independent of 7TM and C terminus) are inherent to several aGPCR (Langenhan *et al.* 2009; Prömel *et al.* 2012; Patra *et al.* 2013; Tu *et al.* 2018; Ward *et al.* 2018). While the *cis* mode is relatively well studied in many cases, knowledge on the molecular details as well as the impact of the *trans* function is sparse, limiting our understanding of how such functions are integrated in multicellular settings. In the present study, we show that the 7TM-independent/*trans* mode is a frequently employed concept involved in different physiological and cellular contexts and that, in contrast to other aGPCR (Tu *et al.* 2018; Ward *et al.* 2018), the latrophilin homolog LAT-1 does not seem to engage in simultaneous bidirectional signaling (*cis* and *trans*) in these contexts. We identified LAT-1 N-terminal activity involved in different aspects of the *C. elegans* reproductive system, jointly balancing the brood size of the nematode. Thereby, the 7TM-independent/*trans* mode of LAT-1 action affects both gamete types and their function with seemingly diverse effects on sperm movement, ovulation, and germ cell apoptosis as well as quality.

Although it does not appear to be involved in sperm development or activation, the LAT-1 *trans* function seems to be essential for sperm locomotion. The corresponding defect caused by the absence of the receptor is characterized by sperm loss occurring in the course of *lat-1* mutant adulthood (Fig. 2), due to impaired sperm movement. Possible reasons for this can generally be faulty sperm guidance cues or defective sperm. Our analyses strongly suggest LAT-1 to be involved in the sperm guidance signaling machinery of the hermaphrodite rather than sperm function per se, thereby affecting sperm movement. Many species use chemo-attractants to guide sperm to oocytes to ensure efficient fertilization. The anatomy of the *C. elegans* reproductive tract stresses the need for such signals, because as oocytes are pushed through the spermatheca and the uterus, sperm are dragged along and could be lost to the environment. Thus, a mechanism to lead them back to the spermatheca and localize them to the next oocyte is essential. Similarly, male sperm need to be able to localize the hermaphrodite's oocytes after being transferred into the uterus (summarized in Han *et al.* 2010). The likely origin of a chemo-attractant in *C. elegans* is the oocytes themselves. However, the spermatheca might also play a role in the establishment of the attractive signal (Kubagawa *et al.* 2006). The most likely candidates for chemo-attractants are F-series prostaglandins that are synthetized from polyunsaturated fatty acids (PUFA), as defects in genes involved in the metabolism of PUFA in the intestine (*fat-1-4*) and their uptake into the oocytes (*rme-2*, *daf-1*) lead to impaired sperm guidance (Kubagawa *et al.* 2006; Hoang *et al.* 2013; Hu *et al.* 2021). Other enzymes (*cyp-31A2*, *cyp-31A3*, and *emb-8*) are thought to downregulate prostaglandin synthesis within eggs in the uterus to uphold the signaling gradient toward the unfertilized oocytes (Hoang *et al.* 2013). Future studies will need to shed light on the question where LAT-1 can be placed in the mechanisms. We hypothesized that the reduced ovulation rate with time is related to the sperm movement defect as it correlates with the observed sperm loss. It is well established that ovulation is coordinated by sperm together with oocytes and gonadal sheath cells (Clandinin *et al.* 1998; Bui and Sternberg 2002; Han *et al.* 2010). However, our data suggest that it is likely that LAT-1 has an additional role in ovulation especially as the defects in ovulation can at least partially be rescued by expression of *lat-1* in the DTC or the gonadal sheath cells, while the sperm guidance defects cannot. It might also be conceivable that the guidance signal by transgenic overexpression is not strong enough to guide the sperm all the way back to the spermatheca but might be strong enough to keep them in the uterus, where they can contribute to signals stimulating ovulation.

We also found increased numbers of apoptotic cells in the proximal part of *lat-1* mutant germlines indicating a role of the receptor in programmed cell death (Fig. 3). Future analyses will need to clarify whether this is due to an increased rate of apoptosis itself or defective clearance of apoptotic germ cell corpses. However, the reduced oocyte size and increased embryonic lethality that can be attributed to the 7TM-independent/*trans* mode of LAT-1 hint toward reduced oocyte quality, which makes the latter hypothesis more likely. A function of LAT-1 in the regulation of apoptosis is intriguing since the mouse latrophilin LPHN1/ADGRL1 (Zuko *et al.* 2016), as well as some other aGPCR (Hsiao *et al.* 2015; Shiu *et al.* 2022), have previously been associated with programed cell death.

As these newly identified roles of LAT-1 are exerted solely by its 7TM-independent mode, but *lat-1* is expressed in germ cells as well as in the surrounding somatic cells, the question arose whether the receptor functions noncell autonomously and thus, in *trans*. Our analyses showed that the function in ovulation can be exerted by the LNT from both the DTC and the gonadal sheath cells, while in apoptosis and oocyte size, its presence is specifically required in the gonadal sheath cells rather than the DTC (Fig. 5). This suggests that the receptor indeed seems to fulfill its functions in these contexts noncell autonomously from the somatic germline. However, as the detected differences are small, which is,

Downloaded from https://academic.oup.com/g3journal/article/14/11/jkae206/7750701 by Universitaets- und Landesbibliothek Duesseldorf user on 04 May 2026

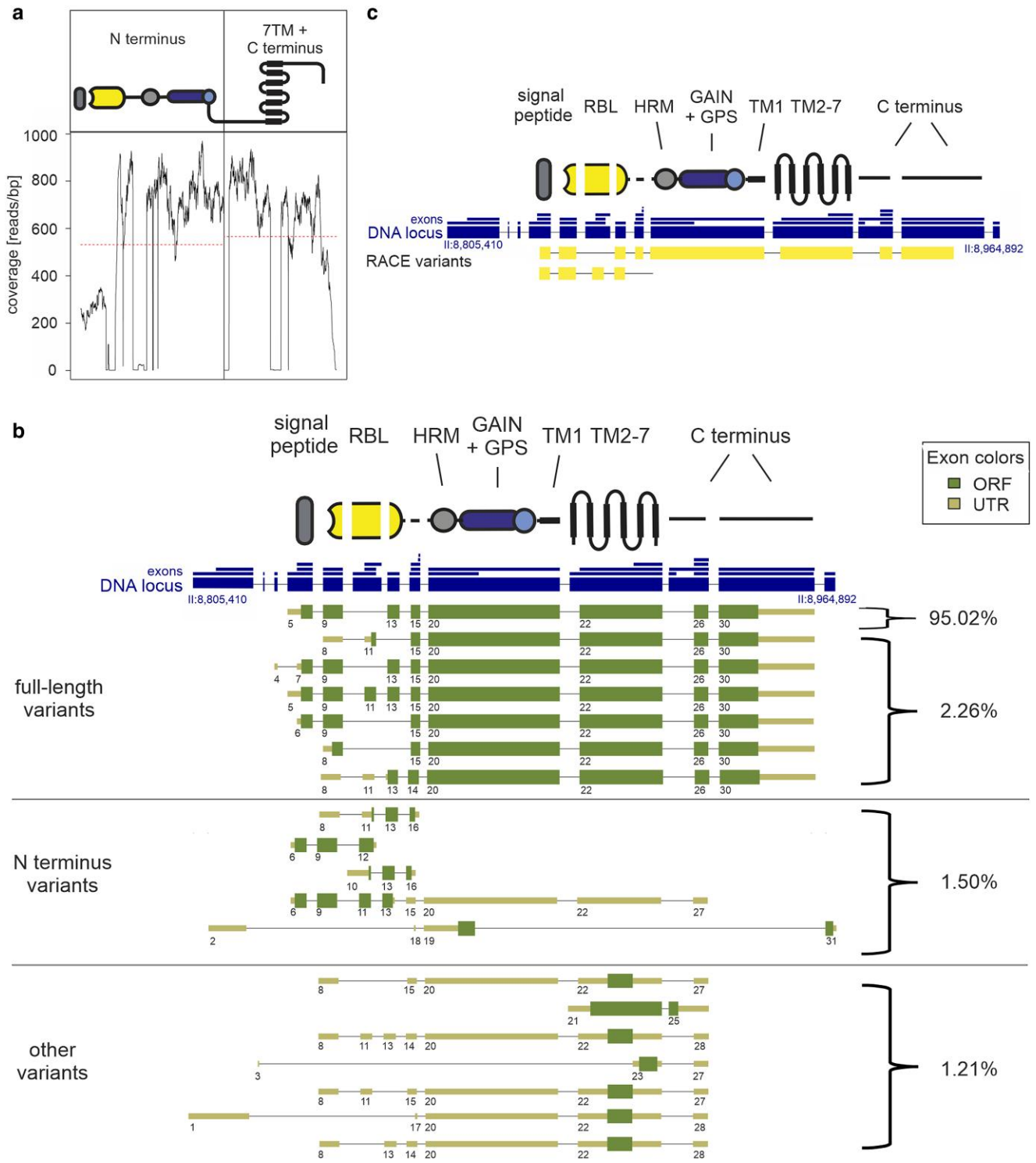


Fig. 6. Several transcripts containing only the N terminus of LAT-1 exist. a) Read coverage of the *lat-1* locus extracted from available RNA-seq data of day 1 adult wild-type hermaphrodites (Chen *et al.* 2015) shows an almost uniform distribution of reads over the entire locus. b) Repertoire of *lat-1* transcript variants identified from RNA-Seq data (Chen *et al.* 2015). Relative abundance of each transcript variants was derived from Fragments Per Kilobase of transcript per Million mapped reads values estimated by StringTie (Supplementary Table 2 in Supplementary File 1). Several full-length variants exist which mostly differ in their N-terminal composition. Variants containing only the N terminus seem mostly not to be membrane-anchored. Other variants, which lack the N terminus, constitute about 1%. Only full-length variants with an incidence of more than 0.01% are depicted. The genomic locus of LAT-1 is shown with its longest exons (large boxes) and size-condensed introns (faint lines). All exons found in the analysis are separately plotted above the locus (small blue boxes). The individual exon arrangements of transcripts are shown numbered. Transcripts were defined as a numeric sequence of exons. The longest bona fide ORF is depicted in thick boxes, while the nonprotein coding 5′ and 3′ UTRs are displayed thinner and lighter. 3′ end exons with minor differences in length but identical 5′ splice acceptor sites are considered as one 3′ end exon. Different compositions of the 5′ start exon, 3′ end exon, and/or exons are considered as individual variants. The exact positions of the exons forming the variants are given in Supplementary Table 4 in Supplementary File 1. c) 5′ RACE analyses of wild-type hermaphrodites rendered among others the full-length variant, which has been shown to be the most abundant one in RNA-seq analyses. Further, a variant comprising the N terminus including RBL and HRM domain, but not the GAIN domain was amplified. RBL, rhamnose-binding lectin domain; HRM, hormone-binding domain; GPS, GPCR proteolytic site; GAIN, GPCR autoproteolysis-inducing domain.

Downloaded from https://academic.oup.com/g3journal/article/14/11/jkae206/7750701 by Universitaets- und Landesbibliothek Duesseldorf user on 04 May 2026

for instance, highlighted by the fact that no significant effect gradations in the rescue levels of the LNT from DTC and gonadal sheath cells were observed (Fig. 5a), an additional contribution from other tissues or the germ cells cannot be fully excluded. This could also apply to sperm locomotion (Fig. 5c), where no significant rescue by LAT-1 in any of the tested tissues was observed. Another possible explanation for this result is that the receptor might need to be present in all tissues simultaneously to effectively influence sperm guidance.

There is a plethora of physiological implications of LAT-1 identified in this study and previously (Prömel *et al.* 2012; Matus *et al.* 2022), and it is conceivable that several more LAT-1 functions exist. However, it remains to be determined which of these functions employ similar mechanisms on a molecular level. Despite the clear evidence that multiple aGPCR are able to engage in 7TM-independent/*trans* modes of action (Prömel *et al.* 2012; Patra *et al.* 2013; Patat *et al.* 2016; Tu *et al.* 2018; Ward *et al.* 2018), it is still debated whether these functions are used for intercellular signaling or if they can be sufficiently explained by a role in adhesion or even other modes of action. While adhesive components of LAT-1 cannot be excluded, the general morphology of *lat-1* mutant gonads seems intact (Fig. 1b) making a sole function as a structural component of cell–cell adhesion complexes less likely.

In the current study, we were not able to identify a clear canonical *cis* function complementing the *trans* function in *C. elegans* fertility (Fig. 5). This was a surprising finding since other aGPCR (Tu *et al.* 2018; Ward *et al.* 2018) seem to engage in simultaneous bidirectional *cis* and *trans* signaling from the same cells. In *C. elegans*, *cis* and *trans* functions seem to be separated both spatially and/or temporally, being involved in different cell types and developmental stages. It is known that the LAT-1 *cis* function is essential for early embryonic development (Langenhan *et al.* 2009). Conversely, neuron morphogenesis in *C. elegans* was found to be mainly regulated by a *trans* function (Matus *et al.* 2022), with some evidence for *cis* functions that were not functionally essential. Similarly, in other postembryonic functions such as sperm guidance, ovulation, and germline apoptosis, *trans* functions seem to dominate. It should be noted that phenotypic analyses are never exhaustive and future analyses could unravel LAT-1 *cis* effects in adult nematodes and *trans* functions in the embryo. Nevertheless, it would be intriguing to find out what molecular switch could cause such differences in the molecular mechanisms employed by LAT-1.

Intriguingly, there is some evidence that *trans* functions can be separated at a molecular level from the *cis* functions due to alternative splicing (Fig. 6). Thereby, isolated N-terminal variants can be expressed in vivo, and it is plausible that they are regulated separately from the full-length receptor. These data are also in concordance with recent studies on other aGPCR showing a huge tissue-specific transcriptional variability as a potential common principle in the regulation of aGPCR function (Boucard *et al.* 2013; Knierim *et al.* 2019; Röthe *et al.* 2019). It should be noted that no information is available on the presence of N-terminal variants selectively in the *C. elegans* somatic gonad or germ cells, only data on whole adult hermaphrodites are accessible. The small proportion of N-terminal variants (~2%) might be due to this heterogeneity of the samples, i.e. the potentially small contribution of *trans* function-exerting cell types (such as the few cells of the somatic gonad) to the total mRNA pool. It remains to be determined whether these N-terminal variants are translated into protein and it is also conceivable that the receptor fulfills its 7TM-independent function as an intact full-length molecule. Alternatively, it cannot be excluded that the full-length aGPCR is produced but mediates the 7TM-independent function by the N terminus liberated through autoproteolysis at the GPS. This mechanism of self-cleavage, which is a hallmark feature of many aGPCR, has been described for LAT-1, but in previous studies we found that cleavage does not have a major impact on receptor function (Prömel *et al.* 2012).

In summary, we show that the LNT acts in *trans* in several, distinct physiological settings, underlining the importance as well as the versatility of this mode of action. We further demonstrate that next to the possibility of liberating the extracellular domains of aGPCR via autoproteolysis, alternative splicing can generate receptor N termini to exert 7TM-independent *trans* functions. It would be highly interesting to see whether the characteristics of *trans* signaling found for the prototypic aGPCR LAT-1 in this study are conserved among species and are moreover applicable to the entire class of aGPCR.

Data availability

C. elegans strains and plasmids are available upon request. The authors affirm that all data necessary for confirming the conclusions of the article are present within the article, figures, and supplementary figures and tables.

Supplemental material available at G3 online.

Acknowledgments

The authors thank Jana Winkler and Sarah Kluczynska for help with establishing fertility and oocyte phenotyping assays, Julia Luterán for assistance in cloning, Sonja Kallendrusch for advice and support with microscopy, and Samantha Hughes for helpful discussions. The authors are very grateful to Oliver Hobert and Ralf Schnabel for kindly providing plasmids and worm strains. A number of strains were supplied by the *Caenorhabditis* Genetics Center (CGC), which is funded by the NIH Office of Research Infrastructure Programs (P40 OD010440).

Funding

This work was supported by grants from the Deutsche Forschungsgemeinschaft (DFG, German Research Foundation) through CRC 1423/2 [project number 421152132; C04 (S.P., T.S.)], FOR 2149 [project number 246212759; P02 (S.P.) and P04 (T.S.)], Pr1534/1-1 [project number 254080357 (S.P.)], and the Federal Ministry of Education and Research (BMBF), Germany (A.B.K., FKZ: 01EO1501).

Conflicts of interest

The authors declare no conflict of interest.

Author contributions

S.P. conceived and designed the study and the experimental approaches. D.M., W.B.P., V.E.G., F.F., A.B.K., D.B.T., and J.L.S. carried out the experiments. D.M., W.B.P., V.E.G., A.B.K., C.K.K., T.S., and S.P. analyzed the data. D.M., W.B.P., V.E.G., and S.P. wrote the manuscript.

Literature cited

Andux S, Ellis RE. 2008. Apoptosis maintains oocyte quality in aging *Caenorhabditis elegans* females. PLoS Genet. 4(12):e1000295. https://doi.org/10.1371/journal.pgen.1000295

Downloaded from https://academic.oup.com/g3journal/article/14/11/jkae206/7750701 by Universitaets- und Landesbibliothek Duesseldorf user on 04 May 2026

Bohnekamp J, Schöneberg T. 2011. Cell adhesion receptor GPR133 couples to Gs protein. J Biol Chem. 286(49):41912–41916. https://doi.org/10.1074/jbc.C111.265934

Boucard AA, Maxeiner S, Sudhof TC. 2013. Latrophilins function as heterophilic cell-adhesion molecules by binding to teneurins: regulation by alternative splicing. J Biol Chem. 289(1):387–402. https://doi.org/10.1074/jbc.M113.504779

Brenner S. 1974. The genetics of *Caenorhabditis elegans*. Genetics. 77(1):71–94. https://doi.org/10.1093/genetics/77.1.71

Bui YK, Sternberg PW. 2002. *Caenorhabditis elegans* inositol 5-phosphatase homolog negatively regulates inositol 1,4,5-triphosphate signaling in ovulation. Mol Biol Cell. 13(5):1641–1651. https://doi.org/10.1091/mbc.02-01-0008

Byrd DT, Knobel K, Affeldt K, Crittenden SL, Kimble J. 2014. A DTC niche plexus surrounds the germline stem cell pool in *Caenorhabditis elegans*. PLoS One. 9(2):e88372. https://doi.org/10.1371/journal.pone.0088372

Carranza-Garcia E, Navarro RE. 2019. Apoptosis contributes to protect germ cells from the oogenic germline starvation response but is not essential for the gonad shrinking or recovery observed during adult reproductive diapause in *C. elegans*. PLoS One. 14(6):e0218265. https://doi.org/10.1371/journal.pone.0218265

Chen C, Fenk LA, de Bono M. 2013. Efficient genome editing in *Caenorhabditis elegans* by CRISPR-targeted homologous recombination. Nucleic Acids Res. 41(20):e193. https://doi.org/10.1093/nar/gkt805

Chen AT, Guo C, Itani OA, Budaitis BG, Williams TW, Hopkins CE, McEachin RC, Pande M, Grant AR, Yoshina S, *et al.* 2015. Longevity genes revealed by integrative analysis of isoform-specific daf-16/FoxO mutants of *Caenorhabditis elegans*. Genetics. 201(2):613–629. https://doi.org/10.1534/genetics.115.177998

Cheng H, Govindan JA, Greenstein D. 2008. Regulated trafficking of the MSP/Eph receptor during oocyte meiotic maturation in *C. elegans*. Curr Biol. 18(10):705–714. https://doi.org/10.1016/j.cub.2008.04.043

Clandinin TR, DeModena JA, Sternberg PW. 1998. Inositol trisphosphate mediates a RAS-independent response to LET-23 receptor tyrosine kinase activation in *C. elegans*. Cell. 92(4):523–533. https://doi.org/10.1016/S0092-8674(00)80945-9

Dickinson DJ, Ward JD, Reiner DJ, Goldstein B. 2013. Engineering the *Caenorhabditis elegans* genome using Cas9-triggered homologous recombination. Nat Methods. 10(10):1028–1034. https://doi.org/10.1038/nmeth.2641

Dobin A, Gingeras TR. 2015. Mapping RNA-seq reads with STAR. Curr Protoc Bioinformatics. 51(1):11.14.1–19. https://doi.org/10.1002/0471250953.bi1114s51

Dolphin CT, Hope IA. 2006. *Caenorhabditis elegans* reporter fusion genes generated by seamless modification of large genomic DNA clones. Nucleic Acids Res. 34(9):e72. https://doi.org/10.1093/nar/gkl352

Einspahr JM, Tilley DG. 2022. Pathophysiological impact of the adhesion G protein-coupled receptor family. Am J Physiol Cell Physiol. 323(2):C640–C647. https://doi.org/10.1152/ajpcell.00445.2021

Francis R, Barton MK, Kimble J, Schedl T. 1995. gld-1, a tumor suppressor gene required for oocyte development in *Caenorhabditis elegans*. Genetics. 139(2):579–606. https://doi.org/10.1093/genetics/139.2.579

Friedland AE, Tzur YB, Esvelt KM, Colaiácovo MP, Church GM, Calarco JA. 2013. Heritable genome editing in *C. elegans* via a CRISPR-Cas9 system. Nat Methods. 10(8):741–743. https://doi.org/10.1038/nmeth.2532

Gartner A, Boag PR, Blackwell TK. 2008. Germline survival and apoptosis. WormBook. 1–20. https://doi.org/10.1895/wormbook.1.145.1

Gibson DG, Young L, Chuang RY, Venter JC, Hutchison CA 3rd, Smith HO. 2009. Enzymatic assembly of DNA molecules up to several hundred kilobases. Nat Methods. 6(5):343–345. https://doi.org/10.1038/nmeth.1318

Gumienny TL, Lambie E, Hartwieg E, Horvitz HR, Hengartner MO. 1999. Genetic control of programmed cell death in the *Caenorhabditis elegans* hermaphrodite germline. Development. 126(5):1011–1022. https://doi.org/10.1242/dev.126.5.1011.

Gupte J, Swaminath G, Danao J, Tian H, Li Y, Wu X. 2012. Signaling property study of adhesion G-protein-coupled receptors. FEBS Lett. 586(8):1214–1219. https://doi.org/10.1016/j.febslet.2012.03.014

Hall DH, Winfrey VP, Blaeuer G, Hoffman LH, Furuta T, Rose KL, Hobert O, Greenstein D. 1999. Ultrastructural features of the adult hermaphrodite gonad of *Caenorhabditis elegans*: relations between the germ line and soma. Dev Biol. 212(1):101–123. https://doi.org/10.1006/dbio.1999.9356

Hamann J, Aust G, Araç D, Engel FB, Formstone C, Fredriksson R, Hall RA, Harty BL, Kirchhoff C, Knapp B, *et al.* 2015. International Union of basic and clinical pharmacology. XCIV. Adhesion G protein-coupled receptors. Pharmacol Rev. 67(2):338–367. https://doi.org/10.1124/pr.114.009647

Hammerquist AM, Yen CA, Curran SP. 2021. Analysis of *Caenorhabditis elegans* sperm number, size, activation, and mitochondrial content. Bio Protoc. 11(11):e4035. https://doi.org/10.21769/BioProtoc.4035

Han SM, Cottee PA, Miller MA. 2010. Sperm and oocyte communication mechanisms controlling *C. elegans* fertility. Dev Dyn. 239(5):1265–1281. https://doi.org/10.1002/dvdy.22202

Hoang HD, Prasain JK, Dorand D, Miller MA. 2013. A heterogeneous mixture of F-series prostaglandins promotes sperm guidance in the *Caenorhabditis elegans* reproductive tract. PLoS Genet. 9(1):e1003271. https://doi.org/10.1371/journal.pgen.1003271

Howe KL, Bolt BJ, Shafie M, Kersey P, Berriman M. 2017. WormBase ParaSite—a comprehensive resource for helminth genomics. Mol Biochem Parasitol. 215:2–10. https://doi.org/10.1016/j.molbiopara.2016.11.005

Hsiao CC, Keysselt K, Chen HY, Sittig D, Hamann J, Lin HH, Aust G. 2015. The adhesion GPCR CD97/ADGRE5 inhibits apoptosis. Int J Biochem Cell Biol. 65:197–208. https://doi.org/10.1016/j.biocel.2015.06.007

Hu M, Tiwary E, Prasain JK, Miller M, Serra R. 2021. Mechanisms of TGFss in prostaglandin synthesis and sperm guidance in *Caenorhabditis elegans*. Dev Dyn. 250(7):932–942. https://doi.org/10.1002/dvdy.296

Jones AR, Francis R, Schedl T. 1996. GLD-1, a cytoplasmic protein essential for oocyte differentiation, shows stage- and sex-specific expression during *Caenorhabditis elegans* germline development. Dev Biol. 180(1):165–183. https://doi.org/10.1006/dbio.1996.0293

Knierim AB, Röthe J, Çakir MV, Lede V, Wilde C, Liebscher I, Thor D, Schöneberg T. 2019. Genetic basis of functional variability in adhesion G protein-coupled receptors. Sci Rep. 9(1):11036. https://doi.org/10.1038/s41598-019-46265-x

Kodama Y, Shumway M, Leinonen R; International Nucleotide Sequence Database Collaboration. 2012. The sequence read archive: explosive growth of sequencing data. Nucleic Acids Res. 40(D1):D54–D56. https://doi.org/10.1093/nar/gkr854

Kubagawa HM, Watts JL, Corrigan C, Edmonds JW, Sztul E, Browse J, Miller MA. 2006. Oocyte signals derived from polyunsaturated fatty acids control sperm recruitment in vivo. Nat Cell Biol. 8(10):1143–1148. https://doi.org/10.1038/ncb1476

Langenhan T, Prömel S, Mestek L, Esmaeili B, Waller-Evans H, Hennig C, Kohara Y, Avery L, Vakonakis I, Schnabel R, *et al.*

Downloaded from https://academic.oup.com/g3journal/article/14/11/jkae206/7750701 by Universitaets- und Landesbibliothek Duesseldorf user on 04 May 2026

2009. Latrophilin signaling links anterior-posterior tissue polarity and oriented cell divisions in the *C. elegans* embryo. Dev Cell. 17(4):494–504. https://doi.org/10.1016/j.devcel.2009.08.008

Leinonen R, Sugawara H, Shumway M; International Nucleotide Sequence Database Collaboration. 2011. The sequence read archive. Nucleic Acids Res. 39(Database): D19–D21. https://doi.org/10.1093/nar/gkq1019

L'Hernault SW. 2006. Spermatogenesis. WormBook. p. 1–14. https://doi.org/10.1895/wormbook.1.85.1

Liebscher I, Cevheroğlu O, Hsiao CC, Maia AF, Schihada H, Scholz N, Soave M, Spiess K, Trajković K, Kosloff M, *et al.* 2022. A guide to adhesion GPCR research. FEBS J. 289(24):7610–7630. https://doi.org/10.1111/febs.16258

Lin HH, Chang GW, Davies JQ, Stacey M, Harris J, Gordon S. 2004. Autocatalytic cleavage of the EMR2 receptor occurs at a conserved G protein-coupled receptor proteolytic site motif. J Biol Chem. 279(30):31823–31832. https://doi.org/10.1074/jbc.M402974200

Matus D, Post WB, Horn S, Schoneberg T, Promel S. 2022. Latrophilin-1 drives neuron morphogenesis and shapes chemo- and mechanosensation-dependent behavior in *C. elegans* via a trans function. Biochem Biophys Res Commun. 589:152–158. https://doi.org/10.1016/j.bbrc.2021.12.006

Müller A, Winkler J, Fiedler F, Sastradihardja T, Binder C, Schnabel R, Kungel J, Rothemund S, Hennig C, Schöneberg T, *et al.* 2015. Oriented cell division in the *C. elegans* embryo is coordinated by G-protein signaling dependent on the adhesion GPCR LAT-1. PLoS Genet. 11(10):e1005624. https://doi.org/10.1371/journal.pgen.1005624

Okajima D, Kudo G, Yokota H. 2010. Brain-specific angiogenesis inhibitor 2 (BAI2) may be activated by proteolytic processing. J Recept Signal Transduct Res. 30(3):143–153. https://doi.org/10.3109/10799891003671139

Patat O, Pagin A, Siegfried A, Mitchell V, Chassaing N, Faguer S, Monteil L, Gaston V, Bujan L, Courtade-Saïdi M, *et al.* 2016. Truncating mutations in the adhesion G protein-coupled receptor G2 gene ADGRG2 cause an X-linked congenital bilateral absence of vas deferens. Am J Hum Genet. 99(2):437–442. https://doi.org/10.1016/j.ajhg.2016.06.012

Patra C, van Amerongen MJ, Ghosh S, Ricciardi F, Sajjad A, Novoyatleva T, Mogha A, Monk KR, Mühlfeld C, Engel FB. 2013. Organ-specific function of adhesion G protein-coupled receptor GPR126 is domain-dependent. Proc Natl Acad Sci U S A. 110(42):16898–16903. https://doi.org/10.1073/pnas.1304837110

Pertea M, Pertea GM, Antonescu CM, Chang TC, Mendell JT, Salzberg SL. 2015. StringTie enables improved reconstruction of a transcriptome from RNA-seq reads. Nat Biotechnol. 33(3):290–295. https://doi.org/10.1038/nbt.3122

Prömel S, Frickenhaus M, Hughes S, Mestek L, Staunton D, Woollard A, Vakonakis I, Schöneberg T, Schnabel R, Russ AP, *et al.* 2012. The GPS motif is a molecular switch for bimodal activities of adhesion class G protein-coupled receptors. Cell Rep. 2(2):321–331. https://doi.org/10.1016/j.celrep.2012.06.015

Radman I, Greiss S, Chin JW. 2013. Efficient and rapid *C. elegans* transgenesis by bombardment and hygromycin B selection. PLoS One. 8(10):e76019. https://doi.org/10.1371/journal.pone.0076019

Robinson JT, Thorvaldsdóttir H, Winckler W, Guttman M, Lander ES, Getz G, Mesirov JP. 2011. Integrative genomics viewer. Nat Biotechnol. 29(1):24–26. https://doi.org/10.1038/nbt.1754

Rosa M, Noel T, Harris M, Ladds G. 2021. Emerging roles of adhesion G protein-coupled receptors. Biochem Soc Trans. 49(4):1695–1709. https://doi.org/10.1042/BST20201144

Röthe J, Thor D, Winkler J, Knierim AB, Binder C, Huth S, Kraft R, Rothemund S, Schöneberg T, Prömel S. 2019. Involvement of the adhesion GPCRs latrophilins in the regulation of insulin release. Cell Rep. 26(6):1573–1584.e1575. https://doi.org/10.1016/j.celrep.2019.01.040

Schindelin J, Arganda-Carreras I, Frise E, Kaynig V, Longair M, Pietzsch T, Preibisch S, Rueden C, Saalfeld S, Schmid B, *et al.* 2012. Fiji: an open-source platform for biological-image analysis. Nat Methods. 9(7):676–682. https://doi.org/10.1038/nmeth.2019

Schneider CA, Rasband WS, Eliceiri KW. 2012. NIH image to ImageJ: 25 years of image analysis. Nat Methods. 9(7):671–675. https://doi.org/10.1038/nmeth.2089

Seufert F, Chung YK, Hildebrand PW, Langenhan T. 2023. 7TM domain structures of adhesion GPCRs: what's new and what's missing? Trends Biochem Sci. 48(8):726–739. https://doi.org/10.1016/j.tibs.2023.05.007

Shiu FH, Wong JC, Yamamoto T, Lala T, Purcell RH, Owino S, Zhu D, Van Meir EG, Hall RA, Escayg A. 2022. Mice lacking full length Adgrb1 (Bai1) exhibit social deficits, increased seizure susceptibility, and altered brain development. Exp Neurol. 351:113994. https://doi.org/10.1016/j.expneurol.2022.113994

Steimel A, Wong L, Najarro EH, Ackley BD, Garriga G, Hutter H. 2010. The Flamingo ortholog FMI-1 controls pioneer-dependent navigation of follower axons in *C. elegans*. Development. 137(21):3663–3673. https://doi.org/10.1242/dev.054320

Tourasse NJ, Millet JRM, Dupuy D. 2017. Quantitative RNA-seq meta-analysis of alternative exon usage in C. elegans. Genome Res. 27(12):2120–2128. https://doi.org/10.1101/gr.224626.117

Tu YK, Duman JG, Tolias KF. 2018. The adhesion-GPCR BAI1 promotes excitatory synaptogenesis by coordinating bidirectional trans-synaptic signaling. J Neurosci. 38(39):8388–8406. https://doi.org/10.1523/JNEUROSCI.3461-17.2018

Tursun B, Cochella L, Carrera I, Hobert O. 2009. A toolkit and robust pipeline for the generation of fosmid-based reporter genes in *C. elegans*. PLoS One. 4(3):e4625. https://doi.org/10.1371/journal.pone.0004625

Waaijers S, Muñoz J, Berends C, Ramalho JJ, Goerdayal SS, Low TY, Zoumaro-Djayoon AD, Hoffmann M, Koorman T, Tas RP, *et al.* 2016. A tissue-specific protein purification approach in *Caenorhabditis elegans* identifies novel interaction partners of DLG-1/discs large. BMC Biol. 14(1):66. https://doi.org/10.1186/s12915-016-0286-x

Ward Y, Lake R, Faraji F, Sperger J, Martin P, Gilliard C, Ku KP, Rodems T, Niles D, Tillman H, *et al.* 2018. Platelets promote metastasis via binding tumor CD97 leading to bidirectional signaling that coordinates transendothelial migration. Cell Rep. 23(3):808–822. https://doi.org/10.1016/j.celrep.2018.03.092

Warming S, Costantino N, Court DL, Jenkins NA, Copeland NG. 2005. Simple and highly efficient BAC recombineering using galK selection. Nucleic Acids Res. 33(4):e36. https://doi.org/10.1093/nar/gni035

Zhou Z, Hartwieg E, Horvitz HR. 2001. CED-1 is a transmembrane receptor that mediates cell corpse engulfment in *C. elegans*. Cell. 104(1):43–56. https://doi.org/10.1016/S0092-8674(01)00190-8

Zuko A, Oguro-Ando A, Post H, Taggenbrock RL, van Dijk RE, Altelaar AF, Heck AJ, Petrenko AG, van der Zwaag B, Shimoda Y, *et al.* 2016. Association of cell adhesion molecules contactin-6 and latrophilin-1 regulates neuronal apoptosis. Front Mol Neurosci. 9:143. https://doi.org/10.3389/fnmol.2016.00143

Editor: S. Lee

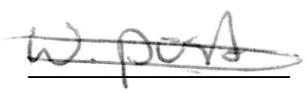
Downloaded from https://academic.oup.com/g3journal/article/14/11/jkae206/7750701 by Universitaets- und Landesbibliothek Duesseldorf user on 04 May 2026

Detailed author contributions

For the publication 'The N terminus-only (*trans*) function of the Adhesion GPCR Latrophilin-1 controls multiple processes in reproduction of *C. elegans*', the following contributions were made by Willem Berend Post:

- Nematode maintenance
- Generation of transgenic lines *via* CRISPR/Cas9
- Ovulation rate assays
- Sperm activation assays
- Oocyte size and area measurements
- SYTO12 staining and imaging
- CED-1::GFP imaging
- Antibody and DAPI staining
- (Confocal) microscopy
- Generation of constructs
- Data analysis
- Manuscript writing

Date: 6th May 2026





Willem Berend Post

Prof. Dr. Simone Prömel

4 Notch activity is modulated by the aGPCR Latrophilin binding the DSL ligand in *C. elegans*

Willem Berend Post[#], Victoria Elisabeth Groß[#], Daniel Matúš[#], Iannis Charnay, Fabian Liessmann, Florian Seufert, Peter Hildebrand, Jens Meiler, Anette Kaiser, Torsten Schöneberg & Simone Prömel

[#] These authors contributed equally to this work

Journal: Nature Communications

Publisher: Nature Publishing Group (npg)

Impact Factor: 15.7

Submitted: 14 November 2024

Accepted: 30 June 2025

Published: 12 July 2025

DOI: https://doi.org/10.1038/s41467-025-61730-0

PubMed ID: 40651965

nature communications

Article

https://doi.org/10.1038/s41467-025-61730-0

Notch activity is modulated by the aGPCR Latrophilin binding the DSL ligand in *C. elegans*

Received: 14 November 2024

Accepted: 30 June 2025

Published online: 12 July 2025

Check for updates

Willem Berend Post[1,10], Victoria Elisabeth Groß[1,10], Daniel Matúš[2,3,10], Iannis Charnay[1], Fabian Liessmann[4], Florian Seufert[5], Peter Hildebrand[5], Jens Meiler[4,6,7], Anette Kaiser[8], Torsten Schöneberg[2,9] & Simone Prömel[1]

The Notch pathway is a highly conserved signaling cascade across metazoans that regulates numerous physiological processes, including cell proliferation, differentiation, and fate determination. Given its fundamental roles, the pathway is tightly regulated by diverse molecules through multiple mechanisms. Here, we identify the Adhesion GPCR latrophilin (LPHN/ADGRL) as a positive modulator of Notch signaling, which increases Notch receptor activation and the translocation of its intracellular domain into the nucleus. Physiologically, this latrophilin role is crucial for balancing the number of proliferating cells in the gonadal stem cell niche of the nematode *C. elegans*. In silico, in vitro, and in vivo analyses demonstrate that the *C. elegans* latrophilin homolog LAT-1 directly interacts with the DSL protein/Notch ligand LAG-2 on the same cell. This interaction is mediated by LAT-1's conserved GAIN and the RBL domain. Importantly, the modulatory effect depends solely on the receptor's N terminus and is independent of G protein signaling. Finally, we explore the implications of this fine-tuning of Notch signaling by an aGPCR.

Adhesion *G* protein-coupled receptors (aGPCRs) are unique receptors involved in various (patho-)physiological processes (summarized in refs. 1–3). Beyond transmitting traditional *G* protein-mediated signals[4,5], their large N termini enable them to perform functions independent of canonical signaling (often referred to as *N* terminus-only, *trans*, or seven transmembrane domain (7TM)-independent functions). These include facilitating cell-cell and cell-matrix adhesion[1,6], as well as influencing other signaling pathways. For instance, some aGPCRs have been shown to modulate Wnt signaling[7–10]. This versatility positions aGPCRs as key integrators of diverse physiological signals.

In this study, we present evidence that the aGPCR latrophilin (LAT/LPHN/ADGRL) interacts with the Notch pathway, modulating its activity by enhancing the activation of the Notch receptor. The Notch pathway is one of the most essential signaling cascades in many organisms governing numerous physiological processes such as development and tissue morphogenesis (summarized in refs. 11,12). Due to its fundamental role, many components of the Notch pathway and the underlying mechanisms are highly conserved across species[13–15]. In the nematode *C. elegans*, the Notch pathway controls, among others, germ cell division and the balance between germ cell proliferation (self-renewal) in the gonadal stem cell niche and

[1]Institute of Cell Biology, Department of Biology, Heinrich Heine University Düsseldorf, Düsseldorf, Germany. [2]Rudolf Schönheimer Institute of Biochemistry, Medical Faculty, Leipzig University, Leipzig, Germany. [3]Department of Molecular and Cellular Physiology, Stanford University, Stanford, CA, USA. [4]Institute for Drug Development, Faculty of Medicine, Leipzig University, Leipzig, Germany. [5]Institute of Medical Physics and Biophysics, Medical Faculty, Leipzig University, Leipzig, Germany. [6]Center for Scalable Data Analytics and Artificial Intelligence ScaDS.AI, Leipzig University, Leipzig, Germany. [7]Department of Chemistry, Center for Structural Biology, Vanderbilt University, Nashville, TN, USA. [8]Department of Anaesthesiology and Intensive Care, Medical Faculty, Leipzig University, Leipzig, Germany. [9]School of Medicine, University of Global Health Equity, Kigali, Rwanda. [10]These authors contributed equally: Willem Berend Post, Victoria Elisabeth Groß, Daniel Matúš. e-mail: proemel@uni-duesseldorf.de

differentiation into germ cell progenitors (entry into meiosis). Thereby, it promotes proliferation while suppressing meiotic entry[16–20]. The signal originates from the distal tip cell (DTC), where LAG-2, a membrane-bound Notch ligand of the Delta, Serrate, LAG-2 (DSL) family, interacts with the Notch receptor GLP-1 on adjacent germ cells[19–21] thereby activating it and initiating the Notch pathway.

Here, we show that LAT-1, the *C. elegans* homolog of the aGPCR latrophilin, directly interacts with the Notch ligand LAG-2 and enhances Notch receptor activation. This interaction increases Notch activity solely via the aGPCR N terminus (N terminus-only/*trans*/7TM-independent function) and modulates cell proliferation within the gonadal stem cell niche.

Results

LAT-1 modulates germ cell proliferation

Recently, we discovered that the 7TM-independent/N terminus-only/*trans* function of LAT-1 in *C. elegans* regulates various processes, including germ cell apoptosis, ovulation, and sperm guidance, ultimately controlling reproduction[22]. In our analysis of hermaphrodites homozygous for the null allele *lat-1(ok1465)* (hereafter referred to as *lat-1*), we also observed a reduced number of germ cells in the distal region of the gonad (Fig. 1a, b). This reduction primarily affects the progenitor zone but also extends to the transition zone and the pachytene stage (Fig. 1a, c). Using mNeonGreen-fused REC-8 as a marker for progenitor zone nuclei[23], we confirmed that the size of the progenitor zone of *lat-1* mutants is indeed modestly yet significantly smaller than in wild-type hermaphrodites (Fig. 1d, e). Time-course analyses revealed that these phenotypes were most prominent in worms aged L4 + 8 h (Supplementary Fig. 1a–c). Consequently, all subsequent experiments were conducted on individuals at this stage.

To further characterize the effects of LAT-1 on distal germ cells, cell proliferation was studied by assessing both mitotic (M) phase (using an anti-phospho-histone H3 (Ser10) (PH3) antibody) and synthesis (S) phase (using EdU staining) nuclei. These analyses revealed a decrease in both mitotic (Fig. 1f–h) and DNA synthesis (Fig. 1i–k) events in *lat-1* mutants.

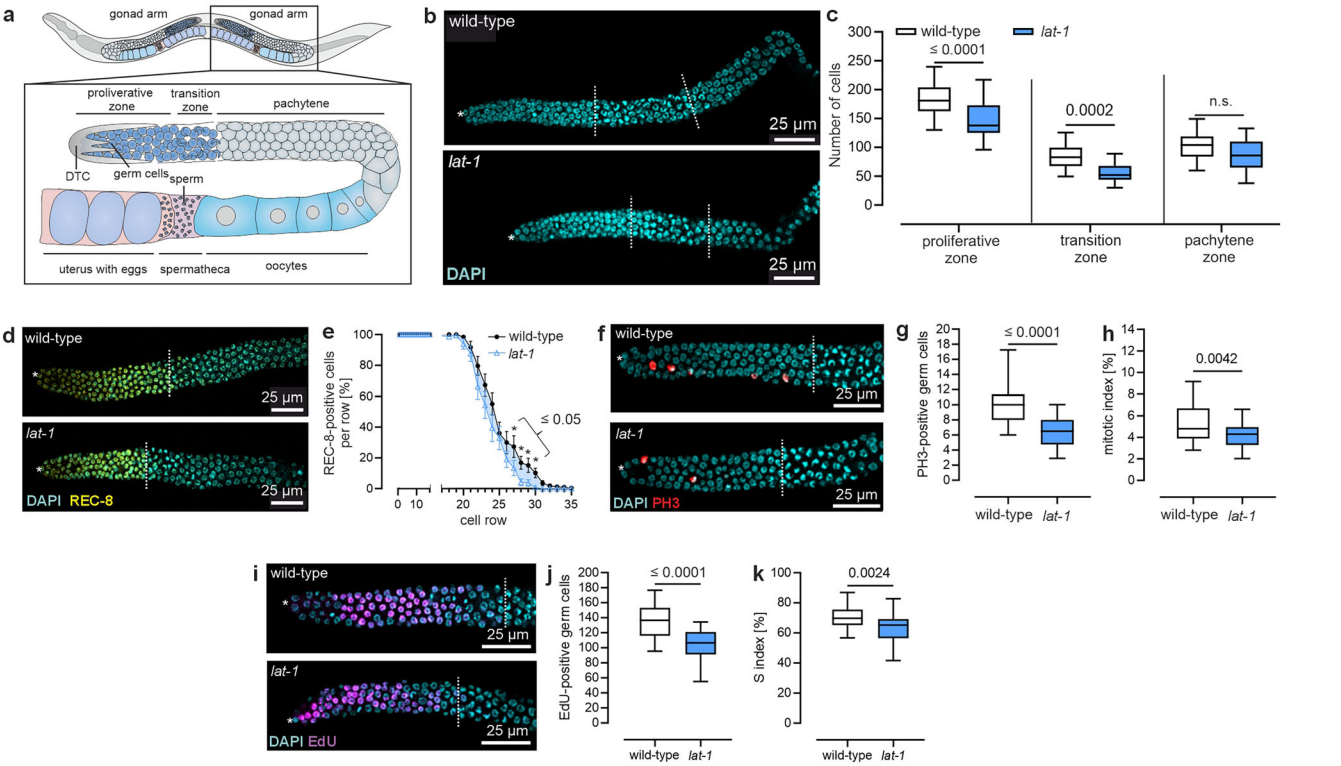


Fig. 1 | Nematodes lacking *lat-1* display a reduction in germ cells. a Schematic depiction of the adult *C. elegans* gonad. The nematode has two symmetrical U-shaped gonads where oocytes are produced during adulthood. The most distal part of each gonad arm, the progenitor zone, is encased by the distal tip cell (DTC). Within this zone, germ cells undergo continuous self-renewal through mitotic divisions. Subsequently, they enter meiosis in the transition zone, where they arrest in the pachytene before cellularizing, growing, and progressing further through meiotic development. Eventually, the oocytes are pushed through the spermatheca, where sperm, produced during the last larval stage, is stored. After fertilization, the eggs move to the uterus and are laid. **b** Hermaphrodite gonads lacking LAT-1 display altered germ cell zone sizes. Shown are two representative images of gonads of L4 + 8 h-old hermaphrodites. Asterisks: DTC; dashed lines: zones (**c**) Quantification of germ cell numbers in (**b**) reveals shorter zones in *lat-1* worms. Wild-type: $n = 33$, *lat-1*: $n = 19$ in four independent experiments. **d** Expression of mNeonGreen-fused *rec-8* ceases in more distal germ cell rows in *lat-1* individuals compared to wild-type controls. Asterisks: DTC; dashed lines: end of progenitor zone. **e** Quantification of REC-8-positive cells per cell row shown in (**d**) confirms the shorter progenitor zone and thus, the earlier change in the transition from progenitor (REC-8-positive cells) to meiotic (REC-8-negative cells) fate in *lat-1* mutant germlines. Wild-type: $n = 23$, *lat-1*: $n = 18$ in four independent experiments. Exact *p* values are provided in the Source Data. **f** Representative images of PH3-stained gonads of 8 h-post-L4 *lat–1* and wild-type individuals. Asterisks: DTC; dashed lines: end of progenitor zone. **g** PH3-stained germlines from (**f**) reveal a lower incidence of M phase nuclei in the progenitor zone of *lat-1* compared to wild-type gonads. Wild-type: $n = 44$, *lat-1*: $n = 38$ in six independent experiments. **h** *lat-1* mutant germlines have a decreased M index (percentage PH3-positive nuclei from all progenitor zone nuclei). Wild-type: $n = 44$, *lat-1*: $n = 38$ in six independent experiments. **i** EdU-stained gonads 8 h-post-L4 worms visualize S phase nuclei. Asterisks: DTC; dashed lines: end of progenitor zone. **j** Quantification of images from (**i**) demonstrates that the distal germline of *lat-1* hermaphrodites has more EdU-positive (S phase) nuclei than wild-type controls. Wild-type: $n = 34$, *lat-1*: $n = 26$ in 6 independent experiments. **k** Quantification of S indices based on images from (**i**). *lat-1* germlines have a decreased S index (percentage of EdU-positive nuclei from all progenitor zone nuclei). Wild-type: $n = 34$, *lat-1*: $n = 26$ in six independent experiments. Graph raw data are provided in the Source Data. Graph details and statistics are: (**c**), (**g**), (**h**), (**j**), (**k**): Box plots with median (center), interquartal range, 5th (lower whisker) and 95th (upper whisker) percentiles. **e**: Mean ± SEM. Two-sided unpaired t-test without multiple comparison correction.

Additionally, we calculated the M (Fig. 1h) and S (Fig. 1k) indices, defined as the percentage of M phase (PH3-positive) (Fig. 1g, Source data) or S phase (EdU-positive) (Fig. 1j, Source data) nuclei within the total number of nuclei in the progenitor zone. These indices, which can account for potential zone size differences, were lower in *lat-1* mutant compared to wild-type hermaphrodites. The observed effects in *lat-1* mutants were persistent at different temperatures (Supplementary Fig. 1d–f).

Taken together, our results indicate that LAT-1 plays a role in controlling cell proliferation and/or regulating zone size during the late L4/very early adult stage.

LAT-1 facilitates Notch signaling in the distal *C. elegans* germline

Various potentially coexisting mechanisms could lead to a reduction in the size of the germline zones, such as a smaller pool of mitotic cells or an altered cell cycle (reviewed in[24]). It is possible that LAT-1 plays a role in one or more of these processes. A key signaling cascade that promotes germ cell proliferation while suppressing meiotic entry, thereby regulating the balance between the two and determining the size of the progenitor zone, is the Notch pathway. Some, albeit by far not all, of the defects in *lat-1* nematodes resemble phenotypes reported in mutants of these Notch pathway components. For instance, a decreased number of proliferating cells and an altered progenitor zone size have been observed in *glp-1* reduction-of-function mutants[16,25], leading us to investigate whether LAT-1 affects the Notch pathway. In the *C. elegans* stem cell niche, the initial signal in this highly conserved cascade originates from the DTC, which expresses the DSL ligand *lag-2*. The interaction of this membrane-bound molecule with the Notch receptor GLP-1 on adjacent germ cells triggers the activation of GLP-1, which is cleaved twice with one cleavage by a γ secretase yielding the release of the Notch intracellular domain (NICD). This NICD acts as a transcription factor for the direct transcriptional targets (*lst-1*/*sygl-1*), which in turn repress *gld-1-3* and other mitosis-inhibiting or meiosis-promoting factors (Fig. 2a) (summarized in[26,27]).

To examine a potential interplay of *lat-1* with Notch, we first analyzed its downstream target *gld-1*, which inhibits cell proliferation[26,28], in *lat-1* mutants using a GLD-1::GFP reporter. In wild-type hermaphrodites, *gld-1* expression begins and intensifies as the repressing effect of the Notch signal diminishes at a certain distance from the DTC[29]. In contrast, *lat-1* mutants showed a significant upregulation of *gld-1* in more distal germ cells, starting from germ cell row ~14 (Fig. 2b, c). This suggests that LAT-1 influences downstream effectors of the Notch pathway. While GLD-1 is a known downstream target of Notch signaling, research indicates that it can also be regulated by other molecules, particularly those involved in cell cycle control[30].

To investigate whether LAT-1 operates within the Notch pathway, we analyzed genetic interactions between *lat-1* and the core Notch pathway components *lag-2* and *glp-1*. Similar to *lat-1* mutants, hermaphrodites carrying single reduction-of-function mutations in *lag-2* (*lag-2(q420)*[21]) and *glp-1* (*glp-1(bn18)*[31]) exhibit defects in germ cell proliferation and meiotic entry, resulting in a shorter progenitor zone (Fig. 2d) and concomitantly, reduced numbers of M phase nuclei (Fig. 2e, Supplementary Fig. 2a)[25,32,33]. The respective *lat-1*; *lag-2* and *lat-1*; *glp-1* double mutants did not show any difference in effect compared to the respective Notch component single mutants (Fig. 2d, e). No additive effects were observed suggesting that *lat-1* might act through key Notch signaling components rather than via another, parallel pathway. To further study the role of LAT-1, we examined a potential direct impact of the aGPCR on the Notch pathway. Upon ligand activation, the Notch receptor undergoes proteolytic processing, allowing for the translocation of its intracellular domain (NICD) to the nucleus, where it promotes the transcription of target genes (see above). Notch activation can be quantified by comparing the ratio of membrane-bound GLP-1 to GLP-1 within germ cell nuclei[34,35]. In *lat-1* nematodes, a decrease in nuclear GLP-1 was observed (Fig. 2f, g), suggesting that the aGPCR impacts Notch signaling. Meanwhile, overall expression levels of both *lag-2* and *glp-1* were unaffected by the absence of *lat-1* (Supplementary Fig. 2b–e).

As many functions of LAT-1 in the germline have been shown to depend solely on its *N* terminus (anchored to the membrane) rather than on G protein signaling[22], we tested whether this was also true for its role in Notch activation. Indeed, expressing only the *lat-1* N terminus tethered to the membrane via its first transmembrane domain (LNT) resulted in similar levels of Notch activation to those observed in wild-type worms (Fig. 2f, g). This confirms that the N terminus alone is sufficient to mediate LAT-1's effect on Notch activation.

Notch signaling is not only required in the germline, it is essential for numerous other processes in the adult nematode. Thus, we asked whether LAT-1 might also be involved in these contexts. As such, during development, Notch signaling is (among others) essential for the formation of the rectum/anus. *lag-2* mutant nematodes do not form a proper rectum/anus, a function that seems also dependent on *glp-1* and the other Notch receptor *lin-12*[20]. As *lat-1* has been shown to be expressed widely during development[36], we tested whether it might interact with Notch signaling here. We observed that *lat-1* mutant animals show anus defects comparable to *lag-2* mutants, albeit at a lower frequency, while the *lat-1; lag-2* double mutant was indistinguishable from the *lag-2* single mutant (Fig. 2h, i). Furthermore, we elucidated a potential interaction of *lat-1* with the Notch pathway in the nervous system where Notch signals control chemosensory avoidance of octanol[37]. As *lat-1* is also expressed on neurons[38], an interaction with *lag-2* in this context is also conceivable. Therefore, we assessed the avoidance behavior of *lat-1* mutants and found that these animals have a similarly delayed response in octanol avoidance compared to *lag-2* mutants, with double mutant animals showing no increased avoidance compared to single mutants (Fig. 2j). Thus, in both contexts, *lat-1* seems to interact with the Notch pathway hinting towards a wider involvement of LAT-1 in Notch signaling within *C. elegans* physiology.

In summary, these results show that LAT-1 cross-talks with the Notch pathway by modulating Notch receptor activity and regulating *gld-1* expression.

LAT-1 directly interacts with the Notch ligand LAG-2 via its RBL and GAIN domains

We next asked how LAT-1 exerts its modulatory effects on Notch-pathway activation. The primary source of the Notch signal controlling cell proliferation in the progenitor region is the DTC (Figs. 1a, 2a)[26], and its integrity is crucial for proper signaling. To determine whether the DTC morphology is affected in *lat-1* mutants, we examined the structure of this cell in hermaphrodites 8 h post-L4 stage. Both the plexus and cap length appeared similar to those in wild-type nematodes (Supplementary Fig. 3) indicating that the effect of LAT-1 on the Notch pathway is not caused by alterations in DTC morphology.

As the aGPCR is present on both the DTC and potentially germ cells[22], it is conceivable that it modulates Notch activity by directly interacting with the Notch receptor or ligand. To test this hypothesis, we predicted and analyzed in silico the potential interactions between the extracellular domains of LAT-1 with GLP-1 and LAG-2, respectively, using AlphaFold2 Multimer[39]. Based on the consistent domain-level contacts observed across multiple predicted structures and various domain combinations, the computational model supported a binding hypothesis with interactions between LAT-1 and LAG-2, but no convergence of binding interfaces between LAT-1 and GLP-1 was observed. The interaction with LAG-2 is mediated via the LAT-1 rhamnose-binding lectin (RBL) and GPCR autoproteolysis-inducing (GAIN) domains (Fig. 3a, b, Supplementary Fig. 4). We analyzed the AlphaFold2 Multimer-predicted complex using Rosetta and its interface analysis tools to further characterize the predicted LAT-1/LAG-2 binding interface. The total buried surface area at the interface was

https://doi.org/10.1038/s41467-025-61730-0

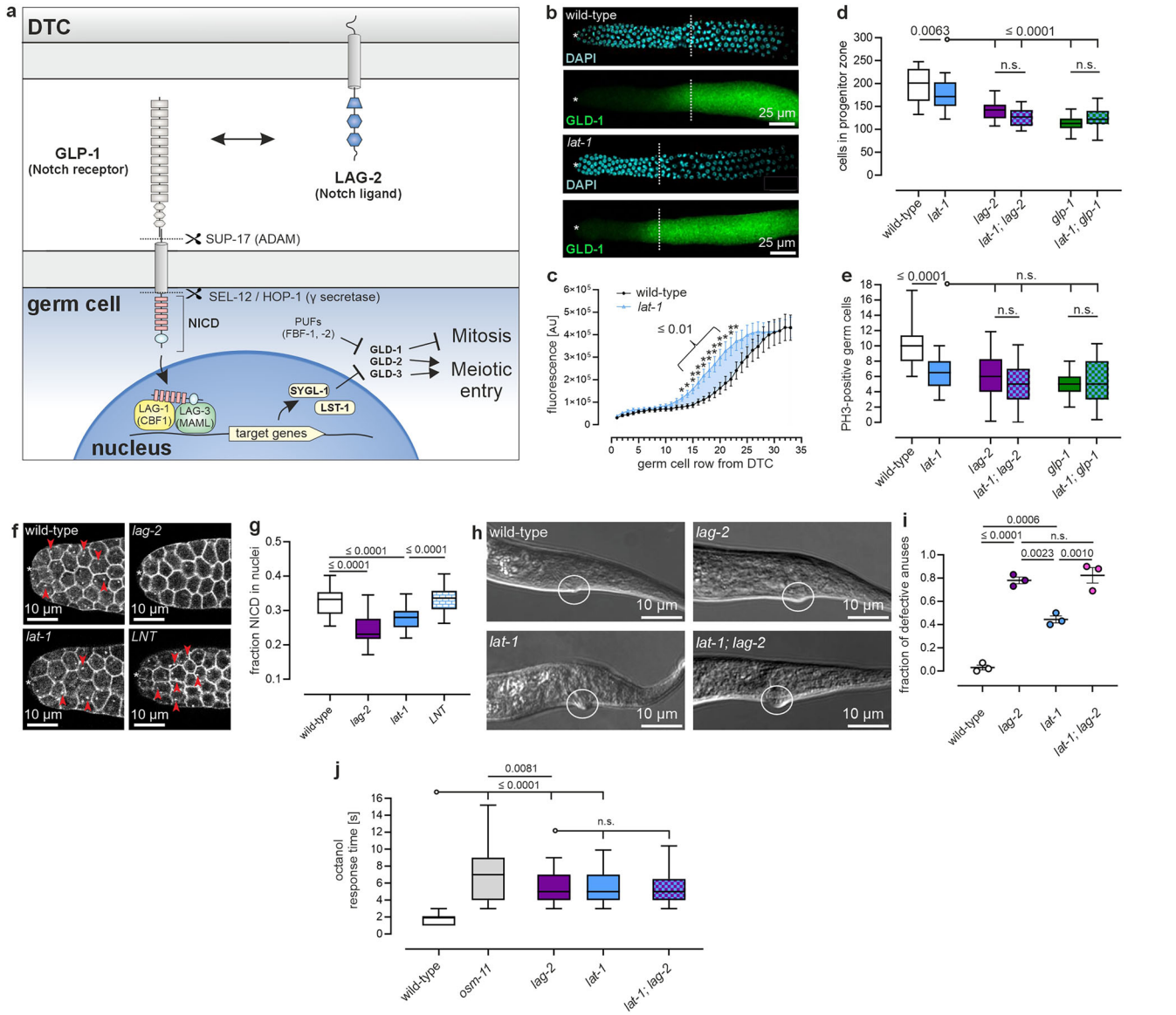


Fig. 2 | LAT-1 modulates Notch signaling in the distal gonad. a In the distal gonad, the Notch pathway controls cell proliferation and the switch between germ cell division and differentiation. It is initiated by the Notch ligand LAG-2 on the distal tip cell (DTC) binding to the Notch receptor GLP-1 present on germ cell membranes. This causes the Notch intracellular domain (NICD) to be cleaved off to translocate to the nucleus, initiating together with LAG-1 and LAG-3 the transcription of downstream effectors such as LST-1 and SYGL-1. In turn, these effectors repress expression of e.g., *gld-1-3*. **b** Expression of *gld-1* occurs more distally in *lat-1* mutant (bottom) than in wild-type (top) L4 + 8 h gonads. Asterisks: DTC, dashed lines: end of the progenitor zone. **c** Quantification of *gld-1::GFP* expression/germ cell row in *lat-1* and wild-type gonads by measuring fluorescence intensity with increasing distance from the distal tip cell based on images from (**b**). Loss of *lat-1* leads to a reduced repression of *gld-1*. Wild-type: $n = 17$, *lat-1*: $n = 22$ in four independent experiments. **d**, **e** Comparison of progenitor zones of Notch pathway component single mutants (*lag-2(q420)*, *glp-1(bn18)*) and respective double mutants with *lat-1(ok1465)*. Analyses are based on DAPI-/PH3-stained dissected gonads to visualize all and specifically M phase nuclei (for images see Supplementary Fig. 2a). The progenitor zone sizes in the double mutants differ from those in *lat-1* single mutants, but are similar to the respective Notch component single mutants (**d**). Overall, no differences in PH3-positive germ cell number were observed in single compared to double mutants (**e**). Replicate values: wild-type: 44, *lat-1*: 38, *lag-2*: 42, *lat-1; lag-2*: 36, *glp-1*: 41, *lat-1; glp-1*: 46 gonads in 6 independent experiments. **f** Notch activation was visualized using the GLP-1 NICD::V5 reporter *glp-1(q1000[glp-1::4xV5]*. In *lat-1* germline nuclei of L4 + 8 h-old hermaphrodites, less NICD is present than in the wild-type (red arrowheads) which is ameliorated by the presence of the *LNT*. The *lag-2(q420)* mutant (positive control) shows severely reduced NICD in cell nuclei. asterisks: DTC. **g** Quantification of the NICD fraction located in germ cell nuclei based on images in (**f**) confirms the reduced activity of Notch in *lat-1* mutants. Replicate values (independent experiments): wild-type: 33 (5), *lat-1*: 33 (3), *lag-2*: 21 (4), LNT: 16 (3). **h** DIC images showing anus morphology defects in L1 nematodes, which occurs both in *lat-1* and *lag-2* mutants. **i** Quantification of the images from (**h**). Wild-type: 127, *lag-2*: 122, *lat-1*: 167, *lat-1; lag-2*: 86 in three independent experiments. **j** *lat-1* mutant nematodes exhibit a similar delayed reversal upon exposure to octanol as *lag-2* mutants. Replicate values (independent experiments): wild-type: 75 (5), *osm-11*: 45 (3), *lat-1*: 75 (6), *lag-2*: 45 (3), *lat-1, lag-2*: 45 (3). Graph raw data are provided in the Source Data. Graph details and statistics are: (**c**): Mean *gld-1::GFP* expression/germ cell row ± SEM (replicates and exact p values in the Source Data). Two-sided unpaired t-test without multiple comparison correction. (**d**), (**e**), (**g**), (**i**), (**j**): Box plots with median (center), interquartal range, 5th (lower whisker) and 95th (upper whisker) percentiles. One-way ANOVA with Bonferroni post-hoc test. (**i**): Mean ± SEM. One-way ANOVA with Bonferroni post-hoc test.

https://doi.org/10.1038/s41467-025-61730-0

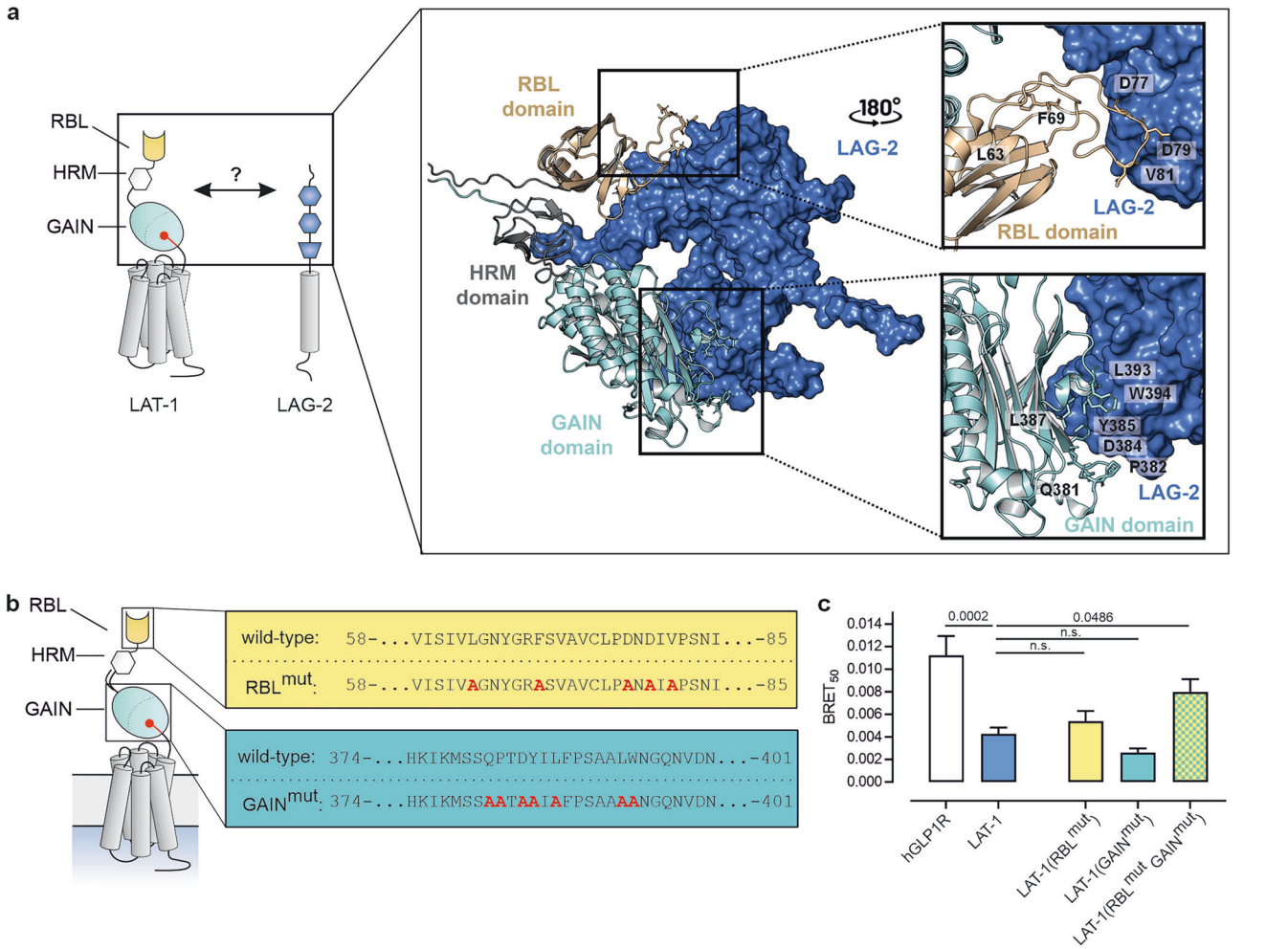


Fig. 3 | LAT-1 interacts with the Notch ligand LAG-2 in silico and in vitro. **a** AlphaFold2 Multimer models suggest an interaction between the extracellular region of LAG-2 (blue, surface representation) and both the RBL (yellow, cartoon representation) and GAIN (cyan, cartoon representation) domains of LAT-1. The interacting regions in LAT-1 include the main protruding loop of the RBL domain and a stretch of the GAIN domain. The HRM domain (gray, cartoon representation) is not involved in binding. Interacting residues are shown as stick representation. Details on energy breakdown values calculated using Rosetta's *per_residue_energies* application are given in Supplementary Fig. 4. **b** Location of the residues within RBL and GAIN domain of LAT-1 identified by models and energetic breakdown analyses (Supplementary Fig. 4) to be candidates to mediate the binding to LAG-2. **c** Nano Bioluminescence Resonance Energy Transfer (NanoBRET) analyses show an interaction of LAT-1 (Venus::LAT-1) with LAG-2 (Nluc::LAG-2) in HEK293 cells. The human GLP1R fused to Venus served as negative control. Note that higher $BRET_{50}$ values correspond to low binding affinity. Introduction of distinct point mutations in single domains predicted to be essential for the interaction (identified in (**a**–**c**)) do not significantly reduce affinity of LAT-1 for LAG-2, however, affinity is decreased when mutations in RBL and GAIN domain are combined. Mean ± SEM, $n = 4$ technical replicates in 11 (LAT-1), 8 (hGLP1R), 4 (LAT-1 (RBL^{mut})), 4 (LAT-1 ($GAIN^{mut}$)), 10 (LAT-1 (RBL^{mut} $GAIN^{mut}$)) independent experiments. One-way ANOVA with Bonferroni post-hoc test. Corresponding netBRET values and curves are shown in Supplementary Fig. 7b.

approximately 2768 Å², involving contributions from both the RBL and GAIN domain of LAT-1. Notably, the GAIN domain accounts for a larger portion of this interface, contributing 2089 Å². According to Rosetta InterfaceAnalyzer calculations, the interface consists of ~42% polar and 58% hydrophobic contacts. Several predicted hydrogen bonds contribute to complex stabilization, with six of these located within the GAIN domain. These findings support a mixed-mode interaction in which both specificity and stability are likely mediated by a combination of electrostatic and hydrophobic contacts.

To validate the AlphaFold2 Multimer-predicted complex and to investigate its conformational stability, we carried out all-atom molecular dynamics (MD) simulations. The structural integrity of the full LAG-2/GAIN-RBL complex was retained in all three repeats of 1-microsecond MD simulations. Within the simulation time, besides some thermal fluctuations of the GAIN and RBL domains against LAG-2, we did not observe major structural re-arrangements, validating the predicted complex (Supplementary Fig. 5).

Further analysis of these models and the per-residue energy breakdown of the interaction identified five amino acids in the RBL and seven in the GAIN domain to be crucial for the interaction (Fig. 3b, Supplementary Fig. 4). An evolutionary analysis showed that residues forming the binding interface are generally highly conserved among *Caenorhabditis* Spp. (Supplementary Fig. 6) potentially indicating that the interation is also conserved.

We next tested whether the predicted interaction between LAG-2 and LAT-1 indeed occurs in a cellular context. For this purpose, we conducted Nano Bioluminescence Resonance Energy Transfer (NanoBRET) experiments in vitro. In this setup, LAG-2 fused to a Nanoluciferase (Nluc::LAG-2) served as energy donor while Venus::LAT-1 was the acceptor. Both tags were in the extracellular *N* termini of the proteins. Constructs were expressed heterologously in HEK293 cells (Supplementary Fig. 7a). As negative control that does not interact with LAG-2, the human glucagon-like peptide-1 receptor (hGLP1R) fused to a Venus protein was employed. The NanoBRET analyses confirmed the

https://doi.org/10.1038/s41467-025-61730-0

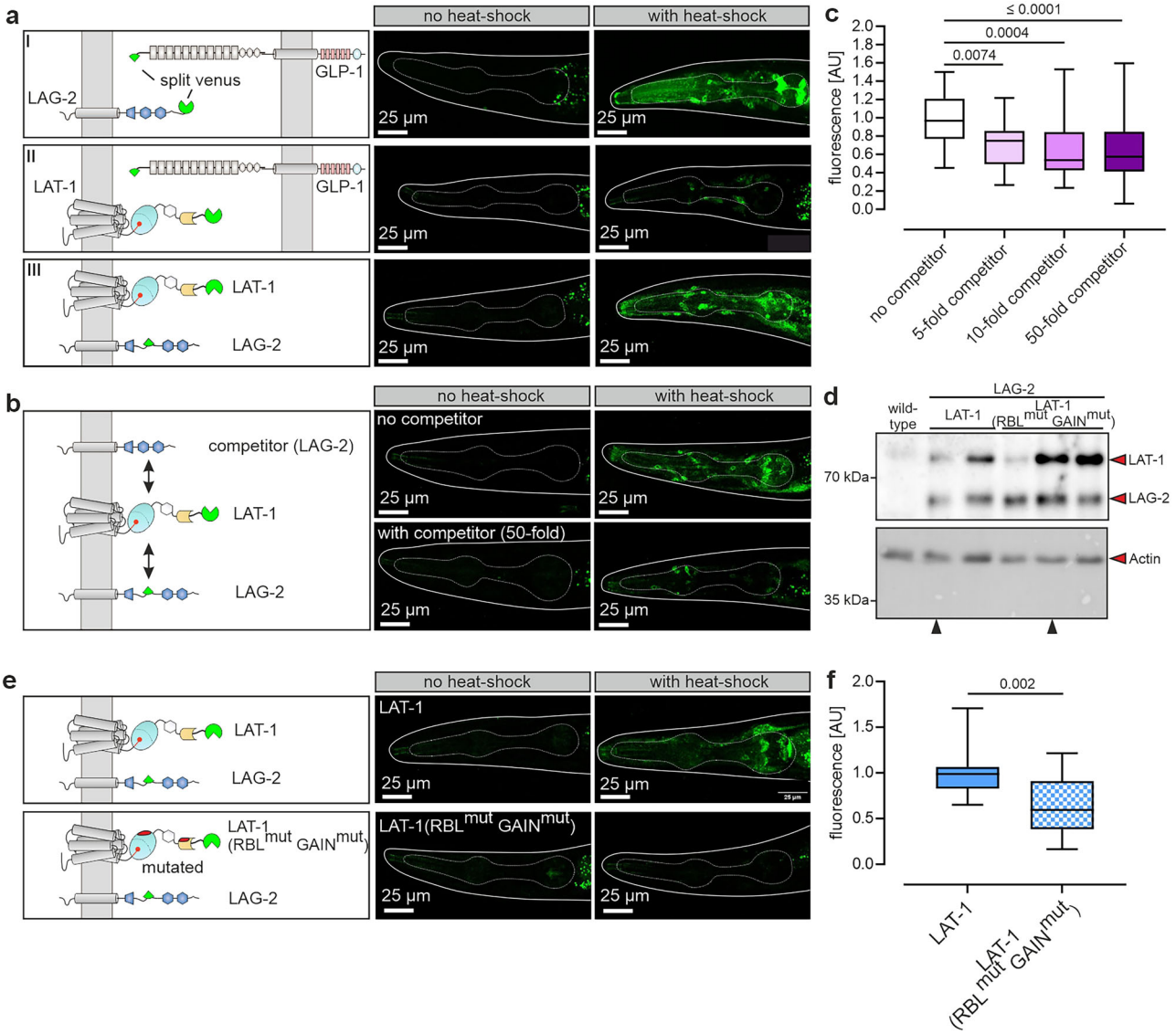


Fig. 4 | LAT-1 binds to LAG-2 in vivo. a, **b**, **e** Bimolecular fluorescence complementation (BiFC) analyses using the two parts of a split Venus protein (VN/VC) fused each to a protein of interest in *C. elegans*. Expression of these constructs is driven by the heat-shock promoter *hsp16.41p*. Upon heat shock, the proteins are produced, and a fluorescent signal occurs if they interact as the split Venus protein parts get into proximity, reconstitute, and fluoresce. For signal monitoring, the pharynx was chosen as the heat-shock promoter is highly active in pharyngeal neurons[43]. **a** LAG-2 binds to GLP-1 yielding a clear fluorescence signal after heat shock (I). Co-expression of *VN::lat-1* and *VC::glp-1* shows a very minor fluorescence signal, indicating that they do not interact (II). A strain harboring *VN::lat-1* and *VC::lag-2* together shows fluorescence after heat shock, indicating binding of the two (III). Shown are representative images of 22 (LAG-2; GLP-1), 35 (GLP-1; LAT-1) and 75 (LAT-1; LAG-2) heat-shocked worms. **b** Competition BiFC assay. In the strain expressing *VN::lat-1* and *VC::lag-2* (employed in (**a**) III), varying amounts of a construct containing an untagged *lag-2* serving as a competitor were introduced. Nematodes stably carrying all three constructs were heat-shocked, and fluorescence was measured. Hermaphrodites with 50-fold excess of untagged *lag-2* competitor relative to *VC::lag-2* (1 ng *VC::lag-2*/ 50 ng untagged *lag-2*) displayed severely less fluorescence. This indicates that LAT-1 interacts with the untagged LAG-2, which competes with VC::LAG-2. Shown are exemplary images. **c** Quantification of the competition BiFC assay from images shown in (**b**). Fluorescence significantly decreases with increasing amounts of untagged *lag-2* asa competitor. Four nematode lines carrying fixed amounts of *VN::lat-1* (1 ng) and *VC::lag-2* (1 ng) together with no competitor (same line as in (**a**) III), 5-fold (5 ng), 10-fold (10 ng), and 50-fold (50 ng) competitor, respectively, were used. To always maintain the same total amount of DNA, pBluescript was supplemented. Replicate values (independent experiments): no competitor: 75 (8), 5-fold: 17 (3), 10-fold: 21 (3), 50-fold: 24 (3). **d** Western Blot analysis confirms the expression of *lat-1* (V5-tagged, 81 kDa (autocatalytically cleaved)), *lag-2* (HA-tagged, 57 kDa), and mutated *lat-1(RBL^{mut} GAIN^{mut})* (V5-tagged, 81 kDa (autocatalytically cleaved)) on protein level in worm lines after heat shock and shows that the point mutations in LAT-1 do not hamper expression. Black arrowheads indicate the lines studied further in (**e**), (**f**). Actin served as a loading control. For full Western blots, see Supplementary Fig. 7e. Western Blot was performed twice with 60-80 worms per sample. **e** Exemplary images of BiFC using VC::LAG-2 and LAT-1(RBL^{mut} GAIN^{mut})::VN showing less fluorescence than in combination with a wild-type VN::LAT-1. **f** BiFC analysis using VC::LAG-2 in combination with VN::LAT-1 carrying the 12 point mutations of residues within the RBL/GAIN domains potentially essential for LAG-2 binding (Fig. 3b). Worm lines selected based on similar LAG-2, LAT-1, and LAT−1(RBL^{mut} GAIN^{mut}) protein levels (d, black arrowheads) were tested. The mutations lead to significantly reduced fluorescence levels compared to wild-type LAT-1. Replicate values (independent experiments): LAT-1: 26 (4), LAT-1 (RBL^{mut} GAIN^{mut}): 17 (3). Graph raw data are provided in the Source Data. Graph details and statistics are: (**c**), (**f**): Box plots with median (center), interquartal range, 5th (lower whisker) and 95th (upper whisker) percentiles. One-way ANOVA with Bonferroni post-hoc test (**c**). Two-sided unpaired t-test without multiple comparison correction (**f**).

proposed LAT-1/LAG-2 interaction, with $BRET_{50}$ values showing a significantly higher affinity of LAG-2 to LAT-1 than to the hGLP1R negative control (Fig. 3c, Supplementary Fig. 7b).

To further investigate the observed LAT-1/LAG-2 interaction, the amino acids in the RBL and GAIN domain of LAT-1 predicted to mediate the contact interface to LAG-2 were mutated to alanine (Fig. 3b). We verified that all mutated receptors remained intact and cell surface expression was similar to the wild-type (Supplementary Fig. 7c). Mutations in the GAIN domain alone did not affect protein-protein affinity ($BRET_{50}$) in the NanoBRET assay, while mutations in the RBL caused a slight, yet insignificant reduction (Fig. 3c). However, combining mutations in both the RBL and GAIN domains (LAT-1(RBL^{mut} $GAIN^{mut}$)) resulted in a significant two-fold decrease in affinity in the NanoBRET assays compared to the wild-type receptor (Fig. 3c), suggesting that LAT-1 indeed binds to LAG-2 via the RBL and the GAIN domains. It should be noted that a LAT-1 interaction with GLP-1 was not further investigated in this setting due to a lack in *glp-1* expression (see above).

In *C. elegans*, LAG-2 is only one of several Notch ligands. One of the other ligands, APX-1, is so closely related to LAG-2 that it can even compensate for its function in some contexts[40]. Thus, we tested whether APX-1 could have a similar affinity to LAT-1 as LAG-2. Upon expression of *Nluc::apx-1* with *Venus::lat-1*, low $BRET_{50}$ values showed that LAT-1 also has an affinity for APX-1 (Supplementary Fig. 7d), suggesting that LAT-1 may engage in a broader interaction mechanism with several Notch ligands. Notably, the five amino acids within the LAT-1 RBL domain and the seven within the GAIN domain, which are critical for LAG-2 binding (Fig. 3), also appear to contribute to the interaction with APX-1 (Supplementary Fig. 7d). This indicates that the mechanism underlying the binding might be a general one.

LAT-1 binds the Notch ligand LAG-2 in vivo

To determine whether the observed LAT-1/LAG-2 interaction occurs in vivo in *C. elegans*, Bimolecular Fluorescence Complementation (BiFC)[41,42] was conducted. For that purpose, the two parts of a split Venus protein (VN/VC) were fused to one of the interaction partners, each under the control of the heat-shock promoter *hsp16.41p*. Upon heat shock, the proteins are produced, and a fluorescent signal occurs if they are in close enough proximity to interact. As the heat-shock promotor is particularly strong in pharyngeal neurons[43], both proteins express at levels sufficient to allow detection of even weak interactions. Thus, we assessed the pharynx region to monitor potential BiFC signals. As a positive control, GLP-1 and LAG-2 were used, showing a clear signal upon heat shock (Fig. 4a I). Only very low signals were detected when assessing GLP-1 and LAT-1 (Fig. 4a II), adding to the in silico prediction that they might not interact. Distinct fluorescence was observed in strains carrying LAT-1 and LAG-2 (Fig. 4a III), suggesting that their interaction also occurs in an in vivo context.

It is important to note that, while all other in vivo experiments involving modified *lat-1* in this study rely on genomic editing, this particular assay used extrachromosomal arrays and heat-shock–induced overexpression for two main reasons: (1) endogenous LAT-1/LAG-2 interaction levels are likely too low to be detected, and (2) the reconstitution of the split Venus protein is nearly irreversible[44], potentially leading to stabilized interactions with detrimental effects, especially during development where both LAT-1[36] and Notch molecules[45–47] have important functions.

To ensure that the observed BiFC interaction was specific and not due to a spontaneous reconstitution of the split Venus fluorophores upon overexpression, competition BiFC was conducted[48,49]. In this assay, *VN::lat-1* and *VC::lag-2* were co-expressed with increasing concentrations of an untagged *lag-2* as competitor (5-fold, 10-fold, and 50-fold compared to *VC::lag-2*). If the interaction was specific, the fluorescent signal would decrease since the unlabeled LAG-2 competed with the labeled version. Indeed, a reduction in fluorescence was detected starting at 5-fold amount of competitor (Fig. 4b, c), indicating the specificity of the interaction.

Next, we tested whether the interaction is mediated via the RBL and GAIN domains in vivo as revealed in silico and in cell culture (see above). Therefore, the LAT-1 construct containing all residues predicted to be essential for LAG-2 binding mutated to alanine residues (LAT-1(RBL^{mut} $GAIN^{mut}$) was analyzed. First, the expression of this construct was verified and found to be consistent, with similar levels observed across several independently generated worm lines (Fig. 4d). BiFC analyses were performed for one line containing LAT-1(RBL^{mut} $GAIN^{mut}$) and LAG-2 at comparable protein levels (Fig. 4e, Supplementary Fig. 7e). Consistent with the in vitro results, LAT-1(RBL^{mut} $GAIN^{mut}$) showed a reduction in affinity to LAG-2 in vivo as indicated by a decrease of BiFC fluorescence (Fig. 4e, f).

These data show that LAT-1 positively modulates Notch signaling by directly interacting with the Notch ligand LAG-2 in vitro and in vivo. This LAT-1/LAG-2 binding appears to occur via the RBL and the GAIN domains.

LAT-1 functions from the DTC on neighboring germ cells

Our results indicate that LAT-1 increases Notch activation by binding to the ligand LAG-2 and that only the extracellular N terminus is essential for this, suggesting a *trans* function of the receptor. As LAT-1 is present on the DTC but also on germ cells[22], this raises the question of whether the LAT-1/LAG-2 interaction occurs *in cis* on the DTC or in trans with LAT-1 on the germ cells. To address this, we separately expressed *Nluc::lag-2* and *Venus::lat-1* in different populations of HEK293 cells and varied their ratio as well as the strength of *Venus::lat-1* expression to obtain a protein gradient similar to the experiments described above. The subsequent NanoBRET analyses revealed that with an increasing number of cells expressing *lat-1::Venus*, no NanoBRET window could be established (Fig. 5a), suggesting that a *cis* rather than a *trans* interaction occured. Similarly, increasing the protein expression in the *lat-1::Venus* expressing cells failed to induce a BRET window (Fig. 5a), further strengthening the hypothesis that the interaction forms in *cis*.

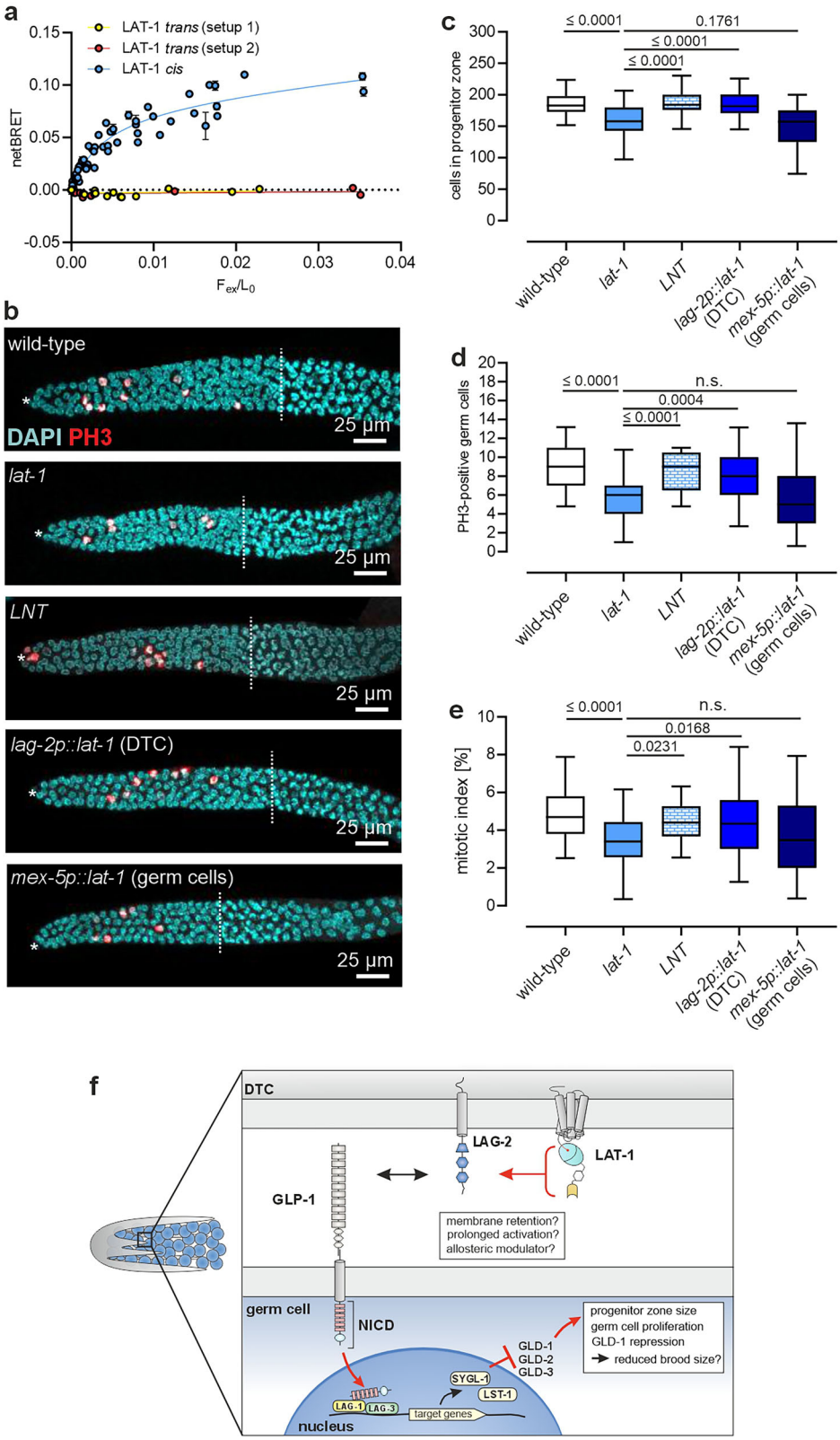
As these in vitro data suggest that the LAT-1/LAG-2 interaction occurs on the same cell, this would mean that LAT-1 must be present on the DTC rather than on germ cells in *C. elegans*. To investigate whether this is the case in vivo, two different worm strains were created: one with *lat-1* expressed only in the DTC by using the DTC-specific *lag-2* promoter (*lag-2p::lat-1*) and another with the receptor expressed exclusively in germ cells, driven by the germ cell promoter of *mex-5* (*mex-5p::lat-1*). Both strains were assessed for the size of the progenitor zone and germ cell proliferation through PH3/DAPI staining. When LAT-1 was present in the DTC, progenitor zone size, number of PH3-positive cells, and mitotic index were similar to those observed in wild-type hermaphrodites (Fig. 5b–e). In contrast, when the receptor was expressed in germ cells, zone sizes, PH3-positive cell counts, and mitotic index resembled those found in *lat-1* mutant gonads (Fig. 5b–e). These data, taken together with the in vitro data, indicate that LAT-1 located on the DTC fulfills the receptor's role in germ cell proliferation.

In summary, our findings suggest that LAT-1 interacts with LAG-2 on the same cell, and that LAT-1 must be localized to the DTC, not the germ cells, to modulate Notch signaling and regulate germ cell proliferation (Fig. 5f).

Discussion

The Notch pathway is a highly conserved signaling mechanism[50] with vital roles in numerous biological processes, especially in development (summarized in refs. 11,51). Unsurprisingly, dysregulated Notch signaling is associated with various diseases, including cancer[52–55]. As such, a tightly regulated network of components exists to control Notch signals (summarized in refs. 56–58). In the present study, we identify the aGPCR latrophilin-1 as a positive modulator of the Notch

https://doi.org/10.1038/s41467-025-61730-0



pathway (Fig. 5f). These highly versatile receptors not only transduce G protein-mediated signals into cells like classical GPCR, but also mediate functions independent of *G* protein signals solely via their extracellular *N* termini[59–62]. Our data show that the latrophilin homolog LAT-1 in *C. elegans* enhances the activation/activity of Notch signaling in the germline (Fig. 2). Specifically, the aGPCR increases the translocation of the Notch receptor GLP-1 intracellular domain (NICD) into the nuclei of distal germ cells, without affecting the overall GLP-1 levels. Once in the nucleus, the NICD functions as a transcription factor, promoting the expression of target genes, thereby regulating the balance between cell proliferation and differentiation into germ cell progenitors (i.e., entry into meiosis) in the distal germline (summarized in ref. 26). In *C. elegans*, two direct target genes of Notch are *sygl-1* and *lst-1*[63], which act in conjunction with the RNA-binding proteins FBF-1 and FBF-2 to

Fig. 5 | LAT-1 elicits its effect on germ cells from the DTC. a BRET analysis indicates that LAT-1 and LAG-2 establish their interaction on the same cell (*cis*) (blue line), whereas expression on opposite cells (*trans*) results in no measurable BRET window (red and yellow lines). $n = 4$ technical replicates in 2 (setup 1), 2 (setup 2) and 11 (LAT-1 *cis*) independent experiments. Note that the *cis* BRET curve is the same as in Supplementary Fig. 7b. **b** Representative images of gonads from L4 + 8 h-old hermaphrodites with tissue-specific expression of *lat-1* in the DTC and germ cells, respectively. Only *lat-1* expression in the DTC but not the germ cells resulted in a higher PH3-positive germ cell number and progenitor zone size than in *lat-1* mutants, comparable to the wild-type. As a positive control, *lat-1* promoter-driven LNT was used that ameliorates the reproductive defects in *lat-1* mutants to wild-type levels. Asterisks: DTC, dashed lines: end of the progenitor zone. **c** Quantification of the progenitor zone (from images shown in (**b**)). Replicate values (independent experiments): wild-type: 71 (9), *lat-1*: 53 (12), *LNT*: 37 (7), *lag-2p::lat-1*: 46 (7), *mex-5p::lat-1*: 30 (8). **d** Quantification of PH3-positive germ cells of images shown in (**b**). Wild-type 71 (9), *lat-1:* 53 (12), *LNT*: 37 (7), *lag-2p::lat-1:* 46 (7), *mex-5p::lat−1:* 31 (8). **e** M index (percentage PH3-positive nuclei from all progenitor zone nuclei). Wild-type 71 (9), *lat-1*: 53 (12), *LNT*: 37 (7), *lag-2p::lat-1*: 46 (7), *mex-5p::lat-1*: 30 (8). Raw data of PH3-positive cell counts and the denominators for index calculations are given in the Source data. **f** Proposed model of LAT-1 function. LAT-1 interacts with LAG-2 on the DTC to boost GLP-1 activation in germ cells. This interaction leads to the modulation of *gld-1* expression and subsequently, an increase in germ cell proliferation and the regulation of progenitor zone size. Red arrows and lines highlight steps investigated in this study. Graph raw data are provided in the Source Data. Graph details and statistics are: (**a**): Mean ± SD. (**c**), (**d**), (**e**): Box plots with median (center), interquartal range, 5th (lower whisker) and 95th (upper whisker) percentiles. One-way ANOVA with Bonferroni post-hoc test.

suppress the mRNAs of downstream targets like *gld-1*[64] (Fig. 2a). Consequently, the reduced Notch activation observed in *lat-1* mutants likely accounts for the detected increase in GLD-1 protein levels and its presence in more distal germ cells (Fig. 2b, c), a phenotype similar to that in *glp-1* reduction-of-function mutants (allele *bn18*)[65].

Through this signaling mechanism, Notch activity regulates the balance between cell proliferation and differentiation into germ cell progenitors (i.e., entry into meiosis) in the distal germline of *C. elegans* (summarized in ref. 26). As germ cells move away from the DTC and thus, from the ligand LAG-2 located on this cell, Notch activity declines, leading to meiotic differentiation (summarized in ref. 26). Worms with reduced GLP-1 function exhibit a smaller progenitor zone and fewer proliferating cells[25,27], a phenotype also observed in the absence of LAT-1 (Fig. 1).

Beyond Notch signaling, there are indications that LAT-1 may also play roles in cell cycle regulation in the germline. This is suggested by the altered M and S phase indices in *lat-1* mutants, implying a faster cell cycle. While altered Notch signaling does not typically affect the mitotic index[25,32], a cross-talk between Notch and cell cycle regulation components has been reported[66,67]. *lat-1* expression in both the DTC and germ cells hints at further roles that warrant investigation.

Notably, although Notch activity is required throughout the reproductive lifespan, time-course analyses indicate that LAT-1 plays a specific role in young adult nematodes (8–12 h post-L4 stage) (Supplementary Fig. 1a), when their reproductive capacity starts to build up[27]. This suggests that LAT-1 enhances Notch signaling during this critical period, interacting with LAG-2, one of two conserved DSL homologs in *C. elegans*[21,68].

In multiple distinct lines of evidence, we show the interaction between LAT-1 and LAG-2 through their extracellular regions. Our AlphaFold2 Multimer-generated models suggest that both the LAT-1 RBL and GAIN domains form the interaction interface with the GAIN domain contributing the larger area. These domains have been previously shown to be crucial for both receptor 7TM-dependent and 7TM-independent/N terminus-only/*trans* functions[62]. Further support for this interaction is provided by BRET and BiFC analyses in both cells and live nematodes identifying the key amino acids involved (Figs. 3, 4). It needs to be noted that a larger interface does not necessarily imply a greater functional contribution and/or physiological effect. Indeed, our mutational analyses (Fig. 3c) reveal that only the combined mutations of both RBL and GAIN domains significantly impairs binding affinity, whereas mutations in either domain alone have little to no effect. This suggest that the two domains function cooperatively to establish a stable and specific interaction.

Further investigation into additional proteins potentially involved in the LAT-1/LAG-2 interaction could provide a deeper understanding, as latrophilin homologs in mice neurons function within large protein super-complexes[69]. For instance, while we could not detect a direct interaction between LAT-1 and GLP-1, it remains possible that LAT-1 forms a complex with LAG-2 and GLP-1 when all three proteins are present.

We provide physiological and mechanistic evidence that only the N terminus of LAT-1 is sufficient to modulate Notch activity indicating that the full-length receptor is not required for this function. Reduced Notch signaling was ameliorated by expression of the *N* terminus tethered to the membrane (LNT), indicating that the LAT-1 function is indeed able to modulate Notch pathway activity in a non-cell autonomous manner. This is consistent with previous findings showing that many functions of the aGPCR in the germline, such as sperm guidance and germ cell apoptosis, rely solely on its *N* terminus[22]. These data raised the question of whether the interaction between LAT-1 and LAG-2 occurs *in cis* (on the same cell) or in trans (on different cells). Both in vitro and in vivo analyses (Fig. 5) support a *cis* interaction, implying that LAT-1 binds to LAG-2 on the same cell and that the *N* terminus-only/7TM-independent function of the aGPCR is based on a *cis* interaction in the DTC, but it exerts an effect in trans on neighboring germ cells.

In summary, our results propose a model in which LAT-1, via its *N* terminus, interacts with LAG-2 on the somatic DTC, directly modulating the Notch ligand-receptor complex to regulate the expansion of the germline stem cell pool in *C. elegans* (Fig. 5f). This role might complement the previously identified functions of LAT-1 in regulating brood size, as the latter was partly rescued by LNT expression in the DTC[22]. Interestingly, our data indicate that LAT-1 may also engage in cross-talk with the Notch pathway in additional contexts, such as anus development and chemosensory regulation (Fig. 2), potentially pointing to a general underlying mechanism.

The question remains how the interaction of latrophilin with the Notch ligand promotes increased Notch activation. Several modulators of the Notch pathway have been identified in the past, acting at different sites, for example regulating expression of key Notch components[70] or influencing their degradation via ubiquitination[71]. LAT-1 does not alter the overall expression of *lag-2* or *glp-1* (Supplementary Fig. 2). However, it may stabilize LAG-2 on the membrane, elevating signal intensity. Alternatively, LAT-1 could increase the effect of LAG-2 on GLP-1. It is well established that for the activation of the Notch pathway, the Notch ligand binds to the Notch receptor on opposing cells (summarized in refs. 58,72). Subsequently, a certain level of force exerted from the Notch ligand is required to activate the receptor, which leads to the exposure of protease recognition sites and receptor cleavage at two sites, one extracellularly and one in the transmembrane domain that releases the NICD (summarized in refs. 58,72). In *Drosophila melanogaster* and vertebrates, this mechanical force needs to be quite strong and is generated by ligand endocytosis, promoting a conformational change within the Notch receptor. In *C.elegans*, much lower force thresholds are in place, tethering the ligand to the membrane is sufficient[73]. A hypothesis could be that LAT-1 acts as an allosteric modulator, enhancing the conformational changes in the LAG-2/GLP-1 complex required for signaling.

This newly discovered mechanism of LAT-1 interacting with LAG-2 could be generalizable and may also be present in other contexts within *C. elegans* or even in other species. Our analyses hint towards a broader involvement of the two at least in the nematode, since in anus development and neurological contexts such as octanol avoidance an interaction is conceivable (Fig. 2). In addition, a cross-talk could occur in embryonic development. Notch signals are required for specifying cell fates in the embryo and for mediating correct embryonic axis formation[45–47] with LAG-2 acting as a key signal in certain embryonic cells[74,75]. As LAT-1 is also present in the early embryo[36], an interaction in this context is plausible.

In mammals, none of the three latrophilin homologs has been directly linked to Notch signaling. However, a cross-talk between aGPCRs and Notch components has been hypothesized. For example, overexpression of human *ADGRL4/ELTD1* leads to a downregulation of the Notch ligand *DLL4* and an upregulation of ligand *JAGI*[76]. Conversely, it was shown in mice that expression of *DLL4* increased *ADGRG6/GPR126* expression[77]. However, a direct interlink was lacking to date. Our work uncovers first mechanistic insights on how an aGPCR interacts with the Notch pathway in a multicellular setting in vivo. This is particularly relevant given the essential role of Notch in development, tissue homeostasis, and pathologies such as cancer[52–55], which makes new potential regulators of the Notch pathway highly relevant for pharmacological and medical research.

Methods

Materials and reagents

All standard chemicals were from Sigma Aldrich, ThermoFisher Scientific or Carl Roth unless stated otherwise. All enzymes were obtained from New England Biolabs unless stated otherwise. Details are given in Supplementary Table 1.

Generation of constructs and plasmids

Constructs were generated using standard restriction-ligation or HiFi assembly (New England Biolabs) (see Supplementary Methods for details). Oligonucleotide sequences are given in Supplementary Table 2 and generated constructs in Supplementary Table 3.

C. elegans maintenance and strains

C. elegans strains were maintained according to standard protocols[78] on *E. coli* OP50 at 15 °C unless stated otherwise. A complete list of used strains is given in Supplementary Table 4. Assays were performed with worms at L4 + 8 h kept at 15 °C unless stated otherwise.

Generation of transgenic *C. elegans* lines

For BiFC experiments, transgenic strains with stably transmitting extrachromosomal arrays were generated employing standard injection techniques into *C. elegans* N2[79]. Nematodes were injected with BiFC plasmids (Supplementary Table 4). Co-injection markers were either pRF4[80] (100 ng/µL), pCFJ90 (2.5 ng/µL)[81] (gift from Erik Jorgensen, Addgene plasmid #19327), pCFJ104 (5 ng/µL)[81] (gift from Erik Jorgensen, Addgene plasmid #19328), or IR98 (30 ng/µL)[82]. pBluescript II SK+ vector DNA (Stratagene) was added as stuffer DNA to achieve a final concentration of 120 ng/µl.

For competition BiFC, plasmid pSP234 was injected in various concentrations (5, 10, 50 ng/µL) into N2 nematodes with IR98 (Hygromycin resistance) as co-injection marker, and crossed into respective BiFC lines, thereby retaining its original extrachromosomal array composition. Transgenic progeny was isolated and stably transmitting lines were selected.

For rescue experiments, strains were generated by CRISPR-Cas9 genome editing. This was accomplished using either a Cas9-RNP complex[83–86], or via a plasmid-based approach[87–90]. For detailed descriptions of modifications see Supplementary Methods, for a list of genetically modified/transgenic strains see Supplementary Table 4.

Antibody and DAPI staining

Antibody and DAPI stainings were performed on extruded germlines. For this purpose, germlines were dissected in PBS and fixed. For anti-phospho histone H3 (anti-PH3) staining, fixation was performed in 3.7% (v/v) formaldehyde in PBS containing 0,1% (v/v) Tween 20 (PBS-T). Gonads were post-fixed in methanol at −20 °C for 5 min. No blocking was required. For staining the NICD::V5, which followed the protocol described in ref. 34, gonads were fixed with 4% (w/v) paraformaldehyde for 10 min. Permeabilization was performed using 0.1% (v/v) Triton X-100 in PBS (PBS-T) for 30 min followed by blocking in 0.5% (w/v) BSA in PBS-T for 20 min. Intermittent washing was done thrice using PBS-T for 5 min per wash. All centrifugation steps were performed at 3000 x *g* for 1 min.

Thereafter, gonads were incubated with the primary antibody overnight at 4 °C (anti-PH3: rabbit anti-phospho histone H3 (Ser10)) 1:200 in PBS-T/0.1% BSA; anti-V5: mouse anti-V5 SV5-Pk1 1:1000 in PBS-T/0.5% BSA) while rotating. After washing three times in PBS-T, gonads were incubated with the secondary antibody (anti-PH3: goat anti-rabbit IRDye 680RD-conjugated 1:1000 in PBS-T/0.1% BSA supplemented with 10 ng/µL DAPI; anti-V5: goat anti-mouse IgG (H + L), F(ab')2 fragment CF 568 1:1000 in PBS-T/0.5% BSA supplemented with 10 ng/µL DAPI) at room temperature for 1 h. Gonads were mounted in Fluoromount G mounting media on 2% agarose pads. For details regarding antibodies or reagents, please refer to Supplementary Table 1.

EdU labeling

5-ethynyl-2´-deoxyuridine (EdU) staining of worms was conducted as previously described[91,92]. For incorporation of EdU into bacteria, an overnight culture of MG1693 bacteria (*E. coli* genetic stock center) was diluted 1:50 in M9 containing 1% glucose, 1.25 µg/mL thiamine, 0.5 µM thymidine, 1 mM $MgSO_4$ and 20 µM EdU (Click-iT EdU Alexa Fluor 647 Imaging Kit, ThermoFisher) and grown for 24 h at 37 °C. Staged adult hermaphrodites (8 h post L4) were transferred to NGM plates seeded with these bacteria and incubated for 30 min in the dark at room temperature. Subsequently, worms were washed off the plates and gonads were extruded and fixed as described for the PH3 staining. EdU staining was completed using the Click-iT EdU Alexa Fluor 488 or 647 Imaging Kit (ThermoFisher) according to the manufacturer's protocol.

Microscopy

Microscopy of nematodes was performed using a Leica TCS SP8 confocal microscope equipped with LAS X software. Z stacks were taken with spatial spacing of 0.5–2 µm, depending on the specimen (2 µm for whole worms, 0.5 µm for gonads) using either 40x or 93x magnification objectives. Microscopic images were evaluated using Fiji[93]. Scoring of anus phenotypes was performed using a Zeiss AXIO Imager.A2 using 63x magnification and DIC.

Notch activation assay

GLP-1 activation was monitored in worms carrying the allele *glp-1(q1000[glp-1::4xV5])* that has a 4x V5 tag located in the GLP-1 intracellular domain (NICD)[34]. These were stained with an anti-V5 antibody as described above, mounted, and subjected to microscopy. Fiji[93] was used to quantify Notch activation as the fraction of NICD present in nuclei in a central *Z* slice. For this purpose, a central slice was selected, and nuclei in the first five rows were annotated as ROI based on DAPI staining. The fluorescent signal of the V5 staining in these areas was quantified. NICD ratio was calculated as: sum [V5 signal in DAPI-annotated ROIs] / total V5 signal in slice.

Assessing DTC morphology

The DTC morphology was quantified in worms carrying allele *qIs153[lag-2p*::MYR::GFP + *ttx-3p*::DsRed] V, which encodes a myristylated GFP marking the DTC membrane. Gonads were extruded,

fixed, stained with DAPI, mounted, and imaged using confocal microscopy as described above. Quantification of DTC structures was performed according to ref. 94. In brief, the DTC cap was defined as from distal to the most proximal extent of signal covering the germ cell surface, whereas the plexus was defending from the most distal signal to the most proximal signal of intercalating processes.

Quantification of GLD-1 levels

Gonads of 8 h post-L4 worms containing *ozIs5[gld-1::gfp + unc-119(+)]* [95] were extruded, fixed, stained with DAPI, and mounted as described above. To compare expression in different strains images were acquired with same exposure and detection settings. Z projections of the image stacks were analyzed as previously described[20] with the "Plot Profile" function in Fiji[93] to generate expression profiles of the distal germ cell rows (ROI: a 5 μm-wide square spanning 35 germ cell rows). Fluorescence intensities of each germ cell row were obtained by dividing the plot profile into 35 equal sections, respectively. For each germ cell row, a mean fluorescence value was calculated by pooling fluorescence intensities of multiple germlines.

Anus absence quantification

Adult nematodes were bleach-synchronized as per standard procedure and hatched overnight at room temperature. L1-arrested nematodes were immobilized using 300 mM levamisole in M9 and mounted on 2% agarose pads. Nematodes were subjected to microscopy, and the absence of the anus was scored based on tail morphology.

Octanol avoidance assay

Nematodes were raised at 25 °C (restrictive temperature for *lag-2* and *lat-1; lag-2* mutants). At 1-day-old adult stage, they were assessed for their chemosensory response as described in ref. 96. Briefly, freshly diluted octanol (70% in ethanol) was soaked into an eyelash and placed in front of a forward-moving animal on an NGM agar plate without food. As a negative control, 100% ethanol was used. The time required to initiate reversing was recorded.

BiFC analysis

Adult nematodes expressing BiFC constructs were heat-shocked for 3 h at 33 °C and recovered for 5 h at 22 °C prior to anesthetizing in 300 μM levamisole in M9.

Z stacks of nematode heads were acquired using confocal microscopy using 2 μm spacing. Images were evaluated using Fiji[93]. Quantification was performed using the "sum slices" function and quantifying the fluorescence using the anterior end of the head until the posterior end of the pharynx. Gut autofluorescence signal recorded from non-heat-shocked nematodes was subtracted to compensate for background signal.

Western blot analysis

60-80 1-day-old adult nematodes were heat-shocked for 3 h at 33 °C, recovered for 5 h at 22 °C, and snap frozen at −80 °C in 20 μL M9. Samples were boiled for 10 min at 95 °C in 1x Laemmli buffer and spun down. 20 μL of supernatant were subjected to PAGE on a 10% SDS polyacrylamide gel and transferred on a nitrocellulose membrane. After blocking with EveryBlot buffer (BioRad) for 5 min at room temperature, the membrane was incubated with a mix of the two primary antibodies mouse anti-V5 SV5-Pk1 (BioRad, MCA1360) and rabbit anti-HA (Abcam, ab236632) (each 1:1000 in EveryBlot buffer) overnight at 4 °C. Unbound antibody was washed off using TBS-T (0.1%) in three washes. Secondary antibody incubation was performed using the anti-rabbit IgG, HRP-conjugated antibody (Cell Signaling Technology, 7074) (1:2500 in EveryBlot buffer) and the goat anti-mouse IgG (H + L)-HRP conjugate (BioRad, 1721011) (1:5000 in EveryBlot buffer) with anti-actin hFAB-rhodamine (Biorad, 12004164) (1:2500 in EveryBlot buffer) as loading control. Incubation with the secondary antibodies was performed for 1 h at room temperature followed by washing as stated above, followed by detection of HRP-conjugated antibodies using SuperSignal West Pico PLUS (Thermo Fisher, 34577) as well as fluorescent detection of actin by exciting at 519 nm and detecting at 605 nm using a UVP Chemstudio (Analytik Jena).

Molecular modeling of LAT-1 and LAG-2

The models of the extracellular regions of LAT-1 and LAG-2 were constructed using AlphaFold2 Multimer[39,97]. The software was downloaded from Github (https://github.com/deepmind/AlphaFold) and installed on the local computing cluster of Leipzig University Rechenzentrum (10/2022, v2.2.2). Sequences of the extracellular domains and combinations thereof were obtained from Uniprot[98] and used as input for various complex combinations of LAG-2 and LAT-1. Here, models of the entire extracellular region of LAG-2 with a) only the GAIN domain, b) GAIN and HRM domain, c) only the RBL domain, d) LAT-1 with an extended linker sequence between RBL domain and GAIN domain and e) the entire extracellular region of LAT-1 were predicted. Input multiple sequence alignment (MSA) features were generated by the AlphaFold2 Multimer pipeline described in ref. 97. For each interaction combination, 50 models were generated, energetically minimized, and ranked. Obtained structures were analyzed and visually inspected in PyMOL (version 2.5.4). Initial root-mean square deviation RMSD calculations were conducted using PyMOL alignment calculation. Each interaction complex combination was analyzed, and common interaction faces inspected. The most promising models, defined by the highest ipTM and pTM as AlphaFold2 scores and with the most commonly observed interactions, were energetically minimized (Rosetta relax) using Rosetta3 (version 3.13)[99]. For each model, 300 minimized structures were generated, and the interface was analyzed. Here, the Rosetta InterfaceAnalzyer was used, and the top-scoring model was selected for further analysis. The quality of the structural model and its interaction were assessed with MD simulations.

To study the energetics of the interaction, a per-residue energy analysis (energy breakdown) was carried out using Rosetta's per_residue_energies application. Based on the individual energies for residue-residue interactions between the different protein domains, a residue contact map (hotspot analysis) was made and plotted with Python (version 3.7). Based on a hotspot analysis and after visual inspection using PyMOL, relevant interactions were analyzed by mutagenesis experiments. In an additional refinement step, the investigated mutations were modeled with AlphaFold2 Multimer and compared to the initial models. The structural model of the mutations was analyzed similarly. A protocol capture can be found in the Supplementary Methods.

To investigate the complex of LAT-1 and GLP-1, the aforementioned computational pipeline was utilized, but in both cases, the predicted complexes had lower in silico scores and lacked a convergence with highlight variable binding interfaces.

MD simulations

The best-scoring complex model containing LAG-*2* and the RBL and GAIN domains of LAT-1 was used as the basis for the MD system. Disordered non-contacting regions were truncated, leaving residues LAT-1 32-137 (RBL) and 182-539 (GAIN) as well as residues 16-273 for LAG-2 in the system. The termini were capped via N-terminal amidation and *C*-terminal acetylation except for the *N*-terminus of LAG-2, putatively *C*-terminal of signal peptide cleavage, which was left as a charged amino group. Disulfide bridges were added according to the respective UniProtKB database entries (*lag-2*: P45442; *lat-1*: G5EDW2)[100]. The truncated complex was processed for residue hetero states and side chain flips by maestro 2024.2. CHARMM-GUI[101,102] was used to normalize bond lengths and generate minimization and equilibration inputs using the CHARMM36 forcefield for GROMACS (version 2024.2). Water boxes

using the TIP3P water model[103] were generated with CHARMM-GUI using a large cubic box size of 150 Å edge length to accommodate expected large-scale rigid body movements and charge-neutralized with 0.15 M NaCl. After minimization using the steepest-descent method for 5000 steps, a 50 ns equilibration with 1 fs time step was performed with backbone restraints of 400 kJ/mol/nm² and side-chain restraints of 40 kJ/mol/nm² to yield the equilibrated model and extensively accommodate equilibration of the predicted structure. After equilibration, triplicate unbiased MD simulations for 1000 ns using the CHARMM36 force field[104] in GROMACS[105,106] were performed at 295 K using the c-rescale barostat, the v-rescale thermostat and a 2 fs time step. MD analysis was carried out with GROMACS 2024.2 within a python3 environment and by using VMD[107]. For a summary of data reliability and reproducibility, see Supplementary Table 5.

Cell culture

HEK293 and HEK293T cells were maintained in Dulbecco's minimum essential medium (DMEM, high glucose, + L-Glutamine)/F12 (1:1, v/v) supplemented with 15% heat inactivated fetal bovine serum (FBS) in humidified atmosphere at 37 °C and 5% CO_2.

Cell surface ELISA

Cell surface expression of receptors carrying an N-terminal HA tag was determined by an indirect enzyme-linked immunosorbent assay (ELISA). HEK293T cells were split into 48-well plates (1.2×10^5 cells/well) that had been pre-coated with 0.0002% poly-L-lysine (Merck) in PBS (30 min at 37 °C). After 24 h, the cells were transfected with 500 ng of receptor-encoding plasmid DNA per well using Lipofectamine 2000 (ThermoFisher), following the manufacturer's instructions. Cells were fixed with 4% formaldehyde for 20 min and blocked with media + 10% FBS for 1 h at 37 °C. After washing with PBS once cells were incubated with an anti-HA peroxidase conjugated antibody (1:1000) (Sigma-Aldrich, 54193500) and detection was performed as previously described[108]. Briefly, after extensive washing, H_2O_2 and o-phenylenediamine were added to the wells (2.5 mM each in 0.1 M phosphate-citrate buffer (pH 5.0). The color debelopment was stopped after 15 min by addition of 1 M H_2SO_4 and cell surface expression was measured at 492 and 620 nm in a Spark plate reader (Tecan).

BRET analyses

HEK293 cells were seeded into 6-well plates (1.25×10^6 cells/well) and transiently transfected with a DNA gradient of *Venus::lat-1* (or its variants; 0-3970 ng DNA/well, six conditions) over a constant amount of *Nluc::lag-2* (30 ng DNA/well) using 3 µl MetafectenePro (Biontex)/ µg DNA (for BRET plasmids see Supplementary Table 3). The total DNA per well was 4000 ng and was balanced out by empty vector. 16 h post transfection, the cells were detached and re-seeded into poly-D-lysine-coated solid white 96-well plates (BRET reading) or clear bottom black 96-well plates (direct fluorescence excitation) (150.000 cells/well) using phenol-red free medium. One day later, the medium was changed to 200 µl Hank's balanced salt solution (+ Ca^{2+}/Mg^{2+}) supplemented with 25 mM HEPES (pH 7.4; BRET-buffer). Protein expression of *Venus::lat-1* and *Venus::hGLP1R* was quantified in the black plates by direct excitation at 485 ± 20 nm, and fluorescence emission was recorded at 544 ± 25 nm (F_{ex}). For the BRET reading, the luciferase substrate coelenterazine H (Nanolight Prolume) was freshly added into the BRET buffer (final concentration 5 µM) and the cells were incubated for 5 min at 37 °C before measuring dual-color luminescence with filters 400–470 nm (L) and 535–650 nm (F) in a Spark plate reader (Tecan) using the well-wise mode and 500 ms signal integration time.

BRET ratios were calculated as (F/L) and subsequently corrected by the BRET ratio observed in donor-only cells (0 ng *Venus::lat-1* variant) to retrieve the netBRET. For any *Venus::lat-1* variant, the change in netBRET was plotted against the protein expression ratio of *Venus::lat-1* over *Nluc::lag-2* luminescence in the donor-only state (F_{ex} /L_0). Results from four independent experiments were combined and fit to a one site total binding hyperbola function (Y=Bmax*X/Kd+X) + NS*X) using GraphPadPrism 10, where Y is the netBRET and X is F_{ex}/L_0, treating the nonspecific component of the binding hyperbola (NS) as a shared optimization parameter due to random collision. Differences in K_d (equivalent to $BRET_{50}$) reflect changed affinity of the specific binding between LAG-2 or APX-1 and the respective LAT-1 variant.

To evaluate whether the proteins interact in trans, i.e., between neighboring cells rather than on the same cell, two distinct HEK293 cell populations were transfected with either *Nluc-lag-2* (200 ng plasmid DNA/T25 flask) or *Venus-lat-1* (4000 ng/T25 flask). One day after transfection, the cells were re-seeded into poly-D-lysine coated white and black 96-well plates in technical quadruplicate using phenol red-free medium, shaping a gradient by increasing the cell number of *Venus::lat-1*-transfected cells and balancing the total number of cells by filling up with untransfected HEK293 (150.000 cells/well in total; 3 cell populations). In an alternative approach, different amounts of *Venus::lat-1* DNA were transfected (0–4000 ng DNA/well in 6-well-plates), and the fluorescent gradient was shaped by using 130.000 cells of these different *Venus::lat-1* expressing cell populations, combined with 20.000 *Nluc::lag-2* expressing cells (150.000 cells/well in total; 2 cell populations). 24 h after re-seeding, the fluorescent gradient was confirmed by direct excitation in black plates and the BRET was measured as described above.

Statistics

Statistical and graphical analyses (except for the molecular modeling data) were performed using Prism version 10.0 (GraphPad Software). When comparing two groups, statistical significance was analyzed using the two-sided unpaired Student's t test. When comparing several groups, a one-way ANOVA was applied with Bonferroni post-hoc tests to correct for multiple comparisons unless stated otherwise. Data are presented as box plots unless stated otherwise. Details are given in the figure legends.

Reporting summary

Further information on research design is available in the Nature Portfolio Reporting Summary linked to this article.

Data availability

Source data and supplementary information are provided with this paper. All other data and worm strains generated in this study are available upon request to the corresponding author.

Code availability

Data from in silico predictions and MD simulations are stored in Zenodo repository under https://doi.org/10.5281/zenodo.15228753. Source data are provided with this paper.

References

1. Hamann, J. et al. International union of basic and clinical pharmacology. XCIV. Adhesion G protein–coupled receptors. *Pharmacol. Rev.* **67**, 338–367 (2015).
2. Rosa, M., Noel, T., Harris, M. & Ladds, G. Emerging roles of adhesion G protein-coupled receptors. *Biochem. Soc. Trans.* **49**, 1695–1709 (2021).
3. Einspahr, J. M. & Tilley, D. G. Pathophysiological impact of the adhesion G protein-coupled receptor family. *Am. J. Physiol. Cell Physiol.* **323**, C640–C647 (2022).
4. Bohnekamp, J. & Schöneberg, T. Cell adhesion receptor GPR133 couples to Gs protein. *J. Biol. Chem.* **286**, 41912–41916 (2011).
5. Gupte, J. et al. Signaling property study of adhesion G-protein-coupled receptors. *FEBS Lett.* **586**, 1214–1219 (2012).

6. Yona, S., Lin, H.-H., Siu, W. O., Gordon, S. & Stacey, M. Adhesion-GPCRs: emerging roles for novel receptors. *Trends Biochem. Sci.* **33**, 491–500 (2008).
7. Cho, C., Smallwood, P. M. & Nathans, J. Reck and Gpr124 are essential receptor cofactors for Wnt7a/Wnt7b-specific signaling in mammalian CNS angiogenesis and blood-brain barrier regulation. *Neuron* **95**, 1056–1073.e5 (2017).
8. Posokhova, E. et al. GPR124 functions as a WNT7-specific coactivator of canonical β-catenin signaling. *Cell Rep.* **10**, 123–130 (2015).
9. Wu, Y. et al. Elevated G-Protein Receptor 125 (GPR125) Expression predicts good outcomes in colorectal cancer and inhibits Wnt/β-catenin signaling pathway. *Med. Sci. Monit.* **24**, 6608–6616 (2018).
10. Vallon, M. et al. A RECK-WNT7 receptor-ligand interaction enables isoform-specific regulation of WNT BIOAvailability. *Cell Rep.* **25**, 339–349.e9 (2018).
11. Sachan, N., Sharma, V., Mutsuddi, M. & Mukherjee, A. Notch signalling: multifaceted role in development and disease. *FEBS J.* **291**, 3030–3059 (2024).
12. Artavanis-Tsakonas, S., Rand, M. D. & Lake, R. J. Notch SIGNALING: CELL FATE CONTROL AND SIGNAL INTEGRATION IN DEVELopment. *Science* **284**, 770–776 (1999).
13. Fleming, R. J. Structural conservation of Notch receptors and ligands. *Semin. Cell Dev. Biol.* **9**, 599–607 (1998).
14. Mizutani, T., Taniguchi, Y., Aoki, T., Hashimoto, N. & Honjo, T. Conservation of the biochemical mechanisms of signal transduction among mammalian Notch family members. *Proc. Natl. Acad. Sci. USA* **98**, 9026–9031 (2001).
15. He, X., Wu, F., Zhang, L., Li, L. & Zhang, G. Comparative and evolutionary analyses reveal conservation and divergence of the notch pathway in lophotrochozoa. *Sci. Rep.* **11**, 11378 (2021).
16. Austin, J. & Kimble, J. *glp-1* Is required in the germ line for regulation of the decision between mitosis and meiosis in C. elegans. *Cell* **51**, 589–599 (1987).
17. Berry, L. W., Westlund, B. & Schedl, T. Germ-line tumor formation caused by activation of glp-1, a caenorhabditis elegans member of the Notch family of receptors. *Development* **124**, 925–936 (1997).
18. Fitzgerald, K. & Greenwald, I. Interchangeability of caenorhabditis *elegans* DSL proteins and intrinsic signalling activity of their extracellular domains in vivo. *Development* **121**, 4275–4282 (1995).
19. Henderson, S. T., Gao, D., Christensen, S. & Kimble, J. Functional domains of LAG-2, a putative signaling ligand for LIN-12 and GLP-1 receptors in Caenorhabditis elegans. *Mol. Biol. Cell* **8**, 1751–1762 (1997).
20. Lambie, E. J. & Kimble, J. Two homologous regulatory genes, *lin-12* and *glp-1*, have overlapping functions. *Development* **112**, 231–240 (1991).
21. Henderson, S. T., Gao, D., Lambie, E. J. & Kimble, J. lag-2 may encode a signaling ligand for the GLP-1 and LIN-12 receptors of C. elegans. *Dev. Camb. Engl.* **120**, 2913–2924 (1994).
22. Matúš, D. et al. The N terminus-only (*trans*) function of the adhesion G protein-coupled receptor latrophilin-1 controls multiple processes in reproduction of *Caenorhabditis elegans*. *G3 Genes Genomes Genet.* **14**, jkae206 (2024).
23. Hansen, D., Albert Hubbard, E. J. & Schedl, T. Multi-pathway control of the proliferation versus meiotic development decision in the Caenorhabditis elegans germline. *Dev. Biol.* **268**, 342–357 (2004).
24. Vanden Broek, K., Han, X. & Hansen, D. Redundant mechanisms regulating the proliferation vs. differentiation balance in the C. elegans germline. *Front. Cell Dev. Biol.* **10**, 960999 (2022).
25. Fox, P. M. & Schedl, T. Analysis of Germline Stem Cell Differentiation Following Loss of GLP-1 Notch Activity in *Caenorhabditis elegans*. *Genetics* **201**, 167–184 (2015).
26. Kimble, J. Germline proliferation and its control. *WormBook* (WormBook, 2005).
27. Albert Hubbard, E. J. & Schedl, T. Biology of the *Caenorhabditis elegans* germline stem cell system. *Genetics* **213**, 1145–1188 (2019).
28. Francis, R., Barton, M. K., Kimble, J. & Schedl, T. gld-1, a tumor suppressor gene required for oocyte development in Caenorhabditis elegans. *Genetics* **139**, 579–606 (1995).
29. Schumacher, B. et al. Translational repression of C. elegans p53 by GLD-1 regulates DNA damage-induced apoptosis. *Cell* **120**, 357–368 (2005).
30. Jeong, J., Verheyden, J. M. & Kimble, J. Cyclin E and Cdk2 control GLD-1, the mitosis/meiosis decision, and germline stem cells in Caenorhabditis elegans. *PLoS Genet.* **7**, e1001348 (2011).
31. Kodoyianni, V., Maine, E. M. & Kimble, J. Molecular basis of loss-of-function mutations in the glp-1 gene of Caenorhabditis elegans. *Mol. Biol. Cell* **3**, 1199–1213 (1992).
32. Michaelson, D., Korta, D. Z., Capua, Y. & Hubbard, E. J. A. Insulin signaling promotes germline proliferation in C. elegans. *Dev. Camb. Engl.* **137**, 671–680 (2010).
33. Fausett, S. R., Sandjak, A., Billard, B. & Braendle, C. Higher-order epistasis shapes natural variation in germ stem cell niche activity. *Nat. Commun.* **14**, 2824 (2023).
34. Sorensen, E. B., Seidel, H. S., Crittenden, S. L., Ballard, J. H. & Kimble, J. A toolkit of tagged glp-1 alleles reveals strong glp-1 expression in the germline, embryo, and spermatheca. *MicroPublication Biol.* **2020**, 271 (2020).
35. Gutnik, S. et al. PRP-19, a conserved pre-mRNA processing factor and E3 ubiquitin ligase, inhibits the nuclear accumulation of GLP-1/Notch intracellular domain. *Biol. Open* **7**, 034066 (2018).
36. Langenhan, T. et al. Latrophilin signaling links anterior-posterior tissue polarity and oriented cell divisions in the C. elegans embryo. *Dev. Cell* **17**, 494–504 (2009).
37. Singh, K. et al. C. elegans notch signaling regulates adult chemosensory response and larval molting quiescence. *Curr. Biol.* **21**, 825–834 (2011).
38. Matúš, D., Post, W. B., Horn, S., Schöneberg, T. & Prömel, S. Latrophilin-1 drives neuron morphogenesis and shapes chemo- and mechanosensation-dependent behavior in C. elegans via a trans function. *Biochem. Biophys. Res. Commun.* **589**, 152–158 (2022).
39. Jumper, J. et al. Highly accurate protein structure prediction with AlphaFold. *Nature* **596**, 583–589 (2021).
40. Gao, D. & Kimble, J. APX-1 can substitute for its homolog LAG-2 to direct cell interactions throughout Caenorhabditis elegans development. *Proc. Natl. Acad. Sci. USA* **92**, 9839–9842 (1995).
41. Shyu, Y. J. et al. Visualization of protein interactions in living Caenorhabditis elegans using bimolecular fluorescence complementation analysis. *Nat. Protoc.* **3**, 588–596 (2008).
42. Hiatt, S. M., Shyu, Y. J., Duren, H. M. & Hu, C.-D. Bimolecular fluorescence complementation (BiFC) analysis of protein interactions in Caenorhabditis elegans. *Methods* **45**, 185–191 (2008).
43. Stringham, E. G., Dixon, D. K., Jones, D. & Candido, E. P. Temporal and spatial expression patterns of the small heat shock (hsp16) genes in transgenic Caenorhabditis elegans. *Mol. Biol. Cell* **3**, 221–233 (1992).
44. Hu, C.-D., Chinenov, Y. & Kerppola, T. K. Visualization of interactions among bZIP and Rel family proteins in living cells using bimolecular fluorescence complementation. *Mol. Cell* **9**, 789–798 (2002).
45. Hutter, H. & Schnabel, R. glp-1 and inductions establishing embryonic axes in C. elegans. *Dev. Camb. Engl.* **120**, 2051–2064 (1994).

46. Mello, C. C., Draper, B. W. & Priess, J. R. The maternal genes apx-1 and glp-1 and establishment of dorsal-ventral polarity in the early C. elegans embryo. *Cell* **77**, 95–106 (1994).
47. Moskowitz, I. P., Gendreau, S. B. & Rothman, J. H. Combinatorial specification of blastomere identity by glp-1-dependent cellular interactions in the nematode Caenorhabditis elegans. *Dev. Camb. Engl.* **120**, 3325–3338 (1994).
48. Don, E. K. et al. In vivo Validation of Bimolecular Fluorescence Complementation (BiFC) to Investigate Aggregate Formation in Amyotrophic Lateral Sclerosis (ALS). *Mol. Neurobiol.* **58**, 2061–2074 (2021).
49. Kodama, Y. & Hu, C.-D. Bimolecular fluorescence complementation (BiFC): a 5-year update and future perspectives. *BioTechniques* **53**, 285–298 (2012).
50. Gazave, E. et al. Origin and evolution of the Notch signalling pathway: an overview from eukaryotic genomes. *BMC Evol. Biol.* **9**, 249 (2009).
51. Siebel, C. & Lendahl, U. Notch signaling in development, tissue homeostasis, and disease. *Physiol. Rev.* **97**, 1235–1294 (2017).
52. Joutel, A. et al. Notch3 mutations in CADASIL, a hereditary adult-onset condition causing stroke and dementia. *Nature* **383**, 707–710 (1996).
53. Guest, R. V. et al. Notch3 drives development and progression of cholangiocarcinoma. *Proc. Natl. Acad. Sci. USA* **113**, 12250–12255 (2016).
54. Iascone, M. et al. Identification of de novo mutations and rare variants in hypoplastic left heart syndrome. *Clin. Genet.* **81**, 542–554 (2012).
55. Isidor, B. et al. Truncating mutations in the last exon of NOTCH2 cause a rare skeletal disorder with osteoporosis. *Nat. Genet.* **43**, 306–308 (2011).
56. Zhou, B. et al. Notch signaling pathway: architecture, disease, and therapeutics. *Signal Transduct. Target. Ther.* **7**, 95 (2022).
57. Henrique, D. & Schweisguth, F. Mechanisms of Notch signaling: a simple logic deployed in time and space. *Dev. Camb. Engl.* **146**, dev172148 (2019).
58. Kopan, R. & Ilagan, M. X. G. The canonical Notch signaling pathway: unfolding the activation mechanism. *Cell* **137**, 216–233 (2009).
59. Patra, C. et al. Organ-specific function of adhesion G protein-coupled receptor GPR126 is domain-dependent. *Proc. Natl Acad. Sci. Usa.* **110**, 16898–16903 (2013).
60. Tu, Y.-K., Duman, J. G. & Tolias, K. F. The Adhesion-GPCR BAI1 promotes excitatory synaptogenesis by coordinating bidirectional trans-synaptic signaling. *J. Neurosci.* **38**, 8388–8406 (2018).
61. Ward, Y. et al. Platelets promote metastasis via binding tumor CD97 leading to bidirectional signaling that coordinates transendothelial migration. *Cell Rep.* **23**, 808–822 (2018).
62. Prömel, S. et al. The GPS motif is a molecular switch for bimodal activities of adhesion class G protein-coupled receptors. *Cell Rep.* **2**, 321–331 (2012).
63. Kershner, A. M., Shin, H., Hansen, T. J. & Kimble, J. Discovery of two GLP-1/Notch target genes that account for the role of GLP-1/Notch signaling in stem cell maintenance. *Proc. Natl Acad. Sci. Usa.* **111**, 3739–3744 (2014).
64. Shin, H. et al. SYGL-1 and LST-1 link niche signaling to PUF RNA repression for stem cell maintenance in Caenorhabditis elegans. *PLoS Genet.* **13**, e1007121 (2017).
65. Brenner, J. L. & Schedl, T. Germline stem cell differentiation entails regional control of cell fate regulator GLD-1 in caenorhabditis elegans. *Genetics* **202**, 1085–1103 (2016).
66. Ambros, V. Cell cycle-dependent sequencing of cell fate decisions in Caenorhabditis elegans vulva precursor cells. *Dev. Camb. Engl.* **126**, 1947–1956 (1999).
67. Nusser-Stein, S. et al. Cell-cycle regulation of NOTCH signaling during C. elegans vulval development. *Mol. Syst. Biol.* **8**, 618 (2012).
68. Tax, F. E., Yeargers, J. J. & Thomas, J. H. Sequence of C. elegans lag-2 reveals a cell-signalling domain shared with Delta and Serrate of Drosophila. *Nature* **368**, 150–154 (1994).
69. Jackson, V. A. et al. Super-complexes of adhesion GPCRs and neural guidance receptors. *Nat. Commun.* **7**, 11184 (2016).
70. Gopal, S., Amran, A., Elton, A., Ng, L. & Pocock, R. A somatic proteoglycan controls Notch-directed germ cell fate. *Nat. Commun.* **12**, 6708 (2021).
71. Chen, Y. & Greenwald, I. hecd-1 modulates notch activity in Caenorhabditis elegans. *G3 Bethesda Md.* **5**, 353–359 (2014).
72. Suarez Rodriguez, F., Sanlidag, S. & Sahlgren, C. Mechanical regulation of the Notch signaling pathway. *Curr. Opin. Cell Biol.* **85**, 102244 (2023).
73. Langridge, P. D., Garcia Diaz, A., Chan, J. Y., Greenwald, I. & Struhl, G. Evolutionary plasticity in the requirement for force exerted by ligand endocytosis to activate C. elegans Notch proteins. *Curr. Biol. CB* **32**, 2263–2271.e6 (2022).
74. Hutter, H. & Schnabel, R. Establishment of left-right asymmetry in the Caenorhabditis elegans embryo: a multistep process involving a series of inductive events. *Dev. Camb. Engl.* **121**, 3417–3424 (1995).
75. Moskowitz, I. P. & Rothman, J. H. lin-12 and glp-1 are required zygotically for early embryonic cellular interactions and are regulated by maternal GLP-1 signaling in Caenorhabditis elegans. *Dev. Camb. Engl.* **122**, 4105–4117 (1996).
76. Favara, D. M. et al. Elevated expression of the adhesion GPCR ADGRL4/ELTD1 promotes endothelial sprouting angiogenesis without activating canonical GPCR signalling. *Sci. Rep.* **11**, 8870 (2021).
77. D'Amato, G. et al. Sequential Notch activation regulates ventricular chamber development. *Nat. Cell Biol.* **18**, 7–20 (2016).
78. Brenner, S. The genetics of Caenorhabditis elegans. *Genetics* **77**, 71–94 (1974).
79. Mello, C. & Fire, A. Chapter 19 DNA transformation. in *Methods in Cell Biology* vol. 48 451–482 (Elsevier, 1995).
80. Mello, C. C., Kramer, J. M., Stinchcomb, D. & Ambros, V. Efficient gene transfer in C.elegans: extrachromosomal maintenance and integration of transforming sequences. *EMBO J.* **10**, 3959–3970 (1991).
81. Frøkjaer-Jensen, C. et al. Single-copy insertion of transgenes in Caenorhabditis elegans. *Nat. Genet.* **40**, 1375–1383 (2008).
82. Radman, I., Greiss, S. & Chin, J. W. Efficient and Rapid C. elegans Transgenesis by Bombardment and Hygromycin B Selection. *PLOS ONE* **8**, e76019 (2013).
83. Prior, H., MacConnachie, L., Martinez, J. L., Nicholl, G. C. B. & Beg, A. A. A rapid and facile pipeline for generating genomic point mutants in C. elegans Using CRISPR/Cas9 ribonucleoproteins. *J. Vis. Exp. JoVE* **134**, 57518 (2018).
84. Eroglu, M., Yu, B. & Derry, W. B. Efficient CRISPR/Cas9 mediated large insertions using long single-stranded oligonucleotide donors in C. elegans. *FEBS J.* **290**, 4429–4439 (2023).
85. Ghanta, K. S., Ishidate, T. & Mello, C. C. Microinjection for precision genome editing in Caenorhabditis elegans. *STAR Protoc.* **2**, 100748 (2021).
86. Ghanta, K. S. & Mello, C. C. Melting dsDNA donor molecules greatly improves precision genome editing in caenorhabditis elegans. *Genetics* **216**, 643–650 (2020).
87. Dickinson, D. J., Ward, J. D., Reiner, D. J. & Goldstein, B. Engineering the Caenorhabditis elegans genome using Cas9-triggered homologous recombination. *Nat. Methods* **10**, 1028–1034 (2013).

88. Dickinson, D. J., Pani, A. M., Heppert, J. K., Higgins, C. D. & Goldstein, B. Streamlined genome engineering with a self-excising drug selection cassette. *Genetics* **200**, 1035–1049 (2015).
89. Chen, C., Fenk, L. A. & Bono, M. Efficient genome editing in Caenorhabditis elegans by CRISPR-targeted homologous recombination. *Nucleic Acids Res.* **41**, e193 (2013).
90. Huang, G. et al. Improved CRISPR/Cas9 knock-in efficiency via the self-excising cassette (SEC) selection method in C. elegans. *MicroPublication Biol.* **2021**, (2021).
91. Kocsisova, Z., Mohammad, A., Kornfeld, K. & Schedl, T. Cell cycle analysis in the C. elegans germline with the thymidine analog EdU. *J. Vis. Exp. JoVE* **140**, 58339 (2018).
92. Fox, P. M. et al. Cyclin E and CDK-2 regulate proliferative cell fate and cell cycle progression in the C. elegans germline. *Dev. Camb. Engl.* **138**, 2223–2234 (2011).
93. Schindelin, J. et al. Fiji: an open-source platform for biological-image analysis. *Nat. Methods* **9**, 676–682 (2012).
94. Byrd, D. T., Knobel, K., Affeldt, K., Crittenden, S. L. & Kimble, J. A DTC niche plexus surrounds the germline stem cell pool in Caenorhabditis elegans. *PloS One* **9**, e88372 (2014).
95. Voronina, E., Paix, A. & Seydoux, G. The P granule component PGL-1 promotes the localization and silencing activity of the PUF protein FBF-2 in germline stem cells. *Dev. Camb. Engl.* **139**, 3732–3740 (2012).
96. Chao, M. Y., Komatsu, H., Fukuto, H. S., Dionne, H. M. & Hart, A. C. Feeding status and serotonin rapidly and reversibly modulate a Caenorhabditis elegans chemosensory circuit. *Proc. Natl. Acad. Sci. USA* **101**, 15512–15517 (2004).
97. Evans, R. et al. *Protein Complex Prediction with AlphaFold-Multimer*. Preprint at *bioRxiv* https://doi.org/10.1101/2021.10.04.463034 (2021).
98. Zaru, R. & Orchard, S. UniProt Tools: BLAST, align, peptide search, and ID mapping. *Curr. Protoc.* **3**, e697 (2023).
99. Leman, J. K. et al. Macromolecular modeling and design in Rosetta: recent methods and frameworks. *Nat. Methods* **17**, 665–680 (2020).
100. UniProt Consortium UniProt: the universal protein knowledgebase in 2023. *Nucleic Acids Res.* **51**, D523–D531 (2023).
101. Lee, J. et al. CHARMM-GUI Input Generator for NAMD, GROMACS, AMBER, OpenMM, and CHARMM/OpenMM Simulations Using the CHARMM36 Additive Force Field. *J. Chem. Theory Comput.* **12**, 405–413 (2016).
102. Jo, S., Kim, T., Iyer, V. G. & Im, W. CHARMM-GUI: a web-based graphical user interface for CHARMM. *J. Comput. Chem.* **29**, 1859–1865 (2008).
103. Jorgensen, W. L., Chandrasekhar, J., Madura, J. D., Impey, R. W. & Klein, M. L. Comparison of simple potential functions for simulating liquid water. *J. Chem. Phys.* **79**, 926–935 (1983).
104. Huang, J. & MacKerell, A. D. CHARMM36 all-atom additive protein force field: Validation based on comparison to NMR data. *J. Comput. Chem.* **34**, 2135–2145 (2013).
105. Van Der Spoel, D. et al. GROMACS: Fast, flexible, and free. *J. Comput. Chem.* **26**, 1701–1718 (2005).
106. Abraham, M. J. et al. GROMACS: High performance molecular simulations through multi-level parallelism from laptops to supercomputers. *SoftwareX* **1–2**, 19–25 (2015).
107. Humphrey, W., Dalke, A. & Schulten, K. VMD: visual molecular dynamics. *J. Mol. Graph.* **14**, 27–28 (1996). 33–38.
108. Stäubert, C., Broom, O. J. & Nordström, A. Hydroxycarboxylic acid receptors are essential for breast cancer cells to control their lipid/fatty acid metabolism. *Oncotarget* **6**, 19706–19720 (2015).

Acknowledgements

We thank Franziska Fiedler, Niko Fleischer, and Anna Tisnikar for help with generating constructs and establishing phenotyping assays, Hannah Mönch and Daniel Fox for support with data analysis, and Claudia Binder, Diane Schmiegelt, Barbara Klüver, and Ronald Weichelt for technical assistance. We are very grateful to Mike Boxem, John Calarco, Oliver Hobert, Erik Jorgensen, Ralf Schnabel, and Allison Woollard for kindly providing plasmids, W. Brent Derry and the *Caenorhabditis Genetics Center* (CGC) (which is funded by the NIH Office of Research Infrastructure Programs (P40 OD010440)) for generously sharing *C. elegans* strains. We would further like to acknowledge the Center for Advanced Imaging (CAi) at the Heinrich Heine University Düsseldorf for providing access to the Leica TCS SP8 STED 3X and the Abberior Facility Line, and especially Sebastian Hänsch for general support with imaging and analysis. This work was supported by a scholarship to D.M. from the Medical Faculty, Leipzig University, and by a Humboldt Professorship to J.M. from the Alexander von Humboldt Foundation. The authors acknowledge grants from the Deutsche Forschungsgemeinschaft (DFG, German Research Foundation) through CRC 1423/2 (project number 421152132; B03 (A.K.), C04 (S.P., T.S.), Z04 (P.W.H., J.M.)), FOR 2149 (project number 246212759; P02 (S.P.) and P04 (T.S.)), and SPP2363 (project number 460865652 (J.M.)). Funding for instrumentation: Leica TCS SP8 STED 3X: DFG INST 208/665-1 FUGG; Abberior Facility Line: DFG INST 208/805-1 FUGG. Financial support was also provided by the Federal Ministry of Education and Research of Germany and by the Sächsische Staatsministerium für Wissenschaft, Kultur und Tourismus in the program Center of Excellence for AI Research, Center for Scalable Data Analytics and Artificial Intelligence Dresden/Leipzig (project identification number SCADS24B (F.L., J.M.)).

Author contributions

S.P. conceived and designed the study. W.B.P.: cloning, transgene generation, genetic modification, worm genetics, PH3 assays, anus phenotyping, Notch activation assays, Western Blot, BiFC assays, and data analysis. V.E.G.: worm genetics, DAPI, PH3, REC-8, EdU, and GLD-1 assays, data analysis. D.M.: worm genetics, design of DAPI, PH3, REC-8, EdU, GLD-1, and DTC morphology assays, data analysis. I.C.: ELISA experiments, octanol reversion assays. F.L. and J.M.: molecular modeling. F.S. and P.W.H.: MD simulations. A.K.: BRET assays. T.S.: data analysis. W.B.P., V.E.G., D.M., and S.P. wrote the manuscript with the consent of all co-authors. All authors agreed to the final version of the manuscript.

Funding

Open Access funding enabled and organized by Projekt DEAL.

Competing interests

The authors declare no competing interests.

Additional information

Supplementary information The online version contains supplementary material available at https://doi.org/10.1038/s41467-025-61730-0.

Correspondence and requests for materials should be addressed to Simone Prömel.

Peer review information *Nature Communications* thanks the anonymous reviewers for their contribution to the peer review of this work. A peer review file is available.

Reprints and permissions information is available at http://www.nature.com/reprints

Publisher's note Springer Nature remains neutral with regard to jurisdictional claims in published maps and institutional affiliations.

Open Access This article is licensed under a Creative Commons Attribution 4.0 International License, which permits use, sharing, adaptation, distribution and reproduction in any medium or format, as long as you give appropriate credit to the original author(s) and the source, provide a link to the Creative Commons licence, and indicate if changes were made. The images or other third party material in this article are included in the article's Creative Commons licence, unless indicated otherwise in a credit line to the material. If material is not included in the article's Creative Commons licence and your intended use is not permitted by statutory regulation or exceeds the permitted use, you will need to obtain permission directly from the copyright holder. To view a copy of this licence, visit http://creativecommons.org/licenses/by/4.0/.

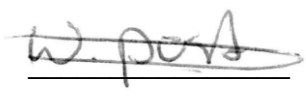
© The Author(s) 2025

Detailed author contributions

For the publication ‘Notch activity is modulated by the aGPCR Latrophilin binding the DSL ligand in *C. elegans*’ the following contributions were made by Willem Berend Post:

- Design and construction of all plasmids
- Maintenance and crossing of C. elegans strains
- Generation of transgenic C. elegans strains using extrachromosomal arrays and CRISPR/Cas9
- BiFC analysis
- PH3-antibody, anti-V5 antibody staining
- Distal Tip Cell morphology quantification
- Western Blot analysis
- Confocal microscopy
- Data analysis
- Manuscript writing

Date: 6th May 2026





Willem Berend Post Prof. Dr. Simone Prömel

5 The Adhesion GPCR ADGRL2/LPHN2 Can Protect Against Cellular and Organismal Dysfunction

Authors: Philipp Jakobs†, Anne Rafflenbeul†, Willem Berend Post†, Niloofar Ale-Agha, Victoria Elisabeth Groß, Stephanie Pick, Sascha Dolata, Fiona F. Cox, Florian von Ameln, Olaf Eckermann, Joachim Altschmied, Simone Prömel and Judith Haendeler

† These authors contributed equally to this work

Journal: Cells

Publisher: Multidisciplinary Digital Publishing Institute (MDPI)

Impact Factor: 5.2

Submitted: 15 October 2024

Accepted: 31 October 2024

Published: 5 November 2024

Keywords: ADGRL2/LPHN2, *Caenorhabditis elegans*, endothelial cells, eNOS, lipopolysaccharide, NRF2, *skn-1*, reactive oxygen species

DOI: 10.3390/cells13221826

PubMed ID: 39594576

cells

MDPI

Article

The Adhesion GPCR ADGRL2/LPHN2 Can Protect Against Cellular and Organismal Dysfunction

Philipp Jakobs [1,†], Anne Rafflenbeul [2,†], Willem Berend Post [3,†], Niloofar Ale-Agha [1], Victoria Elisabeth Groß [3], Stephanie Pick [3], Sascha Dolata [3], Fiona F. Cox [2], Florian von Ameln [2], Olaf Eckermann [1], Joachim Altschmied [2], Simone Prömel [3,*] and Judith Haendeler [1,*]

[1] Cardiovascular Degeneration, Haendeler Group, Clinical Chemistry and Laboratory Diagnostics, Medical Faculty, University Hospital and Heinrich Heine University Düsseldorf, 40225 Düsseldorf, Germany; philipp.jakobs@hhu.de (P.J.); niale001@hhu.de (N.A.-A.); olaf.eckermann@hhu.de (O.E.)

[2] Cardiovascular Degeneration, Altschmied Group, Clinical Chemistry and Laboratory Diagnostics, Medical Faculty, University Hospital and Heinrich Heine University Düsseldorf, 40225 Düsseldorf, Germany; anne.rafflenbeul@hhu.de (A.R.); fiona.cox@hhu.de (F.F.C.); florian.ameln@hhu.de (F.v.A.); joalt001@hhu.de (J.A.)

[3] Institute of Cell Biology, Department of Biology, Heinrich Heine University Düsseldorf, 40225 Düsseldorf, Germany; postw@hhu.de (W.B.P.); grossv@hhu.de (V.E.G.); stephanie.pick@hhu.de (S.P.); sascha.dolata@hhu.de (S.D.)

* Correspondence: proemel@hhu.de (S.P.); juhae001@hhu.de (J.H.); Tel.: +49-211-81-13816 (S.P.); +49-211-8112008 (J.H.)

† These authors contributed equally to this work.

Abstract: The most common trigger of sepsis and septic shock is bacterial lipopolysaccharide (LPS). Endothelial cells are among the first to encounter LPS directly. Generally, their function is closely linked to active endothelial NO Synthase (eNOS), which is significantly reduced under septic conditions. LPS treatment of endothelial cells leads to their activation and apoptosis, resulting in loss of integrity and vascular leakage, a hallmark of septic shock. Hence, therapies that prevent endothelial leakage or restore the endothelial barrier would be invaluable for patients. Adhesion GPCRs (aGPCRs) have been largely overlooked in this context, although particularly one of them, ADGRL2/LPHN2, has been implicated in endothelial barrier function. Our study shows that overexpression of ADGRL2 protects endothelial cells from LPS-induced activation, apoptosis, and impaired migration. Mechanistically, ADGRL2 preserves eNOS activity by shifting its binding from Caveolin-1 to Heat Shock Protein 90. Furthermore, ADGRL2 enhances antioxidative responses by increasing NRF2 activity. Notably, we found that this function may be evolutionarily conserved. In the absence of *lat-2*, a homolog of ADGRL2 in *Caenorhabditis elegans*, worms show higher ROS levels and altered stress response gene expression. Additionally, *lat-2* mutants have a significantly reduced lifespan, altogether indicating a protective role of ADGRL2 against oxidative stress across species.

Keywords: ADGRL2/LPHN2; *Caenorhabditis elegans*; endothelial cells; eNOS; lipopolysaccharide; NRF2; *skn-1*; reactive oxygen species

check for updates

Citation: Jakobs, P.; Rafflenbeul, A.; Post, W.B.; Ale-Agha, N.; Groß, V.E.; Pick, S.; Dolata, S.; Cox, F.F.; von Ameln, F.; Eckermann, O.; et al. The Adhesion GPCR ADGRL2/LPHN2 Can Protect Against Cellular and Organismal Dysfunction. *Cells* **2024**, *13*, 1826. https://doi.org/10.3390/cells13221826

Academic Editor: Aditi Bhargava

Received: 15 October 2024
Revised: 30 October 2024
Accepted: 31 October 2024
Published: 5 November 2024

Copyright: © 2024 by the authors. Licensee MDPI, Basel, Switzerland. This article is an open access article distributed under the terms and conditions of the Creative Commons Attribution (CC BY) license (https://creativecommons.org/licenses/by/4.0/).

1. Introduction

Sepsis can best be described as an overshooting immune response to a microbial infection, which can lead to shock, multiple organ failure, and often death. In 2017, the World Health Organization (WHO) estimated that sepsis affects more than 48 million individuals every year, potentially leading to 11 million deaths annually [1]. The basis for the pathophysiological responses in sepsis and septic shock is multifactorial, which might serve as an explanation why—besides vasopressor agents, which have been in use for several decades—no new therapeutic approaches have been developed for sepsis treatment to date.

The most common trigger for sepsis and septic shock is bacterial lipopolysaccharide (LPS), a serologically reactive bacterial toxin. It is a component of the outer membrane of Gram-negative bacteria, which triggers a strong proinflammatory response in the human immune system, with 1 to 2 mg in the bloodstream potentially being lethal [2]. LPS can enter the bloodstream through intestinal absorption of the LPS produced by gut bacteria. Moreover, gut lesions and diets rich in lipids boost the transport across membranes into the systemic circulation [3]. Therefore, at the cellular level, endothelial cells (ECs) are, besides circulating immune cells, the first cells directly confronted with LPS.

Endothelial functionality is intrinsically tied to the availability of NO produced by endothelial NO Synthase (eNOS). Under septic conditions or during chronic inflammation, this enzymes' activity is severely reduced [2,4]. Moreover, LPS triggers endothelial cell activation, a proinflammatory and procoagulant state of the endothelium, and ultimately apoptosis, resulting in loss of the endothelial integrity and vascular leakage, a mainstay of septic shock [2]. Hence, therapies, which could prevent endothelial cell leakage or even restore the endothelial barrier, would be of enormous value for patients and would address medical needs. However, up to now, the molecular mechanisms by which LPS leads to endothelial activation, apoptosis, and leakage are far from understood.

One class of molecules, which role in endothelial functionality has been underestimated to date, is Adhesion G protein-coupled receptors (aGPCRs). They combine cellular adhesion with intracellular signaling. Many features of aGPCRs, such as their ability to mediate cell–cell interactions and adhesion, makes them interesting candidates to be involved in EC function. Intriguingly, three aGPCRs, which are expressed in ECs, have been firmly linked to their function to date: ADGRF5/GPR116, ADGRL2/LPHN2, and ADGRL4/ELTD1, with the latter two belonging to the group of Latrophilins, which also contains ADGRL1/LPHN1 and ADGRL3/LPHN3 [5].

With respect to barrier function, only ADGRL2 seems to play a role in ECs [6,7]. It is localized at cell-to-extracellular matrix contacts and promotes tight junction assembly. Vascular ECs of ADGRL2-deficient zebrafish embryos are abnormally stretched and, thus, hyperpermeable, such that cells transported by the blood stream extravasate more easily into the surrounding tissues [6]. Further, ADGRL2 regulates flow-induced changes and barrier functions of ECs [7]. These studies suggest essential functions of this aGPCR in the regulation of endothelial integrity and raise the question of whether it also plays a role in LPS-induced endothelial dysfunction.

In the present study, we found protective functions of the Latrophilin ADGRL2 in human ECs, and those are, in part, evolutionarily conserved as *C. elegans* lacking the Latrophilin homolog LAT-2 and have reduced functionality.

2. Materials and Methods

2.1. Cell Culture

Primary human ECs were obtained from LONZA and cultured in endothelial basal medium supplemented with 50 ng/mL amphotericin B, 1 µg/mL hydrocortisone, 50 µg/mL gentamicin, 12 µg/mL bovine brain extract, 10 ng/mL epidermal growth factor (LONZA, Cologne, Germany), and 10% fetal bovine serum until passage 3 was reached in a humidified incubator at 37 °C in an atmosphere containing 5% CO_2.

2.2. Plasmids

To generate a NRF2-dependent firefly luciferase reporter vector, two copies of a 41 bp DNA fragment containing the antioxidant response element (ARE) from the murine Glutathione S-transferase alpha 1 gene promoter [8] were inserted between the *Hind III* and *Bam HI* sites of pTATA LUC+ [9] to generate p$(ARE)_2$TATA-LUC. Then, this tandem ARE was placed directly upstream of the minimal promoter derived from the herpes simplex virus thymidine kinase gene. As specificity control, several point mutations, which had been shown to interfere with the activation of a minimal promoter and/or inducibility by tert-butylhydroquinone conferred by this ARE [8,10], were introduced.

In addition, an invariable A in the ARE consensus derived from polymorphic AREs in the human genome [11] was replaced by a G. These mutations in the resulting plasmid p(AREmut)$_2$TATA-LUC prevented the binding of NRF2 to the mutated ARE. The identity of the newly created plasmids was confirmed by restriction analysis; in addition, the regions containing the AREs were verified by DNA sequencing.

To generate a vector suitable for *ADGRL2* expression in primary human ECs, the SV40 promoter in the pcDps backbone of the previously described expression vector [12] was replaced with the human cytomegalovirus (CMV) immediate early promoter and enhancer. Therefore, a 1.4 kbp *Sca* I/*Eco* RV fragment from pcDNA3.1/myc-His(-)C (Thermo Fisher Scientific, Dreieich, Germany) containing part of the ampicillin resistance gene and the CMV promoter/enhancer was isolated and inserted into the backbone of the pcDps-based expression vector cut with *Sca* I and *Stu* I using the Blunt/TA Ligase Master Mix (New England Biolabs, Frankfurt, Germany). The identity of the newly created expression vector was verified by restriction analysis. Complete plasmid sequences are available upon request.

2.3. Transient Transfection of ECs

Transient transfections of ECs were performed with Effectene (Qiagen, Hilden, Germany). In detail, cells were transfected on 6 cm culture dishes with 2.5 µg plasmid DNA, 20 µL Enhancer, and 25 µL Effectene in 150 µL buffer; subsequently, 1 mL cell culture medium was added. For transfections of luciferase reporter plasmids, 0.25 µg of these were used and made up to 2.5 µg with either an empty vector or the *ADGRL2* expression vector. For transfections in 6-well culture plates, 1 µg plasmid DNA, 8 µL Enhancer, and 10 µL Effectene in 100 µL buffer were used; subsequently, 300 µL medium were added.

2.4. Generation of Sequence Logos

The ARE sequence logo was generated using WebLogo 3 (https://weblogo.threeplusone.com/, accessed on 10 October 2024 [13]) using the matrix profile for the human NRF2-binding site (MA0150.1) from JASPAR 2024 [14].

2.5. Migration Assay

The migration of ECs was quantitated by the scratch wound assay; therefore, the cells were cultivated on 6 cm dishes. Before a wound was set by scraping off a section of the monolayer with a sterile disposable rubber policeman, the bottom of the dishes was labeled with a trace line indicating the wound position. After setting the injury, detached cells were removed by a gentle washing step with culture medium, and 20 h later, the cells were fixed with 4% (*w*/*v*) formaldehyde for 15 min at room temperature and stained with 500 ng/mL 4′,6-diamidino-2-phenylindole (DAPI) (Carl Roth, Karlsruhe, Germany) in PBS, and microscopic pictures were taken using a Zeiss Axio Observer 7. The cells, which had migrated into the wound from the trace line, were automatically counted using the particle analysis feature of ImageJ [15] after watershed separation of overlapping nuclei.

2.6. Immunoblotting

Cells were harvested by detaching them from the culture surface with a rubber policeman followed by centrifugation at 800× *g*. After washing the cells twice with ice cold PBS, the supernatant was completely removed. The pelleted cells were resuspended in radioimmunoprecipitation assay (RIPA) buffer (50 mM Tris-HCl, pH 8.0, 150 mM NaCl, 1% (*v*/*v*) IGEPAL-CA630, 0.1% (*w*/*v*) SDS, and 0.5% (*w*/*v*) Na-deoxycholate) supplemented with 1/100 volume of a protease inhibitor cocktail and phosphatase inhibitor cocktail (Bimake, Munich, Germany). The cell suspension was placed on ice for 30 min for lysis, before the lysates were centrifuged at 18,000× *g* and 4 °C for 15 min. The supernatants containing the cellular proteins were transferred to a fresh tube. Proteins were separated by standard sodium-dodecyl-sulfate polyacrylamide gel electrophoresis and blotted onto polyvinylidene difluoride membranes by wet transfer. The membranes were blocked with

5% (*w*/*v*) milk powder in TBS (200 mM Tris-HCl, pH 8.0, 300 mM NaCl, and 100 mM KCl) with 0.1% (*v*/*v*) Tween-20 (TBS-T) for 1 h at room temperature before they were incubated with primary antibodies overnight at 4 °C. The following day, membranes were washed three times with TBS-T and incubated with horseradish peroxidase-coupled secondary antibodies for 2 h at room temperature. Detection was performed using ECL substrate (Cytiva, Marlborough, MA, USA) and X-ray films. Semi-quantitative analyses were performed on scanned X-ray films using ImageJ 2.9.0. [15]. All antibodies used for immunoblotting are listed in Supplementary Table S1.

2.7. Immunostaining

ECs were seeded on acidified glass slides in 6-well culture plates and transfected as described under Section 2.3, and 5 h after transfection, the cells were treated as indicated, and 20 h later, they were fixed with 4% (*w*/*v*) formaldehyde for 15 min at room temperature. This was followed by a blocking/permeabilization step with 3% (*v*/*v*) normal goat serum (Sigma-Aldrich, Deisenhofen, Germany) diluted in PBS containing 0.3% (*v*/*v*) Triton X-100 for 15 min at room temperature. Then, cells were incubated with primary antibodies overnight at 4 °C and subsequently washed three times with PBS. After that, they were incubated with Alexa Fluor-coupled secondary antibodies for 1 h at room temperature. Nuclei were counterstained with DAPI (500 ng/mL) (Carl Roth, Karlsruhe, Germany) in PBS for 5 min at room temperature. Finally, cells were mounted with ProLong Diamond Antifade Mountant (Thermo Fisher Scientific, Dreieich, Germany). Images were taken using Zeiss Axio Observer 7 (magnification 400× or 200×), and pixel intensities were measured with ImageJ 2.9.0. [15]. All antibodies used for immunostaining are listed in Supplementary Table S2.

2.8. Luciferase Assay

The day after transfection, the cells were lysed with Reporter Lysis Buffer (Promega, Mannheim, Germany) according to the manufacturer's instructions. Identical amounts of cellular protein were made up to 30 µL with Reporter Lysis Buffer, and luciferase activity was measured by the automatic injection of 100 µL Luciferase Assay Reagent (Promega, Mannheim, Germany) using a LB 960 CENTRO XS3 Luminometer (Berthold, Bad Wildbad, Germany).

2.9. Proximity Ligation Assay

Up to the incubation with the primary antibodies, all steps were identical to the procedures described under Section 2.7. *Immunostaining*. After overnight incubation at 4 °C with the primary antibodies, cells were treated with the components of the Duolink In Situ detection kit (Sigma-Aldrich, Deisenhofen, Germany) according to the manufacturer's instructions. The actin cytoskeleton was stained with Phalloidin CF488A (1:70) (Biotium/Biomol, Hamburg, Germany) for 20 min at room temperature; nuclei were stained with DAPI (500 ng/mL) (Carl Roth, Karlsruhe, Germany) in PBS for 5 min at room temperature. The primary antibodies were the same as for immunostaining and are listed in Supplementary Table S2.

2.10. C. elegans Maintenance and Strains

C. elegans were maintained at 22 °C on nematode growth medium (NGM) agar plates seeded with *E. coli OP50* according to standard methods [16]. Experiments were performed at 22 °C unless stated otherwise. Wild-type worms were *C. elegans* var. Bristol strain N2 [16], and *lat-2(knu505(8932 bp deletion)) II* was generated by NemaMetrix Inc. (Eugene, OR, USA) using CRISPR/Cas9 genome editing deleting the entire *lat-2* coding sequence.

2.11. Lifespan Measurements

Synchronized L4 hermaphrodites were transferred to fresh plates daily during the reproductive period and every third day thereafter. Nematode viability was assessed every

2–3 days. An individual was considered dead if there was no movement or response to touch. Those that died from rupture, internal bagging, or were missing were censored from the data.

2.12. Brood Size Assays

L4 hermaphrodites were placed separately on NGM agar plates seeded with *E. coli OP50* and allowed to lay eggs. The individuals were transferred to a fresh plate every 24 h until egg-laying ceased, and eggs were counted. Plates were incubated at 22 °C. To determine survival to adulthood, the number of adult animals was scored 48 h after the mother was removed.

2.13. ROS Quantification in C. elegans

To study ROS levels in nematodes under normal, as well as stress, conditions, ROS were quantified using H_2DCF-DA (Thermo Fisher Scientific, Dreieich, Germany), which readily permeates cell membranes. Bleach-synchronized L4 + 1-day-old nematodes were washed off plates, collected, washed three times with M9 to remove bacteria, and exposed to either 100 µM juglone (in ethanol, prepared fresh before every assay) or vehicle-only (0.9% ethanol) conditions for 1 h in PBS-Tween20 (0.1%) (PBS-T). Worms were washed three times with PBS-T and freeze-cracked once in liquid nitrogen. Sonication was applied for 1 min to disrupt cellular membranes followed by centrifugation at 21,000× *g* for 15 min. Protein amounts were determined with a Bradford assay using RotiQuant (Carl Roth, Karlsruhe, Germany). Subsequently, 50 µL of supernatant was added to a black, clear-bottom 96-well plate, and 50 µL 100 µM H_2DCF-DA was added. Samples were mixed and incubated for 30 min, followed by a 2 h kinetic measurement of the fluorescence levels (excitation: 485 ± 25 nm, emission: 535 ± 20 nm). The ROS levels were quantified by subtracting end measurement values from the starting values and normalizing for nematode quantity based on the protein concentrations determined by the Bradford assay.

2.14. Isolation of Total RNA

Total cellular RNA from ECs was isolated as previously described [17]. In detail, TRIzol (Thermo Fisher Scientific, Dreieich, Germany) was used to extract total RNA from ECs according to the manufacturer's instructions. Further purification of RNA was achieved by using the RNeasy Mini kit (Qiagen, Hilden, Germany), and concentrations were measured using a NanoDrop™ 2000c (Thermo Fisher Scientific, Dreieich, Germany). RNA integrity and purity were analyzed by agarose gel electrophoresis. Nematode RNA was isolated by washing young adult nematodes off NGM plates and washing thrice with M9 buffer. The worms were subsequently resuspended in 200 µL TRI Reagent (Thermo Fisher Scientific, Dreieich, Germany) and snap-frozen in liquid nitrogen, followed by freeze–thawing three times. RNA was isolated using the Direct-zol RNA MiniPrep kit (Zymo Research, Freiburg, Germany) according to the manufacturer's instructions and checked for integrity by agarose gel electrophoresis.

2.15. cDNA Synthesis

RNA from ECs was reverse-transcribed using the QuantiTect Reverse Transcription kit (Qiagen, Hilden, Germany) according to the manufacturer's instructions. cDNA synthesis from *C. elegans* samples was performed using the Luna Script RT Master Mix with Oligo d(T)23 VN primers (both New England Biolabs, Frankfurt, Germany). A total of 500 ng of RNA was transcribed into cDNA following the manufacturer's instructions.

2.16. Polymerase Chain Reaction (PCR)

The transcript levels in ECs were determined by semi-quantitative real-time PCR with cDNA as template and the primaQUANT 2× qPCR-SYBR-Green-Master Mix (Steinbrenner, Wiesenbach, Germany); the transcript for the ribosomal protein L32 (*RPL32*) was used for normalization. Thermal cycling was performed in a Rotor-Gene Q instrument

The transcript levels in ECs were determined by semi-quantitative real-time PCR with cDNA as template and the primaQUANT 2× qPCR-SYBR-Green-Master Mix (Steinbrenner, Wiesenbach, Germany); the transcript for the ribosomal protein L32 (*RPL32*) was used for normalization. Thermal cycling was performed in a Rotor-Gene Q instrument (Qiagen, Hilden, Germany). Relative expression was calculated by the ΔC_t method [18]. Homogeneity of the reaction products was analyzed by melting point analysis, and their size was confirmed by standard agarose gel electrophoresis. Transcript levels of target genes from nematode samples were determined by qPCR using the Luna Universal qPCR Master Mix (New England Biolabs, Frankfurt, Germany) according to the manufacturer's instructions. cDNA from each sample was diluted 1:10 with nuclease-free water, and 2 µL of this diluted cDNA was used in each qPCR reaction. To normalize the gene expression levels, the housekeeping genes *act-1*, *cdc-42*, *pmp-3*, *eif-3.C*, and *tba-1* were used. C_t values of these housekeeping genes were averaged to provide a robust normalization factor. Relative quantification of target gene expression was carried out using the $\Delta\Delta C_t$ method, as described by [19]. For the primer sequences, see Supplementary Table S3.

2.17. Statistics

The number of experiments (n) represents independent biological replicates. The data presented are the mean ± SEM. Normal distribution was confirmed by the Shapiro–Wilk test, and homogeneity of the variances (from means) was verified by Levene's test. Since all data sets represented normal distribution, the multiple comparisons were performed using one-way ANOVA with post hoc Tukey LSD test or two-way ANOVA with post hoc Bonferroni test (for *C. elegans* ROS assays) or Student's *t*-test (for *C. elegans* assays). *C. elegans* lifespan analyses were displayed as Kaplan–Meier curves and a Cox–Mantel test was performed to test for significance. Details are given in the respective figure legends.

3. Results

3.1. ADGRL2 Expression Is Reduced in ECs in Response to LPS

To investigate the effects of LPS on *ADGRL2* expression in ECs, we first treated primary human ECs with 150 ng/mL active LPS or detoxified LPS as the control. As shown in Figure 1, *ADGRL2* expression was significantly reduced in response to LPS.

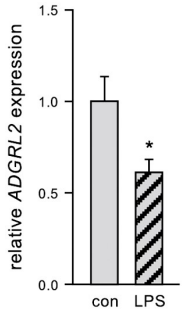


Figure 1. LPS downregulates *ADGRL2* expression in primary human ECs. ECs were treated for 20 h with 150 ng/mL active LPS (LPS) or detoxified LPS as the control (con). Expression of *ADGRL2* was determined by semi-quantitative real-time PCR. *RPL32* was used for normalization (data are the mean ± SEM, n = 4, * $p < 0.05$ vs. con, unpaired, two-sided Student's *t*-test).

We had previously published that LPS induces activation and apoptosis [17] and reduces the migratory capacity of ECs [20]—all of them hallmarks of endothelial dysfunction. Based on the downregulation of *ADGRL2*, we hypothesized that its overexpression could counteract LPS-induced dysfunctionality of ECs.

3.2. ADGRL2 Overexpression Inhibits LPS-Induced EC Activation, Apoptosis, and Preserves Migratory Capacity

To study the impact of ADGRL2 on endothelial cell functions affected by LPS, we generated an expression vector, which contained HA (N-terminus) and FLAG (C-terminus)-epitope tags allowing the identification of the overexpressed protein. We then investigated the effects of HA-ADGRL2-FLAG on EC activation, apoptosis, and migration. Therefore, HA-ADGRL2-FLAG was expressed in ECs, and ECs were treated with 150 ng/mL LPS

for 20 h. For EC activation, ICAM1 (Intercellular Adhesion Molecule 1), a typical marker, was detected. As expected LPS induced an elevation in ICAM1 levels in empty vector (EV) transfected cells. This upregulation was completely inhibited in cells in which HA-ADGRL2-FLAG is overexpressed (Figure 2A,B).

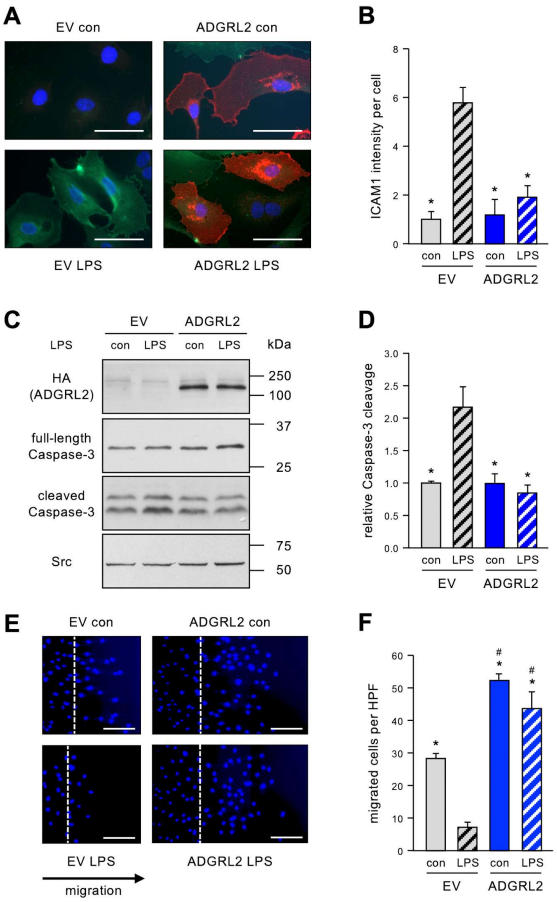


Figure 2. ADGRL2 prevents LPS-induced activation and apoptosis of ECs and enhances the migratory capacity. ECs were transfected with an expression vector for ADGRL2 or a corresponding empty vector (EV). After transfection, the cells were treated for 20 h with 150 ng/mL active LPS (LPS) or detoxified LPS as the control (con). (**A**,**B**) Cells were fixed and stained for ICAM1 (green) and ADGRL2 (red), and nuclei were counterstained with DAPI. (**A**) Representative immunofluorescence staining (scale bars = 50 µm). (**B**) Semi-quantitative analysis of ICAM1 levels per cell (data are the mean ± SEM, n = 4, * $p < 0.05$ vs. EV/LPS, one-way ANOVA with post hoc Tukey LSD test). (**C**,**D**) HA-tagged ADGRL2 (HA(ADGRL2)), uncleaved (full-length Caspase-3), and cleaved Caspase-3 were detected by immunoblot, and Src served as the loading control. (**C**) Representative immunoblots. (**D**) Semi-quantitative analysis of relative amounts of cleaved Caspase-3 (data are the mean ± SEM, n = 5, * $p < 0.05$ vs. EV/LPS, one-way ANOVA with post hoc Tukey LSD test). (**E**,**F**) The migratory capacity was determined by scratch wound assays. Cell nuclei were stained with DAPI. (**E**) Representative DAPI staining. Wounds were set at the dashed lines; right of the lines are the cells that had migrated into them (scale bars = 100 µm). (**F**) Semi-quantitative analysis of migrated cells per high-power field (HPF) (data are the mean ± SEM, n = 5–6, * $p < 0.05$ vs. EV/LPS, # $p < 0.05$ vs. EV/con, one-way ANOVA with post hoc Tukey LSD test).

3.3. ADGRL2 Overexpression Counteracts the LPS-Induced Reduction in Endothelial NO Synthase Activity

Activation and apoptosis induction, as well as the impaired migratory capacity of ECs, are all linked to reduced NO bioavailability. Thus, we next investigated the impact of the effector caspase-3 as the marker for ICAM1 LPS-induced caspase-3 cleavage in EV transfected cells, whereas overexpression of HA-ADGRL2-FLAG blunted apoptosis induction by LPS (Figure 2C,D).

Next, we determined the effect of HA-ADGRL2-FLAG on apoptosis and used the cleavage of caspase-3 as the marker. As for ICAM1, LPS-induced caspase-3 cleavage in EV transfected cells, whereas overexpression of HA-ADGRL2-FLAG blunted apoptosis induction by LPS (Figure 2C,D).

Finally, we measured the migratory capacity of ECs, and 3 h after transfection, a wound was set into the EC layer and cells were treated with LPS for 20 h. As shown in

Figure 2, HA-ADGRL2-FLAG not only inhibited LPS-induced impairment in the migratory capacity but also significantly improved migration when compared to EV transfected cells (Figure 2E,F).

3.3. ADGRL2 Overexpression Counteracts the LPS-Induced Reduction in Endothelial NO Synthase Activity

Activation and apoptosis induction, as well as the impaired migratory capacity of ECs, are all linked to reduced NO bioavailability. Thus, we next investigated the phosphorylation states of the eNOS as a surrogate marker for its activity. Phosphorylation of serine 1177 (S1177) activates the enzyme, whereas phosphorylation of threonine 495 (T495) inactivates it [21]. HA-ADGRL2-FLAG was expressed in ECs, and cells were again treated with 150 ng/mL LPS. As expected, LPS reduced the phosphorylation of eNOS S1177 and increased the phosphorylation of T495 (Figure 3), demonstrating a reduction in active eNOS and, thereby, NO bioavailability. HA-ADGRL2-FLAG completely inhibited LPS-induced dephosphorylation of eNOS S1177, as well as phosphorylation of eNOS T495 (Figure 3), indicating the preservation of enzyme activity. Interestingly, the phosphorylation of eNOS T495 was also reduced when compared to EV transfected cells treated with detoxified LPS (Figure 3C). Thus, we could assume that overexpression of ADGRL2 already under basal conditions increases NO bioavailability.

Cells **2024**, *13*, x FOR PEER REVIEW 9 of 17

active eNOS and, thereby, NO bioavailability. HA-ADGRL2-FLAG completely inhibited LPS-induced dephosphorylation of eNOS S1177, as well as phosphorylation of eNOS T495 (Figure 3), indicating the preservation of enzyme activity. Interestingly, the phosphorylation of eNOS T495 was also reduced when compared to EV transfected cells treated with detoxified LPS (Figure 3C). Thus, we could assume that overexpression of ADGRL2 already under basal conditions increases NO bioavailability.

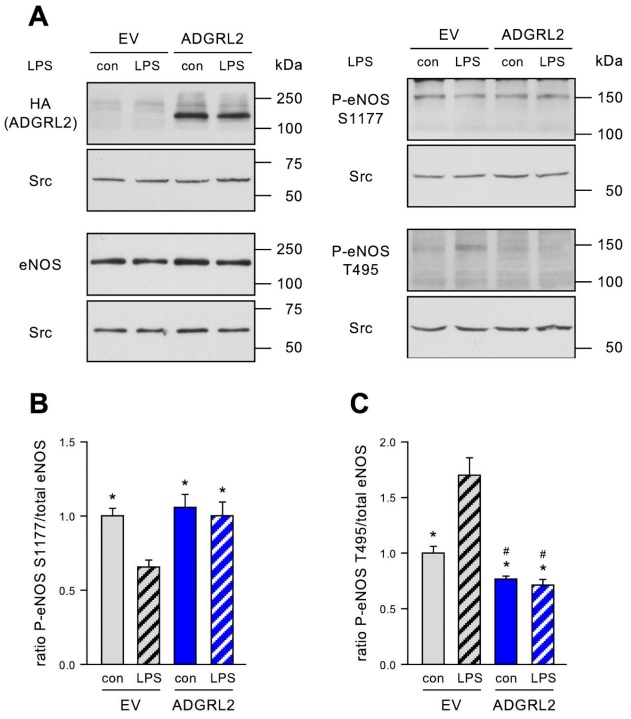


Figure 3. ADGRL2 increases eNOS activity. ECs were transfected with an expression vector for *ADGRL2* or a corresponding empty vector (EV). After transfection, the cells were treated for 20 h with 150 ng/mL active LPS (LPS) or detoxified LPS as the control (con). HA-tagged ADGRL2 (HA (ADGRL2)), total eNOS (eNOS), and eNOS phosphorylated at serine 1177 (P-eNOS S1177) or at threonine 495 (P-eNOS T495), respectively, were detected by immunoblot; in all cases, Src served as the loading control. (**A**) Representative immunoblots; each blot is shown with its respective loading control. (**B**) Semi-quantitative analysis of the ratio of eNOS phosphorylated at serine 1177 to the total eNOS (data are the mean ± SEM, n = 8, * $p < 0.05$ vs. EV/LPS, one-way ANOVA with post hoc Tukey LSD test). (**C**) Semi-quantitative analysis of the ratio of eNOS phosphorylated at threonine 495 to total eNOS (data are the mean ± SEM, n = 5, * $p < 0.05$ vs. EV/LPS, # $p < 0.05$ vs. EV/con, one-way ANOVA with post hoc Tukey LSD test).

For a deeper understanding of the mechanisms underlying the effects of ADGRL2 on eNOS, it has to be noted that the binding of eNOS to Caveolin-1 inhibits its enzymatic activity and, thus, NO production, whereas interaction with Heat Shock Protein 90 (HSP90) enhances the activity of eNOS [22–25]. Therefore, we next investigated the role of ADGRL2 in eNOS binding to Caveolin-1 and HSP90 in ECs.

3.4. ADGRL2 Overexpression Reduces eNOS Interactions with Caveolin-1 and Enhances Binding to HSP90

To determine potential changes in the interactions of eNOS with Caveolin-1 or HSP90, we performed proximity ligation assays (PLAs) in ECs transfected with EV or HA-

For a deeper understanding of the mechanisms underlying the effects of ADGRL2 on eNOS, it has to be noted that the binding of eNOS to Caveolin-1 inhibits its enzymatic activity and, thus, NO production, whereas interaction with Heat Shock Protein 90 (HSP90) enhances the activity of eNOS [22–25]. Therefore, we next investigated the role of ADGRL2 in eNOS binding to Caveolin-1 and HSP90 in ECs.

3.4. ADGRL2 Overexpression Reduces eNOS Interactions with Caveolin-1 and Enhances Binding to HSP90

To determine potential changes in the interactions of eNOS with Caveolin-1 or HSP90, we performed proximity ligation assays (PLAs) in ECs transfected with EV or HA-ADGRL2-FLAG in the presence or absence of active LPS (Figure 4).

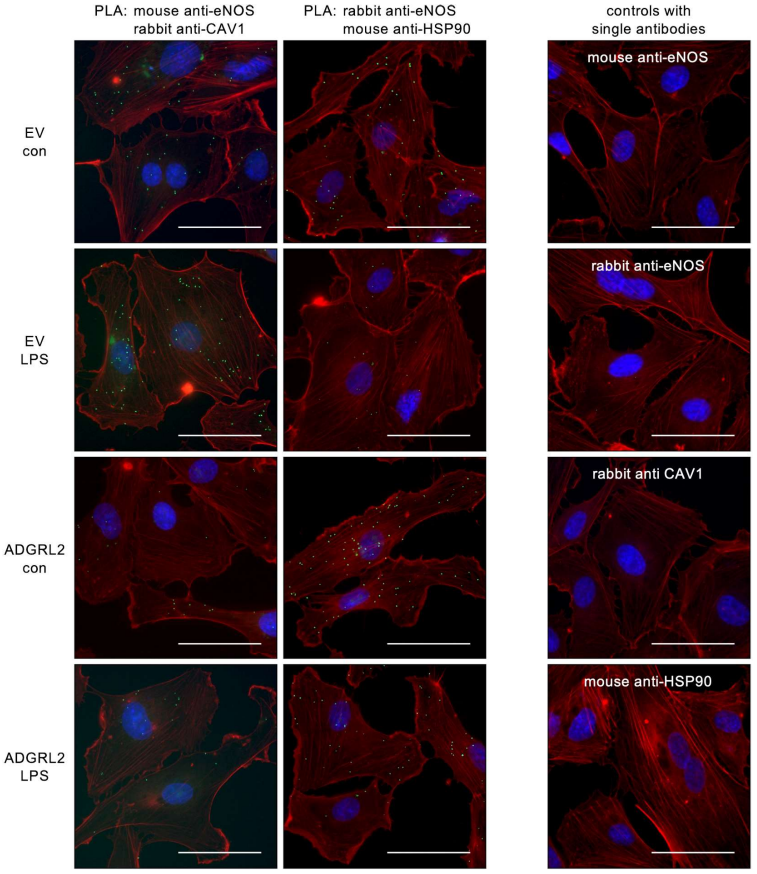


Figure 4. ADGRL2 alters eNOS interactions with Caveolin-1 and HSP90. ECs were transfected with an expression vector for *ADGRL2* or a corresponding empty vector (EV). After transfection, the cells were treated for 20 h with 150 ng/mL active LPS (LPS) or detoxified LPS as the control (con). Interactions between eNOS and Caveolin-1 (CAV1, left panels) and between eNOS and Heat Shock Protein 90 (HSP90, middle panels), respectively, were detected by a proximity ligation assay (green dots). The cytoskeleton was stained with Phalloidin Alexa 594 (red), and nuclei were counterstained with DAPI (blue). Negative controls, in which only one of the primary antibodies was used, are shown in the right panels (scale bars = 50 µm).

From the PLA data in Figure 4, it is obvious that LPS increased the binding of eNOS to Caveolin-1 and reduced its interactions with HSP90 in EV transfected cells. This is in perfect accordance with the previous observations regarding eNOS phosphorylation at S1177 and T495 (Figure 3), which indicated reduced activity. Interestingly, in cells overexpressing ADGRL2, the interaction between eNOS and Caveolin-1 was markedly diminished when compared to EV transfected cells. Moreover, ADGRL2 inhibited the LPS-induced increase in eNOS–Caveolin-1 interactions (Figure 4, left panels). Along the same lines, ADGRL2 maintained eNOS binding to HSP90 even after LPS treatment (Figure 4, middle panels), thereby keeping eNOS active.

In this context, it has to be noted that an increase in intracellular NO can lead to a dissociation of Kelch-like ECH-associated protein 1 (KEAP1) from NRF2 (NFE2-related factor 2), the master regulator of antioxidative defense. This leads to stabilization of NRF2 and nuclear translocation of this transcription factor. Active, nuclear NRF2, besides

again corroborating the phosphorylation data (Figure 3). Thus, this aGPCR maintains the NO bioavailability even under LPS treatment by supporting the interaction of eNOS with HSP90, thereby keeping eNOS active.

In this context, it has to be noted that an increase in intracellular NO can lead to a dissociation of Kelch-like ECH-associated protein 1 (KEAP1) from NRF2 (NFE2-related factor 2), the master regulator of antioxidative defense. This leads to stabilization of NRF2 and nuclear translocation of this transcription factor. Active, nuclear NRF2, besides reducing oxidative stress, has been shown to inhibit EC activation and apoptosis [26], thereby contributing to proper EC functionality. Therefore, it is tempting to speculate that the improved eNOS activity induced by ADGRL2 could lead to increased NRF2 activity.

Cells **2024**, *13*, x FOR PEER REVIEW 11 of 17

reducing oxidative stress, has been shown to inhibit EC activation and apoptosis [26], thereby contributing to proper EC functionality. Therefore, it is tempting to speculate that the improved eNOS activity induced by ADGRL2 could lead to increased NRF2 activity.

3.5. ADGRL2 Overexpression Enhances NRF2 Activity

3.5. ADGRL2 Overexpression Enhances NRF2 Activity

To investigate the effects of ADGRL2 on NRF2 activity, we first generated a NRF2-dependent luciferase reporter vector by inserting a tandem antioxidant response element (ARE), the binding site for NRF2, upstream of a minimal promoter containing only a TATA box driving expression of firefly luciferase. As a specificity control, we generated an identical vector in which bases within the AREs critical for NRF2 binding are mutated (Figure 5A,B).

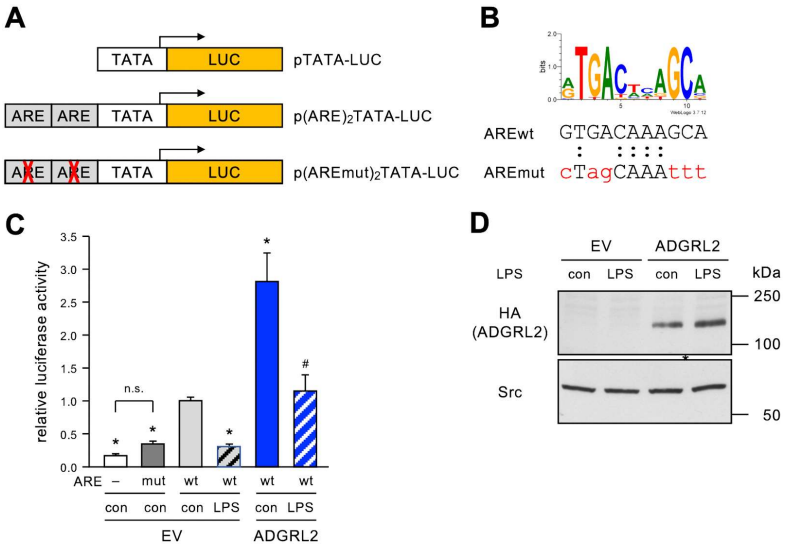


Figure 5. ADGRL2 activates endogenous NRF2 and protects against the LPS-induced loss of NRF2. (**A**) Schematic depiction of luciferase reporter vectors. In all plasmids, expression of firefly luciferase is driven by a minimal promoter derived from the herpes simplex virus thymidine kinase gene containing only a TATA box. The plasmid p(ARE)$_2$TATA-LUC contains two copies of a 41 bl long antioxidant response element (ARE) from the murine Glutathione S-transferase alpha 1 gene promoter directly upstream of the minimal promoter. In p(AREmut)$_2$TATA-LUC, the core sequence of these AREs is mutated to prevent the binding of NRF2. (**B**) Intact and mutated ARE. Shown is the sequence logo of the core binding sequence of human NRF2 and the corresponding sequence in the ARE of p(ARE)$_2$TATA-LUC (AREwt), the mutated bases in p(AREmut)$_2$TATA-LUC are shown in red (AREmut). (**C**,**D**) ECs were co-transfected with the reporter vector containing intact (wt), mutated (mut), or no AREs (–) and an expression vector for ADGRL2 or a or a corresponding empty vector (EV). After transfection, the cells were treated for 20 h with active LPS (LPS) or detoxified LPS as the control (con). (**C**) Luciferase activity was measured in cell lysates and is shown relative to AREwt/EV/con, which reflects the basal endogenous NRF2 activity (data are the mean ± SEM, n = 9–21, * $p < 0.05$ vs. AREwt/EV/con, # $p < 0.05$ vs. AREwt/EV/LPS, n.s. = not significant, one-way ANOVA with post hoc Tukey LSD test). (**D**) Expression of HA-tagged ADGRL2 (HA (ADGRL2)) in the co-transfections with p(ARE)$_2$TATA-LUC was confirmed by immunoblot and Src served as the loading control.

Figure 5. ADGRL2 activates endogenous NRF2 and protects against the LPS-induced loss of NRF2. (**A**) Schematic depiction of luciferase reporter vectors. In all plasmids, expression of firefly luciferase is driven by a minimal promoter derived from the herpes simplex virus thymidine kinase gene containing only a TATA box. The plasmid p(ARE)$_2$TATA-LUC contains two copies of a 41 bl long antioxidant response element (ARE) from the murine Glutathione S-transferase alpha 1 gene promoter directly upstream of the minimal promoter. In p(AREmut)$_2$TATA-LUC, the core sequence of these AREs is mutated to prevent the binding of NRF2. (**B**) Intact and mutated ARE. Shown is the sequence logo of the core binding sequence of human NRF2 and the corresponding sequence in the ARE of p(ARE)$_2$TATA-LUC (AREwt), the mutated bases in p(AREmut)$_2$TATA-LUC are shown in red (AREmut). (**C**,**D**) ECs were co-transfected with the reporter vector containing intact (wt), mutated (mut), or no AREs (–) and an expression vector for ADGRL2 or a or a corresponding empty vector (EV). After transfection, the cells were treated for 20 h with active LPS (LPS) or detoxified LPS as the control (con). (**C**) Luciferase activity was measured in cell lysates and is shown relative to AREwt/EV/con, which reflects the basal endogenous NRF2 activity (data are the mean ± SEM, n = 9–21, * $p < 0.05$ vs. AREwt/EV/con, # $p < 0.05$ vs. AREwt/EV/LPS, n.s. = not significant, one-way ANOVA with post hoc Tukey LSD test). (**D**) Expression of HA-tagged ADGRL2 (HA (ADGRL2)) in the co-transfections with p(ARE)$_2$TATA-LUC was confirmed by immunoblot and Src served as the loading control.

These reporter plasmids were co-transfected with the HA-ADGRL2-FLAG expression vector or the corresponding empty vector, and the cells were treated with LPS as before. Then, luciferase activity as a direct readout for the transcriptional activity of NRF2 was measured (Figure 5C), and ADGRL2 overexpression was confirmed by immunoblot (Figure 5D).

These reporter plasmids were co-transfected with the HA-ADGRL2-FLAG expression vector or the corresponding empty vector, and the cells were treated with LPS as before. Then, luciferase activity as a direct readout for the transcriptional activity of NRF2 was measured (Figure 5C), and ADGRL2 overexpression was confirmed by immunoblot (Figure 5D).

The comparison of the luciferase reporter vector without ARE and the two vectors containing the intact and mutated AREs (Figure 5C, left three bars), respectively, demonstrated the specificity of the reporter system. While the construct with the intact AREs, which reflects basal endogenous NRF2 activity, yielded significantly higher luciferase activity than the one without AREs, the base mutations in the mutated ARE resulted in luciferase activity not different from the vector without AREs.

More importantly, LPS induced a complete loss of NRF2 activity in cells co-transfected with the empty vector instead of the *ADGRL2* expression vector. On the contrary, ADGRL2 overexpression had a striking effect on NRF2. Not only did it increase the basal NRF2 transcriptional activity nearly threefold but also protected the cells from complete loss upon LPS treatment, indicating that ADGRL2 can boost antioxidative defenses in ECs through the upregulation of NRF2 activity.

3.6. The Latrophilin Homolog LAT-2 Is Involved in the Control of Oxidative Stress in the Nematode C. elegans

Latrophilins are evolutionarily highly conserved aGPCRs present in vertebrates and invertebrates, raising the question of whether the function in the protection against oxidative stress observed with mammalian ADGRL2 is conserved. In the nematode *C. elegans*, two homologs, *lat-1* and *lat-2*, exist, whereby no clear one-to-one homology between the mammalian and the nematode homologs can be determined. Previous work indicates though that, in terms of sequence, LAT-1 is most similar to ADGRL1 and also signals through the same G proteins [27]. Thus, we focused our analysis for functional similarities on LAT-2. Indeed, worm strain *lat-2(knu505)* (hereafter referred to as *lat-2* mutant) lacking the entire *lat-2* coding sequence and therefore, being a null mutant, had significantly higher levels of ROS than wild-type individuals (Figure 6A). This was the case for basal ROS amounts, as well as for those produced after stress induction using juglone, suggesting that, in the absence of the receptor, nematodes either produce more ROS or display a reduced ROS defense.

In order to gain further insights into this potential role of LAT-2 in oxidative stress defenses, we analyzed the expression of genes involved in stress protection or control of ROS: *nuo-6* and *isp-1* that code for mitochondrial proteins [28]; the transcription factors *hsf-1* [29], *skn-1* (homolog of NRF2), and *daf-16* (FOXO homolog) [30]; *daf-2*, which encodes a receptor upstream of DAF-16; and the aging-related genes *age-1* [31] and *sir-2.1* [32]. Most of these genes were differentially expressed in *lat-2* mutants (Figure 6B). Therefore, especially the ROS-protective gene *skn-1* [30] was significantly downregulated compared to the wild-type controls, which is consistent with the upregulation of NRF2 after overexpression of ADGRL2 observed in human ECs (Figure 5C).

Oxidative stress damage can severely affect the lifespan of *C. elegans* [30], and indeed, *lat-2* mutant nematodes display a significantly reduced lifespan (Figure 6C), further highlighting that LAT-2 has conserved protective functions across species. In order to exclude the possibility that the effect of *lat-2* deficiency on the lifespan is a secondary effect caused by, e.g., developmental defects, the brood size and survival to adulthood were determined. Both appeared to be indistinguishable from the wild-type individuals (Supplementary Figure S1).

similarities on LAT-2. Indeed, worm strain *lat-2(knu505)* (hereafter referred to as *lat-2* mutant) lacking the entire *lat-2* coding sequence and therefore, being a null mutant, had significantly higher levels of ROS than wild-type individuals (Figure 6A). This was the case for basal ROS amounts, as well as for those produced after stress induction using juglone, suggesting that, in the absence of the receptor, nematodes either produce more ROS or display a reduced ROS defense.

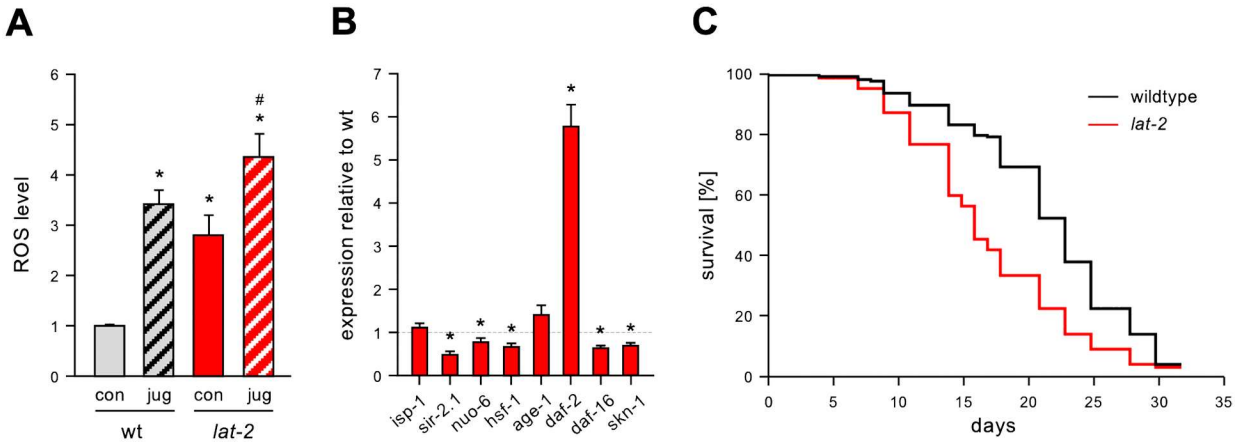


Figure 6. Nematodes lacking the latrophilin homolog *lat-2* show increased ROS levels, altered expression of stress-related genes, and reduced lifespans. (**A**) The ROS levels are increased in *lat-2(knu505)* individuals, both under normal conditions and after exposure to juglone. Worms were lysed after a 1-h treatment with 100 µM juglone (jug), incubated with H2DCF-DA, and DCF conversion was measured over a 2-h period. Control samples (con) were treated with ethanol instead of juglone (data are the mean ± SEM, n = 3, with 5 replicates per n, $^{*}p < 0.05$ vs. wild-type/con, $^{\#}p < 0.05$ vs. wt/jug, two-way ANOVA with post hoc Bonferroni test for comparing multiple groups). (**B**) Expression of stress-related genes in *lat-2(knu505)* mutants. Expression of single genes was determined by semi-quantitative real-time PCR and normalized to the geometric mean of the reference genes *act-1*, *cdc-42*, *pmp-3*, *eif-3.C*, and *tba-1* and is shown relative to wild-type animals (data are the mean ± SEM, n = 3, with 3 replicates per n, $^{*}p < 0.05$ vs. wt, unpaired, two-sided Student's *t*-test. (**C**) *lat-2(knu505)* nematodes have a significantly reduced lifespan (Cox–Mantel test, $p < 0.0001$). The median survival is 16 days for *lat-2(knu505)* hermaphrodites and 23 days for wild-type individuals ($p < 0.001$). n ≥ 200 in 4 independent experiments.

4. Discussion

The major findings of the present study are the protective functions of ADGRL2 in endotoxemia-induced endothelial dysfunction, including increased eNOS activity and upregulation of antioxidative defense systems. The latter function is evolutionarily conserved, as *C elegans* lacking the latrophilin homolog LAT-2 have increased ROS levels and reduced the lifespan.

Our data demonstrate that, in primary human ECs, ADGRL2 preserves or even increases eNOS activity by shifting the binding of eNOS from Caveolin-1 to HSP90, resulting in decreased phosphorylation of T495 and the maintenance of phosphorylation of S1177 within eNOS. Interestingly, Human Cell Map (https://humancellmap.org (accessed on 13 October 2024)), a publicly available resource based on the characterization of the spatial organization of the proteome in HEK293 cells by BioID [33], lists an interaction between Caveolin-1 and ADGRL2. Thus, it is tempting to speculate that an increase in ADGRL2 in ECs sequesters Caveolin-1 by a direct interaction, making it unavailable for interactions with eNOS. In addition, there might be other mechanisms involved in eNOS activation through ADGRL2. It has been shown that Gαi2, one of the G proteins required for ADGRL2 signaling in ECs [7], is required for eNOS activation induced by dehydroepiandrosterone [34]. Taken these findings together, ADGRL2 seems to improve endothelial functionality not only by signaling via Gαi2 but also by changing the binding partners of eNOS.

The increased activation of eNOS induced by AGDRL2 results in protection against EC activation and apoptosis, as well as in maintenance of the migratory capacity. These diverse functions can be explained by an enhanced NO bioavailability induced by ADGRL2. It has been demonstrated that, in Caveolin-1-deficient mice, eNOS is more active, and the NO bioavailability is increased, resulting in the inhibition of LPS-induced ICAM1 expression [35]. This is in line with our data that ADGRL2 overexpression, on the one hand,

leads to more active eNOS, most likely due to the reduced interaction between eNOS and Caveolin-1, and, on the other hand, completely inhibits LPS-induced ICAM1 upregulation and EC activation. With respect to apoptosis protection by ADGRL2, it has been demonstrated that S-nitrosation of Caspase-3 leads to its inactivation of ECs [36,37], resulting in a decreased apoptosis rate. Another important feature of ECs is their capacity to migrate, which is required when the monolayer is disrupted to preserve the endothelial barrier. Notably, the migratory capacity of ECs, another hallmark for their proper functionality, also depends on NO [38]. Taken together, these effects on the cellular level might be due to ADGRL2-mediated protection against the LPS-induced loss of eNOS activity.

Interestingly, not only Caspase-3 is S-nitrosated by NO in ECs. This modification of KEAP1 facilitates its dissociation from NRF2 and thereby contributes to the nuclear accumulation of NRF2 [26]. With our NRF2-dependent luciferase reporter system, we found that LPS treatment significantly reduced NRF2 activity in ECs. Moreover, in accordance with the positive effect of ADGRL2 on eNOS activity observed here, we also demonstrated that ADGRL2 significantly activates NRF2 in untreated ECs and completely restores NRF2 activity in LPS-treated cells. These data suggest that ADGRL2 leads not only to enhanced NO bioavailability but also to reduced oxidative stress due to NRF2 activation.

To address the question whether the protection against oxidative stress and the regulation of NRF2 by ADGRL2 exists across species, we investigated the role of the latrophilin homolog LAT-2 in the nematode *C. elegans* using a LAT-2-deficient strain. ROS levels in the *lat-2* mutant worms were already increased under normal maintenance, as well as after treatment with the ROS generator juglone. These data indicate that, in the absence of LAT-2, nematodes either produce more ROS or do not cope with the radicals well. In line with these results, expression of the genes involved in protection from oxidative stress is altered when LAT-2 is lacking. Thereby, most of the analyzed genes are downregulated, especially the ROS-protective gene *skn-1* [30], which is a homolog of mammalian NRF2. Although *C. elegans* does not have a vasculature, several mechanisms to protect from oxidative stress are conserved between mammals and the worm [39]. The function of SKN-1 is very similar to that of NRF proteins in response to oxidative stress, and *skn-1* is required for oxidative stress resistance and also longevity [40]. Its downregulation can indicate a reduced stress response in *lat-2* mutants, which could be one explanation for the increased ROS levels. This points towards a role of LAT-2 in the protection against oxidative damage like ADGRL2. Oxidative stress can result in a reduced lifespan [41], as is also the case for *lat-2* mutants. Thus, our *C. elegans* data are consistent with the positive impact of ADGRL2 on NRF2 in ECs.

It has to be noted that *C. elegans* harbors two latrophilin homologs, *lat-1* and *lat-2*. No information exists whether LAT-1 also has a function in the control of or protection against oxidative stress. Worms lacking LAT-1 display a plethora of phenotypes such as developmental arrest, only a very small number of individuals reach adulthood, and these have a reduced brood size and neurological defects [42,43]. Thus, delineating a potential role of LAT-1 in oxidative stress is challenging, as such effects, if present, might be secondary. This is in contrast to LAT-2, as the mutant worms seem not to have any developmental defects.

Future analyses will need to clarify whether LAT-2 in *C. elegans*, as well as ADGRL2 in primary human ECs, also have effects on aging and cellular senescence, respectively. As for *C. elegans*, the reduced lifespan of *lat-2* worms can be well explained by increased oxidative stress but might also have an age-related contribution. As for the primary ECs, the positive effects of ADGRL2 on eNOS and NRF2 activation points towards a protective role against cellular senescence induction.

5. Conclusions

In conclusion, ADGRL2 has protective effects across species. An increase in the ADGRL2 levels improves endothelial functionality, and this aGPCR could therefore be a promising therapeutic target for the treatment of sepsis to protect the endothelium and,

thus, to restore endothelial cell integrity. Moreover, it seems to be of interest for the elderly population to determine whether potential protective functions of ADGRL2 also exist in aging and senescence.

Supplementary Materials: The following supporting information can be downloaded at https://www.mdpi.com/article/10.3390/cells13221826/s1: Figure S1: *lat-2(knu505)* nematodes do not show any defects in brood size and survival to adulthood. Table S1: Antibodies used for immunoblots. Table S2: Antibodies used for immunostaining and PLA. Table S3: Primers used for semi-quantitative real-time PCR.

Author Contributions: Conceptualization, S.P. (Simone Prömel) and J.H.; methodology, P.J., A.R., W.B.P., N.A.-A., V.E.G., S.P. (Stephanie Pick), S.D., F.F.C. and J.A.; software, F.v.A. and J.H.; validation, O.E., J.A., S.P. (Simone Prömel) and J.H.; formal analysis, P.J., A.R., W.B.P., N.A.-A., V.E.G., S.P. (Stephanie Pick), F.v.A. and O.E.; investigation, P.J., A.R., W.B.P., N.A.-A., V.E.G., S.P. (Stephanie Pick), F.v.A. and O.E.; resources, J.A., S.P. (Simone Prömel) and J.H.; data curation, S.P. (Stephanie Pick), O.E., J.A., S.P. (Simone Prömel) and J.H.; writing—original draft preparation, P.J., A.R., W.B.P., J.A., S.P. (Simone Prömel) and J.H.; writing—review and editing, P.J., A.R., N.A.-A., J.A., S.P. (Simone Prömel) and J.H.; visualization, N.A-A. and J.A.; supervision, N.A.-A., V.E.G., S.P. (Stephanie Pick), J.A., S.P. (Simone Prömel) and J.H.; funding acquisition, S.P. (Simone Prömel) and J.H. All authors have read and agreed to the published version of the manuscript.

Funding: This research was, in part, funded by intramural funding (9792888) of the University Hospital of the Heinrich Heine University to S.P. and J.H.

Institutional Review Board Statement: Not applicable.

Informed Consent Statement: Not applicable.

Data Availability Statement: Raw data will be made available by the corresponding authors upon reasonable request.

Conflicts of Interest: The authors declare no conflicts of interest.

References

1. Rudd, K.E.; Johnson, S.C.; Agesa, K.M.; Shackelford, K.A.; Tsoi, D.; Kievlan, D.R.; Colombara, D.V.; Ikuta, K.S.; Kissoon, N.; Finfer, S.; et al. Global, regional, and national sepsis incidence and mortality, 1990–2017: Analysis for the Global Burden of Disease Study. *Lancet* **2020**, *395*, 200–211. [CrossRef] [PubMed]
2. Merk, D.; Cox, F.F.; Jakobs, P.; Promel, S.; Altschmied, J.; Haendeler, J. Dose-Dependent Effects of Lipopolysaccharide on the Endothelium-Sepsis versus Metabolic Endotoxemia-Induced Cellular Senescence. *Antioxidants* **2024**, *13*, 443. [CrossRef] [PubMed]
3. Boutagy, N.E.; McMillan, R.P.; Frisard, M.I.; Hulver, M.W. Metabolic endotoxemia with obesity: Is it real and is it relevant? *Biochimie* **2016**, *124*, 11–20. [CrossRef] [PubMed]
4. Shu, Y.; Jin, S. Caveolin-1 in endothelial cells: A potential therapeutic target for atherosclerosis. *Heliyon* **2023**, *9*, e18653. [CrossRef] [PubMed]
5. Hamann, J.; Aust, G.; Arac, D.; Engel, F.B.; Formstone, C.; Fredriksson, R.; Hall, R.A.; Harty, B.L.; Kirchhoff, C.; Knapp, B.; et al. International Union of Basic and Clinical Pharmacology. XCIV. Adhesion G protein-coupled receptors. *Pharmacol. Rev.* **2015**, *67*, 338–367. [CrossRef]
6. Camillo, C.; Facchinello, N.; Villari, G.; Mana, G.; Gioelli, N.; Sandri, C.; Astone, M.; Tortarolo, D.; Clapero, F.; Gays, D.; et al. LPHN2 inhibits vascular permeability by differential control of endothelial cell adhesion. *J. Cell Biol.* **2021**, *220*, e202006033. [CrossRef]
7. Tanaka, K.; Chen, M.; Prendergast, A.; Zhuang, Z.; Nasiri, A.; Joshi, D.; Hintzen, J.; Chung, M.; Kumar, A.; Mani, A.; et al. Latrophilin-2 mediates fluid shear stress mechanotransduction at endothelial junctions. *EMBO J.* **2024**, *43*, 3175–3191. [CrossRef]
8. Wasserman, W.W.; Fahl, W.E. Functional antioxidant responsive elements. *Proc. Natl. Acad. Sci. USA* **1997**, *94*, 5361–5366. [CrossRef]
9. Altschmied, J.; Duschl, J. Set of optimized luciferase reporter gene plasmids compatible with widely used CAT vectors. *Biotechniques* **1997**, *23*, 436–438. [CrossRef]
10. Erickson, A.M.; Nevarea, Z.; Gipp, J.J.; Mulcahy, R.T. Identification of a variant antioxidant response element in the promoter of the human glutamate-cysteine ligase modifier subunit gene. Revision of the ARE consensus sequence. *J. Biol. Chem.* **2002**, *277*, 30730–30737. [CrossRef]
11. Wang, X.; Tomso, D.J.; Chorley, B.N.; Cho, H.Y.; Cheung, V.G.; Kleeberger, S.R.; Bell, D.A. Identification of polymorphic antioxidant response elements in the human genome. *Hum. Mol. Genet.* **2007**, *16*, 1188–1200. [CrossRef] [PubMed]
12. Rothe, J.; Thor, D.; Winkler, J.; Knierim, A.B.; Binder, C.; Huth, S.; Kraft, R.; Rothemund, S.; Schoneberg, T.; Promel, S. Involvement of the Adhesion GPCRs Latrophilins in the Regulation of Insulin Release. *Cell Rep.* **2019**, *26*, 1573–1584.e5. [CrossRef] [PubMed]

13. Crooks, G.E.; Hon, G.; Chandonia, J.M.; Brenner, S.E. WebLogo: A sequence logo generator. *Genome Res.* **2004**, *14*, 1188–1190. [CrossRef] [PubMed]
14. Rauluseviciute, I.; Riudavets-Puig, R.; Blanc-Mathieu, R.; Castro-Mondragon, J.A.; Ferenc, K.; Kumar, V.; Lemma, R.B.; Lucas, J.; Cheneby, J.; Baranasic, D.; et al. JASPAR 2024: 20th anniversary of the open-access database of transcription factor binding profiles. *Nucleic Acids Res.* **2024**, *52*, D174–D182. [CrossRef]
15. Abramoff, M.D.; Magelhaes, P.J.; Ram, S.J. Image Processing with ImageJ. *Biophotonics Int.* **2004**, *11*, 36–42.
16. Brenner, S. The genetics of Caenorhabditis elegans. *Genetics* **1974**, *77*, 71–94. [CrossRef]
17. Merk, D.; Ptok, J.; Jakobs, P.; von Ameln, F.; Greulich, J.; Kluge, P.; Semperowitsch, K.; Eckermann, O.; Schaal, H.; Ale-Agha, N.; et al. Selenoprotein T Protects Endothelial Cells against Lipopolysaccharide-Induced Activation and Apoptosis. *Antioxidants* **2021**, *10*, 1427. [CrossRef]
18. Pfaffl, M.W. A new mathematical model for relative quantification in real-time RT-PCR. *Nucleic Acids Res.* **2001**, *29*, e45. [CrossRef]
19. Livak, K.J.; Schmittgen, T.D. Analysis of relative gene expression data using real-time quantitative PCR and the 2(-Delta Delta C(T)) Method. *Methods* **2001**, *25*, 402–408. [CrossRef]
20. Merk, D.; Greulich, J.; Vierkant, A.; Cox, F.; Eckermann, O.; von Ameln, F.; Dyballa-Rukes, N.; Altschmied, J.; Ale-Agha, N.; Jakobs, P.; et al. Caffeine Inhibits Oxidative Stress- and Low Dose Endotoxemia-Induced Senescence-Role of Thioredoxin-1. *Antioxidants* **2023**, *12*, 1244. [CrossRef]
21. Forstermann, U.; Sessa, W.C. Nitric oxide synthases: Regulation and function. *Eur. Heart J.* **2012**, *33*, 829–837. [CrossRef] [PubMed]
22. Ju, H.; Zou, R.; Venema, V.J.; Venema, R.C. Direct interaction of endothelial nitric-oxide synthase and caveolin-1 inhibits synthase activity. *J. Biol. Chem.* **1997**, *272*, 18522–18525. [CrossRef] [PubMed]
23. Ghosh, S.; Gachhui, R.; Crooks, C.; Wu, C.; Lisanti, M.P.; Stuehr, D.J. Interaction between caveolin-1 and the reductase domain of endothelial nitric-oxide synthase. Consequences for catalysis. *J. Biol. Chem.* **1998**, *273*, 22267–22271. [CrossRef] [PubMed]
24. Gratton, J.P.; Fontana, J.; O'Connor, D.S.; Garcia-Cardena, G.; McCabe, T.J.; Sessa, W.C. Reconstitution of an endothelial nitric-oxide synthase (eNOS), hsp90, and caveolin-1 complex in vitro. Evidence that hsp90 facilitates calmodulin stimulated displacement of eNOS from caveolin-1. *J. Biol. Chem.* **2000**, *275*, 22268–22272. [CrossRef]
25. Wei, Q.; Xia, Y. Roles of 3-phosphoinositide-dependent kinase 1 in the regulation of endothelial nitric-oxide synthase phosphorylation and function by heat shock protein 90. *J. Biol. Chem.* **2005**, *280*, 18081–18086. [CrossRef]
26. Mann, G.E.; Rowlands, D.J.; Li, F.Y.; de Winter, P.; Siow, R.C. Activation of endothelial nitric oxide synthase by dietary isoflavones: Role of NO in Nrf2-mediated antioxidant gene expression. *Cardiovasc. Res.* **2007**, *75*, 261–274. [CrossRef]
27. Muller, A.; Winkler, J.; Fiedler, F.; Sastradihardja, T.; Binder, C.; Schnabel, R.; Kungel, J.; Rothemund, S.; Hennig, C.; Schoneberg, T.; et al. Oriented Cell Division in the *C. elegans* Embryo Is Coordinated by G-Protein Signaling Dependent on the Adhesion GPCR LAT-1. *PLoS Genet.* **2015**, *11*, e1005624. [CrossRef]
28. Yang, W.; Hekimi, S. A mitochondrial superoxide signal triggers increased longevity in Caenorhabditis elegans. *PLoS Biol.* **2010**, *8*, e1000556. [CrossRef]
29. Sonani, R.R.; Singh, N.K.; Awasthi, A.; Prasad, B.; Kumar, J.; Madamwar, D. Phycoerythrin extends life span and health span of Caenorhabditis elegans. *Age* **2014**, *36*, 9717. [CrossRef]
30. Miranda-Vizuete, A.; Veal, E.A. Caenorhabditis elegans as a model for understanding ROS function in physiology and disease. *Redox Biol.* **2017**, *11*, 708–714. [CrossRef]
31. Zhang, M.; Li, Z.; Gao, D.; Gong, W.; Gao, Y.; Zhang, C. Hydrogen extends Caenorhabditis elegans longevity by reducing reactive oxygen species. *PLoS ONE* **2020**, *15*, e0231972. [CrossRef] [PubMed]
32. Guo, X.; Garcia, L.R. SIR-2.1 integrates metabolic homeostasis with the reproductive neuromuscular excitability in early aging male Caenorhabditis elegans. *Elife* **2014**, *3*, e01730. [CrossRef] [PubMed]
33. Go, C.D.; Knight, J.D.R.; Rajasekharan, A.; Rathod, B.; Hesketh, G.G.; Abe, K.T.; Youn, J.Y.; Samavarchi-Tehrani, P.; Zhang, H.; Zhu, L.Y.; et al. A proximity-dependent biotinylation map of a human cell. *Nature* **2021**, *595*, 120–124. [CrossRef] [PubMed]
34. Liu, D.; Dillon, J.S. Dehydroepiandrosterone activates endothelial cell nitric-oxide synthase by a specific plasma membrane receptor coupled to Galpha(i2,3). *J. Biol. Chem.* **2002**, *277*, 21379–21388. [CrossRef]
35. Garrean, S.; Gao, X.P.; Brovkovych, V.; Shimizu, J.; Zhao, Y.Y.; Vogel, S.M.; Malik, A.B. Caveolin-1 regulates NF-kappaB activation and lung inflammatory response to sepsis induced by lipopolysaccharide. *J. Immunol.* **2006**, *177*, 4853–4860. [CrossRef]
36. Hoffmann, J.; Dimmeler, S.; Haendeler, J. Shear stress increases the amount of S-nitrosylated molecules in endothelial cells: Important role for signal transduction. *FEBS Lett.* **2003**, *551*, 153–158. [CrossRef]
37. Rossig, L.; Fichtlscherer, B.; Breitschopf, K.; Haendeler, J.; Zeiher, A.M.; Mulsch, A.; Dimmeler, S. Nitric oxide inhibits caspase-3 by S-nitrosation in vivo. *J. Biol. Chem.* **1999**, *274*, 6823–6826. [CrossRef]
38. Haendeler, J.; Mlynek, A.; Buchner, N.; Lukosz, M.; Graf, M.; Guettler, C.; Jakob, S.; Farrokh, S.; Kunze, K.; Goy, C.; et al. Two Isoforms of Sister-of-Mammalian Grainyhead Have Opposing Functions in Endothelial Cells and In Vivo. *Arterioscler. Thromb. Vasc. Biol.* **2013**, *33*, 1639–1646. [CrossRef]
39. Rodriguez, M.; Snoek, L.B.; De Bono, M.; Kammenga, J.E. Worms under stress: *C. elegans* stress response and its relevance to complex human disease and aging. *Trends Genet.* **2013**, *29*, 367–374. [CrossRef]
40. An, J.H.; Blackwell, T.K. SKN-1 links *C. elegans* mesendodermal specification to a conserved oxidative stress response. *Genes Dev.* **2003**, *17*, 1882–1893. [CrossRef]
41. Zhou, K.I.; Pincus, Z.; Slack, F.J. Longevity and stress in Caenorhabditis elegans. *Aging* **2011**, *3*, 733–753. [CrossRef] [PubMed]

42. Langenhan, T.; Promel, S.; Mestek, L.; Esmaeili, B.; Waller-Evans, H.; Hennig, C.; Kohara, Y.; Avery, L.; Vakonakis, I.; Schnabel, R.; et al. Latrophilin signaling links anterior-posterior tissue polarity and oriented cell divisions in the *C. elegans* embryo. *Dev. Cell* **2009**, *17*, 494–504. [CrossRef] [PubMed]
43. Matus, D.; Post, W.B.; Horn, S.; Schoneberg, T.; Promel, S. Latrophilin-1 drives neuron morphogenesis and shapes chemo- and mechanosensation-dependent behavior in *C. elegans* via a trans function. *Biochem. Biophys. Res. Commun.* **2022**, *589*, 152–158. [CrossRef]

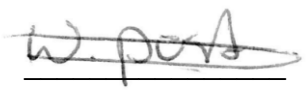
Disclaimer/Publisher's Note: The statements, opinions and data contained in all publications are solely those of the individual author(s) and contributor(s) and not of MDPI and/or the editor(s). MDPI and/or the editor(s) disclaim responsibility for any injury to people or property resulting from any ideas, methods, instructions or products referred to in the content.

Detailed author contributions

For the publication ‘The Adhesion GPCR ADGRL2/LPHN2 Can Protect Against Cellular and Organismal Dysfunction’ the following contributions were made by Willem Berend Post:

- Nematode maintenance
- Measurement of *in vivo* ROS levels
- Data analysis
- Manuscript writing

Date: 6th May 2026





Willem Berend Post

Prof. Dr. Simone Prömel

6 Discussion

Within cellular and wider organismal functioning, proper propagation of signals received from extracellular stimuli is essential. aGPCRs have been described as transducer molecules of stimuli in many different scenarios. Unusual for GPCRs, aGPCRs can realize molecular functions in a variety of manners: in addition to canonical G protein signaling, they are capable of mediating *trans*/N terminus-only/7TM independent functions, as well as cell-cell and cell-matrix adhesion.

Especially the N terminus-only function is highly intriguing leading to the ultimate question of how an aGPCR integrates different functions. However, this function is also only poorly understood, as it does not rely on G proteins, yet it can have a large variety of physiological consequences (reviewed by [31]). Due to this almost complete lack in mechanistic understanding, *in vitro* approaches to study the N terminus-only function of aGPCRs are difficult to design and not very informative.

The work presented in this thesis uses the nematode *C. elegans* to study the physiological and molecular effects of the N terminus-only functions of the aGPCR Latrophilin *in vivo*. For this purpose, several biological processes in which the Latrophilin homolog LAT-1 plays an essential role were identified, which are all confined to reproduction. We found N terminus-only functionality in sperm guidance, germ cell apoptosis as well as oocyte health and ovulation rate, indicating that LAT-1 plays an integral part in overall *C. elegans* reproductivity, driving brood size using the long N terminus.

Once clear functionality of the LAT-1 N terminus was determined, we sought to investigate how LAT-1 mechanistically affects the germline. For this purpose, we identified an influence of LAT-1 on the germline progenitor zone, with a reduction of the progenitor zone in *lat-1* mutant animals. We found that LAT-1 likely modulates Notch activity in this tissue, which was corroborated by our finding that the LAT-1 N terminus is able to physically interact with LAG-2. To our knowledge, this is the first time a direct connection of aGPCRs to Notch signaling has been identified.

Lastly, the research was extended towards the second Latrophilin homolog, LAT-2. In this thesis, we identified a physiological role of LAT-2 towards protection against ROS, affecting nematode lifespan. These initial physiological roles are a starting point on which mechanistic studies can be based in future research.

6.1 Notch and aGPCRs: a conserved mechanism uncovered?

This thesis describes the first detailed instance of an aGPCR modulating Notch signaling, down to mechanistic insight (**chapter 4**) [66]. We have shown how LAT-1 interacts with the Notch ligand LAG-2, modulating the progenitor zone in *C. elegans*. Cross-talk between aGPCRs and conserved pathways has been shown before. A key example is the *trans* function of ADGRA2/GPR124, which was described in **chapter 1.1.4**.

In other organisms, research has indicated ADGRL2 as a mediator of Notch activity in the context of fluid shear stress, in which the aGPCR acts again independent of its G protein signaling function [67], showing close similarity to our findings. Additionally, ADGRG6 has been implicated in affecting myocardial Notch activity in zebrafish [68]. Both these findings add to our findings in *C. elegans*, hinting towards a broad implication of aGPCRs in Notch, which to date has been hinted towards, but never systematically studied. Therefore, it would be of high value if a systematic approach would be taken to screen aGPCR-mediated Notch modulation. The outcomes of such a study would provide numerous insights and clarify how aGPCRs and Notch are connected on a broader level, for example within cell types and organisms.

Additionally, our data suggests that an *in vitro* interaction with Notch ligand APX-1 is also possible, indicating how a broader mechanism might be acting in *C. elegans*, strengthening the potential for a systemic study of aGPCR-modulated Notch signaling. Within *C. elegans*, it would be fascinating to more closely study Notch signaling in the embryo and vulva, since Notch plays key roles in these tissues (described in **chapter 1.2.3**), and LAT-1 is expressed in these tissues as well [16]. Especially in the developing embryo, LAT-1 has essential functions in establishing cell polarity, but a ligand has not yet been identified.

Within the germline, a link between the lipoprotein VIT-3 and Notch has recently been proposed [69]. This is fascinating, coming from the context that Vitellogenins have been identified by the Prömel lab as potential interactors with LAT-1 (unpublished data), linking towards a highly elaborate network of proteins that are able to affect Notch, in which aGPCRs might play a central yet poorly characterized role. Further research into Vitellogenins and their effect on LAT-1 would help in further elucidation.

6.2 The role of alternative splicing to establish N terminus-only functions

One key, unanswered question is how a single receptor is able to integrate *cis* and N terminus-only functions. Can an aGPCR mediate both functions as a single entity, or are there processes at work that generate separate entities for each function? A logical avenue is NTF-CTF dissociation due to receptor autoproteolysis. In the case of LAT-1, this seems to be unlikely however, since previous studies have found no discernible function for receptor cleavage [17]. Another method in which different receptor variants can be generated is alternative splicing, which was speculated as a way for LAT-1 to fulfill its N terminus-only function in **chapter 3** [70]. Alternative splicing allows for the generation of various distinct transcripts, with potentially varying functionality, of a single gene. Indeed, alternative splicing is very common for many aGPCRs [71,72]. For LAT-1, a large number of variants were identified, including variants consisting solely of the N terminus, albeit at extremely low abundancies. However, taken together with the prominence of alternative splicing in aGPCRs, the hypothesis that N terminus-only functions are realized in this manner is tempting.

To date, *in vivo* studies that couple a function to a specific aGPCR splice variant remain scarce. One study has shown that in the mouse hippocampus, alternative splicing of *Lphn3* results in a receptor with an altered C terminus, preferentially coupling to $G\alpha_{12/13}$ instead of the conventional $G\alpha_s$ coupling, affecting synapse formation [73]. Another recent study in *Drosophila* hypothesizes an interplay between the full-length version of Cirl and a 1TM version, generated as a result of intron retention [74], together acting in mechanosensory signal propagation. Interestingly, in both these studies the alternatively composed receptor coexists with the native receptor, however for *Lphn3*, the different variants have distinct roles, whereas for Cirl, the

1TM and 7TM variant are proposed to work together, physically binding to each other. Additionally, there are several recent works that show that splice variants at the C terminal tail of ADGRLs show modified arrestin recruitment or signaling via G proteins, progressing on the research on *Lphn3* [75,76], however, evidence of N terminus-only signaling mediated by splice variants does not yet exist.

In order to study this question in more detail, one can exploit the findings in this thesis as an entry point. Knowing the existence and sequence of variants, one promising starting point would be determining where these variants are expressed in the nematode, either using tissue specific transcriptomics or by generating strains expressing reporters coupled to these transcripts. Additionally, knockouts of these variants could be made, or knockdown by either RNA interference (RNAi) or auxin inducible degradation (AID) could give hints towards their functionality on a temporal or spatial level [77,78]. This would significantly contribute to the field of aGPCR signaling by providing novel contexts for splice variants, as well as potential new mechanistic insight into how these receptors can transduce signals in such a variety of manners, and is currently ongoing research.

One important note is that alternative splicing and cleavage are not the only explanations how N terminus-only functioning can occur. Since it has been shown that N-C separation is not essential for *cis* signaling in some aGPCRs [30,79], and since it has been shown that abolishing autoproteolytic cleavage of LAT-1 does not affect either fertility or lethality [17], a likely hypothesis is that a full length receptor is able to both transduce *cis* and *trans* signals, without the need of specific variants existing for regulating *trans* signals. In this context, it would be valuable to study function-specific interaction partners, resulting in either a *cis* or a *trans* signal.

Taken together, this thesis has described the enigmatic *trans* signaling capacity of LAT-1 in thorough detail, exploiting the well-defined structure and properties of the *C. elegans* gonad to pinpoint *trans* signaling to specific phenotypes and cell types. Additionally, this thesis has significantly aided in the poorly understood field of aGPCR signaling, particularly in relation to Notch. To date, there were some undirect hints towards aGPCRs modulating Notch signaling, but no direct link has been characterized. We have provided evidence from phenotypic to

molecular level that show how an aGPCRs and a Notch ligand can interact physically, affecting Notch activity directly. This provides ample openings for additional research to shed light on how adhesion GPCRs and Notch act together in more detail, and how prevalent these interactions are within the aGPCR class.

Additionally, this thesis provides new insights into the functions provided by LAT-2, opening up new avenues to find signaling mechanisms for this poorly characterized aGPCR, further advancing our knowledge of the physiological roles supplied by ADGRLs.

7 References

1. Dryja, T. P. *et al.* A point mutation of the rhodopsin gene in one form of retinitis pigmentosa. *Nature* **343**, 364–366 (1990).

2. Inglehearn, C. F. *et al.* A 3-bp deletion in the rhodopsin gene in a family with autosomal dominant retinitis pigmentosa. *Am. J. Hum. Genet.* **48**, 26–30 (1991).

3. Nathans, J. & Hogness, D. S. Isolation and nucleotide sequence of the gene encoding human rhodopsin. *Proc. Natl. Acad. Sci.* **81**, 4851–4855 (1984).

4. McGee, J. *et al.* The very large G-protein-coupled receptor VLGR1: a component of the ankle link complex required for the normal development of auditory hair bundles. *J. Neurosci. Off. J. Soc. Neurosci.* **26**, 6543–6553 (2006).

5. Yagi, H. *et al.* Vlgr1 is required for proper stereocilia maturation of cochlear hair cells. *Genes Cells Devoted Mol. Cell. Mech.* **12**, 235–250 (2007).

6. Fredriksson, R., Lagerström, M. C., Lundin, L.-G. & Schiöth, H. B. The G-Protein-Coupled Receptors in the Human Genome Form Five Main Families. Phylogenetic Analysis, Paralogon Groups, and Fingerprints. *Mol. Pharmacol.* **63**, 1256–1272 (2003).

7. Bjarnadóttir, T. K. *et al.* The human and mouse repertoire of the adhesion family of G-protein-coupled receptors. *Genomics* **84**, 23–33 (2004).

8. Hamann, J. *et al.* International Union of Basic and Clinical Pharmacology. XCIV. Adhesion G Protein–Coupled Receptors. *Pharmacol. Rev.* **67**, 338–367 (2015).

9. Liebscher, I. *et al.* A guide to adhesion GPCR research. *FEBS J.* **289**, 7610–7630 (2022).

10. Langenhan, T. *et al.* Adhesion G protein-coupled receptors. *Pharmacol. Rev.* 100116 (2026) doi:10.1016/j.pharmr.2026.100116.

11. Ke, N. *et al.* Biochemical characterization of genetic mutations of GPR56 in patients with bilateral frontoparietal polymicrogyria (BFPP). *Biochem. Biophys. Res. Commun.* **366**, 314–320 (2008).

12. Boyden, S. E. *et al.* Vibratory Urticaria Associated with a Missense Variant in ADGRE2. *N. Engl. J. Med.* **374**, 656–663 (2016).

13. Araç, D. *et al.* A novel evolutionarily conserved domain of cell-adhesion GPCRs mediates autoproteolysis. *EMBO J.* **31**, 1364–1378 (2012).

14. Lin, H.-H. *et al.* Autocatalytic Cleavage of the EMR2 Receptor Occurs at a Conserved G Protein-coupled Receptor Proteolytic Site Motif *. *J. Biol. Chem.* **279**, 31823–31832 (2004).

15. Chang, G.-W. *et al.* Proteolytic cleavage of the EMR2 receptor requires both the extracellular stalk and the GPS motif. *FEBS Lett.* **547**, 145–150 (2003).

16. Langenhan, T. *et al.* Latrophilin signaling links anterior-posterior tissue polarity and oriented cell divisions in the C. elegans embryo. *Dev. Cell* **17**, 494–504 (2009).

17. Prömel, S. *et al.* The GPS motif is a molecular switch for bimodal activities of adhesion class G protein-coupled receptors. *Cell Rep.* **2**, 321–331 (2012).

18. Dates, A. N. *et al.* Heterogeneity of tethered agonist signaling in adhesion G protein-coupled receptors. *Cell Chem. Biol.* **31**, 1542-1553.e4 (2024).

19. Liebscher, I. *et al.* A tethered agonist within the ectodomain activates the adhesion G protein-coupled receptors GPR126 and GPR133. *Cell Rep.* **9**, 2018–2026 (2014).

20. Stoveken, H. M., Hajduczok, A. G., Xu, L. & Tall, G. G. Adhesion G protein-coupled receptors are activated by exposure of a cryptic tethered agonist. *Proc. Natl. Acad. Sci.* **112**, 6194–6199 (2015).

21. Demberg, L. M., Rothemund, S., Schöneberg, T. & Liebscher, I. Identification of the tethered peptide agonist of the adhesion G protein-coupled receptor GPR64/ADGRG2. *Biochem. Biophys. Res. Commun.* **464**, 743–747 (2015).

22. Sun, Y. *et al.* Optimization of a peptide ligand for the adhesion GPCR ADGRG2 provides a potent tool to explore receptor biology. *J. Biol. Chem.* **296**, 100174 (2021).

23. Wilde, C. *et al.* The constitutive activity of the adhesion GPCR GPR114/ADGRG5 is mediated by its tethered agonist. *FASEB J.* **30**, 666–673 (2016).

24. Bui, D. L. H. *et al.* The adhesion GPCRs CELSR1–3 and LPHN3 engage G proteins via distinct activation mechanisms. *Cell Rep.* **42**, 112552 (2023).

25. Scholz, N. *et al.* Mechano-dependent signaling by Latrophilin/CIRL quenches cAMP in proprioceptive neurons. *eLife* **6**, e28360 (2017).

26. Müller, A. *et al.* Oriented Cell Division in the C. elegans Embryo Is Coordinated by G-Protein Signaling Dependent on the Adhesion GPCR LAT-1. *PLOS Genet.* **11**, e1005624 (2015).

27. Seufert, F., Chung, Y. K., Hildebrand, P. W. & Langenhan, T. 7TM domain structures of adhesion GPCRs: what's new and what's missing? *Trends Biochem. Sci.* **48**, 726–739 (2023).

28. Liebscher, I., Schöneberg, T. & Thor, D. Stachel-mediated activation of adhesion G protein-coupled receptors: insights from cryo-EM studies. *Signal Transduct. Target. Ther.* **7**, 1–2 (2022).

29. Beliu, G. *et al.* Tethered agonist exposure in intact adhesion/class B2 GPCRs through intrinsic structural flexibility of the GAIN domain. *Mol. Cell* **81**, 905-921.e5 (2021).

30. Kordon, S. P. *et al.* Conformational coupling between extracellular and transmembrane domains modulates holo-adhesion GPCR function. *Nat. Commun.* **15**, 10545 (2024).

31. Lehmann, L., Groß, V. E., Behlendorf, R. & Prömel, S. The N terminus-only function of adhesion GPCRs: emerging concepts. *Trends Pharmacol. Sci.* **46**, 231–248 (2025).

32. Posokhova, E. *et al.* GPR124 Functions as a WNT7-Specific Coactivator of Canonical β-Catenin Signaling. *Cell Rep.* **10**, 123–130 (2015).

33. Chang, J. *et al.* Gpr124 is essential for blood–brain barrier integrity in central nervous system disease. *Nat. Med.* **23**, 450–460 (2017).

34. Cho, C., Smallwood, P. M. & Nathans, J. Reck and Gpr124 Are Essential Receptor Cofactors for Wnt7a/Wnt7b-Specific Signaling in Mammalian CNS Angiogenesis and Blood-Brain Barrier Regulation. *Neuron* **95**, 1056-1073.e5 (2017).

35. Vallon, M. *et al.* A RECK-WNT7 Receptor-Ligand Interaction Enables Isoform-Specific Regulation of Wnt Bioavailability. *Cell Rep.* **25**, 339-349.e9 (2018).

36. Patra, C. *et al.* Organ-specific function of adhesion G protein-coupled receptor GPR126 is domain-dependent. *Proc. Natl. Acad. Sci.* **110**, 16898–16903 (2013).

37. Petersen, S. C. *et al.* The Adhesion GPCR GPR126 Has Distinct, Domain-Dependent Functions in Schwann Cell Development Mediated by Interaction with Laminin-211. *Neuron* **85**, 755–769 (2015).

38. Feltri, M. L. *et al.* Conditional disruption of β1 integrin in Schwann cells impedes interactions with axons. *J. Cell Biol.* **156**, 199–210 (2002).

39. Kaur, B., Brat, D. J., Devi, N. S. & Van Meir, E. G. Vasculostatin, a proteolytic fragment of Brain Angiogenesis Inhibitor 1, is an antiangiogenic and antitumorigenic factor. *Oncogene* **24**, 3632–3642 (2005).

40. Kaur, B. *et al.* Vasculostatin Inhibits Intracranial Glioma Growth and Negatively Regulates In vivo Angiogenesis through a CD36-Dependent Mechanism. *Cancer Res.* **69**, 1212–1220 (2009).

41. Cork, S. M. *et al.* A proprotein convertase/MMP-14 proteolytic cascade releases a novel 40 kDa vasculostatin from tumor suppressor BAI1. *Oncogene* **31**, 5144–5152 (2012).

42. Rosenthal, L. & Meldolesi, J. α-latrotoxin and related toxins. *Pharmacol. Ther.* **42**, 115–134 (1989).

43. Lelianova, V. G. *et al.* α-Latrotoxin Receptor, Latrophilin, Is a Novel Member of the Secretin Family of G Protein-coupled Receptors *. *J. Biol. Chem.* **272**, 21504–21508 (1997).

44. Krasnoperov, V. G. *et al.* The Calcium-Independent Receptor of α-Latrotoxin Is Not a Neurexin. *Biochem. Biophys. Res. Commun.* **227**, 868–875 (1996).

45. Sugita, S., Ichtchenko, K., Khvotchev, M. & Südhof, T. C. α-Latrotoxin Receptor CIRL/Latrophilin 1 (CL1) Defines an Unusual Family of Ubiquitous G-protein-linked Receptors: G-PROTEIN COUPLING NOT REQUIRED FOR TRIGGERING EXOCYTOSIS*. *J. Biol. Chem.* **273**, 32715–32724 (1998).

46. Moreno-Salinas, A. L. *et al.* Latrophilins: A Neuro-Centric View of an Evolutionary Conserved Adhesion G Protein-Coupled Receptor Subfamily. *Front. Neurosci.* **13**, (2019).

47. Röthe, J. *et al.* Involvement of the Adhesion GPCRs Latrophilins in the Regulation of Insulin Release. *Cell Rep.* **26**, 1573-1584.e5 (2019).

48. Brenner, S. The genetics of Caenorhabditis elegans. *Genetics* **77**, 71–94 (1974).

49. Sulston, J. E. & Horvitz, H. R. Post-embryonic cell lineages of the nematode, Caenorhabditis elegans. *Dev. Biol.* **56**, 110–156 (1977).

50. C. elegans Sequencing Consortium. Genome sequence of the nematode C. elegans: a platform for investigating biology. *Science* **282**, 2012–2018 (1998).

51. Kimble, J. E. & White, J. G. On the control of germ cell development in *Caenorhabditis elegans*. *Dev. Biol.* **81**, 208–219 (1981).

52. Byrd, D. T., Knobel, K., Affeldt, K., Crittenden, S. L. & Kimble, J. A DTC Niche Plexus Surrounds the Germline Stem Cell Pool in Caenorhabditis elegans. *PLOS ONE* **9**, e88372 (2014).

53. Austin, J. & Kimble, J. *glp-1* Is required in the germ line for regulation of the decision between mitosis and meiosis in C. elegans. *Cell* **51**, 589–599 (1987).

54. Henderson, S. T., Gao, D., Lambie, E. J. & Kimble, J. lag-2 may encode a signaling ligand for the GLP-1 and LIN-12 receptors of C. elegans. *Dev. Camb. Engl.* **120**, 2913–2924 (1994).

55. Berry, L. W., Westlund, B. & Schedl, T. Germ-line tumor formation caused by activation of glp-1, a Caenorhabditis elegans member of the Notch family of receptors. *Development* **124**, 925–936 (1997).

56. Hall, David H., Herndon, Laura A., & Lints, Robyn. Reproductive System - Somatic Gonad. https://doi.org/10.3908/WORMATLAS.1.22 doi:10.3908/WORMATLAS.1.22.

57. Hall, David H., Herndon, Laura A., & Lints, Robyn. Reproductive System - Germ Line. https://doi.org/10.3908/WORMATLAS.1.23 doi:10.3908/WORMATLAS.1.23.

58. Gumienny, T. L., Lambie, E., Hartwieg, E., Horvitz, H. R. & Hengartner, M. O. Genetic control of programmed cell death in the Caenorhabditis elegans hermaphrodite germline. *Development* **126**, 1011–1022 (1999).

59. Zhou, B. *et al.* Notch signaling pathway: architecture, disease, and therapeutics. *Signal Transduct. Target. Ther.* **7**, 95 (2022).

60. Hubbard, E. J. A. & Schedl, T. Biology of the Caenorhabditis elegans Germline Stem Cell System. *Genetics* **213**, 1145–1188 (2019).

61. Greenwald, I. Development of the Vulva. in *C. elegans II* (eds Riddle, D. L., Blumenthal, T., Meyer, B. J. & Priess, J. R.) (Cold Spring Harbor Laboratory Press, Cold Spring Harbor (NY), 1997).

62. Priess, J. R. Notch signaling in the C. elegans embryo. *WormBook* https://doi.org/10.1895/wormbook.1.4.1 (2005) doi:10.1895/wormbook.1.4.1.

63. Matúš, D., Post, W. B., Horn, S., Schöneberg, T. & Prömel, S. Latrophilin-1 drives neuron morphogenesis and shapes chemo- and mechanosensation-dependent behavior in C. elegans via a trans function. *Biochem. Biophys. Res. Commun.* **589**, 152–158 (2022).

64. Guest, M. *et al.* The calcium-activated potassium channel, SLO-1, is required for the action of the novel cyclo-octadepsipeptide anthelmintic, emodepside, in *Caenorhabditis elegans*. *Int. J. Parasitol.* **37**, 1577–1588 (2007).

65. Willson, J. *et al.* Latrotoxin Receptor Signaling Engages the UNC-13-Dependent Vesicle-Priming Pathway in *C. elegans*. *Curr. Biol.* **14**, 1374–1379 (2004).

66. Post, W. B. *et al.* Notch activity is modulated by the aGPCR Latrophilin binding the DSL ligand in C. elegans. *Nat. Commun.* **16**, 6461 (2025).

67. Tanaka, K. *et al.* Latrophilin mediates flow activation of Notch to control vascular endothelial phenotype and atherosclerosis. 2025.07.01.662676 Preprint at https://doi.org/10.1101/2025.07.01.662676 (2025).

68. Srivastava, S. *et al.* Adgrg6/Gpr126 is required for compact wall integrity and establishing trabecular identity during cardiac trabeculation. *Nat. Commun.* **17**, 1484 (2026).

69. Kloock, A. & Hubbard, E. J. A. Intestinal RICT-1 regulates the larval germline progenitor pool via the vitellogenin VIT-3 in C. elegans. *BioRxiv Prepr. Serv. Biol.* 2025.01.08.632040 (2025) doi:10.1101/2025.01.08.632040.

70. Matúš, D. *et al.* The N terminus-only (trans) function of the adhesion G protein-coupled receptor latrophilin-1 controls multiple processes in reproduction of Caenorhabditis elegans. *G3 GenesGenomesGenetics* **14**, jkae206 (2024).

71. Knierim, A. B. *et al.* Genetic basis of functional variability in adhesion G protein-coupled receptors. *Sci. Rep.* **9**, 11036 (2019).

72. Kuhn, C. K. *et al.* The repertoire and structure of adhesion GPCR transcript variants assembled from publicly available deep-sequenced human samples. *Nucleic Acids Res.* **52**, 3823–3836 (2024).

73. Wang, S. *et al.* Alternative splicing of latrophilin-3 controls synapse formation. *Nature* **626**, 128–135 (2024).

74. Bormann, A. *et al.* Intron retention of an adhesion GPCR generates 1TM isoforms required for 7TM-GPCR function. *Cell Rep.* **44**, 115078 (2025).

75. Ribalta-Mena, S. *et al.* Adhesion GPCR ADGRL1/Latrophilin-1 mobilizes β-arrestins as a prerequisite for endosomal restriction of G protein activation and splice-dependent scaffolds. *Biochim. Biophys. Acta BBA - Mol. Cell Res.* **1873**, 120132 (2026).

76. Garbett, K. A. *et al.* Cytoplasmic tail diversity determines the effector bias of the adhesion GPCR ADGRL2. *Cell Chem. Biol.* **33**, 364-378.e6 (2026).

77. Fire, A. *et al.* Potent and specific genetic interference by double-stranded RNA in Caenorhabditis elegans. *Nature* **391**, 806–811 (1998).

78. Zhang, L., Ward, J. D., Cheng, Z. & Dernburg, A. F. The auxin-inducible degradation (AID) system enables versatile conditional protein depletion in *C. elegans*. *Development* dev.129635 (2015) doi:10.1242/dev.129635.

79. Bui, D. L. H. *et al.* The adhesion GPCRs CELSR1-3 and LPHN3 engage G proteins via distinct activation mechanisms. *Cell Rep.* **42**, 112552 (2023).

Declaration of the use of generative AI and AI-assisted technologies

AI by means of ChatGPT was occasionally used, solely for improving language and readability of this thesis. After using the tool, the content was reviewed and edited. I take full responsibility for the content of this thesis.

8 Supplementary material

8.1 Supplementary material for 'The N terminus-only (*trans*) function of the Adhesion GPCR Latrophilin-1 controls multiple processes in reproduction of *C. elegans*'

SUPPLEMENTAL INFORMATION

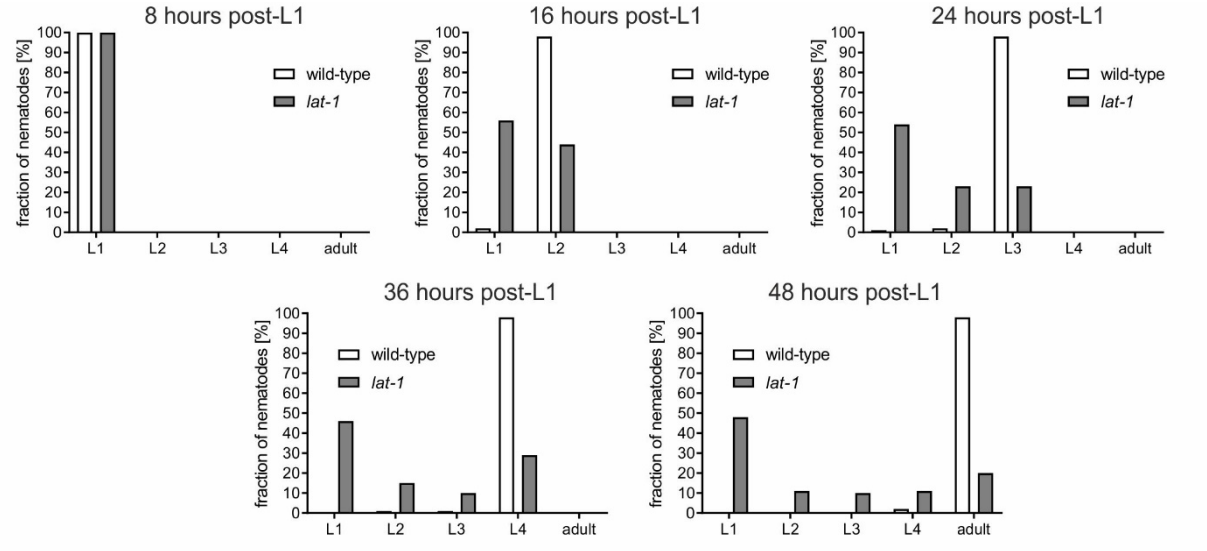


Figure S1. *lat-1* nematodes display an impaired larval development. A synchronized L1 population of nematodes was evaluated for progression through the larval stages up to adulthood at 8, 16, 24, 36, and 48 hours post-L1. While wild-type worms show a fast and synchronized progression, some *lat-1* nematodes arrest in early larval stages. However, a small percentage of *lat-1* mutants reach L4/adulthood at the same time as wild-type animals. Data from 4 independent experiments, n ≥ 700.

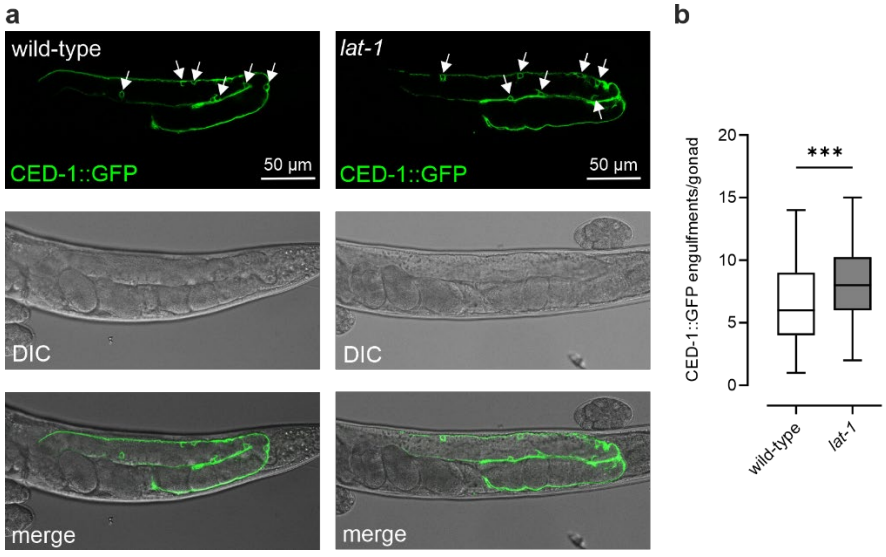


Figure S2. The number of engulfments visualized by CED-1::GFP is increased in *lat-1* hermaphrodites. (a) Representative images of CED-1::GFP in wild-type and *lat-1* hermaphrodites. (b) Quantification of GFP shown in (a) reveals that the number of engulfments is increased in *lat-1* hermaphrodites compared to wild-type nematodes. n ≥ 20 in 3 independent experiments. *** $p < 0.001$.

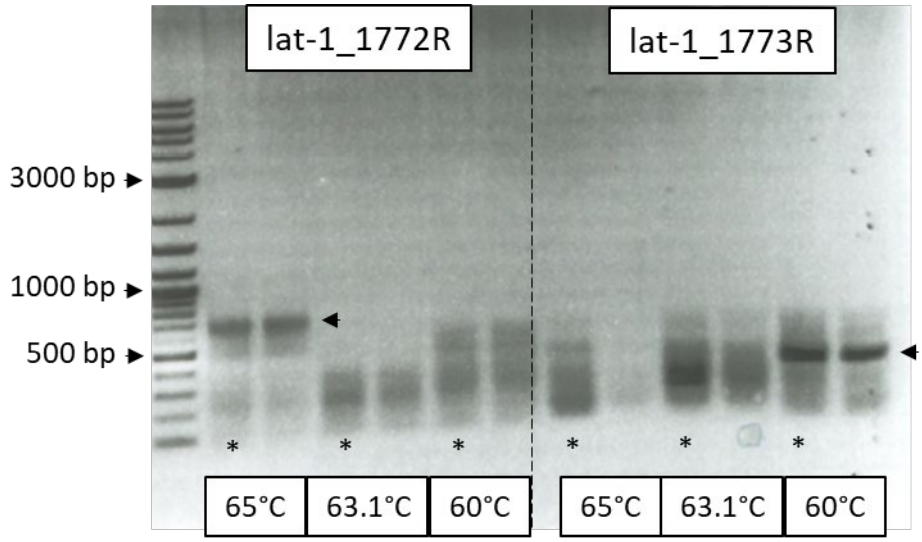


Figure S3. Exemplary gel picture of the 5' rapid amplification of cDNA-ends with PCR (RACE-PCR). The RACE was performed with wild-type RNA with two different primers (lat-1_1772R binding in exon 5 and lat-1_1773R binding to the exon 4/exon 5 junction) at three different annealing temperatures (65 °C, 63.1 °C and 60 °C). Every sample was used both undiluted (*) and diluted (1:20 in water) within the PCR and then separated on a 2% agarose gel containing ethidium bromide gel. Band sizes for variants are 516 bp/505 bp (arrow left) and around 635 bp (arrow right) depending on the selected primers. Other visible bands did not yield any product.

Table S1. Sequences of primers used in the study.

Primer	Sequence 5'-3'
lat1_1080F	TTGTTTGTGAGTTTTCGTTTTCGCCTTTATCTTGTTATTTGAATCCGAATCCCTATAGTGAGTCGTATTACATGGTCATA
lat1_1081R	ATTGCTGCAGGATCTTTTCTACGGGGTCTGACGCTCAGTG
lat1_1082F	GATCCTGCAGCAATGCTTCCGAAAACCTCCGAGTTTTTCG
lat1_1083R	GCTACCAGAATCGTTTGGAGCAACGAATAAGTCGTTTTGTTACGTCGCATGCCGTTGAACAGATATAGAAGTTTGTGATT
lat1_1084F	CTTAACTGTCAGATTTCAAAAAAAAAAGGA
lat1_1085R	CTGTAATTGTCTCATATTTTGATTTTAAAA
lat1_1086F	GATCCTGCAGCTTAACTGTCAGATTTCAAAAAA
lat1_1087R	GCTACCAGAATCGTTTGGAGCAACGAATAAGTCGTTTTGTTACGTCGCATCTGTAATTGTCTCATATTTTGATTTTAAAAGAGTAAACAC
lat1_1088F	TTTGAATCCGAAAAAGTCTCAAAAAGCAAA
lat1_1089R	AAAAGGCAAATTTGAAAAGTGTTGTTGGCT
lat1_1090F	GATCCTGCAGTTTGAATCCGAAAAAGTCTCAAAAAGCAAA
lat1_1091R	GCTACCAGAATCGTTTGGAGCAACGAATAAGTCGTTTTGTTACGTCGCATAAAAGGCAAATTTGAAAAGTGTTGTTGGC
lat-1_1772R	AACGTCCGAATTGAGGGCAT
lat-1_1773R	TGAGGGCATCCTTTTGAGCC
lat1_1896F	CAGCGGATAACAATTTCACAtgcattttattttagcaatttaatgg
lat1_1897R	CTCCTTGCGTTCATCTTCATAACACCCCTTGTATTACTGT
lat1_1898F	ACAGTAATACAAGGGGTGTTATGAAGATGAACGCAAGGAG
lat1_1921R	acgcatcaaagatatggagaAGTTGAAACAGTTATGTTTGGT
lat1_1900F	ATTTAAATTTTCAGGAGTAAtctccatatctttgatgcgt
lat1_1901R	GGTTTTGGCGCGCCTTTAAAactgtcaaactttgagagattg
lat1_1902F	atctctcaaagtttgacagtTTTAAAGGCGCGCCAAAACC
lat1_1903R	aattgctaaaataaaatgcaTGTGAAATTGTTATCCGCTG
Oligo d(T)-Anchor Primer	GACCACGCGTATCGATGTCGACTTTTTTTTTTTTTTTV (V=A, C or G)
PCR Anchor Primer	GACCACGCGTATCGATGTCGAC

Table S2. Raw FPKM values derived from StringTie deduced from (CHEN *et al.* 2015).

	Transcripts		FPKM Sample1	% (of all *lat-1* transcripts)	FPKM Sample2	% (of all *lat-1* transcripts)	FPKM Sample3	% (of all *lat-1* transcripts)	% (mean)	
lat-1 transcripts	all transcripts in samples		46.29	100%	52.30	100%	44.4995	100%	100%	
Full-length complete	5,9,13,15,20,22,26,30	ADGRL1_wt_1.19 ADGF	43.75	94%	50.03	95.66%	42.23	94.90%	95.019%	**95.02%**
Full-length variants										
	4 7 9 13 15 20 22 26 30	ADGRL1_wt_1.15	0.836475	1.81%	0.00	0.00%	0.00	0.00%	0.602%	**2.29%**
	5 9 11 13 15 20 22 26 30	ADGRL1_wt_1.16_(mo)	0.459209	0.99%	0.00	0.00%	0.00	0.00%	0.331%	
	6 9 15 20 22 26 29	ADGRL1_wt_3.19_(mo)	0	0.00%	0.00	0.00%	0.38	0.84%	0.281%	
	8 11 13 14 20 22 26 29	ADGRL1_wt_3.12	0	0.00%	0.00	0.00%	0.09	0.20%	0.067%	
	8 11 15 20 22 26 30	ADGRL1_wt_1.28 ADGRL1_wt_3.17	0.399316	0.86%	0.00	0.00%	0.57	1.28%	0.713%	
	8 15 20 22 26 30	ADGRL1_wt_1.36	0.37441	0.81%	0.00	0.00%	0.00	0.00%	0.270%	
N terminus variants										
	10 13 16	ADGRL1_wt_3.35	0.0000	0.00%	0.0000	0.00%	0.2254	0.51%	0.253%	**1.50%**
	2 18 19 31	ADGRL1_wt_1.56	0.0615	0.13%	0.0000	0.00%	0.0000	0.00%	0.044%	
	6 9 11 13 15 20 22 27	ADGRL1_wt_2.2	0.0000	0.00%	0.2350	0.45%	0.0000	0.00%	0.225%	
	6 9 12	ADGRL1_wt_2.6	0.0000	0.00%	0.3024	0.58%	0.0000	0.00%	0.289%	
	8 11 13 16	ADGRL1_wt_2.5 ADGRL1_wt_3.34	0.0000	0.00%	0.6791	1.30%	0.0353	0.08%	0.689%	
other variants										
	8 11 15 20 22 27	ADGRL1_wt_2.3	0.000	0.00%	0.257	0.49%	0.000	0.00%	0.16%	**1.21%**
	8 13 14 20 22 28	ADGRL1_wt_3.24	0.000	0.00%	0.000	0.00%	0.023	0.05%	0.02%	
	8 15 20 22 27	ADGRL1_wt_2.4	0.000	0.00%	0.518	0.99%	0.000	0.00%	0.33%	
	21 25	ADGRL1_wt_3.36	0.000	0.00%	0.000	0.00%	0.231	0.52%	0.17%	
	3 23 27	ADGRL1_wt_2.7	0.000	0.00%	0.207	0.40%	0.000	0.00%	0.13%	
	1 17 20 22 28	ADGRL1_wt_3.28	0.000	0.00%	0.000	0.00%	0.116	0.26%	0.09%	
	8 11 13 14 20 22 28	ADGRL1_wt_3.18	0.000	0.00%	0.000	0.00%	0.408	0.92%	0.31%	

Table S3. Accession numbers and mapping statistics for transcript analysis of *lat-1* variants.

GEO Accession	SRA run	raw reads	uniquely aligned raw reads [%]
GSM1862268	SRR2185654	2 x 57999404	94.52
GSM1862269	SRR2185655	2 x 40607164	94.76
GSM1862270	SRR2185656	2 x 49090847	94.62

Table S4. Exon positions of *lat-1* variants analyzed in this study. Given are the identified exons for the *lat-1* gene (numbering refers to the reference *C. elegans* genome (WBcel235)).

Exon	Chromosome	Start	End
1	II	8805410	8805979
2	II	8805628	8805979
3	II	8846108	8846118
4	II	8890831	8890855
5	II	8896750	8896987
6	II	8896839	8896987
7	II	8896841	8896987
8	II	8899797	8899984
9	II	8899798	8899984
10	II	8903278	8903494
11	II	8903388	8903494
12	II	8903300	8903521
13	II	8903607	8903719
14	II	8903832	8903929
15	II	8903844	8903929
16	II	8903844	8903930
17	II	8903913	8903929
18	II	8903916	8903929
19	II	8904012	8904492
20	II	8904012	8905264
21	II	8905967	8906846
22	II	8906060	8906846
23	II	8906575	8906846
24	II	8906914	8906981
25	II	8906915	8907289
26	II	8907152	8907287
27	II	8907152	8907288
28	II	8907152	8907289
29	II	8907725	8908630
30	II	8907725	8908636
31	II	8964794	8964892

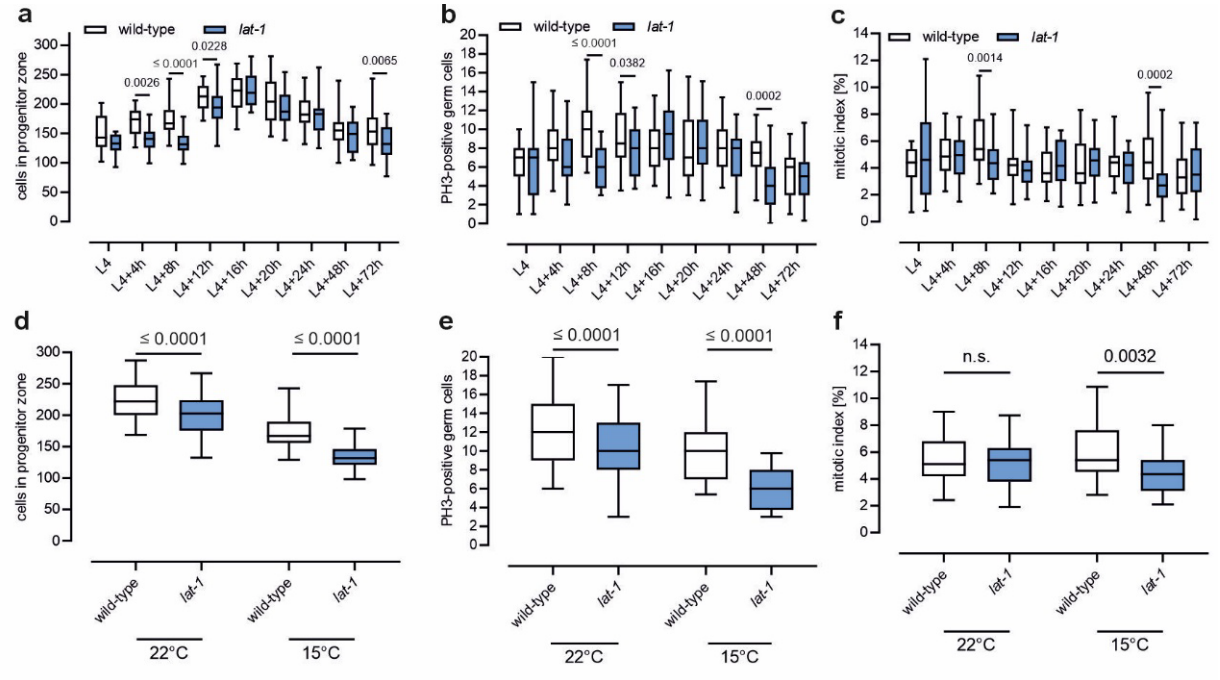
REFERENCES

Chen, A. T., C. Guo, O. A. Itani, B. G. Budaitis, T. W. Williams *et al.*, 2015 Longevity Genes Revealed by Integrative Analysis of Isoform-Specific daf-16/FoxO Mutants of Caenorhabditis elegans. Genetics 201**:** 613-629.

8.2 Supplementary material for ‘Notch activity is modulated by the aGPCR Latrophilin binding the DSL ligand in *C. elegans*’

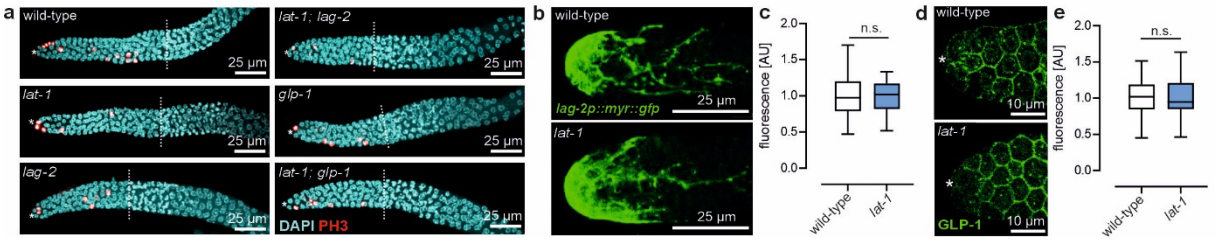
SUPPLEMENTARY INFORMATION

Supplementary Figures and Figure Legends



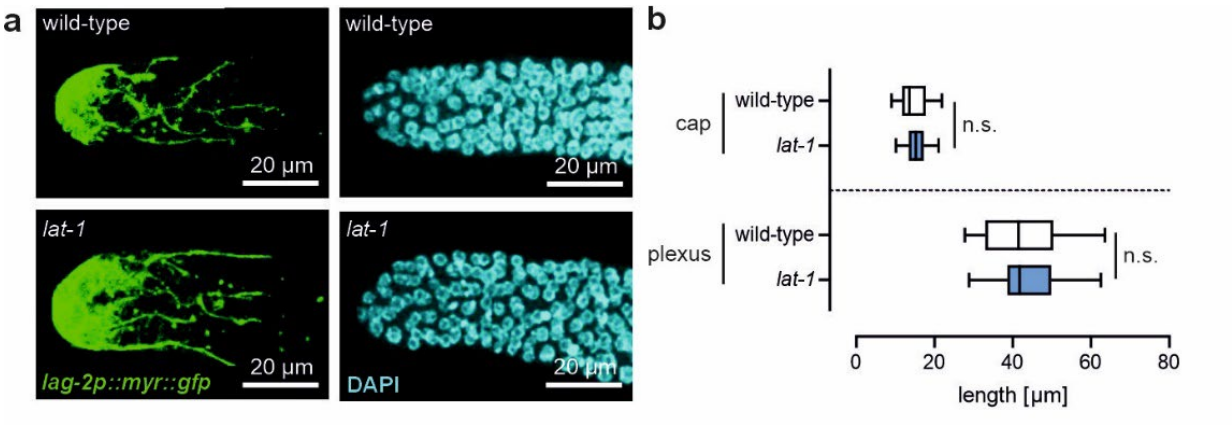
Supplementary Figure 1. LAT-1 affects germ cell proliferation at specific time points during very early adult stages, an effect that persists at different temperatures. (a)-(c) Gonads of *lat-1* animals at different ages after L4 at 15°C stained with DAPI and anti-PH3 antibody show differences compared to wild-type controls. (a) In *lat-1* mutant gonads, the size of the progenitor zone is smaller than in wild-type controls at the age of L4 + 4 h to L4 + 12 h as well as L4 + 72 h. (b) Likewise, the number of PH3-positive germ cells at L4 +8 h to L4 + 12 h and L4 + 48 h was significantly decreased in the progenitor zone of *lat-1* hermaphrodites. (c) The mitotic index was significantly altered in *lat-1* mutants only at L4 + 8 h and L4 + 48 h compared to wild-type levels. (d)-(f) The observed alterations in progenitor zone size (d), PH3-positive germ cells (e), but not the mitotic index (f) in *lat-1* gonads at the age of L4 + 8 h persist at 22 °C compared to 15 °C.

Data are based on DAPI- and anti-PH3-stained gonads. n = 22 in 4 independent experiments. Graph raw data and p values are provided in the Source Data. Graph details and statistics are: Box plots with median (center), interquartal range, 5th (lower whisker) and 95th (upper whisker) percentiles. One-way ANOVA with Bonferroni post-hoc test (a)-(c). Two-sided unpaired t-test without multiple comparison correction (d)-(f).



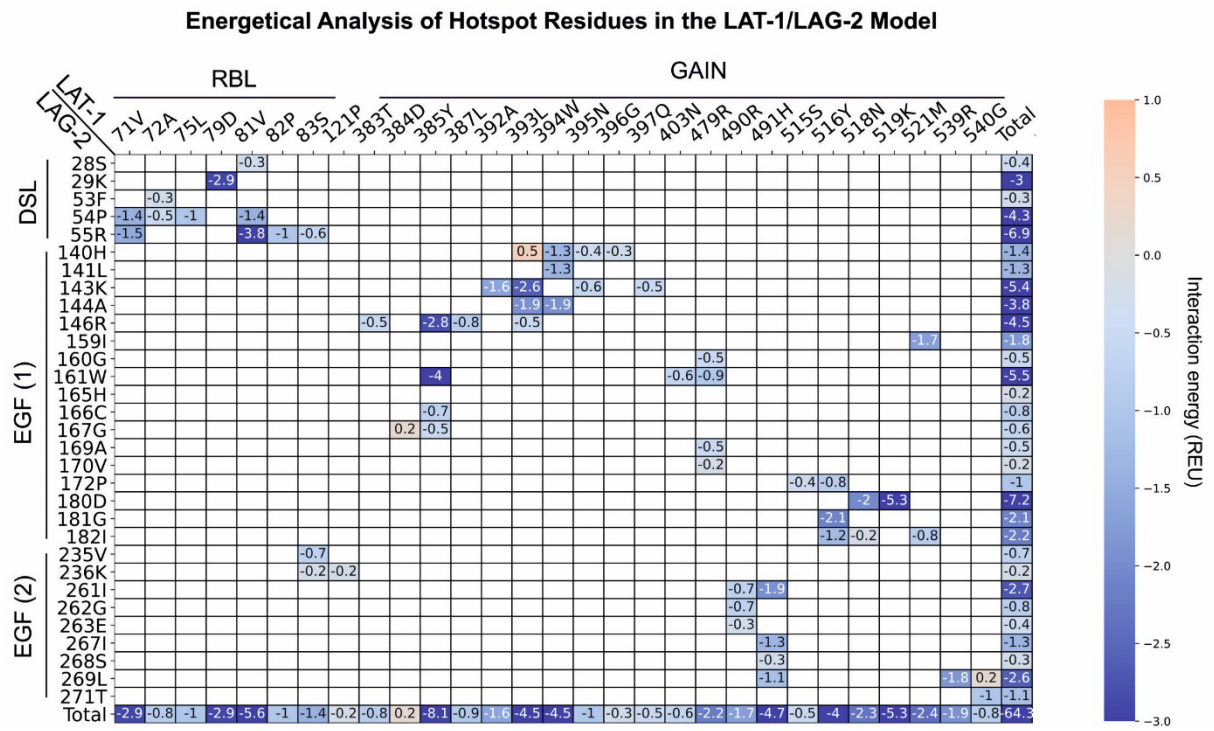
Supplementary Figure 2. Gonads of *lat-1*, *lag-2*, and *glp-1* single and double mutants and expression of Notch pathway components in *lat-1* gonads. (a) Representative DAPI- and PH3-stained gonads of L4 + 8 h-old hermaphrodites carrying *lat-1(ok1465)*, *lag-2(q420),* or *glp-1(bn18)* as well as of hermaphrodites harboring the double mutants *lat-1(ok1465); lag-2(q420)* or *lat-1(ok1465); glp-1(bn18)*. These images formed the basis for the quantification of proliferative zone size (Fig. 2d) and PH3-positive germ cell numbers (Fig. 2e). (b), (c) Expression of *lag-2* is not altered in *lat-1* gonads. Representative images of the distal gonads of L4 + 8 h-old hermaphrodites expressing *lag-2p::myr::gfp* (b). These images were used to quantify *lag-2* expression based on fluorescence intensity of the reporter in wild-type and *lat-1* mutants (c). Wild-type: n = 27 in 4 independent experiments, *lat-1*: n = 23 in 4 independent experiments. (d), (e) Expression of *glp-1* in the gonads of *lat-1* hermaphrodites, assessed using the GLP-1 NICD::V5 reporter *glp-1(q1000[glp-1::4xV5])* is not different from that in wild-type individuals (d). Shown are exemplary images of distal gonads. Quantification of these images confirms that total *glp-1* expression does not change in the absence of *lat-1* (e). Note that subcellular distribution of the reporter changes as described in Fig. 2f, g. Wild-type: n = 31 in 6 independent experiments, *lat-1*: n = 28 in at least 4 independent experiments.

Graph raw data and p values are provided in the Source Data. Graph details and statistics are: (c), (e): Box plots with median (center), interquartal range, 5th (lower whisker) and 95th (upper whisker) percentiles. Two-sided unpaired t-test without multiple comparison correction. n.s. = not significant.

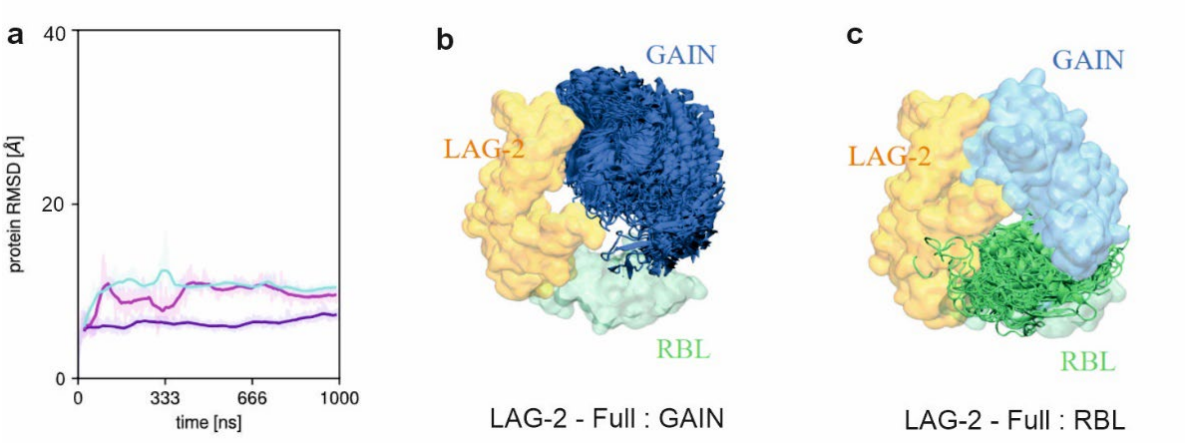


Supplementary Figure 3. The morphology of the DTC is unaltered in *lat-1* mutants. (a) Wild-type and *lat-1* mutant DTC visualized by *lag-2p::myr::gfp* expression in 8-h-post-L4 animals. The morphology of the *lat-1* mutant DTC is largely intact compared to the wild-type DTC. The extension of the plexus over the proliferative zone is unchanged. (b) Quantification of images from (a). Cap as well as plexus lengths in *lat-1* gonads are indistinguishable from those in wild-type animals. n.s. = not significant. Cap measurements: wild-type: 28 replicates in 4 independent experiments, *lat-1*: 23 replicates in 3 independent experiments. Plexus: wild-type: 27 replicates in 4 independent experiments, *lat-1*: 22 replicates in 3 independent experiments.

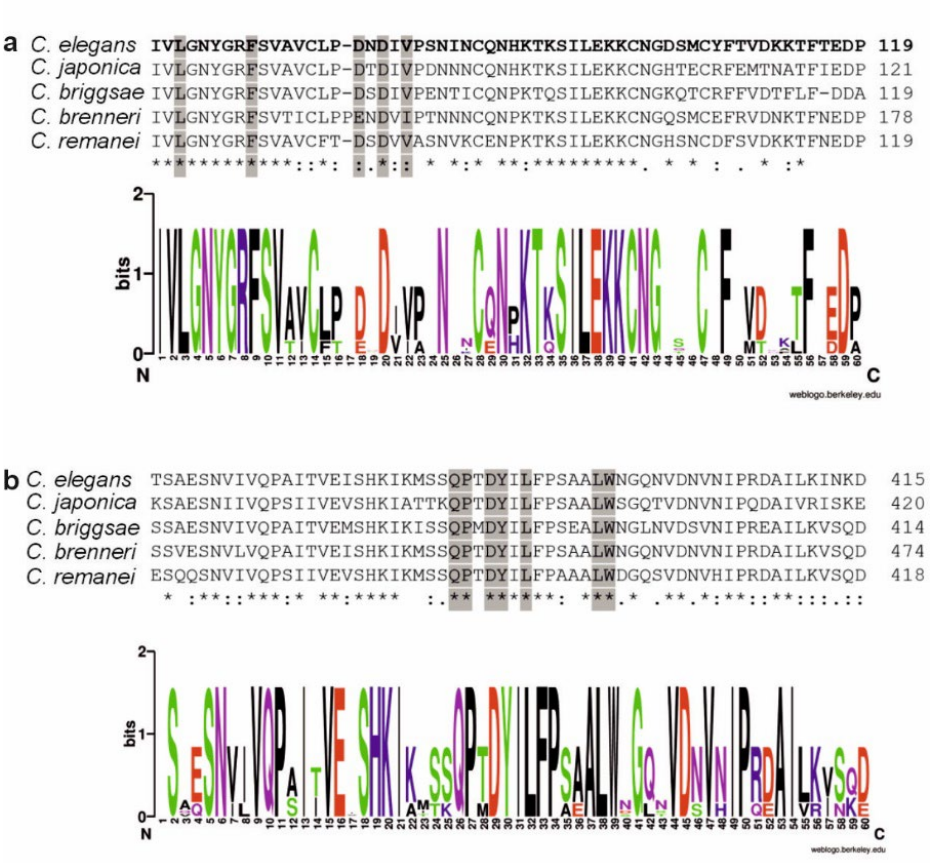
Graph raw data and p values are provided in the Source Data. Graph details and statistics are: (b): Box plots with median (center), interquartal range, 5th (lower whisker) and 95th (upper whisker) percentiles. Two-sided unpaired t-test without multiple comparison correction. n.s. = not significant.



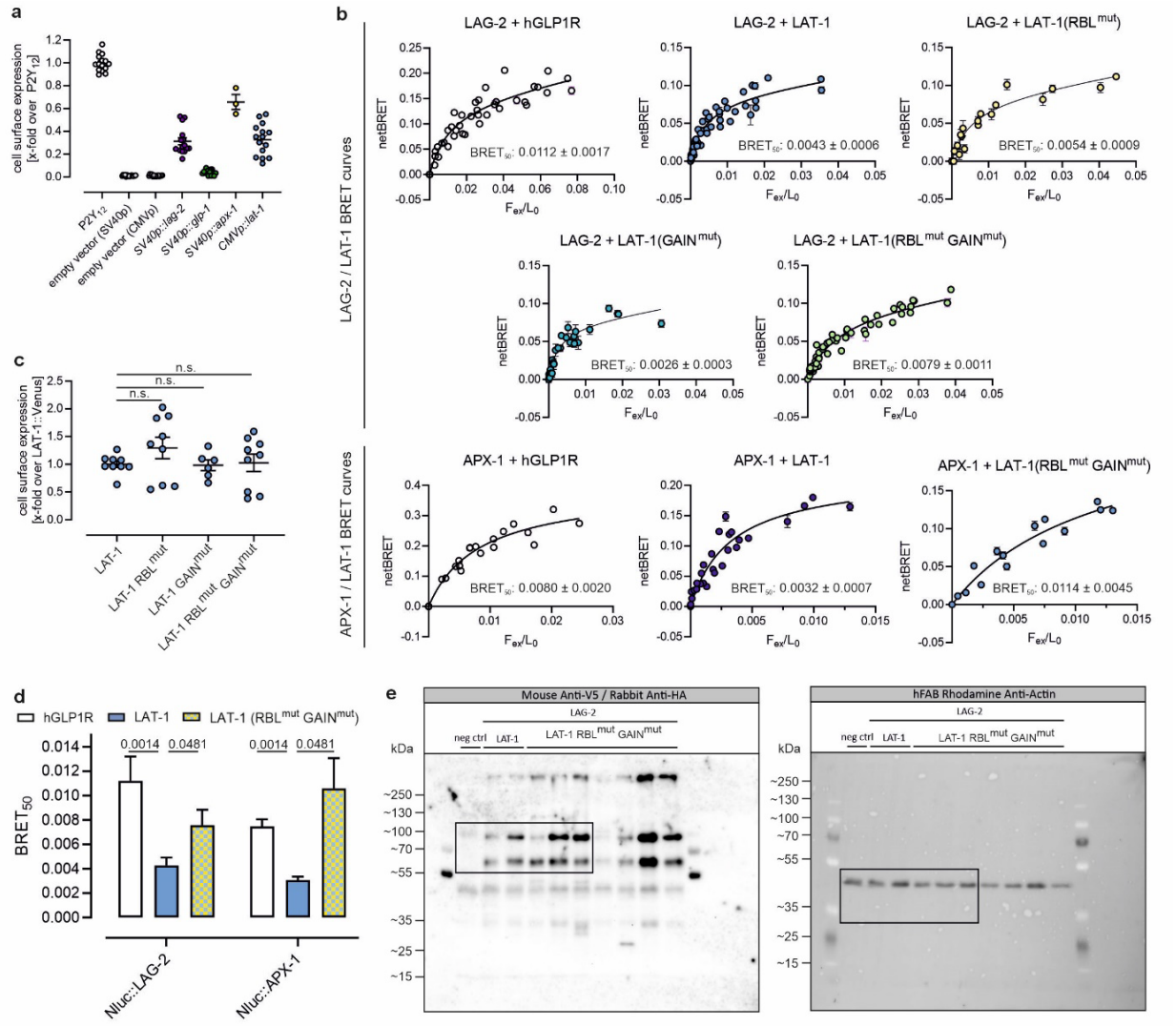
Supplementary Figure 4. Contact map for the per residue energy contribution of wild-type LAT-1 and LAG-2 interface. An energy breakdown based on the final energetically minimized Rosetta models of the AlphaFold2 Multimer model shows the average pairwise energetical contribution in Rosetta Energy Units (REU). REU are internal scoring units used by the Rosetta modeling software to estimate the energetic contribution of individual residues to the protein-protein interface. They are not equivalent to kcal/mol and should be interpreted comparatively. More negative values represent stronger stabilizing interactions. A negative number and darker color correlate with stronger energetical contribution between the extracellular regions of LAT-1 and LAG-2. Shown residues were selected by score, with a calculated binding energy higher than +0.2 REU or lower than -0.2 REU.



Supplementary Figure 5. Molecular Dynamics (MD) Simulations of the best ranked LAG-2/LAT-1 complex show stable LAG-2-GAIN interactions. (a) Root-mean square deviation (RMSD) traces of the simulated complex model. Opaque traces represent moving average over 50 ns for three independent trajectories colored in cyan, magenta and purple, with raw data shown transparent in the background. (b), (c) Flexibility of RBL (green) and GAIN (blue) protein domains relative to LAG-2 (orange) shown in snapshots overlaid with time-dependent conformations every 100 ns shown as cartoon: The full complex trajectory with time-dependent GAIN conformations shows stable interaction regions (b) with a stable relative conformation of the RBL domain in the full complex (c).



Supplementary Figure 6. The residues comprising the binding interface of LAT-1 are conserved in *Caenorhabditis* species. (a) Top: Multiple sequence alignment of related Latrophilin 1 proteins in *Caenorhabditis* species, focusing on the interaction interface of the RBL domain with LAG-2. Residues essential for binding mutated in the course of the study are shaded in grey. Bottom: Sequence logo of the LAT-1 RBL domain shows residue conservation across various nematode species, with highly conserved positions represented by taller letters. (b) Top: Multiple sequence alignment of Latrophilin 1 proteins in *Caenorhabditis* species, focusing on the GAIN interaction interface with LAG-2. Bottom: Sequence logo of the LAT-1 GAIN domain indicates residue conservation across various nematode species, with highly conserved positions represented by taller letters.



Supplementary Figure 7. Characterization of NanoBRET and BiFC constructs. (a) Cell surface expression of *lag-2*, *glp-1*, *apx-1*, and *lat-1* in HEK293 cells by ELISA displayed. Human $P2Y_{12}$ served as positive control. The non-specific OD values are: empty vector (SV40p): 0.0072 ± 0.0042; empty vector (CMVp): 0.0075 ± 0.0040, $P2Y_{12}$: 0.6564 ± 0.1511 (set to 1). *lag-2*, *glp-1*, and *apx-1* are under the control of the SV40 promoter and *lat-1* is CMV promoter-driven. Number of independent experiments (all in triplicates): *SV40p::apx-1*: 3 independent experiments; all other samples: 5 independent experiments. (b) Plots displaying netBRET values from the NanoBRET analyses of LAT-1 (LAT-1::Venus) and respective constructs carrying point mutations in RBL and/or GAIN domain with LAG-2 (Nluc::LAG-2) or APX-1 (Nluc::APX-1) in HEK293 cells over increasing amounts of transfected acceptor plasmid. The human hGLP1R::Venus served as negative control. Note that LAG-2 + hGLP1R shows a higher $netBRET_{max}$ value due to the different orientation of this complex. Different $BRET_{50}$ values reflect different protein-protein affinities. $BRET_{50}$ values are stated for each donor:acceptor pair. All experiments were performed in technical quadruplicate. Independent replicates: LAG-2 + hGLP1R: 8, LAG-2 + LAT-1: 11, LAG-2 + LAT-1(RBL^{mut}): 4, LAG-2 + LAT-1($GAIN^{mut}$): 6, LAG-2 + LAT-1(RBL^{mut} $GAIN^{mut}$): 5, APX-1 + hGLP1R: 4, APX-1 + LAT-1: 6, APX-1 + LAT-1(RBL^{mut} $GAIN^{mut}$): 3. (c) ELISA reveals an unaltered cell surface expression of *lat-1(*RBL^{mut} $GAIN^{mut}$*)::Venus* mutants compared to unmutated LAT-1 in HEK293 cells. 3 independent experiments for all plasmids, except *Venus::lat-1* $GAIN^{mut}$ (2 independent replicates), all performed in triplicate. (d) APX-1 and LAT-1 interact *in vitro.* NanoBRET assays indicate a similar affinity of APX-1 for LAT-1 as LAG-2. Introducing point mutations in RBL and GAIN domain reduces the affinity in a comparable manner to LAG-2 and LAT-1, indicating that

the same residues in LAT-1 are required to mediate the interaction. Number of independent replicates (each in quadruplicate): LAG-2 + hGLP1R: 8, LAG-2 + LAT-1: 11, LAG-2 + LAT-1(RBL^{mut} $GAIN^{mut}$): 10, APX-1 + hGLP1R: 4, APX-1 + LAT-1: 6, APX-1 + LAT-1(RBL^{mut} $GAIN^{mut}$): 3. Corresponding netBRET values and curves are shown in (b). (e) Uncropped Western blots (related to Fig. 4d). Left: LAT-1 (V5-tagged, 81 kDa (autocatalytically cleaved)), LAG-2 (HA-tagged, 57 kDa), and mutated LAT-1(RBL^{mut} $GAIN^{mut}$) (V5-tagged, 81 kDa (autocatalytically cleaved)). Right: reference protein actin (~42 kDa). Boxes indicate crops displayed in Fig. 4d. Western Blot was performed twice with 60-80 worms per sample.

Graph raw data and p values are provided in the Source Data. Graph details and statistics are: (a), (c), (d): Mean ± SEM. One-way ANOVA with Bonferroni post-hoc test. n.s. = not significant.

Supplementary Tables and Table legends

Supplementary Table 1. Reagents and resources

REAGENT or RESOURCE	SOURCE	IDENTIFIER
Bacterial and Virus Strains		
E. coli DH5α	ThermoFisher Scientific	18258012
E. coli OP50	CGC	N/A
Primary antibodies		
Rabbit anti-phospho histone H3 (Ser10)	Merck Millipore	06-570
Mouse anti-V5 SV5-Pk1	BioRad	MCA1360
Anti-HA-peroxidase, High Affinity	Sigma	54193500
Secondary antibodies		
Goat anti-Rabbit IRDye 680RD-conjugated	LiCor	926-68071
Goat anti-Mouse IgG (H+L), F(ab')2 Fragment CF 568	Biotium	20109
Anti-rabbit IgG, HRP-linked Antibody	Cell Signaling Technology	7074
Goat Anti-Mouse IgG (H+L)-HRP Conjugate	BioRad	1721011
anti-Actin hFAB-Rhodamine	BioRad	12004164
Chemicals		
4,6 diamidine-2-phenylindole (DAPI)	Sigma	D9542
Fluoromount G	ThermoFisher Scientific	00-4958-02
Levamisole hydrochloride	BLDpharm	MFCD00012675
Enzymes		
Alt-R S.p. HiFi Cas9 Nuclease V3, 100 µg	Integrated DNA Technologies, Inc	1081060
Critical Commercial Assays		
Click-iT EdU Alexa Fluor 488 Imaging Kit	ThermoFisher Scientific	C10337
Click-iT EdU Alexa Fluor 647 Imaging Kit	ThermoFisher Scientific	C10340
NEBuilder HiFi DNA Assembly	New England Biolabs	E2621L
Zero Blunt TOPO PCR Cloning Kit	ThermoFisher Scientific	450245
Experimental Models: Cell Lines		
HEK293	German Collection of Microorganisms and Cell Cultures (DSMZ)	ACC 305
HEK293T	German Collection of Microorganisms and Cell Cultures (DSMZ)	ACC 635
Experimental Models: Organisms/Strains		
Caenorhabditis elegans strains, see *C. elegans* maintenance and strains and Table S3	This paper	N/A
Oligonucleotides		
See Supplementary Table 1	Sigma-Aldrich, IDT, Microsynth	N/A
Scientific instruments		
TCS SP8 STED 3X	Leica	
Spark plate reader	Tecan	

Supplementary Table 2. Oligonucleotides used in this study

Primer	Sequence (5' -> 3')
Bifc_1F	CACAACATCGAGAGTTTAAACTAAGCGGCCGCAG
Bifc_2R	CTGCGGCCGCTTAGTTTAAACTCTCGATGTTGTG
Bifc_3Fp	GAATTCATCTCGAGATGGTGAGCAAGGGCGAGGAGCTGTTCACC
Bifc_4Rp	GGTGGGCCCGCGGGTACAATTGCTAGCCAA
Bifc_5F	AGGTTTAAACGCCGCCGCAGCAGCCAGCAACAAGCCGACAACGGATGAAAGTGGA
lat-1_881F	GCCAATCTTTCCCTACTCTCCTCT
lat-1_1467Fp	GGCGAAAGTTGGAGTAACAGTCAG
lat-1_1468Rp	GCATGTACTGCCAGGACCTGGATTACAAGGATGACGACGATAAGTAAG
lat-1_1469Fp	GCTCCATGGATGCGGCCGCAGGATCCAGACA
lat-1_1470Rp	CGCTGCGGCAGCCTTGTACAGCTCGTCCATGC
lat-1_1473Fp	ACGGTACCTCACTTATCATCGTCGTCCTTGT
lat-1_1474Rp	TGAGGTACCGAGCTCGAATTCA
lat-1_1481F	CTCGAGATGATCGCTTACTTCCTCTT
lat-1_1482R	TCTCGAGCAGAAGAACGGCATCAAGGC
lat-1_1483Fp	ACCTGCCTCCCAGTCCTCCAAGCCCAGAAGAACGGCATCAAGGC
lat-1_1483Fp	TCGGTGGTAGGCTTGTTGCTGGCGTAGTCGGGGACGTCGT
lat-1_1484Rp	GAGGAGTAAGAGGAAGTAAGCGATCATCTCGAGATGAATTCGGTGGG
lat-1_1484Rp	ACGACGTCCCCGACTACGCCAGCAACAAGCCTACCACCGA
lat-1_1694Fp	TCGTCGTCATCCTTGTAATCCAGGTCCTGGCAGTACATGC
lat-1_1695Rp	TGAACGGCAGCTTCTACTGCGATTACAAGGATGACGACGATAAG
lat-1_1695Rp	GCAATTGCATTCCCGTCAGCCGCTTTATG
lat-1_1700F	TGCTGTTGCCTGTGACGACATCTTTATTTTGTGTG
lat-1_1703R	TGGCGTCAGGCGGTGGAGGTCAAACATCTAGTAATGAGCAGCTC
lat-1_1708F	TCTCCGCCCATCAGTTGGCTGGCGTAGTCGGGGACGTCGT
lat-1_1709R	GCGTTTTTTGCGCCAATCGCCCAGAAGAACGGCATCAAGGC
lat-1_1709R	ACGACGTCCCCGACTACGCCAGCCAACTGATGGGCGGAGA
lat-1_1712F	TGAATTCGGTGGGCCCGCGGGTACAAT
lat-1_1713R	GCTCCATGGATGCGGCCGCAGGATCCAGACA
lat-1_1714F	CGCTGCGGCAGCCTTGTACAGCTCGTCCATGC
lat-1_1731Fp	GCCTCCCAGTCCTCCAAGCCGACTACAAAGACGATGACGACAAGGCCGC
lat-1_1732Rp	TCGTCATCGTCTTTGTAGTCGGCTTGGAGGACTGGGAG
lat-1_1819F	TCGTCGTCATCCTTGTAATCGCAGTAGAAGCTGCCGTTCA
lat-1_1822R	ACGTCGTAGGGGTAGCTGGCGATAGGGGCGAAG
lat-1_1852R	GCTTTCTTCGCCCCTATCGCCTACCCCTACGACGTCCCCGAC
lat-1_1853F	CAGCAGGATCAGCAGCACCCGCATGGTGGCGGTACCAGATCTCCCG
lat-1_1869Fp	CCCCGACTACGCCCAACTGATGGGCGGAGAGTG
lat-1_1870Rp	GCCCGGGGCCACCATGATCGCCTACTTCCTGCT
lat-1_1927Fp	GAGTAAAATTAGAAGAACTCGCATCTCGAGATGAATTCGGTGGG
lat-1_1928Rp	CTCGAGATGATCGCTTACTTCCTCTT
lat-1_2006Rp	TCTATATCACCGCCGACAAGCAGAAGAACGGCATCAAGGC
lat-1_2009Fp	GCCTTGATGCCGTTCTTCTGCTTGTCGGCGGTGATATAGACGTT
lat-1_2036Rp	GAGGTTCTGGTGGCGGAGGTTCTAGCAACAAGCCGACAACGGA
lat-1_2167F	CGTGATTACAAGGATGACGATGACAAGAGACCTCGCCGTTTCACATACCTAC
lat-1_2168R	TTCACACAGGAAACAGCTATGACCATTTATCCAGTTGAACTATTTACTCCAGGTGAC
lat-1_2169F	CATCGATGCTCCTGAGGCTCCCGATGCTCCATCTGATGGGAAAACTTCAGTGAGC

lat-1_2170R	CGTGATTACAAGGATGACGATGACAAGAGACCTCGCCGTTTCACATACCTAC
lat-1_2175F	TTCACACAGGAAACAGCTATGACCATTTATCCAGTTGAACTATTTACTCCAGGTGAC
lat-1_2176R	TCTTGGTGAAACGGCGAGGATCTGA
lat-1_2177F	AAACTCAGATCCTCGCCGTTTCACC
lat-1_2178R	CACGCTGGCTCTTCCGTAGTTGCCCGCCACGATGCTGATCACTTTGC
lat-1_2179F	GCTGTCTGCCTGCCCGCTAACGCCATCGCGCCAAGCAACATCAACTGCCAG
lat-1_2180R	GACAGAGGCTCTTCCATAGTTTCCTGCGACAATCGAGATTACTTTTCCAGC
lat-1_2240R	GACAGAGGCTCTTCCATAGTTTCCTGCGACAATCGAGATTACTTTTCCAGC
lat-1_2241F	GCTGTTTGCCTTCCTGCCAATGCCATCGCTCCATCCAACATCAACTGCCAAAAC
lat-1_2284F	GCTGTTTGCCTTCCTGCCAATGCCATCGCTCCATCCAACATCAACTGCCAAAAC
lat-1_2285R	CTTGCCAGGCCTCCTGCAGCTAATCTAGAGGGCCCGTTTAAACCC
lat-1_2402F	TCGGGGACGTCGTAGGGGTACCTGCCCACCATCCCGAG
lat-1_2403R	TGCTCGGGATGGTGGGCAGGTACCCCTACGACGTCCCCG
lat-1_2491F	TGCAGCGGCTGACGGGAATGCAA
lat-1_2492R	TTTCCCTCTGCCGCCGCAGCTAACGGCCAAAATGTCGATAATG
lat-1_2499F	TAAACGGGCCCTCTAGATTAGCTGCAGGAGGCCTGGCAAGTGG
lat-1_2500R	TCCAGATTACGCTGCCGCCGCAGCAGCCCGAG
lat-1_2501F	CCCTGGGGGCGGGGGCCGGCTGAACCTCCTCCACCGGAGT
lat-1_2502R	ACTCCGGTGGAGGAGGTTCAGCCGGCCCCCGCCCCCAG
lat-1_2503F	ACATCGTATGGGTAGGCTTGGAGGACTGGGAGGC
lat-1_2504R	CTCCTCGGACTTGATAGCACCGCCGCCGCAGCAGCCATG
lat-1_2505F	TGGGTTAGGGATAGGCTTACCCTCGAGGGCGAAAGTTGGAGTAAC
lat-1_2506R	GGGGTCTGGTGAGCGGTGAGAAGGGCGAATTCTGCAGATA
lat-1_2511F	TGCGATAGCAGCGGTTGCTGCGCTAGACATCTTGATCTTGTG
lat-1_2512R	ACGTTGTAAAACGACGGCCAGTCGCCGGCAGTCGTTTGCCAGGGCTGTTG
lat-1_2513F	AGACTTTTGGACCGTGCGCCAAGGGCGAATTCCAGCACAC
lat-1_2514R	GTGTGCTGGAATTCGCCCTTGGCGCACGGTCCAAAAGTCT
lat-1_2527F	AGTTTAAACGCCGCCGCAGC
lat-1_2528R	CTCGATGTTGTGGCGGATCTTGAA
lat-1_2529F	GCGGCCGCCTAGACATAGTGACAGGCTG
lat-1_2529F	CGAGTAGAAGTCCATCAAGAGTTCAT
lat-1_2530R	ACCTGCCTCCCAGTCCTCCAAGCCCAGAAGAACGGCATCAAGGC
lat-1_2530R	GGCTTGGAGGACTGGGAG
lat-1_2531F	TCGTCGAGTGTAAGAGTTTCTCTCTGTCTGAAACATTCAATTGATTATC
lat-1_2532R	AAACTCAGATCCTCGCCGTTTCACC
lat-1_2616R	GGGGTCTGGTGAGCGGTGAGAAGGGCGAATTCTGCAGATA
lat-1_2617F	AGACTTTTGGACCGTGCGCCAAGGGCGAATTCCAGCACAC
lat-1_2618R	ACGACGTCCCCGACTACGCCATGGTGAGCAAGGGCGAGGA
lat-1_2618R	GCGAATGGGCAGAATGTTGATAATGTAAATATTC
lat-1_2619F	TCCTCGCCCTTGCTCACCATGGCGTAGTCGGGGACGTCGT
lat-1_2619F	GGTAGGCTTGTTGCTTGAACCTCCTCCACCGGAGTCGAGCGCTCGCCGAG
lat-1_2628F	CCAACTTTTCTTCTTTGCAGTTTGAATCCGAAAAAGTCTC
lat-1_2629R	TCGTCGAGTGTAAGAGTTTCAAAAGGCAAATTTGAAAAGTG
lat-1_2630F	GAGACTTTTTCGGATTCAAACTGCAAAGAAGAAAAGTTGGAAAAATAGAG
lat-1_2631R	CCAACTTTTCTTCTTTGCAGTTTGAATCCGAAAAAGTCTC
lat-1_2632F	GTGTGCTGGAATTCGCCCTTGGCGCACGGTCCAAAAGTCT
lat-1_2633R	GAGACTTTTTCGGATTCAAACTGCAAAGAAGAAAAGTTGGAAAAATAGAG

lat-1_2652F	ACTGAGCCTCCGCCACCACTATTAGGCTGAGAGGGGTGGA
lat-1_2653R	TCCACCCCTCTCAGCCTAATAGTGGTGGCGGAGGCTCAGT
lat-1_2654F	TGCTCATTACTAGATGTTTGACCTCCACCGCCTGACGCCA
lat-1_2655R	GCTCGACTCCGGTGGAGGAGGTTCAAGCAACAAGCCTACCACCGATG
lat-1_2691F	GCGTAATCTGGAACATCGTATGGGTAGGCGATTGGCGCAAA
lat-1_2691F	TTGAATGTTTCAGACAGAGAGAAACTCTTACACTCGACGA
lat-1_2692R	GATCCATGGAGTCAACTTATGGGTGGA
lat-1_2692R	GAAAATGTATTTTCTTGCAGCTGCAAAGAAGAAAAGTTGG
lat-1_2693F	GAGGAGTAAGAGGAAGTAAGCGATCATCTCGAGATGAATTCGGTGGG
lat-1_2693F	ACTTTTCAAATTTGCCTTTTGAAACTCTTACACTCGACGAACA
lat-1_2694R	TGCCGCCGCAGCAGCCCAGAAGAACGGCATC
lat-1_2694R	TATCTGCAGAATTCGCCCTTCTCACCGCTCACCAGACCCC
lat-1_2695F	ACCTGCCTCCCAGTCCTCCAAGCCCAGAAGAACGGCATCAAGGC
lat-1_2695F	TCGTCGAGTGTAAGAGTTTCAAAAGGCAAATTTGAAAAGTG
lat-1_2696R	GAGGAGTAAGAGGAAGTAAGCGATCATCTCGAGATGAATTCGGTGGG
lat-1_2696R	ACTTTTCAAATTTGCCTTTTGAAACTCTTACACTCGACGAACA
lat-1_2697F	TGCCGCCGCAGCAGCCCAGAAGAACGGCATC
lat-1_2697F	TATCTGCAGAATTCGCCCTTCTCACCGCTCACCAGACCCC
lat-1_2698R	GCGTAATCTGGAACATCGTATGGGTAGGCGATTGGCGCAAA
lat-1_2698R	TTGAATGTTTCAGACAGAGAGAAACTCTTACACTCGACGA
lat-1_2708F	GATGCGGCCGCCTAGACATAGTGACAGGCTG
lat-1_2708F	CCAACTTTTCTTCTTTGCAGCTGCAAGAAAATACATTTTC
lat-1_2709R	GATGCGGCCGCCTAGACATAGTGACAGGCTG
lat-1_2709R	TCGTCGAGTGTAAGAGTTTCTCTCTGTCTGAAACATTCAATTGATTATC
lat-1_2710F	GATGCGGCCGCTTAACAGTAGAAGGAGCCAT
lat-1_2710F	GAAAATGTATTTTCTTGCAGCTGCAAAGAAGAAAAGTTGG
lat-1_2711R	GATGCGGCCGCATCGAGTAGAAGTCCATCAAGA
p indicates 5' phosphorylation	
ssODN	**Sequence**
ssODN 1	TAAACTCAGTTATCATAATAAGACAATGACGTCATGTGACTGTACTGCTCTCACACA CTTCGCAGTACTGATGGATGTACGAGGACACGATCTGAATGAAATCGACCAAACGCT TCTCAC
ssODN 4	ATTGTTTCCTGCATTATTCAAATTCGTTGCTGCCGTTTGTTTGTCGATATGGAAGAT AAATACCGTTCTACTTTTGTTACAGAACTTTTTTTATTGTTAAAAAGTTTAATATAA TTGCTC
crRNA	**Sequence**
crRNA 2	UUCCAACUUUUCUUCUUUGC
crRNA 5	ACAAAAGUAGAACGGUAAGA
crRNA 6	UCGAUAUGGAAGAUAAACAA
tracrRNA	**Sequence**
Alt-R CRISPR-Cas9 tracrRNA	N/A

Supplementary Table 3. Plasmids generated in this study

Plasmid	Open reading frame	Used for	Worm strain
pNF001	*hsp-16.41p::HA::VC155::ala* [*Nco*I and *Not*I restriction sites]	Subcloning	n.a.
pNF002	*hsp-16.41p::HA::VC155::ala* [*Xho*I and *Eco*RI restriction sites]	Subcloning	n.a.
pNF017	*hsp-16.41p::lag-2sp::FLAG::ala::lag-2(1-193)::VC155::lag-2(194-401)*	BiFC analysis	APR771, APR834, APR841, APR842
pSP188	*hsp16.41p::lat-1sp::FLAG::VN173::ala::lat-1*	BiFC analysis	APR751
pSP228	*hsp16.41p::lag-2sp::VN173::lag-2*	BiFC analysis	APR739
pSP229	*hsp16.41p::glp-1sp::VC155::glp-1*	BiFC analysis	APR751
pSP234	*hsp16.41p::lag-2*	Competition BiFC	APR834, APR841, APR842
pSP246	*hsp16.41p::lat-1sp::FLAG::VN173::gly-ser::lat-1*	BiFC analysis	APR771, APR834, APR841, APR842
pSP314	*SV40p::glp-1sp::HA::glp-1::FLAG*	Surface ELISA	n.a.
pSP318	*SV40p::lag-2sp::HA::lag-2::FLAG*	Surface ELISA	n.a.
pSP334	*CMVp::lphn-1sp::HA::lat-1::FLAG*	Surface ELISA	n.a.
pSP359	*SV40p::lag-2sp::HA::lag-2(18-193)::gly-ser::Nluc::gly-ser::lag-2(194-401)*	BRET	n.a.
pSP360	*CMVp::lphn-1sp::HA::Venus::lat-1::FLAG*	BRET	n.a.
pSP371	*CMVp::lphn-1sp::HA::Venus::lat-1[GAIN^{mut}]::FLAG*	BRET	n.a.
pSP392	*CMVp::lphn-1sp::HA::Venus::lat-1[RBL^{mut} GAIN^{mut}]::FLAG*	BRET	n.a.
pSP395	*CMVp::lphn-1sp::HA::Venus::lat-1[RBL^{mut}]::FLAG*	BRET	n.a.
pSP396	*CMVp::GLP1Rsp::HA::Venus::GLP1R*	BRET	n.a.
pSP403	*hsp-16.41p::lag-2sp::HA::ala::lag-2(1-193)::vc155::lag-2(194-401)*	BiFC analysis	APR920, APR974
pSP404	*hsp16.41p::lat-1sp::V5::VN173::lat-1*	BiFC analysis	APR920
pSP406	*hsp16.41p::lat-1sp::V5::VN173::lat-1[RBL^{mut} GAIN^{mut}]*	BiFC analysis	APR974
pSP427	*CMVp::lag-2sp::HA::apx-1(21-191)::gly-ser::Nluc::gly-ser::(192-515)*	BRET	n.a.

Supplementary Table 4. *C. elegans* strains used in this study

Strain	Genotype	Used for	Source	Reference
Bristol N2	N/A	Phenotyping assays (PH3, EdU), Western blot	CGC	[11]
APR873	*lat-1(ok1465) II*	Phenotyping assays (PH3, EdU), Western blot, anus phenotyping, octanol assays	CGC	
WD881	*on172(rec-8::mNeonGreen) IV*	REC-8 analysis	Brent Derry	[9]
APR886	*lat-1(ok1465) II; on172(rec-8::mNeonGreen)IV*	REC-8 analysis	This paper	
JH2874	*pgl-1(ct131) him-3(e1147) III; ozIs5 [gld-1::GFP + unc-119(+)]*	GLD-1 analysis	CGC	[12]
APR756	*pgl-1(ct131) him-3(e1147) III; ozIs5 [gld-1::GFP + unc-119(+)] (outcrossed 4x)*	GLD-1 analysis	This paper	
JK1277	*lag-2(q420) V*	Epistasis analysis, anus phenotyping, octanol assays	CGC	[13]
APR569	*lat-1(ok1465) II; lag-2(q420) V*	Epistasis analysis, anus phenotyping, octanol assays	This paper	
HA1019	*osm-11(rt142) X.*	Octanol assays		[14]
DG2389	*glp-1(bn18) III*	Epistasis analysis	CGC	[15]
APR768	*lat-1(ok1465) II; glp-1(bn18) III*	Epistasis analysis	This paper	
JK5933	*glp-1(q1000[glp-1::4xV5]) III*	Notch activation analysis, *glp-1* expression quantification	CGC	[16]
APR778	*lat-1(ok1465) II ; glp-1(q1000[glp-1::4xV5]) III*	Notch activation analysis, *glp-1* expression quantification	This paper	
APR868	*lat-1(apr1[lat-1[1-581]::GFP^HygR]) II; glp-1(q1000[glp-1::4xV5]) III*	Notch activation analysis	This paper	
APR862	*glp-1(q1000[glp-1::4xV5]) III; lag-2(q420) V*	Notch activation analysis	This paper	
JK4475	*qIs153 [lag-2p::MYR::GFP + ttx-3p::DsRed] V.*	DTC morphology, *lag-2* expression quantification	CGC	[17]
APR524	*lat-1(ok1465) II, qIs153 [lag-2p::MYR::GFP + ttx-3p::DsRed] V.*	DTC morphology, *lag-2* expression quantification	This paper	
APR739	*aprEX301 [pSP228 pSP229 pRF4]*	BiFC analysis, pSP228 and pSP229 injected at 3 ng/µL	This paper	
APR751	*aprEX304 [pSP188 pSP229 pRF4]*	BiFC analysis, pSP188 and pSP229 injected at 1 ng/µL	This paper	
APR771	*aprEx309[pSP246 pNF17 pRF4]*	BiFC analysis, pSP246 and pNF017 injected at 1 ng/µL	This paper	

APR834	*aprEx309[pSP246 pNF17 pRF4]; aprEX341[pSP234 [50 ng/µL] IR98 pBlueScript SKII]*	Competition BiFC, pSP234 injected at 50 ng/µL	This paper	
APR841	*aprEx309[pSP246 pNF17 pRF4], aprEx342[pSP234 [5 ng/uL], IR98 pBlueScript SKII]*	Competition BiFC, pSP234 injected at 5 ng/µL	This paper	
APR842	*aprEx309[pSP246 pNF17 pRF4], aprEx343[pSP234 [10 ng/uL], IR98 pBlueScript SKII]*	Competition BiFC, pSP234 injected at 10 ng/µL	This paper	
APR920	*aprEx370[pSP403 pSP404 pRF4]*	BiFC analysis, pSP403 and pSP404 injected at 15 ng/µL	This paper	
APR974	*aprEx384[pSP406 pSP403 pRF4]*	BiFC analysis, pSP406 and pSP404 injected at 15 ng/µL	This paper	
APR742	*lat-1(apr1[lat-1[1-581]::GFP^HygR]) II*	Phenotyping assays		8
APR867	*lat-1 (apr9 [lat-1 (1-650)::eGFP^loxP^3xFLAG::lat-1 (651-1015) II*	Phenotyping assays	This paper	
APR965	*lat-1(apr15[Δlat-1p(7kb)::lag-2p::lat-1 (1-650)::eGFP^loxP^3xFLAG::lat-1 (651-1015)]) II*	Phenotyping assays	This paper	
APR970	*lat-1(apr16[Δlat-1p(7kb)::mex-5p::lat-1 (1-650)::eGFP^loxP^3xFLAG::lat-1 (651-1015)]) II*	Phenotyping assays	This paper	

Supplementary Table 5. Reliability and Reproducibility of the MD simulations

Reliability and reproducibility checklist for molecular dynamics simulations	Yes	No	Response (Please state where this information can be found in the text)
1. Convergence of simula6ons and analysis			
1a. Is an evaluation presented in the text to show that the property being measured has equilibrated in the simulations (*e.g.* time-course analysis)?	X	☐	Supplementary Fig. 5 shows such a time-course analysis. Note, the system is too big to become fully equilibrated within the simulation time. However, plotting the RMSD over simulation time shows that a plateau is reached in all three simulations, indicating that the system equilibrated at its local minimum.
1b. Then, is it described in the text how simulations are split into equilibration and production runs and how much data were analyzed from production runs?	X	☐	Methods section: MD simulations
1c. Are there at least 3 simulations per simulation condition with statistical analysis?	X	☐	Methods and results.
1d. Is evidence provided in the text that the simulation results presented are independent of initial configuration?	X		Simulations generally depend heavily on the starting model. Simulations were equilibrated independently and started after equilibration with different velocities, providing a certain level of independency.
2. Connec6on to experiments			
2a. Are calculations provided that can connect to experiments (*e.g.* loss or gain in function from mutagenesis, binding assays, NMR chemical shifts, J-couplings, SAXS curves, interaction distances or FRET distances, structure factors, diffusion coefficients, bulk modulus and other mechanical properties, *etc*.)?	X		Mutational analysis of predicted interface residues in the manuscript
3. Method choice			
3a. Do simulations contain membranes, membrane proteins, intrinsically disordered proteins, glycans, nucleic acids, polymers, or cryptic ligand binding?	☐	X	Response not needed if **No**

Supplementary Methods

Generation of *C. elegans* constructs

hsp16.42p::lag-2(1-194)::VC155::lag-2(195-401) (*VC::lag-2*, pNF17), *hsp16.42p::lag-2 (HA)* (*lag-2(HA)*, pSP403)

Plasmid pAW722 (kind gift of Alison Woollard) containing *hsp16.42p* followed by the C-terminal part of the split Venus (*VC155*) was modified by outward PCR using phosphorylated primers lat-1_1469Fp/lat-1_1470Rp, removing the C-terminal stop codon and introducing a 5x alanine linker as well as *Nco*I and *Not*I restriction sites (plasmid pNF1). Subsequently, the *lag-2* signal peptide sequence (annotated with SignalP 5.0) was introduced behind the *hsp16.42p* using primers lat-1_1483Fp/lat-1_1484Rp. *lag-2* without signal peptide was amplified from N2 genomic DNA using primers lat-1_1481F/lat-1_1482R and cloned into pCR2.1 using the Zero Blunt TOPO PCR Cloning Kit (Invitrogen). *lag-2(1-193)* was amplified using primers lat-1_1712F/lat-1_1713R, introducing *Xho*I sites, allowing for cloning upstream *VC155*. *lag-2(194-401)* was introduced into this vector by amplification of *lag-2* with primers lat-1_1714F/lat-1_1709R, introducing *Not*I sites. Subsequent digestion and ligation were performed, resulting in plasmid pNF17.

The FLAG tag of pNF17 was swapped with lat-1_2652F and lat-1_2653R that were phosphorylated prior to amplification, resulting in plasmid pSP403.

hsp16.42p::VN173::lat-1 (*VN::lat-1*, pSP246), *hsp16.42p::VN173::lat-1 (V5)* (pSP404)

pAW721 (kind gift of Alison Woollard) containing *hsp16.42p* followed by the N-terminal part of the split Venus (VN173) was modified in two steps using primers Bifc_1F/Bifc_2R introducing a *Pme*I restriction site and primers Bifc_3Fp/Bifc_4Rp to remove the multiple cloning site and a Myc tag in the vector as well as to introduce *Eco*RI/*Xho*I sites (all by outward PCR). *lat-1* cDNA without signal peptide was amplified from pSP101 [1] with primers Bifc_5F/Bifc_6R, introducing *Pme*I sites. PCR product and backbone were digested and ligated. The *lat-1* signal peptide sequence (annotated with SignalP 5.0) was separately amplified (primers Bifc_7F/Bifc_8R) and ligated before VN173 via the previously added *Xho*I sites. C-terminal of *lat-1* signal peptide sequence, a FLAG tag was added using primers lat-1_1731Fp/lat-1_1732Rp (plasmid pSP188) together with a 3x GGGGS linker sequence (primers lat-1_2009Fp/lat-1_2006Rp), resulting in pSP246. Subsequently, the FLAG tag was exchanged for a V5 tag by outward PCR using phosphorylated lat-1_2654F/lat-1_2655R.

hsp16.42p::VN173::lag-2 (*VN::lag-2*, pSP228)

In plasmid pNF1 (see above) *Xho*I/*Eco*RI sites were introduced by outward PCR with primers lat-1_1467Fp/lat-1_1468Rp (resulting in plasmid pNF2). The sequence of the *lag-2* signal peptide was added by outward PCR using primers lat-1_1483Fp/lat-1_1484Rp, followed by addition of a FLAG tag with primers lat-1_1694Fp/lat-1_1695Rp. *lag-2* without signal peptide was amplified from N2 genomic DNA and introduced into this construct using *Not*I restriction sites previously introduced by lat-1_1708F/lat-1_1709R. To exchange *VC155* for *VN173*, *VN173* was amplified with lat-1_1819F/lat-1_1852R from pSP188 while amplifying the backbone with lat-1_1853F/lat-1_1822R. *VC155* was subsequently removed using primers lat-1_1869Fp/lat-1_1870Rp using outward PCR.

hsp16.42p::VC155::glp-1 (*VC::glp-1*, pSP229)

In plasmid pNF2 (see above) the sequence of the *glp-1* signal peptide was inserted using primers lat-1_1473Fp/lat-1_1474Rp. Subsequently, an HA tag was introduced with primers lat-

1_1694Fp/lat-1_1695Rp. *glp-1* was amplified from N2 genomic DNA using primers lat-1_1700F/lat-1_1703R and ligated into the plasmid, incorporating *Nco*I and *Not*I restriction sites.

hsp16.42p::lag-2 (*lag-2*, pSP234)

VN173, 3x GGGGS linkers, and the FLAG tag were removed from pSP228 by outward PCR using the 5' phosphorylated primers lat-1_1927Fp/lat-1_1928Rp and the resulting product was religated resulting in pSP234.

hsp16.42p::lat-1 (V5) RBL^{mut} GAIN^{mut} mutations (*lat-1 RBL^{mut}* GAIN^{mut}, pSP406)

Five point mutations were introduced in the *lat-1* RBL domain based on the AlphaFold2 Multimer models (Fig. 3b-c) by outward PCR using phosphorylated primers lat-1_2619F/lat-1_2618R. Thereby, the respective nucleotides were changed to yield alanine residues.

The resulting construct was modified so that seven amino acids amino acids in the LAT-1 GAIN domain identified to be potentially involved in LAG-2 binding (Fig. 3c) were mutated to code for alanines. This was achieved by outward PCR using primers lat-1_2491F/lat-1_2492R, as well as lat-1_2511F/lat-1_2512R.

Generation of cell culture constructs

HA::lat-1::FLAG (*lat-1*, pSP334)

Codon harmonized *lat-1* cDNA (Genscript) was amplified without its signal peptide using primers lat-1_2169F/lat-1_2170R. In parallel, the backbone of pSP101 [1] containing an N-terminal HA tag followed by the mouse LPHN1 signal peptide, and a C-terminal FLAG tag was amplified using primers lat-1_2167F/lat-1_2168R. Both products were assembled using NEBuilder HiFi DNA Assembly Master Mix (New England Biolabs) according to manufacturer's instruction as described above, resulting in plasmid pSP360. *Kpn*I and *Eco*RI were used to excise this *lat-1* construct and ligate it into pcDNA5.1 (Thermo Fisher).

HA::glp-1 (*glp-1*, pSP314)

Codon harmonized *glp-1* cDNA (Genscript) was inserted into pSP101 [1] employing the same strategy as for *lat-1* (pSP334), using primers lat-1_2175F/lat-1_2176R and lat-1_2177F/lat-1_2178R. The endogenous *glp-1* signal peptide (annotated with SignalP 5.0) was introduced by phosphorylated primers lat-1_2179F/lat-1_2180R performing a PCR on the previously generated plasmid, and ligation, resulting in plasmid pSP301. An N-terminal HA tag was introduced by outward PCR using phosphorylated primers lat-1_2240R/ lat-1_2241F.

HA::lag-2 (*lag-2*, pSP340)

Codon harmonized *lag-2* cDNA (Genscript) with an N-terminal HA and a C-terminal FLAG tag (Genscript) was amplified with primers lat-1_2284F/lat-1_2285R, incorporating *Xma*I/*Kpn*I sites, respectively. Insertion into vector pcDps [2] was performed using restriction ligation as described above, resulting in plasmid pSP318. Subsequently, the FLAG tag was removed by outward PCR using phosphorylated primers lat-1_2402F/lat-1_2403R.

Nluc::lag-2 (pSP359)

The nanoluciferase (Nluc) was amplified from previously generated plasmid pSP184 [3] using primers lat-1_2501F/lat-1_2502R. As backbone, pSP340 was amplified using primers lat-1_2499F/lat-1_2500R, incorporating a 20 bp sequence homology to the Nluc. The fragments were assembled using NEBuilder HiFi DNA Assembly Master Mix (New England Biolabs) according to manufacturer's instruction as described above, with the Nluc incorporated at the same place as VC155 in pSP403.

Nluc::apx-1 (pSP427)

Plasmid pSP427 was synthesized by GenScript and cloned into pcDNA3.1. *Nluc* was inserted at the homologues site as for pSP359.

Venus::lat-1 (pSP360)

As backbone, pSP334 was amplified using primers lat-1_2503F/lat-1_2504R, incorporating 20 bp overhangs to Venus. The Venus sequence was generated by PCR using primers lat-1_2505F/at-1_2506R. Both fragments were subsequently assembled using NEBuilder HiFi DNA Assembly Master Mix (New England Biolabs) according to manufacturer's instruction as described above.

Venus::lat-1(RBLmut) (pSP395)

For this construct, pSP360 served as backbone and the mutations leading to the change of the five residues within the RBL potentially involved in LAG-2 binding (Fig. 3c) to alanines were introduced using phosphorylated primers lat-1_2616R/lat-1_2617F and the resulting product was ligated.

Venus::lat-1(GAIN^{mut}) (pSP371)

In pSP360, mutations were introduced that result in seven amino acid point mutations (to alanines) within the GAIN domain identified to be potentially involved in LAG-2 binding (Fig. 3c). This was achieved by outward PCR of pSP360 with phosphorylated primes lat-1_2513F/lat-1_2514R and subsequent ligation.

Venus::lat-1(RBL^{mut} GAIN^{mut}) (pSP392)

To generate a construct containing all point mutations, pSP371 was amplified using phosphorylated primers lat-1_2616F/ lat-1_2617R which introduce the RBL mutations. The resulting product was ligated.

Venus::hGLP1R (pSP396)

Human *GLP1R* was amplified from plasmid GLP1R-N-EGFP_pcDNA3.1 [3] using primers lat-1_2632F/lat-1_2633R. *HA::Venus* was amplified from pSP360 using primers lat-1_2630F/lat-1_2631R. As backbone, pcDNA3.1 was amplified using lat-1_2628F/lat-1_2629R. All three fragments assembled as described above using NEBuilder

HiFi DNA Assembly Master Mix (New England Biolabs) according to manufacturer's instruction.

Genetic engineering of the *lat-1* locus

lat-1(1-650)::eGFP::3xFLAG::lat-1(651-1015) (strain APR867)

To edit the *lat-1* locus by CRISR-Cas9 genome editing, a self-excising cassette system where flanking sites corresponding to the endogenous *lat-1* as were incorporated as suggested [4]. Briefly, this construct was produced by amplification of a 629 bp 5'-flanking site as well as a 571 bp 3´-flanking site from plasmid pTL2 [6] using primers lat-1_2527F/lat-1_2528R and lat-1_2529F/lat-1_2530R, respectively. Flanking sites were incorporated into plasmid pJJR82 (gift from Mike Boxem, Addgene plasmid #75027) as instructed [5].

In parallel, an sgRNA targeting the *lat-1* locus was generated by cloning a suitable sgRNA (determined using Benchling [Biology Software]. (2024). Retrieved from https://benchling.com) into pJJR50 as previously described [5] using primers lat-1_2531F/lat-1_2532R (pSP373). pJJR50 was a gift from Mike Boxem (Addgene plasmid #75026).

Plasmids pSP372 and pSP373 were injected together in the syncytial germline of wild-type adult nematodes with *eft-3p::cas9-SV40_NLS::tbb-2 3'UTR* [6], pCFJ104, and pCFJ90 according to the instructions and at the concentrations indicated in [4]. Construct *eft-3p::cas9-SV40_NLS::tbb-2 3'UTR* was a gift from John Calarco (Addgene plasmid #46168 [6]). pCFJ104 and pCFJ90 were gifts from Erik Jorgensen (Addgene plasmids #19328 and #19327 [7]). Rolling, non-red F1 worms were recovered. The marker was removed using the embedded *hsp::*Cre recombinase, driven by a heat-shock promoter. Rolling L1/L2 animals were heat-shocked for 3 h and non-rolling offspring were recovered.

lag-2p::lat-1(1-650)::eGFP::3xFLAG::lat-1(651-1015) (strain APR965)

To modify the *lat-1* genomic locus to achieve tissue-specific expression in the DTC, 7 kb of the *lat-1* promoter were exchanged for the *lag-2* promoter (2 kb).

For this purpose, a plasmid containing *lag-2p* and *lat-1* flanking sites (pSP412) was generated. *lag-2p* was amplified from plasmid pJL1 [8] using primers lat-1_2695F/ lat-1_2696R. Primer pairs lat-1_2693F/lat-1_2694R and lat-1_2697F/lat-1_2698R were used to amplify 5' and 3' flanking sites (450 and 571 bp, respectively). pCR2.1 TOPO (Invitrogen) was used as backbone and was amplified using primers lat-1_2691F/lat-1_2692R. The resulting PCR products were assembled using NEBuilder HiFi DNA Assembly Master Mix (New England Biolabs) according to manufacturer's instruction. Subsequently, the *lag-2* promoter sequence and homology arms were amplified from this plasmid (pSP412) using primers lat-1_881F/lat-1_2036Rp. The phosphorylated strand of the PCR product was digested with λ-exonuclease, purified and injected together with RNPs containing crRNA 2 in adult nematodes of strain APR867 as described by [9]. Progeny was screened using the marker-free screening method as described in the same paper, resulting in strain APR934. The endogenous *lat-1p* was deleted using ssODN4 as repair template as well as crRNA 5 and 6 to cleave at the extremities of the anticipated promoter. This was performed as described by [10]. The resulting lines were outcrossed and homozygous lines isolated.

mex-5p::lat-1(1-650)::eGFP::3xFLAG::lat-1(651-1015) (strain APR970)

To modify the *lat-1* genomic locus to achieve tissue-specific expression of *lat-1* in the germ cells, 7 kb of the *lat-1* promoter were exchanged for the *mex-5* promoter (0.5 kb).

First, a construct containing the *mex-5p* and *lat-1* flanking sites (450 and 571 bp, respectively) was generated (pSP422). *mex-5p* was amplified from N2 genomic DNA using primers lat-1_2710F/lat-1_2711R. pSP412 was used as backbone, already containing the correct flanking sites, and was amplified using lat-1_2708F/lat-1_2709R. The resulting PCR products were assembled as described for pSP412. Subsequently, the promoter sequence and homology arms were amplified from plasmid pSP422 using primers lat-1_881F/lat-1_2036Rp, followed by the same procedure as described for *lag*-2p resulting in strain APR945.

The endogenous *lat-1p* was deleted using ssODN4 as repair template as well as crRNA 5 and 6 to cleave at the extremities of the anticipated promoter. This was performed as described by [10]. The resulting lines were outcrossed and homozygous lines isolated.

Supplementary Capture Molecular Modeling

Generation of initial LAT-1 and LAG-2 interactions using AlphaFold2 Multimer

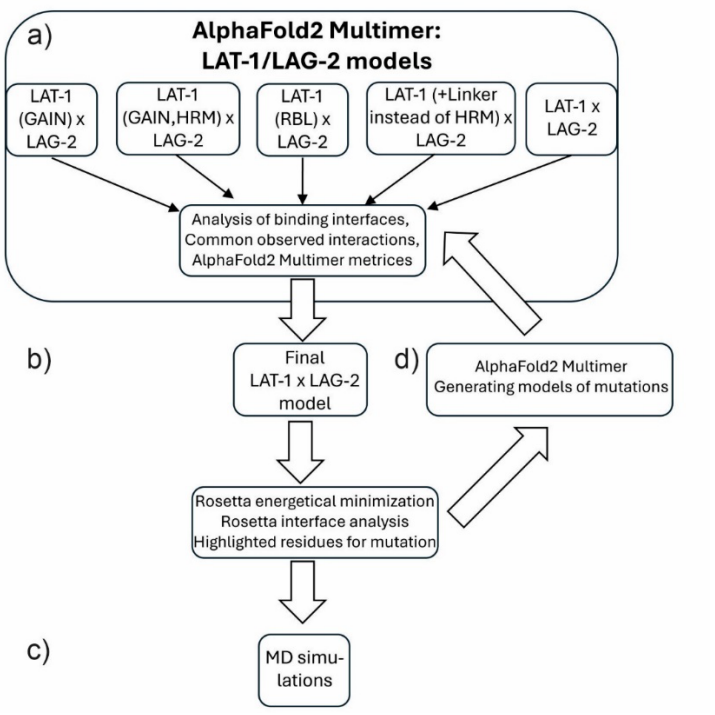
Structural models of the interaction interface between the two extracellular regions (ECR) were obtained through AlphaFold2 Multimer [18]. Respective sequences were downloaded from Uniprot [19] (LAT-1 of *C. elegans* G5EDW2, GLP-1 of *C. elegans* P13508, and LAG-2 of *C. elegans* P45442, accessed on 19 January 2023). Here, various combinations of domains were investigated, including:

- LAT-1 GAIN domain and full-length ECR of LAG-2
- LAT-1 GAIN domain + HRM and full-length ECR of LAG-2
- LAT-1 RBL domain and full-length ECR of LAG-2
- Full-length LAT-1 ECR with linker instead of HRM and full-length ECR of LAG-2
- Full-length ECR of LAT-1 and full-length ECR of LAG-2
- Full-length ECR of LAT-1 with investigated mutation in the GAIN domain and full-length ECR of LAG-2
- Full-length ECR of LAT-1 with investigated mutation in the GAIN domain and RBL domain, and full-length ECR of LAG-2
- Full-length ECR of GLP-1 and full-length ECR of LAT-1
- Short length ECR of GLP-1 (including residues 400-620, including EGF-like domain 9-10 and LNR 1-3) and full-length ECR of LAT-1

The first 30 N-terminal residues of LAT-1 were predicted to form an unstructured, flexible coil with no defined secondary structure. Such regions often introduce noise or variability in computational structure predictions and are unlikely to contribute directly to stable protein-protein interactions. Therefore, these residues were removed prior to modeling in order to improve model convergence and focus computational analysis on the structured, interaction-relevant domains of LAT-1.

After generating the various complexes, the models were visually inspected and common interaction sites highlighted. The best ranked models by AlphaFold2 Multimer internal scoring function was energetically minimized with the standard Rosetta3 energetical minimization (relax) function.

The workflow summarizes as follows:



Protein sequences for various LAT-1 and LAG-2 complex were prepared and modeled using AlphaFold2 Multimer to predict initial complex structures (a)). The best-ranked models were assessed visually and computationally. A common binding interface between various models and combinations was highlighted. Based on the initial findings, the best structure from the entire LAT-1/LAG-2 complex was retrieved and structure prepared with the Rosetta Suite (b)). After energetical minimization, for the best-scoring models the interaction interface was analyzed using Rosetta InterfaceAnalyzer to estimate buried surface area, hydrogen bonding, and per-residue energetic contributions. Furthermore, promising residues in LAT-1 relevant for binding were highlighted for experimental analysis. To assess model quality, the structure was subject to molecular dynamics (MD) simulations (c)). Furthermore, AlphaFold2 Multimer was used again, to generate structural models of the proposed mutations (d)). These were analyzed within the established computational pipeline but without further quality validation with MD simulations. Structural visualizations were generated in PyMOL with domain annotations corresponding to functional regions of LAT-1 and LAG-2.

Sequence for LAT-1 and LAG-2 models

>LAT-1(https://www.uniprot.org/uniprotkb/G5EDW2/entry):

>N-ter

#first residues excluded as unstructured coil

MRRNKTTYSLLQTILVACLLTVTPTFASNK

PTTDESGTISHT

>RBL

ICDGEAAELSCPAGKVISIVLGNYGRFSVAVCLPDNDIVPSNINCQNHKTKSILEKKCNGDSMCYFTVDKKTFTE
DPCPNTPKYLEVKYNCV

>HRM

VPATTTTTTTTTSTTTTDSSLIVDEEEEAQKDALNSDVIKPVKKKEDVFCSATNRRGVNWQNTKSGTTSSAPCPE
GSSGKQLWACTEEGQWLTEFPNSAGCESNWISSRNSVLSGVISSEDVSGLP

An additional linker was investigated instead of HRM

>linker

VPATTTGGGGGGGGGGGGGGGGG

>GAIN

EFLRNLGSETRRPMVGGDLPKVLHLLEKTVNVIAEESWAYQHLPLSNKGAVEVMNYMLRNQEIWGSWDVTKRKEF
ASRFILAAEKAMVASAKGMMTSAESNVIVQPAITVEISHKIKMSSQPTDYILFPSAALWNGQNVDNVNIPRDAIL
KINKDETQVFFSSFDNLGAQMTPSDVTVAIAGTDQTEVRKRRVVSRIVGASLIENGKERRVENLTQPVRITFYHK
ESSVRHLSNPTCVWWNHHELKWKPSGCKLSYHNKTMTSCDCTHLTHFAVLMDVRGHDLNEIDQTLL

>Transmembrane area and intracellular region (deleted in the modeling step)

(TLLTYVGCIISIICLLLTFFAYLIFSRNGGDRVFIHENLCLSLAIAEITFLAGITRTEDSLQCGIIAVALMYMF
LSALTWMLLEGYHIHRMLTEVFPSDPRRFTYLLVGYIPPAIITLVAYLYNSDGFGTPDHCWLSTQNNFIWFFAGP
ACFIFCANSLVLVKTLCTVYQHTSGGYLPCRHDVDSGRSIRNWVKGSLALASLLGVTWIFGLFWVEDSRSIVMAY
VFTISNSLQGLFIFLFHVVFAEKMRKDVGHWMYRRGCGGSSNSSPNHKRHNVQRDLMSPGVNSSTGSDFLYNTND
KYLTNSDTTNRLVYNGIMNHPNQMSVYQQHPHHQIYEQQPGTYDYATIAYGDMMPGHRVAAPPAYQRLAVAEGRY
GSQHQLYQGWHHRPPPEFSPPPPPLSTGPPNSRHYGTGSSGRRPPSSKMSDDSAYSDGSSSMLTTEVTPQGQTVL
RIDLNKPSMYCQD)

in the refinement step, the tested mutations were introduced in AlphaFold Multimer, resulting in the two following LAT-1 sequence:

>LAT-1 refined (GAIN domain mutation)

PTTDESGTISHTICDGEAAELSCPAGKVISIVLGNYGRFSVAVCLPDNDIVPSNINCQNHKTKSILEKKCNGDSM
CYFTVDKKTFTEDPCPNTPKYLEVKYNCVVPATTTTTTTTSTTTTDSSLIVDEEEEAQKDALNSDVIKPVKKKE
DVFCSATNRRGVNWQNTKSGTTSSAPCPEGSSGKQLWACTEEGQWLTEFPNSAGCESNWISSRNSVLSGVISSED
VSGLPEFLRNLGSETRRPMVGGDLPKVLHLLEKTVNVIAEESWAYQHLPLSNKGAVEVMNYMLRNQEIWGSWDVT
KRKEFASRFILAAEKAMVASAKGMMTSAESNVIVQPAITVEISHKIKMSS**AA**T**AA**I**A**FPSAA**AA**NGQNVDNVNIP
RDAILKINKDETQVFFSSFDNLGAQMTPSDVTVAIAGTDQTEVRKRRVVSRIVGASLIENGKERRVENLTQPVRI
TFYHKESSVRHLSNPTCVWWNHHELKWKPSGCKLSYHNKTMTSCDCTHLTHFAVLMDVRGHDLNEIDQTLL

>LAT-1 refined (GAIN domain and RBL domain mutation)

PTTDESGTISHTICDGEAAELSCPAGKVISIV**A**GNYGR**A**SVAVCLP**A**N**A**I**A**PSNINCQNHKTKSILEKKCNGDSM
CYFTVDKKTFTEDPCPNTPKYLEVKYNCVVPATTTTTTTTSTTTTDSSLIVDEEEEAQKDALNSDVIKPVKKKE
DVFCSATNRRGVNWQNTKSGTTSSAPCPEGSSGKQLWACTEEGQWLTEFPNSAGCESNWISSRNSVLSGVISSED
VSGLPEFLRNLGSETRRPMVGGDLPKVLHLLEKTVNVIAEESWAYQHLPLSNKGAVEVMNYMLRNQEIWGSWDVT
KRKEFASRFILAAEKAMVASAKGMMTSAESNVIVQPAITVEISHKIKMSS**AA**T**AA**I**A**FPSAA**AA**NGQNVDNVNIP
RDAILKINKDETQVFFSSFDNLGAQMTPSDVTVAIAGTDQTEVRKRRVVSRIVGASLIENGKERRVENLTQPVRI
TFYHKESSVRHLSNPTCVWWNHHELKWKPSGCKLSYHNKTMTSCDCTHLTHFAVLMDVRGHDLNEIDQTLL

>LAG-2 https://www.uniprot.org/uniprotkb/P45442/entry

>N-ter

MIAYFLLLLTCLPVLQARVEVHQEFISSKRVSVRFEIVTESHSPNRPVTFDLFPRGPKTNIILLDTFNPVFNFSI
QLVQPFTGQPLGDRIYRKVQFSGTNQPWINDTFTTTSGISLSVATE

>DSL

VTCARNYFGNRCENFCDAHLAKAARKRCDAMGRLRCDIGWMGPHC

>EGF

GQAVDPRKCSCENDGICVSSMIHPSQPNQTSSNEQLICECTNGFTGTRCEIFGFNQFQLTAP

>EGF

RPDACSVKDACLNGAKCFPNGPKVFCSCAVGFIGEFCEISLTTTTP

>Transmembrane area (deleted in the modeling step)

TTVEITVSTSGYSSAVYITVALFVIFSIIIGCFKYKFKPMRQQALARGQVPEPYKMPETKSMLIDPEA
SEAQKKVFTIEGSVQKIDEEVRYTSAPRKYESNNEYAVIQKSTPPPPSLSPPSIPACHYV

Sequence for LAG-2 and GLP-1 models

>GLP-1(https://www.uniprot.org/uniprotkb/P13508/entry):

>N-ter

MRVLLILLAFFAPIASQLMGGECGREGACSVNGKCYNGKLIETYWCRCKKGFGGAFCERECDLDCKRG
EKCIYDVYGENPTCICQDCEDETPPTERTQKGCEEGYGGPDCKTPLFSGVNPCDSDPCNNGLCYPFYG
GFQCICNNGYGGSYCEEGIDHCAQNECAEGSTCVNSVYNYYCDCPIGKSGRYCERTECALMGNICNHG
RCIPNRDEDKNFRCVCDSGYEGEFCNKDKNECLIEETCVNNSTCFNLHGDFTCTCKPGYAGKYCEEAI
DMCKDYVCQNDGYCAHDSNQMPICYCEQGFTGQRCEIECPSGFGGIHCDLPLQRPHCSRSNGTCYNDG
RCINGFCVCEPDYIGDRCEINRKDFKFPDIQSCKYNPCVNNATCIDLKNSGYSCHCPLGFYGLNCEQH
LLCTPTTCANGGTCEGVNGVIRCNCPNGFSGDYCEIKDRQLCSRHPCKNGGVCKNTGYCECQYGYTGP
TCEEVLVIEKSKETVIRDLCEQRKCMDLASNGICNPECNLEECNFDGGDCSGGQRPFSKCQYPARCAD

QFANGVCNQECNNEECLYDGLDCQSELFRCPAHIRKHCIERRGDGVCNLECSFIGCGFDGGDCNNGTE
AIILSDIRIKVQIDPIEFQ

>Transmembrane area and intracellular region (deleted in the modeling step)

ATGGETLMQISANLRATVRIQRDELGPLVFRWDGEHEMERVEMNSSKLEDQFVLSHHVRRYRQAVVTGIVLYLEV
EEICKPEFCRFSTAQSVVDLIAAGLVKSDGRMSLGLPITEAMVAVPKRNEIDEGWSRSQVILFACIAFLAFGTVV
AGVIAKNGPERSRKRKMVNATVWMPPMESTNEKGRRNQSNHSSQCSLLDNSAYYHPNTKRHCSDYSTGYNGEQYS
QIYPQTLANGYPGDYNELNFDFQSETFAPADLPADEIPLHVQAAGPDAITAPITNESVNQVDSKYRRRVLHWLAA
NVRGKPEDVITTEAIRCLKAGADVNARDCDENTALMLAVRAHRVRLSVVLLREGANPTIFNNSERSALHEAVVNK
DLRILRHLLTDKRLLKEIDELDRNGMTALMLVARELGKHQVEMAELLLSKGAKLDYDGAARKDSNKYKGRTALHY
AAMHDNEEMVIMLVRRSSNKDKQDEDGRTPIMLAAKEGCEKTVQYLALNDASLGIVDSMDMTAAQVAEASYHHEL
AAFLRQVANERHRNDIMRQQIVKSGHGAKSGRQTVKNIKRAGSRKTPTSAASSRETNHLTPPPSDGSFSSPSPHY
YPTTTSTPNRMETSPEYMFNHEMAPPVNAMWYTTPPPYQDPNYRHVPPNTAFQNAEQMNGSFYC

>shorten to res 400-620 including EGF-like domain 9-10 and LNR1-3

GFYGLNCEQHLLCTPTTCANGGTCEGVNGVIRCNCPNGFSGDYCEIKDRQLCSRHPCKNGGVCKNTGYCECQYGY
TGPTCEEVLVIEKSKETVIRDLCEQRKCMDLASNGICNPECNLEECNFDGGDCSGGQRPFSKCQYPARCADQFAN
GVCNQECNNEECLYDGLDCQSELFRCPAHIRKHCIERRGDGVCNLECSFIGCGFDGGDCNNGTEAIILSDIRIKV
QIDPIEFQATGGETLMQISANLRATVRIQRDELGPLVFRWDGEHEMERVEMNSSKLEDQFVLSHHVRRYRQAVVT
GIVLYLEVEEICKPEFCRFSTAQSVVDLIAAGLVKSDGRMSLGLPITEAMVAVPKRNEIDEG

Sequence for LAT-1 models

AlphaFold Multimer SLURM script at Leipzig Rechenzentrum

```
-------------------------------
#!/bin/bash
#SBATCH --job-name=alphafold-test
#SBATCH --output=alphafold-test-job-out.%J
#SBATCH --time=12:00:00
#SBATCH --nodes=1
#SBATCH --ntasks-per-node=16
#SBATCH --gres=gpu:a30:1
#SBATCH --partition=paula

module purge
ml AlphaFold/2.2.2-foss-2021b-CUDA-11.4.1

export ALPHAFOLD_DATA_DIR=/software/databases/alphafold
export ALPHAFOLD_HHBLITS_N_CPU=12

alphafold --fasta_paths=/home/sc.uni-
leipzig.de/<user>/LAT1_LAG2/just_GAIN.fasta --max_template_date=2100-05-14
--data_dir=/software/databases/alphafold --output_dir=/home/sc.uni-
leipzig.de/<user>/LAT1_LAG2/alphafold_output --db_preset=full_dbs  --
model_preset=multimer  --use_gpu_relax=True  --
num_multimer_predictions_per_model=10  --
pdb_seqres_database_path=/software/databases/alphafold/pdb_seqres/pdb_seqre
s.txt

-------------------------------
###input example for GAIN domain of LAT-1 and full ECR of LAG-2

>LAG2
```

```
MIAYFLLLLTCLPVLQARVEVHQEFISSKRVSVRFEIVTESHSPNRPVTFDLFPRGPKTNIILLDTFNPVFNFSI
QLVQPFTGQPLGDRIYRKVQFSGTNQPWINDTFTTTSGISLSVATVTFDLFPRGPKTNIILLDTFNPVFNFSIQL
VQPFTGQPLGDRIYRKVQFSGTNQPWINDTFTTTSGISLSVATVTCARNYFGNRCENFCDAHLAKAARKRCDAMG
RLRCDIGWMGPHCGQAVDPRKCSCENDGICVSSMIHPSQPNQTSSNEQLICECTNGFTGTRCEIFGFNQFQLTAP
RPDACSVKDACLNGAKCFPNGPKVFCSCAVGFIGEFCEISLTTTTP

>GAIN

NWISSRNSVLSGVISSEDVSGLPEFLRNLGSETRRPMVGGDLPKVLHLLEKTVNVIAEESWAYQHLPLSNKGAVE
VMNYMLRNQEIWGSWDVTKRKEFASRFILAAEKAMVASAKGMMTSAESNVIVQPAITVEISHKIKMSSQPTDYIL
FPSAALWNGQNVDNVNIPRDAILKINKDETQVFFSSFDNLGAQMTPSDVTVAIAGTDQTEVRKRRVVSRIVGASL
IENGKERRVENLTQPVRITFYHKESSVRHLSNPTCVWWNHHELKWKPSGCKLSYHNKTMTSCDCTHLTHFAVLMD
VRGHDLNEIDQTLL
```

Options for Energy Minimization (300 generated structures in 30 runs)

```
/$Rosetta/main/source/bin/relax.static.linuxggcrelease @flags.options -s
<selected_model>.pdb
-------------------------------
#flags.options
# i/o
-out:pdb
-out:path:all output/
-nstruct 10

# relax options
-default_max_cycles 200
-relax:min_type lbfgs_armijo_nonmonotone
-relax:constrain_relax_to_start_coords

# reduce memory footprint
-chemical:exclude_patches LowerDNA  UpperDNA Cterm_amidation SpecialRotamer
VirtualBB ShoveBB VirtualDNAPhosphate VirtualNTerm CTermConnect sc_orbitals
pro_hydroxylated_case1 pro_hydroxylated_case2 ser_phosphorylated
thr_phosphorylated  tyr_phosphorylated tyr_sulfated lys_dimethylated
lys_monomethylated  lys_trimethylated lys_acetylated glu_carboxylated
cys_acetylated tyr_diiodinated N_acetylated C_methylamidated
MethylatedProteinCterm

-linmem_ig 10

# run multiple processes to produce output for one file
-multiple_processes_writing_to_one_directory
-------------------------------
```

Based on the built structures, the RMSD to the respective best model for each model generation was calculated, a *rmsd-total_score* plot generated, and the structures investigated. It must be noted that most structures had an RMSD-value of below 2 Å and clustering was omitted.

An additional interface analyzer for all energetically minimized structures was run to highlight the best interactions.

```
-------------------------------
```

```
/$Rosetta/main/source/bin/rosetta_scripts.static.linuxggcrelease -
parser:protocol InterfaceAnalyzer.xml -s <selected_model>.pdb
------------------------------
#InterfaceAnalyzer.xml
<ROSETTASCRIPTS>
    <TASKOPERATIONS>
    </TASKOPERATIONS>
    <SCOREFXNS>
        <ScoreFunction name="r15" weights="ref2015" symmetric="0" />
    </SCOREFXNS>
    <FILTERS>
    </FILTERS>
    <RESIDUE_SELECTORS>
    </RESIDUE_SELECTORS>
    <MOVERS>
        <InterfaceAnalyzerMover name="Ana" scorefxn="r15"
pack_separated="false" pack_input="false" resfile="false" packstat="false"
interface_sc="false" tracer="false" use_jobname="false" interface="A_B" />
    </MOVERS>
    <APPLY_TO_POSE>
    </APPLY_TO_POSE>
    <PROTOCOLS>
        <Add mover_name="Ana"/>
    </PROTOCOLS>
</ROSETTASCRIPTS>
------------------------------
```

Energetical investigation and energy breakdown

The best docked models were selected for an energetical hotspot analysis with the Rosetta *per_residue_energies* application:

```
------------------------------
/$Rosetta/main/source/bin/residue_energy_breakdown.default.linuxgccreleas
e -s *.pdb -out:file:silent data.out
------------------------------
```

A following python script was utilized to investigate the output and select the per residue energy contributions relevant for the peptide and generating a contact map:

```
------------------------------
import pandas as pd
import seaborn as sns
import matplotlib.pyplot as plt
import numpy as np

from datetime import date

df1 = pd.read_csv('data.out', sep='\s+')

df2 = df1.loc[(df1['resi2'] != '--')]
df2['resi1'] = df2['resi1'].astype(int)
df2['resi2'] = df2['resi2'].astype(int)
df3 = df2.loc[(df2['resi1'] < 287) & (df2['resi2'] > 286)]
df3.to_csv('selected_ia_h.list', sep='\t', index=None)
df3.to_csv('selected_ia.list', sep='\t', index=None, header=None)
peptide_res = df3['resi2'].to_list()
peptide_res = list(set(peptide_res))
```

```
TM_res = df3['resi1'].to_list()
TM_res = list(set(TM_res))
filler = []
for lines in open('selected_ia.list', 'r').readlines():
    line = lines.split('\t')
    filler.append(line)
fil = open('energy_ia.list', 'w')
for TM in TM_res:
    for peptide in peptide_res:
        counter = 0
        for ele in filler:
            if int(ele[5]) == peptide and int(ele[2]) == TM:
                counter += float(ele[27])
        print(TM, peptide, counter, counter/1)
        print(TM, peptide, counter, counter/1, file=fil)
fil.close()

fil = open('summed_energy.list' ,'w')
final_energy = []
energy_ia = pd.read_csv('energy_ia.list', sep=' ', header=None)
for TM in TM_res:
    filler = energy_ia.loc[energy_ia[0] == TM]
    print(TM, filler[3].sum(), file=fil)
    final_energy.append((TM, filler[3].sum()))
fil.close()
filler = []
for lines in open('selected_ia.list', 'r').readlines():
    line = lines.split('\t')
    filler.append((line[5], line[7]))
    filler.append((line[2], line[4]))
filler = list(set(filler))

my_dict = {key: value for key, value in filler}
print(my_dict)
fil = open('energy_header.list', 'w')
for lines in open('energy_ia.list', 'r').readlines():
    line = lines.split()
    print(line[0] + "_" + my_dict[line[0]], line[1] + "_" +
my_dict[line[1]], line[2], line[3], file=fil)
fil.close()

df = pd.read_csv('energy_header.list', sep='\s+', header=None)
df = df.sort_values(by=[0])
# pivot the dataframe to create the desired format
df_pivoted = df.pivot(index=0, columns=1, values=3)
df_pivoted = df_pivoted.sort_index()
df_pivoted.to_csv('final_matrix.list', sep='\t')

#Heat Map
df = df_pivoted
fig, ax = plt.subplots(figsize=(6,8))
mask_con_corr = df[(df >= 0.1) | (df <= -0.1)]
label = df.columns.values.tolist()
index = df.index.tolist()

heat_map = sns.heatmap(mask_con_corr,
                       linewidths=1,linecolor='black',
                       #center=0,
                       cmap="BuPu_r",
                       cbar=True,
                       yticklabels=index, xticklabels=label,
```

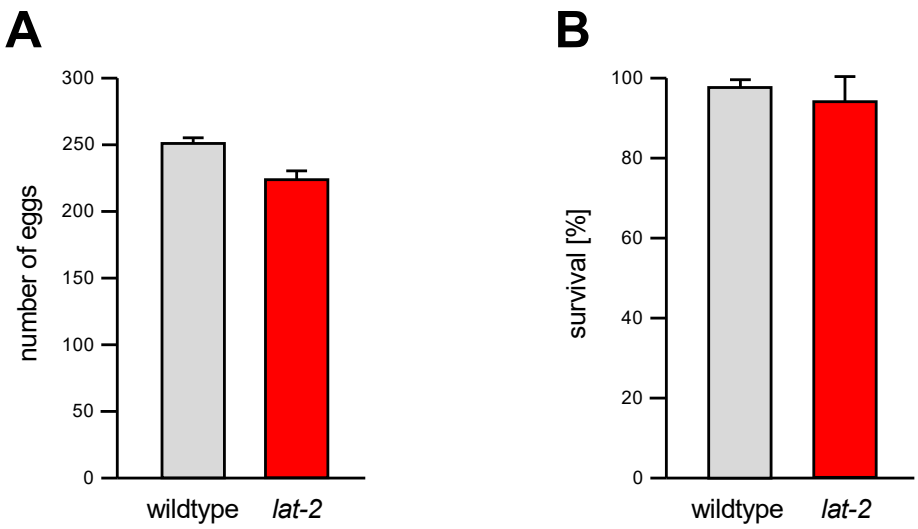
```
vmin=-3, vmax=1)#, annot=True, fmt='g')
ax.xaxis.tick_top()
plottitle = "Energetical Analysis of Hotspot Residues in the \n
LAT-1/LAG-2 Interface"
plt.title(plottitle, fontsize=12)
plt.xticks(size=8)
plt.yticks(size=8)
heat_map.set_xticklabels(heat_map.get_xticklabels(), rotation=30)
heat_map.set_yticklabels(heat_map.get_yticklabels(), rotation=30)

ax.tick_params(left=False, bottom=False)
fig.savefig("_matrix_interaction.png", dpi=600)
--------------------------------
```

Supplementary References

1. Müller, A. *et al.* Oriented Cell Division in the C. elegans Embryo Is Coordinated by G-Protein Signaling Dependent on the Adhesion GPCR LAT-1. *PLoS Genet.* **11**, e1005624 (2015).
2. Okayama, H. & Berg, P. A cDNA cloning vector that permits expression of cDNA inserts in mammalian cells. *Mol. Cell. Biol.* **3**, 280–289 (1983).
3. Wygas, M. M., Laugwitz, J. M., Schmidt, P., Elgeti, M. & Kaiser, A. Dynamics of the Second Extracellular Loop Control Transducer Coupling of Peptide-Activated GPCRs. *Int. J. Mol. Sci.* **24**, (2023).
4. Dickinson, D. J., Pani, A. M., Heppert, J. K., Higgins, C. D. & Goldstein, B. Streamlined Genome Engineering with a Self-Excising Drug Selection Cassette. *Genetics* **200**, 1035–1049 (2015).
5. Waaijers, S. *et al.* A tissue-specific protein purification approach in Caenorhabditis elegans identifies novel interaction partners of DLG-1/Discs large. *BMC Biol.* **14**, 66 (2016).
6. Friedland, A. E. *et al.* Heritable genome editing in C. elegans via a CRISPR-Cas9 system. *Nat. Methods* **10**, 741–743 (2013).
7. Frøkjaer-Jensen, C. *et al.* Single-copy insertion of transgenes in Caenorhabditis elegans. *Nat. Genet.* **40**, 1375–1383 (2008).
8. Matúš, D. *et al.* The N terminus-only (trans) function of the Adhesion GPCR Latrophilin-1 controls multiple processes in reproduction of C. elegans. *G3 Bethesda Md* (2024) doi:10.1093/g3journal/jkae206.
9. Eroglu, M., Yu, B. & Derry, W. B. Efficient CRISPR/Cas9 mediated large insertions using long single-stranded oligonucleotide donors in C. elegans. *FEBS J.* **290**, 4429–4439 (2023).
10. Ghanta, K. S., Ishidate, T. & Mello, C. C. Microinjection for precision genome editing in Caenorhabditis elegans. *STAR Protoc.* **2**, 100748 (2021).
11. Brenner, S. The genetics of Caenorhabditis elegans. *Genetics* **77**, 71–94 (1974).
12. Voronina, E., Paix, A. & Seydoux, G. The P granule component PGL-1 promotes the localization and silencing activity of the PUF protein FBF-2 in germline stem cells. *Dev. Camb. Engl.* **139**, 3732–3740 (2012).
13. Henderson, S. T., Gao, D., Lambie, E. J. & Kimble, J. lag-2 may encode a signaling ligand for the GLP-1 and LIN-12 receptors of C. elegans. *Dev. Camb. Engl.* **120**, 2913–2924 (1994).
14. Komatsu, H. *et al.* OSM-11 Facilitates LIN-12 Notch Signaling during Caenorhabditis elegans Vulval Development. *PLoS Biol.* **6**, e196 (2008).
15. Kodoyianni, V., Maine, E. M. & Kimble, J. Molecular basis of loss-of-function mutations in the glp-1 gene of Caenorhabditis elegans. *Mol. Biol. Cell* **3**, 1199–1213 (1992).
16. Sorensen, E. B., Seidel, H. S., Crittenden, S. L., Ballard, J. H. & Kimble, J. A toolkit of tagged glp-1 alleles reveals strong glp-1 expression in the germline, embryo, and spermatheca. *MicroPublication Biol.* **2020**, (2020).
17. Byrd, D. T., Knobel, K., Affeldt, K., Crittenden, S. L. & Kimble, J. A DTC niche plexus surrounds the germline stem cell pool in Caenorhabditis elegans. *PloS One* **9**, e88372 (2014).
18. Evans, R. *et al. Protein Complex Prediction with AlphaFold-Multimer*. (2021). doi:10.1101/2021.10.04.463034.
19. Zaru, R. & Orchard, S. UniProt Tools: BLAST, Align, Peptide Search, and ID Mapping. *Curr. Protoc.* **3**, e697 (2023).

8.3 Supplementary material for ‘The Adhesion GPCR ADGRL2/LPHN2 Can Protect Against Cellular and Organismal Dysfunction’



Supplementary figure 1: *lat-2(knu505)* nematodes do not show any defects in brood size and survival to adulthood. (**A**) Nematodes lacking LAT-2 function produce a brood size that is not significantly different to that of wild-type controls (data are mean ± SEM, n = 20 in 3 independent experiments, Student´s t-test). (**B**) Wild-type and *lat-2(knu505)* individuals develop to adulthood at similar, not significantly different rates (data are mean ± SEM, n = 20 in 3 independent experiments, unpaired, two-sided Student´s t-test).

Supplementary table 1: antibodies used for immunoblots.

primary antibodies

target protein	mono-/ polyclonal	species of origin	dilution	source	order nr.
Caspase-3	polyclonal	rabbit	1:1.000 (full-length Caspase-3) 1:300 (cleaved Caspase-3)	Cell Signaling Technology	9662
eNOS	monoclonal clone EPR19296	rabbit	1:2.000	Abcam	ab199956
Phospho-eNOS (Ser1177)	polyclonal	rabbit	1:500	Cell Signaling Technology	9571
Phospho-eNOS (Thr495)	polyclonal	rabbit	1:250	Cell Signaling Technology	9574
HA-tag	monoclonal clone GT4810	mouse	1:500	Sigma-Aldrich	SAB2702217
Src	monoclonal clone 32G6	rabbit	1:1.000	Cell Signaling Technology	2123

secondary antibodies

antibody	species of origin	dilution	source	order nr.
ECL anti-mouse IgG, horseradish peroxidase linked whole antibody	sheep	1:5.000	Cytiva	NA931
ECL anti-rabbit IgG, horseradish peroxidase linked whole antibody	sheep	1:5.000	Cytiva	NA934

Supplementary table 2: antibodies used for immunostaining and PLA

primary antibodies

target protein	mono-/ polyclonal	species of origin	dilution	source	order nr.
FLAG-tag	monoclonal clone M2	mouse	1:200	Sigma-Aldrich	F3165
FLAG-tag	monoclonal clone 8H8L17	mouse	1:200	Invitrogen	701629M
eNOS	monoclonal clone 6H2	mouse	1:100	Cell Signaling Technology	5880
eNOS	monoclonal clone EPR19296	rabbit	1:200	Abcam	ab199956
HSP90	monoclonal clone 68	mouse	1:250	BD Biosciences	610418
Caveolin-1	polyclonal	rabbit	1:200	Cell Signaling Technology	3238
ICAM-1	monoclonal clone 15.2	mouse	1:100	Santa Cruz Biotechnology	sc-107

secondary antibodies

antibody	species of origin	dilution	source	order nr.
anti-mouse IgG (H+L) Cross-Adsorbed Secondary Antibody, Alexa Fluor™ 488	goat	1:500	Invitrogen	A11001
anti-mouse IgG (H+L) Cross-Adsorbed Secondary Antibody, Alexa Fluor™ 594	goat	1:500	Invitrogen	A11005
anti-rabbit IgG (H+L) Cross-Adsorbed Secondary Antibody, Alexa Fluor™ 488	goat	1:500	Invitrogen	A11008
anti-rabbit IgG (H+L) Cross-Adsorbed Secondary Antibody, Alexa Fluor™ 594	goat	1:500	Invitrogen	A11012

Supplementary table 3: Primers used for semi-quantitative real-time PCR.
Shown are the sequences of the primers in 5'→3' direction and the expected amplification products.

transcript	primer		sequence		amplification product
human *ADGRL2*	hADGRL2 Ex17 for1	5'-	CTCTGGGCATCAAAGGAGCA	-3'	223 bp
	hADGRL2 Ex18/19 rev1	5'-	GGATCAATGTGTGGCAGGGT	-3'	
human *RPL32*	hmRPL32 Ex02 for1	5'-	GTGAAGCCCAAGATCGTCAA	-3'	257 bp
	hmRPL32 Ex03 rev1	5'-	TTGTTGCACATCAGCAGCAC	-3'	
C. elegans act-1	fwd_act-1	5'-	GCTGGACGTGATCTTACTGATTACC	-3'	114 bp
	rev_act-1	5'-	GTAGCAGAGCTTCTCCTTGATGTC	-3'	
C. elegans age-1	fwd_age-1	5'-	GACGGAACTCCCGACGTATC	-3'	567 bp
	rev_age-1	5'-	TCGTACGAGCCCAGAGAGAA	-3'	
C. elegans cdc-42	fwd_cdc-42	5'-	CTGCTGGACAGGAAGATTACG	-3'	111 bp
	rev_cdc-42	5'-	CTCGGACATTCTCGAATGAAG	-3'	
C. elegans daf-2	fwd_daf-2	5'-	GCTCTCGGAACAACCACTGA	-3'	132 bp
	rev_daf-2	5'-	GACAAGTCGAAGCCGTCTCA	-3'	
C. elegans daf-16	fwd_daf-16	5'-	CTAACTTCAAGCCAATGCCACTA	-3'	260 bp
	rev_daf-16	5'-	TCCAGCTTGACTCAGCTCATGTC	-3'	
C. elegans eif-3.c	fwd_eif-3.c	5'-	ACACTTGACGAGCCCACCGAC	-3'	191 bp
	rev_eif-3.c	5'-	TGCCGCTCGTTCCTTCCTGG	-3'	
C. elegans hsf-1	fwd_hsf-1	5'-	AAAATGGGGCAATTGGTGGC	-3'	333 bp
	rev_hsf-1	5'-	CACCTTGGGACAGTGGAGTC	-3'	
C. elegans isp-1	fwd_isp-1	5'-	AACGTCGTGCTCTTCCAACT	-3'	235 bp
	rev_isp-1	5'-	TTGGCAATCTCAGCCTTGGT	-3'	
C. elegans nuo-6	fwd_nuo-6	5'-	CTCCGAAACTGTGGCAGGAT	-3'	448 bp
	rev_nuo-6	5'-	GTTGGAGCAAAGAGACCGGA	-3'	
C. elegans pmp-3	fwd_ pmp-3	5'-	TGGCCGGATGATGGTGTCGC	-3'	190 bp
	rev_pmp-3	5'-	ACGAACAATGCCAAAGGCCAGC	-3'	
C. elegans sir-2.1	fwd_sir-2.1	5'-	GTCACGTGATAGTGGCAACG	-3'	544 bp
	rev_sir-2.1	5'-	AAGATCGGGAAACTCGCTCC	-3'	
C. elegans skn-1	fwd_skn-1	5'-	GACGTCAATTTATGGAGTGTCG	-3'	137 bp
	rev_skn-1	5'-	GAAGATGTTTTGTCGTGATCCG	-3'	
C.elegans tba-1	fwd_tba-1	5'-	GTACACTCCACTGATCTCTGCTGACAAG	-3'	149 bp
	rev_tba-1	5'-	CTCTGTACAAGAGGCAAACAGCCATG	-3'	

8.4 Curriculum Vitae

8.5 List of publications

Post, W. B.,* Groß, V. E.,* Matúš, D.,* Charnay, I., Liessmann, F., Seufert, F., ... & Prömel, S. (2025). Notch activity is modulated by the aGPCR Latrophilin binding the DSL ligand in *C. elegans*. Nature Communications, 16(1), 6461. https://doi.org/10.1038/s41467-025-61730-0

Matúš, D.,* **Post, W. B.**,* Groß, V. E., Knierim, A. B., Kuhn, C. K., Fiedler, F., ... & Prömel, S. (2024). The N terminus-only (trans) function of the adhesion G protein-coupled receptor latrophilin-1 controls multiple processes in reproduction of *Caenorhabditis elegans*. G3: Genes, Genomes, Genetics, 14(11). https://doi.org/10.1093/g3journal/jkae206

Jakobs, P.,* Rafflenbeul, A.,* **Post, W. B.**,* Ale-Agha, N., Groß, V. E., Pick, S., Dolata, S., Cox, F. F., von Ameln, F., Eckermann, O., Altschmied, J., Prömel, S., & Haendeler, J. (2024). The Adhesion GPCR ADGRL2/LPHN2 Can Protect Against Cellular and Organismal Dysfunction. *Cells*, *13*(22), 1826. https://doi.org/10.3390/cells13221826

Schön, J. L., Groß, V. E., **Post, W. B.**, Daum, A., Matúš, D., Pilz, J., Schnorr, R., Horn, S., Bäumers, M., Weidtkamp-Peters, S., Hughes, S., Schöneberg, T., & Prömel, S. (2024). The adhesion GPCR and PCP component flamingo (FMI-1) alters body size and regulates the composition of the extracellular matrix. *Matrix biology: journal of the International Society for Matrix Biology*, *128*, 1–10. https://doi.org/10.1016/j.matbio.2024.02.005

Matúš, D., **Post, W. B.**, Horn, S., Schöneberg, T., & Prömel, S. (2022). Latrophilin-1 drives neuron morphogenesis and shapes chemo- and mechanosensation-dependent behavior in *C. elegans* via a trans function. Biochemical and biophysical research communications, 589, 152–158. https://doi.org/10.1016/j.bbrc.2021.12.006

Orsi, E., Mougiakos, I., **Post, W**. et al. Growth-uncoupled isoprenoid synthesis in *Rhodobacter sphaeroides*. Biotechnol Biofuels 13, 123 (2020). https://doi.org/10.1186/s13068-020-01765-1

Koendjbiharie, J.G., **Post, W.B.**, Palmer, M.M. et al. Effects of CO2 limitation on the metabolism of *Pseudoclostridium thermosuccinogenes*. BMC Microbiol 20, 149 (2020). https://doi.org/10.1186/s12866-020-01835-2

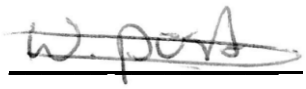
Mougiakos, I., Orsi, E., Ghiffary, M. R., **Post, W.**, de Maria, A., Adiego-Perez, B., ... & van der Oost, J. (2019). Efficient Cas9-based genome editing of *Rhodobacter sphaeroides* for metabolic engineering. Microbial cell factories, 18(1), 1-13. https://doi.org/10.1186/s12934-019-1255-1

*: these authors contributed equally to this work

9 Statement of Authorship

I declare under oath that I have produced my thesis independently and without any undue assistance by third parties under consideration of the ‘Principles for the Safeguarding of Good Scientific Practice at Heinrich Heine University Düsseldorf‘.

Date: 06.05.2026

Signature:  (Willem Berend Post)

10 Acknowledgments

I would first like to express my sincere gratitude to Prof. Dr. Simone Prömel. Simone, it has been a joy working under your supervision. Your knowledge, perseverance and passion for the field has always been motivational, especially in times where progress was slow, and your high standard for scientific integrity has been exemplary for me. Similarly, I would like to thank Prof. Dr. Torsten Schöneberg for his supervision and expertise, allowing me to start this project at his lab in Leipzig and transferring it to Düsseldorf. I also would like to thank Prof. Dr. Sebastian Fraune for being my second supervisor and taking the time to read this thesis.

During the last five years I have had the joy to work with many amazing people. First of all, I would like to thank all colleagues at Leipzig University for making me feel at home straight away. Daniel, Johanna, Max, André, Isabell and many more, thank you for all your support.

Additionally, I am very grateful for Victoria Groß, who helped me get started in Leipzig and was always there for me in Düsseldorf. Victoria, it has been such a joy working and bouldering with you, and I hope we are able to stay in touch!

Many thanks also go to my colleagues in Düsseldorf, for the supportive environment, creating a pleasant work atmosphere and the many laughs. Diane, Anastasia, Kai, Stephanie, Rene, Iannis and Laura, thank you for everything!

I would like to thank all collaborators that have played pivotal roles in the various projects. This thesis would not have been there without your valuable contributions. Specifically, I would like to thank Prof. Dr. Samantha Hughes for introducing me to the wonderful world of the worm in the first place and sharing some of her passion for the research. I am excited to continue collaborating on various projects!

To all my friends, from the Netherlands, from church, and beyond: thank you for your support, your care, and for helping me take my mind off the science every now and then.

To my parents, Ben and Stijnie: I am profoundly grateful for everything you have done for me and for your unwavering support — even when it meant I would move to Germany. I would also like to thank my parents-in-law, Paul and Jenny, for their encouragement and enthusiasm, even from the other side of the world. Finally, I want to thank my grandparents and extended family; although my work was not always easy to explain, I have always felt your support and encouragement.

To Sarah, I cannot thank you enough for your support throughout these five years. The biggest joy in these past years has been getting to know you and even to marry you. I am sorry for the never-ending worm-talk at the dinner table, the long days in the lab and having to deal with a cranky husband when experiments failed. I am deeply grateful for your unconditional care in all circumstances.

Lastly, *Soli Deo Gloria*, all thanks be to God who gave me life and strength throughout these years!